Forschungszentrum Jülich



Institut für Chemie und Dynamik der Geosphäre 4:
Erdöl und Organische Geochemie

Petroleum Generation and Migration in the Berkine (Ghadames) Basin, Eastern Algeria: An Organic Geochemical and Basin Modelling Study

Noureddine Yahi

Jül-3677

Petroleum Generation and Migration in the Berkine (Ghadames) Basin, Eastern Algeria : An Organic Geochemical and Basin Modelling Study

Noureddine Yahi

Berichte des Forschungszentrums Jülich ; 3677
ISSN 0944-2952
Institut für Chemie und Dynamik der Geosphäre 4:
Erdöl und Organische Geochemie Jül-3677
D82 (Diss. RWTH Aachen, 1999)

Zu beziehen durch: Forschungszentrum Jülich GmbH · Zentralbibliothek
D-52425 Jülich · Bundesrepublik Deutschland
☎ 02461/61-6102 · Telefax: 02461/61-6103 · e-mail: zb-publikation@fz-juelich.de

Abstract

In this study the petroleum system of one of the most important hydrocarbon bearing basins in Algeria, the Berkine Basin, was reconstructed by combining the geological knowledge of the basin and the results of geochemical and basin modelling studies. In this order, total organic carbon (C_{org}) measurements, Rock-Eval pyrolyses, vitrinite reflectance measurements, gas chromatography (GC) analyses as well as gas chromatography-mass spectrometry (GC-MS) analyses were performed in order to evaluate the source rocks with respect to organic richness, kerogen type, depositional environment and maturity.

Following the previous evaluation, the burial, erosion and temperature developments within the basin were reconstructed applying both one-dimensional (PDI/1D) and two-dimensional (PetroMod/2D) basin modelling programs. The hydrocarbon generation history of two major Palaeozoic source rocks was reconstructed based on the pre-determined temperature history and a kinetic model for hydrocarbon (oil and gas) generation. The basin has the benefit of multiple hydrocarbon sources deposited during the Silurian and the Frasnian periods within a continental shelf environment. The development of anoxic to dysoxic bottom water conditions was a prerequisite for the deposition of these organic rich units. While increasing the commercial value of the basin by increasing the hydrocarbon potential, these source rocks by generating hydrocarbons at different epochs during the basin evolution generally complicate the understating of the petroleum system and the oil and gas accumulations. Therefore, the 2D finite element program PetroMod was used to discuss the history of hydrocarbon generation, expulsion and accumulation along a 205 km long selected transect which crosses various oil and gas fields. The major goal was to understand these hydrocarbon accumulations of which the origin and emplacement are still unsolved up to date. The understanding of such important petroleum geology aspects can considerably reduce exploration risks. The PetroMod 2D program was also applied in order to understand overpressure developments and the contribution of the major faults to fluid movements.

The results of both 1D and 2D numerical simulations indicate that the maturity reached by the source rocks reflects mainly the Cretaceous-Tertiary burial. The results show no imprint of any higher than normal heat flow during maximum burial time and that the

maturation generally proceeded with time and burial. The results show also that the temperature reached by the source rocks prior to the Hercynian uplift and erosion is of great importance because it determines how much hydrocarbon generation potential was conserved. For instance, the timing of hydrocarbon generation and conservation, particularly for the Silurian source rock, is highly dependant on the pre-Mesozoic burial. Furthermore, the 2D numerical simulations show that the faults related to the Triassic-Early Jurassic rifting are permeable. These faults seem to have a great control on reservoir pressure dessipation towards the more open systems by connecting these reservoirs vertically and putting them in hydraulic communication. The fold-related faults are, in contrast, closed to fluid movements. This fact might be one reason which explains the development of overpressured deep Ordovician reservoirs.

From the above-cited temperature evolution and hydrocarbon generation reconstructions associated with the evolution of the basin through time, expulsion, migration (based on three phase flow; water, oil and gas) and accumulation was reconstructed. The simulation results explain well the filling of the fault block structures in the central part of the basin. It can be argued that oil fields such as Wed Teh, Berkine East, Sif Fatima and undrilled in-between structures were supplied by the Frasnian source rock in which the present oil was generated only during the Late Cretaceous and Tertiary. High drainage capabilities are associated with major extensional faults. Other nearby oil fields such as Rhourd Khrouf, Rhourd Messaoud, Rhourd El Rouni and Bir Berkine may be placed in this context.

A sensitivity analysis shows, on the other hand, the importance of the pre-Mesozoic burial and related residual hydrocarbon generation potential for the Silurian source rock. In fact the oil fields located in the western part of the basin along the Amguid El Biod- Hassi Messaoud ridge (Gassi El Adem, Nezla North, Gassi Touil and others) can be explained only if relatively moderate Palaeozoic burial is assumed. In other words, a Mesozoic generation is the most accurate hypothesis which increases the oil entrapment efficiencies. It is argued that a Palaeozoic generation implies a large destruction of the generated hydrocarbons, particularly oil, by the Hercynian erosion.

Kurzfassung

In dieser Arbeit wurde das Petroleumsystem des wichtigsten kohlenwasserstoffführenden Beckens Algeriens, des Berkine Beckens, durch die Kombination von fundierten regionalgeologischen Erkenntnissen über das Becken sowie den Ergebnissen von geochemischen Untersuchungen und Beckensimulationsstudien rekonstruiert. Um Aussagen über die Kohlenwasserstoffmuttergesteine hinsichtlich des Gehaltes an organischem Material, des Kerogentyps, des Ablagerungsmilieus und der Reife zu manchen, wurden TOC Messungen (total organic carbon), Rock-Eval Pyrolysen, Vitrinitreflexionsmessungen, gaschromatographische Analysen (GC) wie auch gaschromatographisch-massenspektrometrische Analysen (GC-MS) durchgeführt.

Aufbauend auf diesen Ergebnissen wurden Absenkungs-, Erosions- und Temperaturgeschichten sowohl eindimensional als auch zweidimensional mit Hilfe der Beckensimulationsprogramme PDI/PC und PetroMod modelliert. Die Kohlenwasserstoffgenese zweier paläozoischer Muttergesteine wurde auf der Basis der zuvor ermittelten Temperaturgeschichte sowie eines kinetischen Modells zur Genese sowohl von Öl als auch von Gas rekonstruiert. Das Becken ist kohlenwasserstoff-höffig, weil zwei bedeutende Kohlenwasserstoffmuttergesteine während des Silurs und des Fransnians im Bereich des Kontinentalschelfs abgelagert wurden. Die Entwicklung von anoxischen und dysoxischen Bedingungen im Bodenwasser war die Grundvoraussetzung für die Ablagerung dieser Einheiten, die reich an organischem Material sind. Einerseits wird der kommerzielle Wert des Beckens durch das hohe Kohlenwasserstoffpotential gesteigert, andererseits wird durch die Bildung von Kohlenwasserstoffen während unterschiedlichen Zeiten in der Beckenentwicklung und aus den verschiedenen Muttergesteinen das Verständnis des Petroleumsystems sowie der heutigen Öl- und Gas Akkumulationen generell erschwert. Aus diesem Grund wurde das 2D-Finite-Elemente-Programm PetroMod verwendet, um die Kohlenwasserstoffgenese, -Expulsion und -Migration zu simulieren. Dazu wurde ein 205 km langes Profil untersucht, das mehrere Öl- und Gasfelder quert. Hauptziel war es, die Gründe für diese Kohlenwasserstoffakkumulationen, deren Herkunft und Platznahme bis jetzt ungelöst sind, aufzuklären. Das Verständnis dieser wichtigen

Aspekte der Petroleumgeologie kann die Explorationsrisiken beträchtlich reduzieren. Das PetroMod-Programm wurde auch verwendet, um die Entwicklung von Überdrucken und die Bedeutung von Hauptstörungen für die Fluidbewegungen zu verstehen.

Die Ergebnisse sowohl der 1D- als auch der 2D-Simulationsrechnungen zeigen, daß die heutige Reifeverteilung der Muttergesteine hauptsächlich durch die kretazisch-tertiäre Versenkung verursacht wurde. Die Simulationsergebnisse zeigen keine erhöhten Wärmeflüsse zum Zeitpunkt der maximalen Versenkung an. Generell nahm die Reife mit fortschreitender Zeit und Versenkung zu. Die Ergebnisse zeigen weiterhin, daß die Temperaturen, denen die Muttergesteine vor der herzynischen Heraushebung und Erosion ausgesetzt waren, von größter Bedeutung sind, denn sie bestimmen wieviel Kohlenwasserstoffgenesepotential für die folgende Entwicklung konserviert wurde. Beispielsweise ist die Zeitlichkeit der Kohlenwasserstoffgenese in höchstem Maße abhängig von der prä-mesozoischen Versenkung. Dies gilt besonders für das silurische Muttergestein. Darüber hinaus zeigt die 2D-Simulation, daß die Störungen, die in Zusammenhang mit dem Rifting in der Trias und Unterkreide stehen, permeabel sind. Diese Störungen scheinen einen großen Einfluß auf den Reservoirdruck zu haben, indem sie diese vertikal verbinden und damit hydraulisch verknüpfen. Es handelt sich daher um ein eher offenes System. Im Gegensatz dazu stehen die Störungen, die in Zusammenhang mit dem Faltenbau entstanden sind. Sie sind für Fluidbewegungen geschlossen. Diese Tatsache könnte eine Erklärung für die Entstehung von Überdrucken in den tiefen ordovizischen Speichergesteinen bereitstellen.

Aus der oben beschriebenen Temperaturgeschichte und der Rekonstruktion der Kohlenwasserstoffgenese in Zusammenhang mit der zeitlichen Entwicklung des Beckens wurden Expulsion, Migration und Akkumulation modelliert. Die Kohlenwasserstofffüllung der Horst- und Graben-Strukturen (fault block structures) im Zentralbereich des Beckens kann gut durch die Simulationsergebnisse erklärt werden. Es zeigte sich, daß Ölfelder wie Wed Teh, Berkine Ost, Sif Fatime und noch nicht erbohrte Strukturen, die dazwischen liegen, durch Kohlenwasserstoffe aus dem Muttergestein des Frasnian gefüllt wurden, wobei das heute vorhandene Öl nur während der Oberkreide und des Tertiär gebildet wurde. Die Hauptextensions-

Störungen sind gekennzeichnet durch hohe Permeabilitäten und dienen der Drainage des Systems. Andere Ölfelder in der Nähe, wie Rhourd Khrouf, Rhourd Massaoud, Rhourd El Rouni und Bir Berkine, sind in diesem Kontext zu verstehen.

Andererseits zeigt die Sensitivitätsanalyse die Wichtigkeit der prä-mesozoischen Versenkung und das damit zusammenhängende Residual-Potential für die Kohlenwasserstoffgenese des silurischen Muttergesteins. Die Ölfelder, die im westlichen Teil des Beckens entlang des Amguid El Boid - Hassi Messoud Rückens liegen (Gassi El Adem, Nezla Nord, Gassi Touil und andere) können nur erklärt werden, wenn eine moderate paläozoische Versenkung angenommen wird. Dies ist eine geeignete Hypothese zur Erklärung der erhöhten Effizienz der Fallenbildung. Schließlich zeigte sich, daß eine paläozoische Kohlenwasserstoffgenese eine Zerstörung der generierten Kohlenwasserstoffe, besonders von Öl, durch die herzynische Erosion impliziert.

Preface

First, I would like to express my full gratitude to Prof. Dr. Ralf Littke for his constant interest, guidance, supervision, very helpful discussions and encouragements throughout the study. I am also very grateful to Prof. Dr. Dr. h.c. D.H. Welte for his support and permission to carry out this study at the Institute of Petroleum and Organic Geochemistry (ICG-4) of which he is the director.

Very special thanks are due to Dr. R.G. Schaefer and Dr. H.S. Poelchau for reviewing the thesis and for their invaluable help during its completion.

The present study would not have been possible without the support of many other sources. The author gratefully acknowledges the help of Dr. B. Koopmann, the exploration manager of Veba Öl Algerien GmbH, which provided the financial support. I am also grateful to SONATRACH which provided the samples and data necessary for this study. Special thanks are due to M. Hamel, the head of SPT for his orientation and help.

I would also like to thanks all the scientists and technicians at ICG-4 for their assistance and support during the analytical procedures in the different laboratories. Special thanks are due to H. Willsch, W. Laumer, A. Ropertz, U. Disco and W. Benders.

This thesis would never have been completed without the support of a person that had the greatest influence on my education, **my father**, whom I lost during writing this thesis. **This study is dedicated to his memory**. I would also like to thank my mother for her encouragement to get the power to finish this work after this unfortunate event.

Finally, I want to thank my wife, Karima, my daughter, Nesrine, and my son, Hamza, who always managed to get my mind off scientific problems as soon as I arrived at home.

CONTENTS

Abstract/Kurzfassung

Preface

Contents

1. Introduction 1

1-1 Problems and Objectives 1

1-2 Tectonic Evolution of North and West-Central Africa 3

1-3 Petroleum Geology of Northern Africa 7

1-4 History of Petroleum Exploration and Production in Algeria 10

2. Geology of the Ghadames Basin 14

2-1 Regional Geology and Basin Development 14

2-2 Lithostratigraphy and Paleogeography 17

3. Petroleum Geology: An Overview 22

3-1 The Silurian and Upper Devonian Petroleum Systems 22

3-2 Trap Types, Reservoirs, and Sealing Strata 24

3-3 Oil to Oil and Oil to Source Rock Correlations 25

3-4 Some Remarks on Pressure Development in the Ghadames Basin 26

4. Samples and Geochemical Methods 29

4-1 Samples and Sample Documentation 29

4-2 Screening Analyses 30

4-2-1 Total Organic Carbon and Sulfur Content 30

4-2-2 Rock-Eval Pyrolysis 30

4-3 Petrographic Analyses 31

4-4 Molecular Geochemical Analyses 32

4-4-1 Solvent Extraction and Sample Preparation 32

4-4-2 Liquid Chromatography 33

4-4-3 Capillary Gas Chromatography (GC) 33

4-4-4 Gas Chromatography/ Mass Spectrometry (GC/MS) 34

5. Results of Geochemical Analyses 34
5-1 Characterisation of the Solid Organic Matter 34
5-1-1 Organic Matter Abundance and Sulfur Content 35
5-1-2 Kerogen Type and Generation Potential 41
5-1-3 Maturity 45
5-2 Characterisation of Bitumen (EOM) and Crude Oils 49
5-2-1 Total EOM Yields and Compound Class Composition 49
a/ Yields as a Function of Organic Carbon Content 50
b/ Yields as a Function of Maturity 53
c/ Compound Class Composition 55
5-2-2 Molecular Characterisation 57
a/ Aromatic Hydrocarbons 57
b/ Saturated Hydrocarbons 61
5-3 Summary 76

6. Basin Modelling 78
6-1 Principles of Computer-Aided Basin Modelling 78
6-1-1 Application and Material 78
6-1-2 The Conceptual Model 80
6-1-3 The Horizontal Discritization and the Generation of the Grid Net .. 82
6-1-4 Petrophysical Properties of Rocks 83
6-1-5 Input Parameters 86
6-1-6 Calibration Parameters 91
6-2 Petroleum Generation and Migration 94
6-2-1 Kinetics of Petroleum Generation 94
6-2-2 Fluid Flow in Sedimentary Rocks 96
6-3 1D Simulation Results 97
6-3-1 Geothermal Gradient in the Ghadames Basin 97
6-3-2 Burial and Thermal History 99
6-3-3 Maturation History 117
6-3-4 Hydrocarbon Generation History 119

6-3-5 Significance of the Triassic-Liassic Thermal Anomaly to Hydrocarbon Generation..... 130
6-3-6 Significance of Thermal Properties of Rocks to Hydrocarbon Generation..... 131
6-3-7 Data Limitations..... 132
6-3-8 Summary..... 134
6-4 2D Simulation Results.....136
6-4-1 Present-Day Temperature Distribution..... 137
6-4-2 Maturity Distribution and Evolution.....138
6-4-3 Compaction Induced Overpressures and Fault Transmissibility..... 143
6-4-4 History of Hydrocarbon Generation and Migration..... 146
6-4-5 The Alternative Hydrocarbon Generation and Migration Model..... 151

7. Conclusions.....156

8. References..... 160

APPENDIX

1. Introduction

1-1 Problems and Objectives

Located on the eastern Saharan Platform at around 30°N latitude and 8° E longitude and extending into Libya (Fig. 1), the Berkine (former Ghadames) Basin has become one of the most important petroleum bearing basins in Algeria. Thirty discoveries were made in the last decade comprising ten oil fields. However, the estimated petroleum reserves of the basin (Chapter 1.3) are still considered to be insignificant compared to the possible amounts of hydrocarbon generated by both the Silurian and the Frasnian basal "radioactive shales" (Malla et al., 1997). Therefore, with respect to the future exploration strategy, considerable efforts should be applied to search for further hydrocarbon accumulations in the basin. In order to do this, it is important to understand the major factors controlling the success or failure of petroleum exploration at a basin scale such as, the timing of hydrocarbon generation and expulsion related to trap formation, the dynamics of petroleum through time and the destructive events.

Despite the architecture of the basin which is relatively simple, its overall hydrocarbon system is not well understood, particularly with respect to the origin, migration and entrapment of petroleum. Indeed, the basin shows inconsistencies in the liquid and gaseous hydrocarbon distributions. Oil and gas fields are located in different trap types and reservoir levels and are located very close to each other (Fig. 1). This distribution seems to be related to, and complicated by, the effective contribution of each source rock horizon, generating hydrocarbons at different times of the basin evolution. Understanding the contribution of each source to the present oil and gas accumulations is highly required, particularly when correlations of crude oils to their possible source rock horizons are difficult to constrain.

The present study represents a multidisciplinary approach, including geochemical, geological and thermal history studies, used to assess the generation potential, the history of oil and gas generation, as well as areas of oil and gas generation and hydrocarbon migration through geological time. Detailed geochemical studies of the basin are generally missing. Therefore, geochemical techniques have been applied to evaluate source rock attributes such as lithology, depositional environment, organic richness, kerogen type and maturity, and eventually to correlate oils to source rocks.

As pointed out by Waples (1985), geochemistry must be used in the context of a comprehensive model of the entire hydrocarbon system, including hydrocarbon generation, migration pathways and entrapment. Building a consistent model for the petroleum systems in a given sedimentary basin requires an integration of organic geochemistry with geology, geophysics, paleogeography, hydrodynamics and geothermics. As a holistic approach, integrated basin models were used to reconstruct sedimentation, paleopressures, fluid dynamics, and those factors related to hydrocarbon generation, as well as migration routes and to develop an overall framework of the petroleum charge along a selected cross-section through the basin.

The different wells and fields investigated in this study, the wells submitted to one-dimensional (1D) modelling, as well as the position of the seismic line used for two-dimensional (2D) modelling are shown on Fig. 1. The basin modelling concepts and materials, and their importance for the present study area are described in detail in Chapter VI.

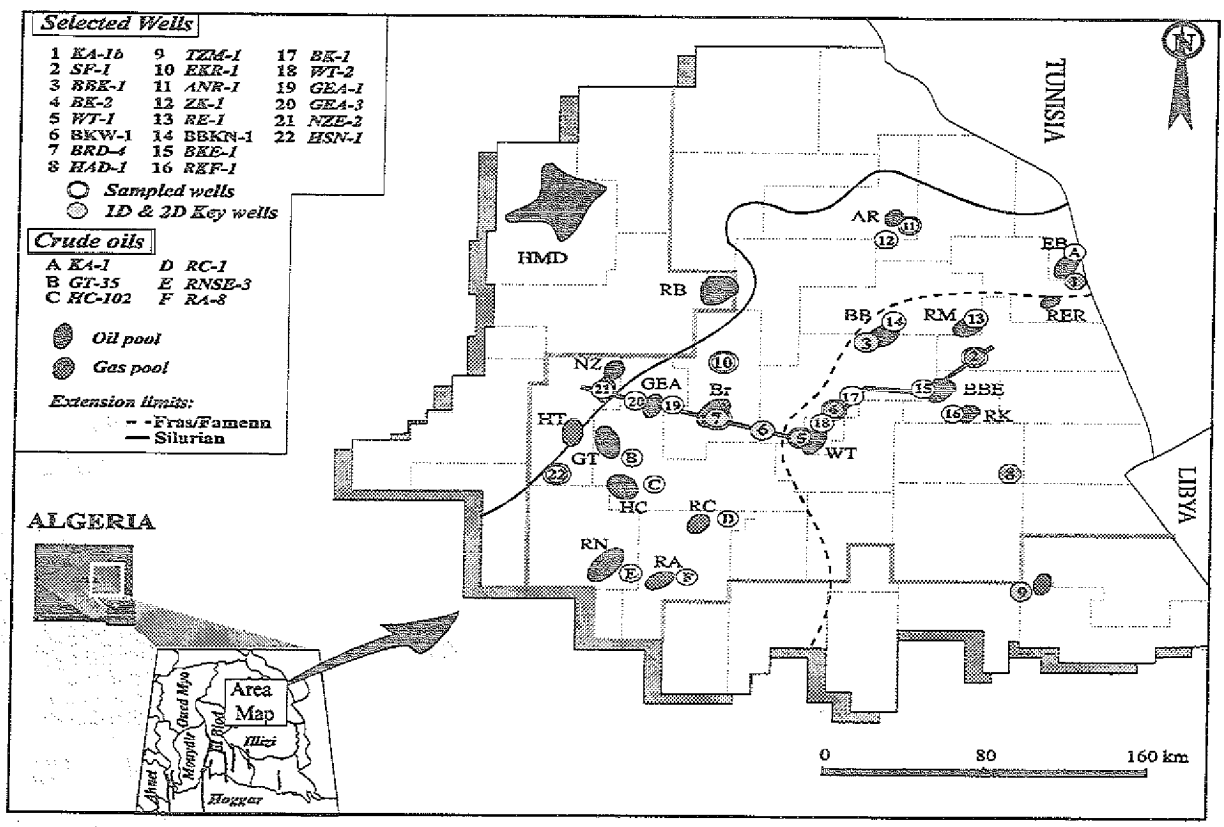


Fig. 1: Base map of the study area showing the location of the evaluated wells, the 1D calibrated key wells, the 2D regional seismic line and discoveries within the basin. HMD, Hassi Messaoud; RB, Rhourd El Baguel; Nz, Nezla; HT, Hassi Touareg; GT, Gassi Touil; HC, Hassi Chergui; Br, Brides; WT, Wed Teh; BB and BBE, Bir Berkine and East; SF, Sif Fatima; EB, El Borma; GEA, Gassi El Adem; AR, Ain Romana; RN, Rhourd.Nouss; RA, Rh.Adra; RC, Rh.Chouf.

1-2 Tectonic Evolution of North and West-Central Africa

About 50% of the total area of Africa (approximately 30 million km^2) is covered by sedimentary basins of various types and ages. Passive margin rift basins, interior sag basins, foreland basins, interior fracture basins, marginal sag basins, as well as basins related to thermal subsidence of hot-spot domes can be differentiated (Clifford, 1987; Sahagian, 1993, Petters, 1991, Hartly and Allen, 1994). Their ages vary from Precambrian to Tertiary (Clifford, 1987; Genik, 1992, Hartly and Allen, 1994). The basin fill thicknesses vary from a few thousand meters to more than 15,000 m of both marine and continental sediments. The greatest sediment thicknesses are documented in extensional basins overlying weak continental lithosphere. Examples are the Cretaceous basins of West-Central Africa (Hartly and Allen, 1994).

This chapter gives an overview of the tectonic evolution of the west-central part of the African plate and its northern margin. Situated between 5° and 36°N latitude, this area is bounded to the North by the Mediterranean sea and extends from the Atlantic in the West to the Red Sea in the East (Fig. 2 and 3).

West-Central Africa is essentially composed of 2 major tectonics unit (Fig. 2): the West African Precambrian craton, stable since 2000 Ma, and the surrounding mobile belts of Upper Proterozoic age (Lesquer et al., 1990). The basement of the West African craton is exposed in the Reguibat and Leo uplifts and remained essentially undisturbed through the Pan-African orogeny (Hartly and Allen, 1994). The Taoudeni basin occupies the center of the West African craton. The West African craton is surrounded by Panafrican mobile belts (Anti Atlas, Hoggar shield, Benin-Nigeria shield, Tibesti and others) (Fig. 2, 3). These structural highs resulted from collisional processes at around 600 Mabp (Lesquer et al., 1984; Dallmeyer and Lecorché, 1989). They are aligned along major lineaments (Guiraud et al., 1987), and are commonly associated with volcanic activity and intervening large Paleo-Mesozoic and Cretaceous-Tertiary interior/marginal sag sedimentary basins. Examples are the Sahara basins (Algeria and Libya), Iullmedden (Niger), Sudan and Chad basins (Fig.3).

The main structural features of the African continental domain are linked to old zones of weakness of Panafrican origin, and to the fact that some major fractures will show an episodic instability during long periods of geological time (Conrad, 1969; Guiraud

et al., 1987). They are generally associated with the dominant influence of the Africa-Europe collision and the opening of the Atlantic ocean (Guiraud et al., 1991).

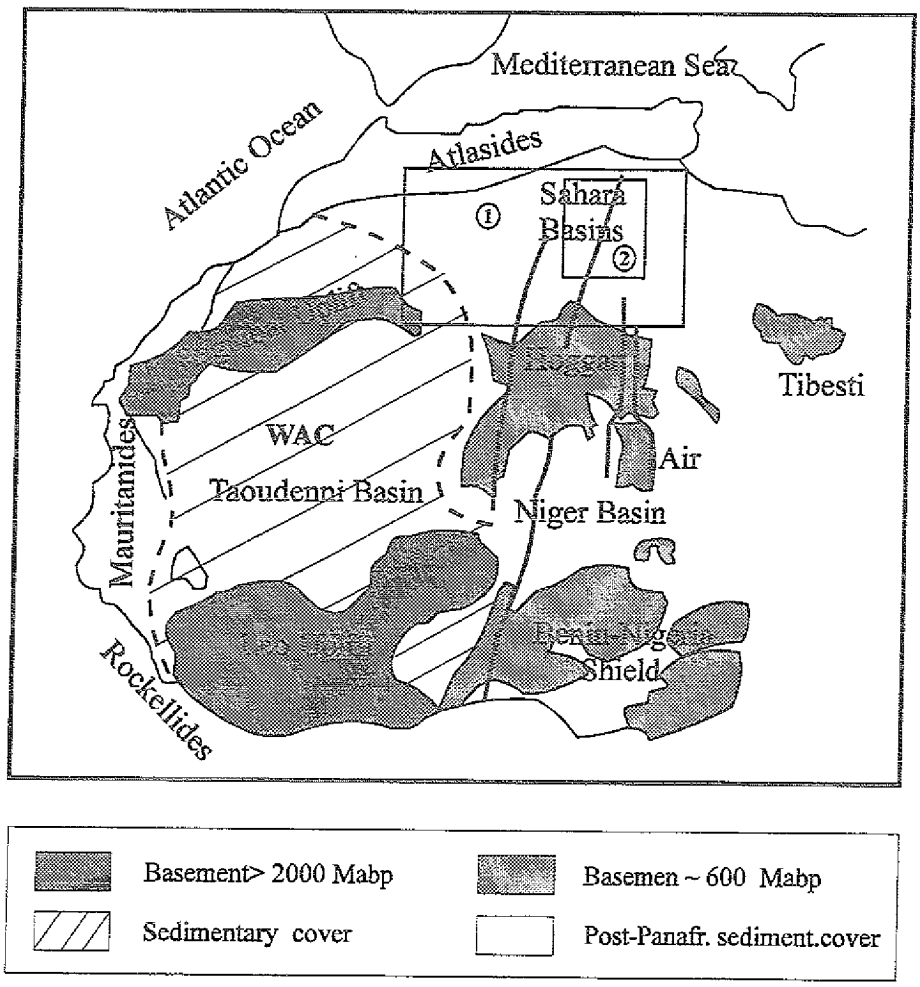


Fig. 2: Major tectonic units of West Africa showing the relative position of the stable West African Craton (WAC) in relation to the Panafrican mobil belts (after Lesquer et al., 1990). Outlined rectangles 1& 2 are areas of Fig. 6 and 7 respectively.

Since the Panafrican orogeny and up to the Triassic-Jurassic rifting phase, the African plate is believed to have been a stable entity (Dautria and Lesquer, 1989; Goudarzi, 1970, Klitzch, 1984, 1993). No definitive continental break-up has been documented before this time for the Platform phase (Genik, 1993), although a significant faulting phase in the Cambro-Ordovician time was reported by Klitzch (1970) and Boudjema (1987). Accordingly most of the Palaeozoic basins in northern Africa are sag features over earlier rift systems.

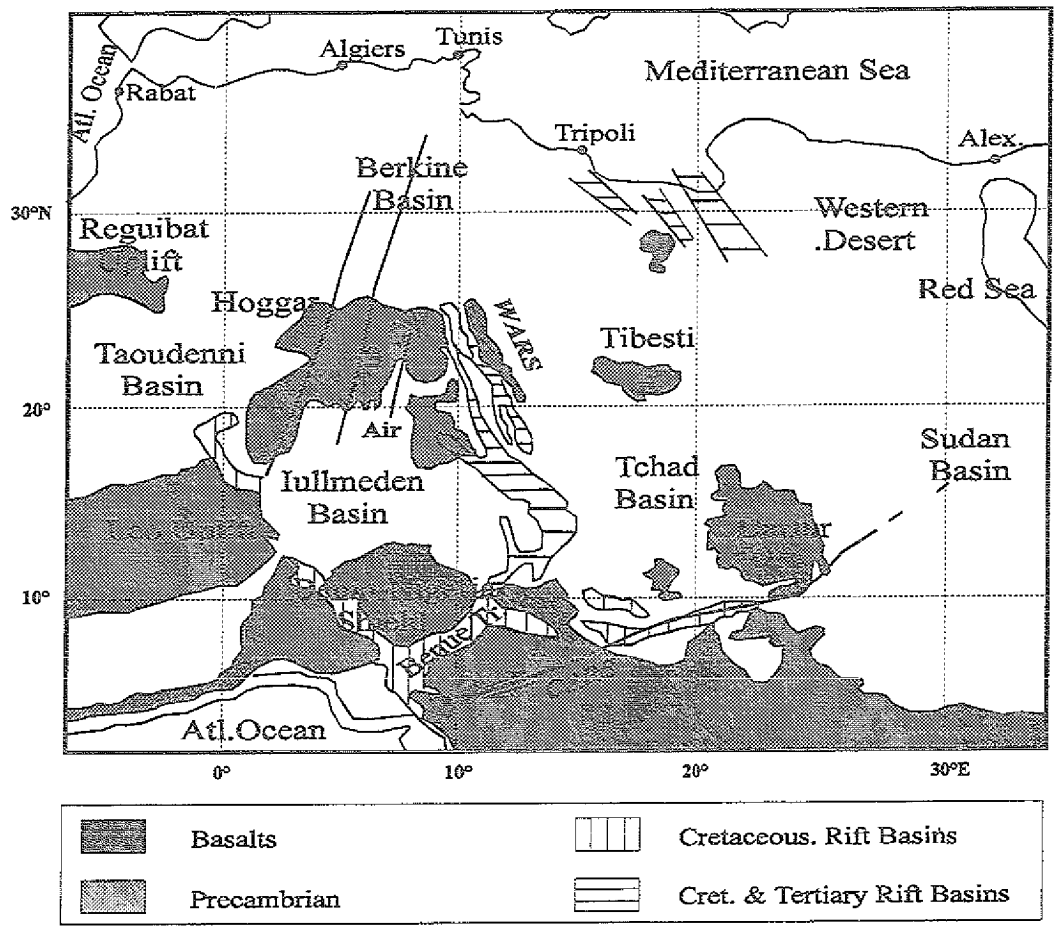


Fig. 3: Schematic geological framework of West-Central Africa (after Genik, 1992, completed) showing its major tectonic units and the position of the West and Central African Rift systems (WARS and CARS) with respect to the Berkine Basin.

The Late Carboniferous Hercynian (Variscan) movements resulting from a plate collision with Europe and responsible for the formation of the Mauritanides and the Atlasic fold belts (Lesquer et al., 1990) ended this Early Palaeozoic rifting phase.

The whole of the continental domain situated between the Alpine chain (Atlasides) accreted in the Tertiary, and Central African lineaments (southern Chad) was further subjected to post-Hercynian deformations (Guiraud et al., 1987). A rifting phase started in the Early Mesozoic time in response to the opening of the central Atlantic (Guiraud et al., 1987; Mengoli and Spenci, 1985). The strike-slip displacements caused by the extensional movements led to the formation of a series of Mesozoic passive margin basins and failed rifts, extending from the Moroccan margin through the Atlas and Pelagian basins to the Abu Gharadig basin in the western desert of Egypt (Awad,

1984). Oblique extension during the drift phase affected much of the North African margin leading to occasional transpressional structures (Macgregor, 1996).

During the Late Cretaceous-Tertiary time the interior of Gondwana was a site of numerous mega-shear zones, related to the formation of a series of rifts such as the West and Central African rift systems (Burke and Whiteman, 1973; Genik, 1992,1993; Guiraud and Maurin, 1992; Guiraud et al., 1992; Guiraud, 1993; Hartly and Allen, 1994). Accordingly, the eastward motion of Central and South Africa along ENE-WSW strike-slip trending movements resulted in the opening of North-South and NNW-SSE fractures inherited from Panafrican and older structures. Complex rift systems were then initiated in Nigeria, Niger, Chad, Central Africa and Sudan. The Western African rift system (Fig. 3) directly underlies the Chad basin and extends from the Benue Trough in the south-west to lake Chad in the north-east and then in a northerly direction towards Niger and Chad (Termit, Tenere and other basins). The Central African rift system, bordering the Chad basin to the South, extends in a roughly E-W direction from the Benue Trough to Sudan (Fig. 3). The rift systems were developed during the initial opening of the North Atlantic in the Early Cretaceous and preceded the definitive break-up of the Central Atlantic in the Late Cretaceous-Tertiary time, and consequently the separation of Africa from North and South America (Burke and Dewey, 1974; Thiessen et al., 1976; Guiraud et al., 1987; Guiraud and Maurin, 1992). These lithospheric cracks were responsible for the formation of strongly subsiding basins. The related extensional sub-basins (e.g. Termit basin) contain exceptionally up to 14 km thick continental and marine sediments of Lower Cretaceous to Tertiary age (Hartly and Allen, 1994).

The change in relative motion vector of the African and European plate from left-lateral translation to convergence in the Late Cretaceous (Savostin et al., 1986, Le Pichon et al., 1988) led to regional scale inversions particularly in the Atlas area and the Western desert area (Mengoli and Spenci, 1985).

Renewed rift activity, related to the opening of the Eastern Mediterranean (Guiraud and Maurin, 1992; Savostin et al., 1986) started in the Late Campanian with major subsidence occurring during the Palaeocene and Eocene times (Gumati and Kanes, 1985). This rifting phase was responsible for the formation of the Sirte basin in Libya (Guiraud and Maurin, 1992).

The effect of the Alpine orogeny at the late Tertiary (Savostin et al., 1986) was again largely confined to the Atlas area and adjoining basins. Thrust sheets, usually of flysch deposits and sometimes also of carbonate rocks occurred in the northern Atlas (Guiraud et al., 1987) passing into milder inversions in the northern Pelagian basin (Bishop, 1975; Clifford, 1987).

A final isolated event was the rifting of the Gulf of Suez in the Miocene (Richardson and Arthur, 1988; Macgregor, 1996). According to Brown (1978) more than 15,000 m of sediments were accumulated during the Miocene time suggesting a deep structure.

1-3 Petroleum Geology of Northern Africa

This chapter provides an overview of the petroleum systems of the northern margin of the African plate, bounded by the Atlantic to the North-west, the Mediterranean sea to the North and the Arabian plate to the East (Fig. 4). This area includes Morocco, Algeria, Tunisia, Libya and Egypt. As well as forming a geographically continuous unit, this region also shows a common geological history forming part of a single geological plate through Phanerozoic history (Chapter 1.2).

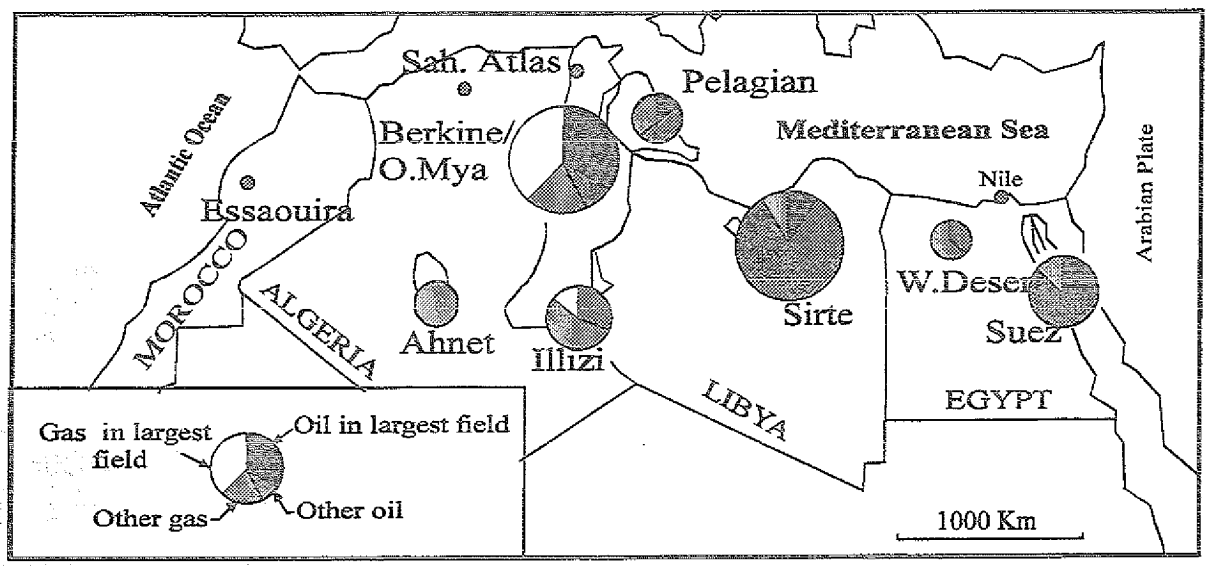


Fig. 4: Distribution of proven hydrocarbon resources in North Africa (After Macgregor, 1996). Note that the proven oil reserves in the Sirte basin are higher than those of Algerian Basins which contain a higher proportion of gas.

The five countries include a sequence of mature sedimentary basins. Such examples are the basins of Essaouira, Ahnet, Triassic (Oued Mya and Berkine), Illizi, Murzuk,

Sirte and the Golf of Suez (Fig. 4). To these should be added the offshore pelagian basin of Tunisia and Libya. The basins are generally separated by structural highs of various age, origin and orientations. Examples are the Ougarta chain, the Amguid El Biod- Hassi Messaoud ridge, and the Hoggar and Tibesti volcanic swells (Figs. 2, 6). The well known hydrocarbon provinces in the five countries concerned are located, according to Clifford, 1987, within marginal sag/interior sag basins that overlie earlier interior sag basins (Berkine and Oued Mya basins in Algeria), interior sag basins (Ahnet and Illizi basins in Algeria), interior fractures basins (Syrte and Gulf of Suez basins in Egypt), Wrench modified (Pelagian basin of Tunisia and Essaouira basin of Morocco). As outlined by Macgregor (1996), petroleum resources tend to be concentrated in a small number of significant provinces (Fig. 4).

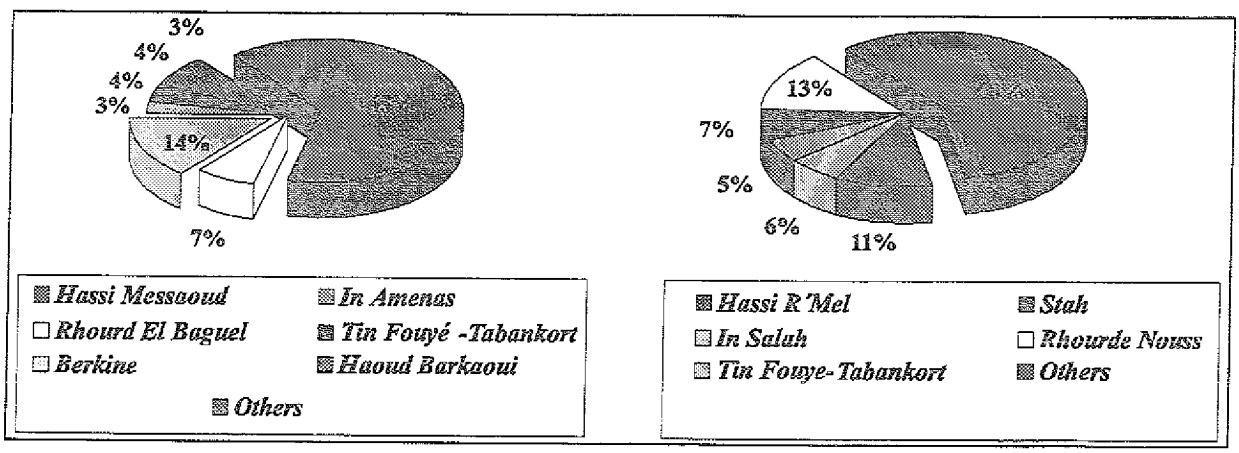


Fig. 5: Distribution of oil and gas reserves in Algeria (SONATRACH source in Oil and gas Journal, 1998). Note the high proportion of basin reserves in two major Algerian fields (Hassi Messaoud and Hassi R´Mel) and the relatively high contribution of the Berkine Basin to the Algerian oil reserves.

The largest oil and gas fields of Algeria are located in the Berkine/Oued Mya basins. These are the Hassi Messaoud and Hassi R´Mell fields with, respectively, nine billion BBL (barrel) of crude oil and 70 TCF (trillion cubic feet) gas plus 2.6 billion BBL of crude oil (Clifford, 1987; Macgregor, 1996). The former, which straddles a North to South trending regional arch (Balbucchi and Pommier, 1970) constitutes 65% of the Algerian total oil reserves (Fig. 5). The oil is produced from fractured Cambrian quartzitic reservoirs. The latter field is situated on the Northwest side of the Oued Mya basin and produces gas and condensate from a Triassic reservoir on a similar arch to Hassi Messaoud (Magliore, 1970). This field accounts for 58% of the total gas reserves

of Algeria (Fig. 5). Many other Triassic discoveries have been made during the last decade in the Berkine Basin. Estimated reserves in these fields are 5.904 billion BBL oil, 200 million BBL of condensate and 2.5 TCF of natural gas. The new oil discoveries account for about 14% of total Algeria's oil reserves (Fig. 5).

Another important hydrocarbon province in Algeria is the Illizi Platform. Edjeleh, Zarzaitine and Alrar are the most important fields with estimated reserves of 220 million BBL oil, 900 million BBL oil plus 2.8 TCF gas and 4.7 TCF gas, respectively (Clifford, 1987). Hydrocarbons are produced from sandstone reservoirs throughout the Palaeozoic (Cambro-Ordovician, Devonian and Carboniferous). Trap types include extensional faulted blocs and inversion structures of Carboniferous age. For instance, the Illizi Platform contains one of the largest known hydrodynamic traps world-wide. This is the Tin Fouyé-Tabankort field (Chiarelli, 1978) with approximately 1.2 billion BOE (barrel oil equivalent) oil and gas reserves in the Devonian and Ordovician reservoirs. The field contributes for about 3% and 6% to the total oil and gas reserves, respectively (Fig. 5).

The main source rock horizons for the Algerian fields are the Silurian and Upper Devonian radioactive shales, developed particularly in the Berkine, Illizi and Ahnet basins.

In the Sirte basin reserves are more widespread. A census of 21 Eocene-Oligocene carbonate fields was made in the basin (Clifford, 1987). Other reservoirs of importance are Cambrian and Lower Cretaceous sandstones. For instance, the Cretaceous sandstones constitute the main reservoir of one of the largest oil field, Sarir, with 6.5 billion BBL of recoverable oil (Clifford, 1987). This field contributes of about 18% to the total basin reserves (Macgregor, 1996). The traps consist mainly of extensional blocs and overlying drape anticlines. Hydrocarbons are mainly sourced from Cenomanian shales, filling the Aptian rift system (Shardanov et al., 1983).

It should be pointed out that the Sirte and Illizi/Ttriassic provinces contain reserves in the range of 30-35 billion BOE, placing them among the world's largest. Together they contain 85 % of the oil and 80 % of the gas discovered in North Africa (Macgregor, 1996).

The Gulf of Suez constitutes the third most important province in North Africa with areal productivity of 7 billion BOE in an area of only 26,000 km^2 (Macgregor, 1996).

The traps consist mainly of extensional blocks. The main hydrocarbon source rock is the Santonian Brown Limestone (Bishop, 1988).

The offshore Pelagian basin of Tunisia and Libya ranks fourth with 3 billion BOE of reserves concentrated in an Eocene carbonate fairway (Macgregor, 1996). The most important source rocks are the carbonate facies of the Eocene and the Turonian black shales (Bishop, 1988). Moderate-sized gas provinces are located in Algeria and Egypt (Ahnet, Western Desert) with proven reserves each of around 1 billion BOE (Macgregor, 1996). The Essaouira basin is another onshore hydrocarbon generating basin in western Morocco. Gas and condensate are produced in the Mescala field from a Triassic reservoir associated with horst fault blocs. Fractured Jurassic carbonate reservoirs associated with closed drapes above buried salt dome are producing in other fields such as Kechoula, Jeer, N´dark and Toukimt in the eastern Essaouira basin (Broughton and Trepanier, 1993). Hydrocarbons are sourced from Jurassic (Oxfordian) shales accumulated within the Neknafa syncline in the western part of the basin and deeply buried Carboniferous coals underlying the eastern basin area.

The petroleum geology of North Africa is summarized in Table 1. The petroleum systems and the contribution of Algeria to the to the North African petroleum reserves are summarized in Table 2.

1-4 History of Exploration and Production in Algeria

The history of exploration in Algeria started with the geological study of Killian (1925). He was the first geologist who described, in the northern Hoggar, the Silurian micaceous bituminous shales, proven later to be one of the most important hydrocarbon source rock in all the Algerian Saharan Platform. Despite this, strong contrasts in the level of exploration can be observed in Algeria. Hydrocarbon exploration was limited to the most accessible zones. Platforms and broad arches were the prime targets. For example about 1800 exploration wells were drilled in the Illizi Platform, but only very few hundred wells in the huge Triassic province (Oued Mya and Berkine Basins).

The eastern Saharan region, including Triassic (Berkine and Oued Mya) and Illizi Platform and the associated ridges, is the most important hydrocarbon-bearing province in Algeria.

Tab.1: Estimated recoverable reserves per field (oil and gas) and per country (total hydrocarbon) in North Africa. Values with asterisk indicate condensate. bBBL, TCF and BOE are billion barrel, trillion cubic feet and barrel oil equivalent, respectively. The data are culled from the references cited in the text.

Contry	Basin	field	Trap Type	Source Rock	Reservoirs	Estimated Reserves Oil (bBBL)	Gas (TCF)	Tot.Est. Rec.Reserves (bBOE)
ALGERIA			*See Table below*					36.5
LIBYA	Sirte	Sarir	Fault block	Cenomanian	L. Cret.	6.5		
		Beda	Drape anticline	Cenomanian	Eocene	0.09		
		Raguba	Drape anticline	Cenomanian	Camb/Eocene	0.75		
		Nasser	Drape anticline	Cenomanian	Paleocene	2.2		
		Waha	Drape anticline	Cenomanian	Eocene	1.4		39.5
		Defa	Drape anticline	Cenomanian	Eocene	1.8		
		Intisser	Fault block	Cenomanian	Eocene	2.4		
		Amal	Fault block	Cenomanian	Camb/L.Cret/Eoc	4.2		
		Nafoora	Fault block	Cenomanian	Camb/L.Cret/Eoc	1.8		
EGYPT	Gulf of Suez	July	Fault block	Santonian	Miocene	0.750		7.3
		Ramadan	Fault block	Santonian	Miocene	0.350		
	Western Desert	Abu Gharadiq	Fault block	Cenomanian	L. Cret.		6	
MOR.+TUNISIA	Essaouira	Mescala	Fault block	Jurassic	Triassic	0.1*	1.1	2.5
	Pelagian		Stratigraphic	Eoc/Turon	Eocene		18	

Tab. 2: Hydrocarbon distribution in Algeria. The estimated recoverable oil and gas reserves per basin and field can be find out in the text.

Basin	field	Trap Type	Source Rock	Reservoirs
Oued Mya	Hassi R'Mel	Arch	Silurian/Devonian	Triassic
Berkine	Hassi Messaoud	Arch	Silurian	Cambrian
Berkine	Berkine	Fault block	Sil/Devon	Triassic
Illizi	Edjeleh	Anticline	Sil/Devon	Ord/Dev/Carb
	Zarzaitine	Anticline	Sil/Devon	Ord/Dev/Carb
	Alrar	Stratigraphic	Sil/Devon	Ord/Dev
	Tin Fouye-Tbkt	Hydrodynamic	Sil/Devon	Ord/Dev
Ahnet	Krechba	Anticline	Devonian	Dev/Carb

Hydrocarbon exploration started in this part of Algeria between 1950 and 1960, particularly when the Algerian government granted oil prospecting licences to oil companies. The first oil was discovered in 1956 at Edjeleh in the south-eastern part of the Illizi Platform by the C.R.E.P.S (Compagnie de Recherche et d´Exploitation de Pétrole en Algérie). This discovery can be considered as the trigger mechanism for further hydrocarbon exploration. Full reconnaissance survey led to the discoveries of the Zarzaitine (1958), Tin Fouyé-Tabankort (1960) and others fields such as Hassi Mazoula, Ohanet, Stah and Mereksen. In the mean time, S.N.REPAL (Société de Recherche et d´Exploitation des Pétroles en Algérie) in association with C.F.P.A (Compagnie Francaise des Pétroles Algérie), now TOTAL, obtained a licence for a prospecting area of about 250,000 km² in the north-eastern Saharan region. The first stratigraphic reconnaissance drilling was carried out between the cities of Ghardaia and Laghouat, 400 km southeast of Algiers. The well Berriane-1 (Be-1) penetrated about 3000 m of sediments and revealed hydrocarbon shows beneath a thick salt cover. Since this encouraging operation, the petroleum companies intensified their geological subsurface surveys. Seismic reflection and refraction acquisitions combined with field geology located, respectively in 1952 and 1956, the culminations of Hassi R´Mel and Hassi Messaoud at around 480 and 560 km southeast of Algiers. In 1956, after complementary seismic survey the Hassi R´Mel-1 (HR-1) was drilled. The well recovered a high pressure Triassic reservoir saturated with gas, and consequently the discovery of the Hassi R´Mel, one of the most important gas field in the world. In the Hassi Messaoud arch, the first well drilled in 1955 was relatively unsuccessful. The MD-1 hole crosses oil stained quartzitic sandstones attributed later to the Ordovician. Extensional wells carried out later on revealed the existence of a large oil accumulation, the production of which started in 1958. Since their discoveries, the Hassi R´Mel and Hassi Messaoud fields have been under continuous developments. By 1957 Algeria has become the tenth largest oil producing country in the world with an average daily production, in 1967, of approximately 830, 000 BBL oil (Balbucchi and Pommier, 1970). The Hassi Messaoud oil field contributed about 40%. By March 1961, the Hassi R´Mel gas field has produced a total of 430 billion CF (cubic feet) of gas and around 20 million BBL of condensate.

The intensification of exploration surveys later led to discoveries of several relatively small fields, but collectively making this area a significant hydrocarbon province. Examples are El Gassi-El Agreb (1959), Nezla (1961) Rhourd El Baguel and Rhourd Nouss (1962) and many others. After the independence of Algeria in 1962 and the creation of SONATRACH (Société Nationale de Transport et de Commercialisation des Hydrocarbures) in 1963, the Algerian and French states agreement created the ASCOOP (Association Cooperative) in 1965. SONATRACH in association with SOPEFAL (Société des Pétroles France-Algerie) made new hydrocarbon discoveries such as Mesdar (1967), Keskasa, El Borma and Oued Noumer (1969). After the nationalisation of hydrocarbons reserves in February, 1971, SONATRACH became the main operator and new fields were discovered particularly in the Ouargla area, such as Draa El Temra (1971), Guellala Nord-Est (1973), Ngoussa (1975), Takhout (1976) and Garet El Chouf (1978).

As previously mentioned, the low lying areas, such as the Berkine Basin, are still not well explored. This region is known to be difficult to access, either in the surface or in the subsurface. This is mainly due to the existence of wide sand dunes and because of the thick Mesozoic deposits (up to 4000 m) and particularly the thick Jurassic evaporites. This, generally, makes the interpretation of seismic data difficult. The partnership between SONATRACH and other companies in the last 15 years has very much enlarged Algeria's oil and gas industry. 38 exploration agreements have been signed with 22 foreign oil companies. 18 are now operating in Algeria on 28 distinct blocs. Exploration efforts of SONATRACH and its partners led to 30 discoveries in the last decade; 11 of which are oil fields and are concentrated mainly in the Berkine area (Berkine Basin). These discoveries are the results of new seismic acquisition and processing. For instance, about 57,000 km of 2D and 670 km of 3D seismic were realised.

In northern Algeria, exploration started in the Southeast Mesozoic basin (Saharan Atlas) in the late 1940s. Despite the discovery of Djebel Onk field in 1954, exploration remained very sparse and unsuccessful due to the geological complexity of the region. The Ras Toumb oil field was discovered only 20 years later. The new discovery of the Guerguit El Kihal oil field (1988) located in the marginal zone of the Saharan flexure renewed the interests of explorationists in this region. Nevertheless, this large

Mesozoic basin is still devoid of giant field discoveries probably as a consequence of the Alpine orogeny effect.

Although exploration started early (1950s) in western Algeria, only medium sized gas fields were discovered and are located mainly in the In Salah area (Ahnet basin). Western Algeria which is thought to be of gas potential, with very local exception such as the Sbaa basin, is still not well explored compared to eastern Algeria.

2. Geology of the Berkine Basin

2-1 Regional Geology and Basin Development

The Berkine Basin is classified as a cratonic sag basin in which a Palaeozoic sag basin is truncated by the Hercynian unconformity and overlain by a Mesozoic marginal sag basin (Clifford, 1987). As inferred from seismic interpretation, the basin shows the imprint of most of the tectonic movements documented in the Algerian Saharan Platform which is believed to have been a single cratonic entity from the Cambrian to Holocene (Burrolet, 1967). Although a significant neofracturing phase affected the structural development of the basin, the orientation of the principal structural elements is inherited from Precambrian and older trending structures (Burrolet, 1967; Boudjema, 1987, Petters, 1991). Depending on the nature of the prevailed stress regime, the reactivation of N-S Precambrian basement faults, particularly along the northern margin of the Hoggar shield, created horsts and grabens with folds in Palaeozoic and Mesozoic strata (Burrolet, 1967; Boudjema, 1987; Clifford, 1987).

Following the structural evolution of the Saharan Platform, the basin has undergone deformation under different stress regimes. A rifting phase, accompanied by spilitic lava flows, affected the basin during Cambro-Ordovician time and can be shown to be a sag feature over these earlier rift systems (Clitzch, 1970; Boudjema, 1987). This early Palaeozoic rifting phase was followed by a thermal sagging of the lithosphere which allowed deposition of up to 4000 m of interlayered marine and continental siliclastic, Cambrian to Carboniferous sediments. Frequent interruptions are mainly concentrated within the Illizi Platform as evidenced by reduced thickness of the sediments (Fig.6). Furthermore, the eastern and central Sahara was an area of slower

subsidence in contrast to the western Saharan synclines, containing mainly Palaeozoic sediments and subjected to rapid subsidence during that time (Fig.6).

During the Late Carboniferous time and according to a plate collision with Europe, the ancient faulted blocs were reactivated under a compressional stress regime and reverse faults developed. Broad Hercynian folding, superimposed on Early Palaeozoic structures (i.e. from Caledonian movements) led to the development of arches on which fields such as the Hassi-Messaoud and Hassi R´Mel oil and gas fields (Fig. 6) are now situated (Magliore, 1970; Balbucchi and Pommier, 1978).

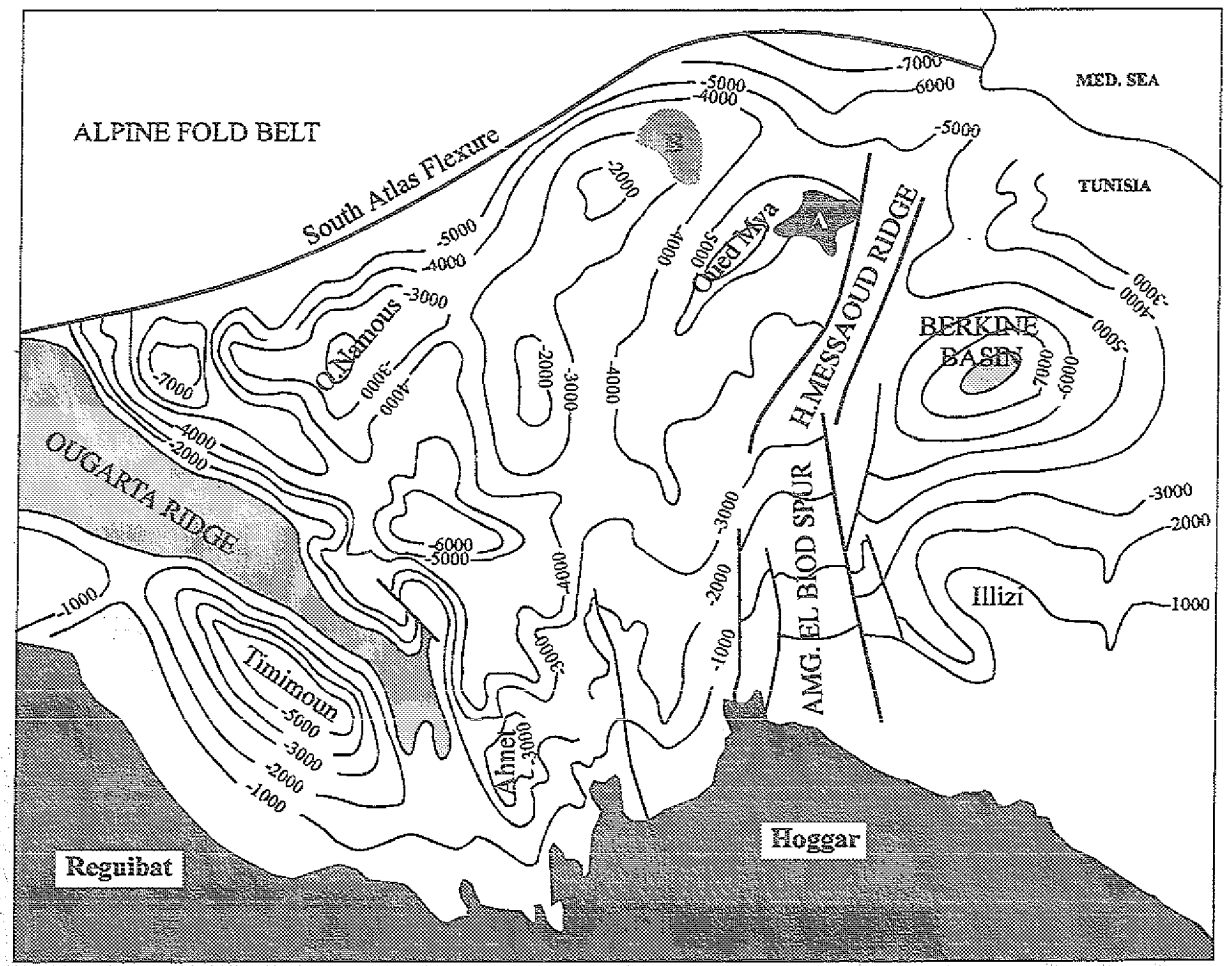


Fig. 6: Structure map of the Saharan Platform with depth of basement (after, Makhous, 1997, simplified). A and B refer to the Hassi Messaoud and Hassi R´Mel oil and gas fields, respectively.

It is, however, notable that the E-W Hercynian compressional event decreases in intensity along a roughly NW-SE direction and does not seem to extend significantly into Libya (Fig. 7). A prominent Hercynian feature projecting northwards from the

Hoggar cristalline basement is the Amguid El Biod spur and its northern extension the Hassi Messaoud-El Agreb ridge (Fig. 6) dividing the Mesozoic basin into 2 low lying areas: Oued Mya and Berkine Basins. This uplift consists of horst and grabens bounded by local, north-south trending faults with displacements of up to 1500 m. Block movements probably were controlled by Precambrian basement faults.

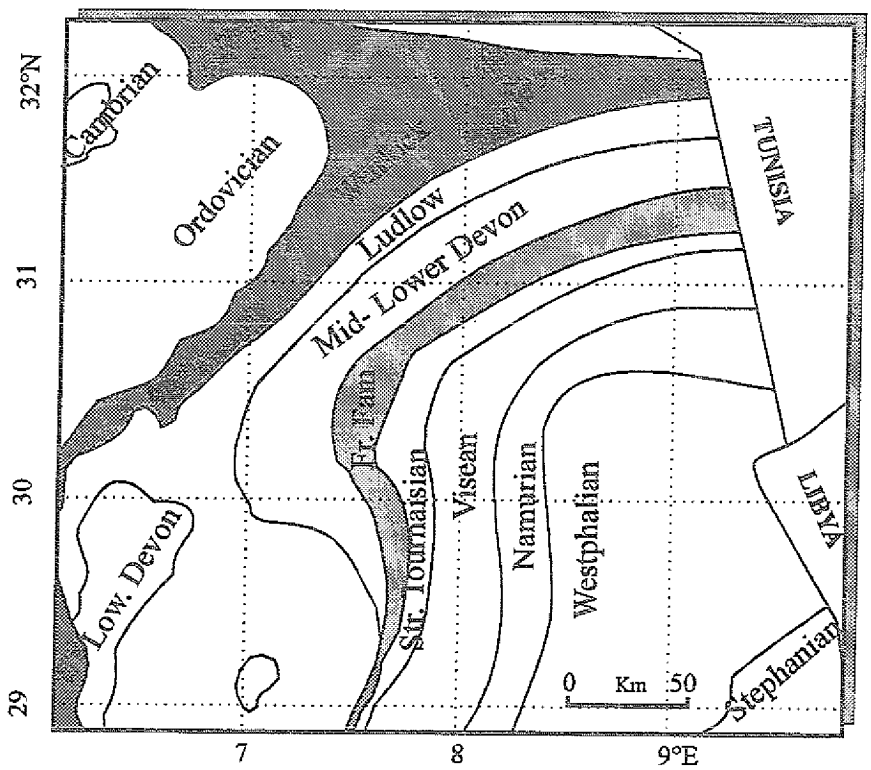


Fig. 7: Simplified Hercynian subcrop map of the Berkine Basin (after BEICIP-SONATRACH, 1991). The highlighted areas correspond to the Frasnian-Famennian (light grey) and Silurian (dark grey) shale formations, which are defined as the main source rocks in the basin.

After the Variscan orogeny, initiated during the Visean and strongly accentuated during the Stephanian time (Boudjema,1987), the Palaeozoic sediments were stripped-off during the Permian- Middle Triassic. The absence of the Permian sediments in the Algerian region and the age of the first Mesozoic sediments (Keuper; BEICIP/SONATRACH, 1979; Boudjema, 1987) suggests that this area remained uplifted. Marine transgression taking place during the Permian lead to the deposition of thick marine sediments in Tunisia and Libya to the East (Klitzch, 1971).

A new rifting phase accompanied by volcano-detritic and evaporitic sedimentation, took place during the Early Mesozoic time (Busson, 1967, Boudjema, 1987). This rift

system is linked to the opening of the central Atlantic. The consequent extension and normal faulting result in the formation of the Oued Mya half graben syncline (Boudjema, 1987). The initiation of the Mesozoic basin is difficult to constrain. Early Jurassic (Hettangian) is a reasonable choice since the deposition of more than 1500 m of thick salt deposits, at around 33°N, 7°E (Sahagian, 1993) indicates an abrupt increase in subsidence rate during a very short period (about 4 Ma). This Early Mesozoic rifting phase was at the origine of the formation of structural lows in which further sedimentation occurred.

An orogenic phase commonly called the Austrian phase, occurred during pre-Aptian time (Claret and Tempere, 1967; Boudjema,1987). This compressive phase has strongly accentuated the main Hercynian structures. Following this phase, the structures were stripped off, down to various levels of the Jurassic (Claret and Tempere, 1967).

Relative movements of Africa and Eurasia during the Eocene led to more regional scale inversions particularly in the Atlas area, in northern Algeria (Bishop, 1975; Mengoli and Spenci, 1985 Guiraud et al., 1987), with additional minor effects in the Berkine-Oued Mya basins (Boudjema, 1987).

The Alpine orogeny uplifted the instable parts of the African Plate and formed a multitude of folds and complex structures represented now by the Atlas fold belts in northern Algeria (Fig. 2, 6). These fold belts isolated interior sedimentary basins of north-western Algeria from the Mediterranean sea to the North. Thereafter, interior sag basins developed and filled with clastic sediment from the rising mountains.

2-2 Lithostratigraphy and Paleogeography

Between the uplifted zones of central Algeria, extensive Palaeozoic sequences fill great depressions, the largest of which are the Ahnet-Timimoun basin, the Oued Mya basin, the Berkine Basin and the Illizi Platform (Fig. 6). Sediment depocenters were mainly controlled by the Panafrican orogeny, accentuated later by Caledonian, Hercynian and more recent structures (Beuf et al., 1971; Boudjema, 1987; Petters, 1991). The oldest sediments of the Saharan Platform are encountered in the South and consist of metamorphic and igneous rocks of Precambrian age (Bishop, 1975). The

first sedimentation occurred after the regional peneplanation prevailed in North Africa, after the final assess of Precambrian orogeny (Beuf et al., 1971). The huge Berkine depression contains sediments from Cambrian to Neogene in age. Lower Palaeozoic strata are well exposed in the South with the Tassili n´Adjer among the largest Palaeozoic exposures (Deynoux, 1983). They form particularly a girdle around the Hoggar cristalline massif (Fig. 7). Otherwise the Palaeozoic strata are subcropping Mesozoic sediments at the Hercynian unconformity. A brief description of the main sequences making up the sedimentary fill of the Berkine Basin is given here. The description presented below is based on Beuf et al. (1971), Whiteman (1972), Balbucchi and Pommier (1970), Bishop (1975), Furon (1963), Busson (1967), Massa and Moreau-Benoit (1976), Massa and Vachard (1979), Benacef et al. (1971), Deynoux et al. (1985), Burrolet (1989), Klitzch (1990) and Beicip/Sonatrach (1991). The vertical distribution of sediments is shown in Figure 8.

2-2-1 The Palaeozoic Cycle

Cambrian to Carboniferous sediments build up the Palaeozoic sedimentary cycle of the Berkine Basin. It consists mainly of interlayered continental and marine clastic deposits with sandstones and shales being predominant.

Quartz-rich sandstones with tiggilites suggesting a marine influence began to accumulate in Cambrian time along northern Africa. The progressive marine transgression continued through the Ordovician time, segregated into 7 distinct units from base to top: El Gassi shales, El Atchane sandstone, Hamra quartzite, Ouargla sandstones, Azzel shales, Oued Saret sandstone and microconglomeratic shale units. Strong marine inundations are generally documented by shallow marine sedimentary rocks as evidenced by black micaceous shale deposits with graptolites, trilobites and the presence of brachiopodes. The strongest marine transgression occurred during the Middle and Late Ordovician (Llanvirnian and Ashgill-Caradocian). The Late Ordovician transgression is presumably due to the partial ablation of the glaciers then present in central Africa.

No substantial interruption in sedimentation between the Ordovician and the Silurian is observed. Repeated marine transgressions during the Early Silurian resulted in a

deposition of a thick black to dark grey graptolitic micaceous shale formation, one of the most important hydrocarbon source rocks in the Algerian Saharan Platform. During that time, the Berkine Basin was a major depocenter for the accumulations of argilites. This thick formation, which is the equivalent of the Tanezouft formation in Libya, is considered to be a result of the total melting of the Ordovician glaciers. The basal Silurian member passes upwards into the Ludlow F6 and known as the Accacus formation in Libya and southern Tunisia. This formation consists of interlayered marine and continental clastic sediments with marine rocks being more prevalent in the North.

The Devonian time is characterised by a fluctuation between open marine and transitional (deltaic) depositional conditions, episodically interrupted by continental influences (e.g. emergence, paleosoils). Alternating sequences of clays and sandstones reflect an extended cycle of transgressive-regressive deposition periods. Sediments of Early Devonian age overlie Silurian sediments with local unconformities. The variation of related thicknesses observed in the low lying areas (Central Berkine Basin) and the Caledonian structural highs (e.g. Ahara high, at the junction zone with the Illizi Platform) might indicate that the gradation from Silurian shales to Early Devonian (Gedinnian) sandstones is likely to be a result of epirogenic rather than orogenic movements. The Early Devonian sandstones grade up into interbedded sandstones and shales and finally to silty shales and shales, indicating a progressive marine inundation. The Middle Devonian section comprises carbonate and shale sequences indicating deep water and more stable tectonic conditions.

At some localities erosion has removed a part or all of the Middle Devonian units, but the Frasnian unconformity is not present everywhere. By the Late Devonian (Frasnian-Famennian), the basin was inundated and thick shaly calcareous and shaly to silty shaly formations were deposited. The whole sequence known as the Tin Meras formation in the eastern Saharan Platform constitutes the second hydrocarbon source of the basin.

Some of the topographic highs formed islands in the transgressive sea, leading to the development of reservoirs such as the Emsian F4, the Eifelian F3 and the Strunian F2 formations of the south-eastern part of the basin.

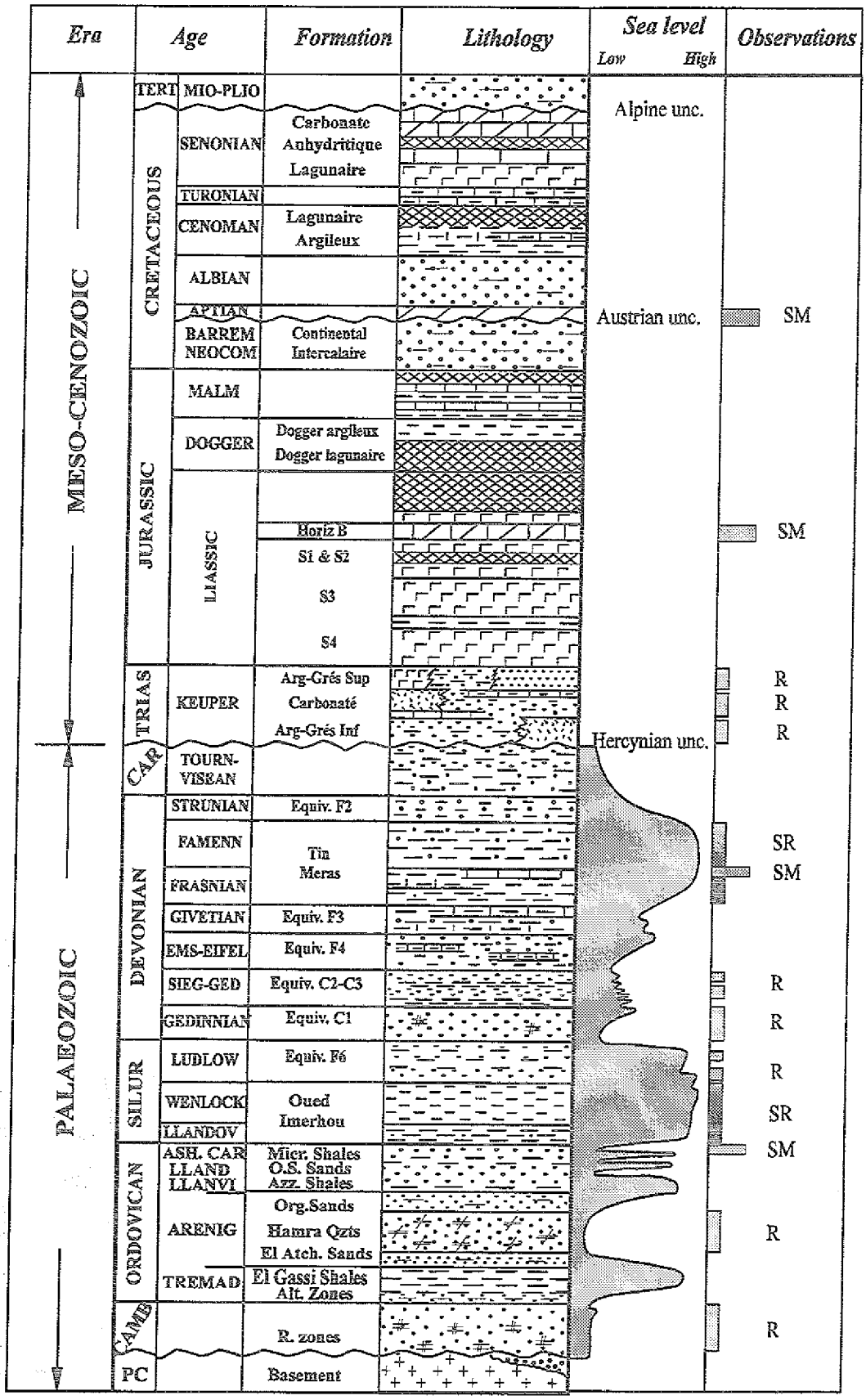


Fig. 8: Typical stratigraphic column of the Berkine Basin. R, SR and SM are reservoir, source rock and seismic marker, respectively.

Stable conditions terminated at the end of the Devonian and the early pulses of the Variscan orogeny seem to be of an epirogenic nature. The sea transgressed for the first time from the north-east and shallow marine sediments including shales, evaporites, limestones, marls and fine sandstones were deposited across the Berkine Basin and the Illizi Platform. The presence of ferugenous and hematitic levels suggest deltaic conditions. The general uplift resulting from the Hercynian orogeny at the Late Carboniferous led to a major withdrawal of the sea.

2-2-2 The Meso-Cenozoic Cycle

Restriction of the western Tethys basin and post-Hercynian and Triassic subsidence along the margin of the African landmass led to a new cycle of sediment deposition. Late Triassic fluvial and shallow marine sandstones commonly overlay the irregular Hercynian unconformity. The Early Jurassic (Liassic) is characterised by the deposition of thick confined shallow marine (lagoonal) sediments, consisting of massive beds of salt and anhydrite. The Late Triassic and Early Jurassic sediments which constitute one of the most important reservoir/seal plays are widespread in the Berkine Basin, as well as in parts of the northern flank of the Illizi Platform.

The Middle Jurassic and younger section are dominated by relatively thin lagoonal dolomites, evaporites and shales, although continental sands were important during certain periods.

Cretaceous sediments consist of alternating sandstones, evaporites, shales, limestones and dolomites. The Lower Cretaceous (Neocomian-Albian) consists mainly of continental siliclastic sediments. Continental conditions were episodically interrupted during the Aptian time during when a nearshore carbonate facies was deposited. The Late Cretaceous sediments grade-up from shales and evaporites to carbonates, as a result of a shallow marine embayment of the neo-Tethys which inundated large parts of the North African desert.

Thin Tertiary sedimentation occurred within the basin and are of Mio-Pliocene and Quaternary age. They overlie the partly eroded Senonian and consist of mostly continental sandstones. Tertiary sedimentation is particularly developed in Tunisia with thicknesses of up to 7000 m.

3. Petroleum Geology: An Overview

3-1 The Silurian and Upper Devonian Petroleum Systems

Parts of the Berkine Basin benefit from multiple hydrocarbon sources attributed to the Silurian graptolitic black shales (Oued Imerhou formation), omnipresent on the Saharan Platform, and the Middle-Upper Devonian shales (Tin Meras Formation). A good overview of the spatial distribution of these hydrocarbons source formations was given by Chaouche (1991). These hydrocarbon source systems seem to be related to a widespread global sea level rise which flooded a sag basin overlying the early Cambro-Ordovician rift phase, and consequently created a series of restricted depositional environments. The Silurian system started with thick graptolitic micaceous black shales member with a thickness of more than 500 m being drilled in the western edge of the basin. This member is, however, pinching out in the north-western and northern parts of the basin below the Hercynian unconformity (Figs. 1 and 7). This formation has been attributed a Llandoverian-Wenlockian age (Fabre, 1976; Legrand, 1981) and is likely to be homogenous all over the basin. Sequence stratigraphic study of BEICIP/SONATRACH (1991) suggests that the Silurian graptolitic black shale formation was deposited during the maximum of the Silurian transgression. As previously outlined by Furon (1963), this thick unit indicates transgression and a deeper, but still epicontinental sea. The organic matter in the Silurian source rock formation consists of phytoplancton and zooplancton associations such as chitinozoa, acritarchs, tasmanes and graptolites (Chaouche, 1991) as well as primitive spore associations (Richardson and Ioannides, 1973).

The Frasnian-Famennian formation, a second hydrocarbon source, is generally sandwiched between 2 major important reservoirs in the Illizi Platform (F2 and F6 of Fig. 8). The organic facies of the Frasnian-Famennian is composed of tasmanites and acritarchs at the base, whereas chitinozoa and some microspores characterise its top (Massa and Moreau-Benoit, 1976). The presence of faunal associations such as goniatites and brachiopodes clearly proves marine depositional conditions.

The entire Frasnian-Famennian formation ranges in thickness from a maximum of more than 900 m, encountered near the Tunisian boundary, to an erosional pinch-out in the western and northern parts of the basin (Figs. 1 and 7).

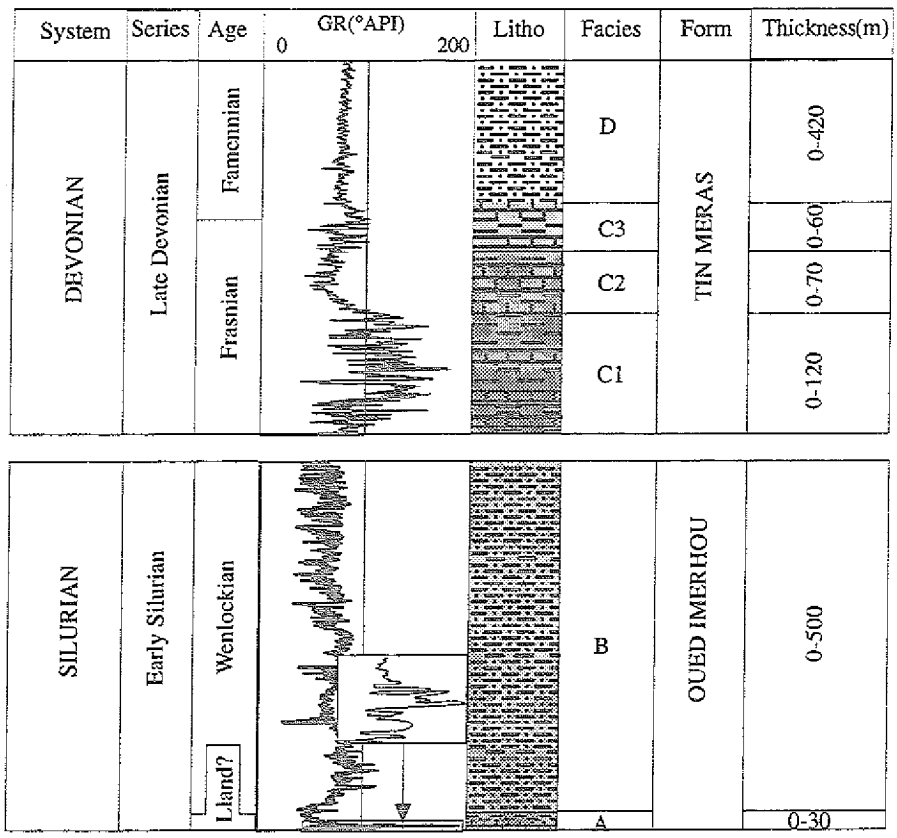


Fig. 9: Lithofacies distribution within the Early Silurian (bottom) and Late Devonian (top) as deduced from lithological and electrical log features. Lld, Llandoverian.

Due to some practical reasons, as well as small scale facies variations and electrical log features, the Silurian and the Frasnian-Famennian formations are discretized vertically into more than one distinct member (Fig. 9). The major emphasis is to distinguish potential dissimilarities with respect to organic matter quantity and quality between the different units and are therefore treated separately in the present study. At the type section, the Silurian is about 500 m thick and consists of a highly to medium laminated, black shaly to shaly calcareous Lower member (subfacies A on Fig. 9), and a dark grey to black micaceous shaly silty Upper member (subfacies B). The nearly 700 m thick marine Frasnian-Famennian sequence is, on the other hand, segregated into four members, which are respectively from base to top: 1) a black laminated shaly and shaly calcareous Lower member (C1), 2) a predominantly grey to dark grey shaly silty to limestone silty member (C2), 3) a dark grey to black micaceous shales

alternating with shaly calcareous strata (C3) and 4) a dark grey shaly to silty shaly strata (D). The subfacies A and C1 are, respectively, about 20-30 and 100 m thick, contain up to 30% CaCO3, and are highly radioactive. They are easily recognized on wireline logs, as they have usually very high gamma-ray readings (up to 200 °API). They correspond to an electrical log marker which is well identified within the basin.

3-2 Trap Types, Reservoirs and Sealing Strata

The Berkine Basin is characterised by a variety of trap types. Compressional and inversion structures are of Cretaceous age or younger and characterise the western part of the basin. Extensional fault block structures of Triassic-Liassic age are common in the central and, to a lesser extent, the north-western parts of the basin (e.g. Rhourd El Baguel, Bir Berkine and Berkine East). Pure stratigraphic traps are uncommon, but Cambro-Ordovician and Devonian pinch-out below volcanic rocks, acting as a seal, may also be possible.

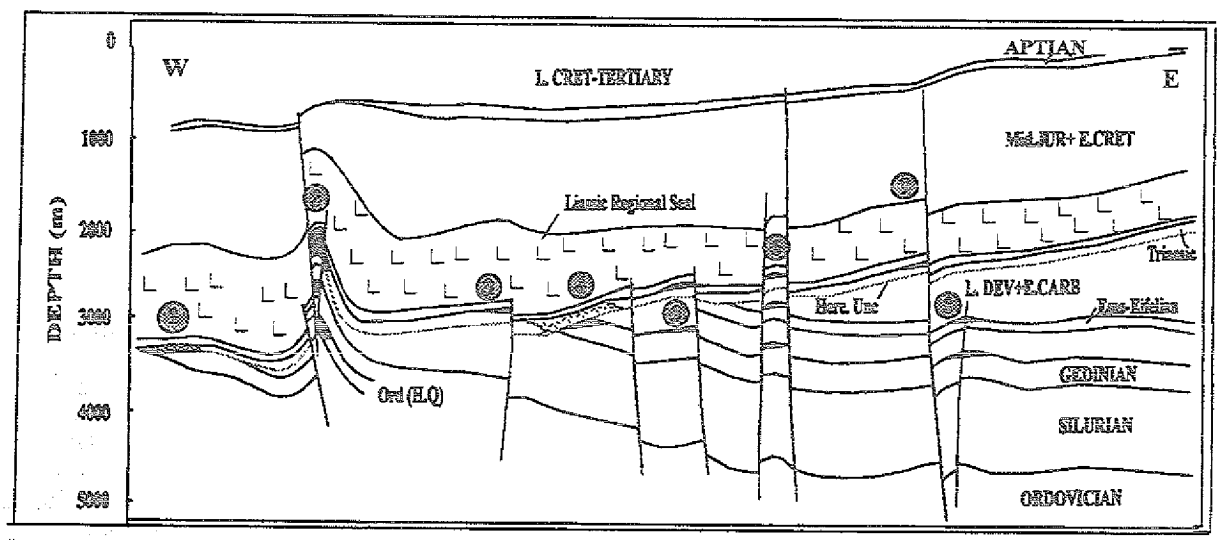


Fig. 10: East-West synthetic cross section showing the different reservoirs, the regional seal, and the distribution of the different trap types as inferred from seismic data (after, BECIP-SONATRACH, 1991). 1-Locally Cambro-Ordovician pinch-out below volcanic sediments, 2-Cretaceous and Tertiary compressional and inversion structures, 3- small sized compressional structure with a Triassic closure, 4- locally possible Devonian pinch-out, 5-Liassic fault bloc structure with Triassic and Devonian closures, 6-Liassic/Tertiary fault bloc structure, 7, 8- traps linked to a Tertiary reactivation of a pre-Mesozoic fault.

The main reservoirs in the basin are, in order of importance, the Triassic, Ordovician (Hamra quartzites), and the Lower Devonian (Gedinnian). However, since the discovery of oil and gas at Rhourd Khrouf, Menzel Ledjmat East, El Merk East and Berkine East, the Lower Carboniferous, considered up to date as a secondary objective, became also an important play particularly in the northern, north-western and western parts of the basin. The high efficiency of the Liassic salt and evaporites which act as a retensive seal (Boudjema, pers. com.) leads to the high degree of petroleum preservation in the basin. The Silurian and the Upper Devonian shales provide cap-rocks for the Palaeozoic reservoirs. The different reservoirs as well as the different trap types are summarized along a West-East cross section through the basin (Fig. 10).

3-3 Oil to Oil and Oil to Source Rock Correlations

The discrimination of petroleum systems in Eastern Algeria are still the matter of debate since the different studies carried out up to now have shown many controversies. Oil to oil and oil to source rock correlations were first carried out by Tissot et al. (1973). For this purpose, oils and rock extracts from the potential source rocks of the Illizi Platform were analyzed by gas chromatography and mass spectrometry. The author argued that the oils exhibit the same overall composition and that the saturated hydrocarbon fraction is fairly uniform. This fact was attributed to the very advanced maturation of the source rocks of the oils making, consequently, difficult to distinguish different oil types and their corresponding stratigraphic sources. The analyses of the aromatic hydrocarbons, especially the compounds of the steroid type, containing one or several aromatic rings, allowed, however, the differentiation between three oil groups, which were related to their respective source rocks. In this order, oils from Carboniferous, Upper Devonian and Lower Devonian reservoirs were correlated to Middle-Upper Devonian source rocks, whereas Ordovician oils were attributed to the Upper Silurian source rock.

On the other hand, Chaouche (1991), using different classification parameters showed in his study great similarities in the hydrocarbon genetic types making correlations very difficult. The oils could be classified according to their relative maturity.

However, the same overall composition was observed. The apparent homogeneity of the Algerian oils was related to the similarity of the organic facies from the period of Ordovician to Upper Devonian time.

Further geochemical investigations were made by Gontcharov (1992) using biological markers as a tool to establish a classification of the Algerian oils. His study allowed the differentiation between three oil families grouped with respect to the di/triterpanes ratio. The three groups defined are, respectively, the Hassi Messaoud and Rhourd Nouss oils, the Illizi oils and the northern Algeria oils.

As a part of its hydrocarbon evaluation in the Illizi and Berkine Basins by analysis of many Palaeozoic oil samples, BHP Petroleum proposed three oil groups. The classification was based on the relative abundance of tricyclic and pentacyclic terpanes. In this order, the first group was associated to the Hassi Messaoud area and nearby regions, and was characterised by their higher concentrations in tricyclic terpanes. The oils were attributed to an unproven Devonian or Silurian source rock located further to the North. The Illizi oils, characterised according to their high concentration in pentacyclic terpanes, constitute the second group, attributed to the Silurian source rock. The third group located geographically between the two first groups in the Tin Fouyé-Tabankort area (Illizi Platform) showed approximately equal proportions of tri- and pentacyclics. For this latest group a contribution from both source rocks (i.e. Silurian and Upper Devonian) was proposed.

More recently Illich et al. (1997, oral presentation) studied oil and sediments from the Berkine Basin and the Illizi Platform. According to their study based on biomarkers, isotope and other geochemical attributes, oils possessing a high degree of similarity were identified and grouped into four families. In this manner, one group of oils was associated with Silurian shales, mainly occurring in the northern part of the basin. Another more widespread family was associated with sediments of Frasnian age. They also suggested that oil mixtures from both the Silurian and Frasnian occur in the north-western part of the basin.

3-3 Some Remarks on Pressure Development in the Berkine Basin

Formation pore pressures are of great importance for petroleum geologists at various stages such as drilling production, reservoir engineering and geological modelling. It

is generally accepted that the principal stresses which can increase fluid pressures in sedimentary basins are: 1) compassion desequilibrium as a result of rapid sediment loading, 2) aquathermal pressuring, 3) compression by tectonic forces and 4) hydrocarbon generation (e.g. Chapman, 1994). Lateral permeability barriers such as large faults and facies changes interrupt generally the continuity of reservoirs and create obstacles to pressure dissipation (Chiarelli and Duffaud, 1980) and hence, fluid migration.

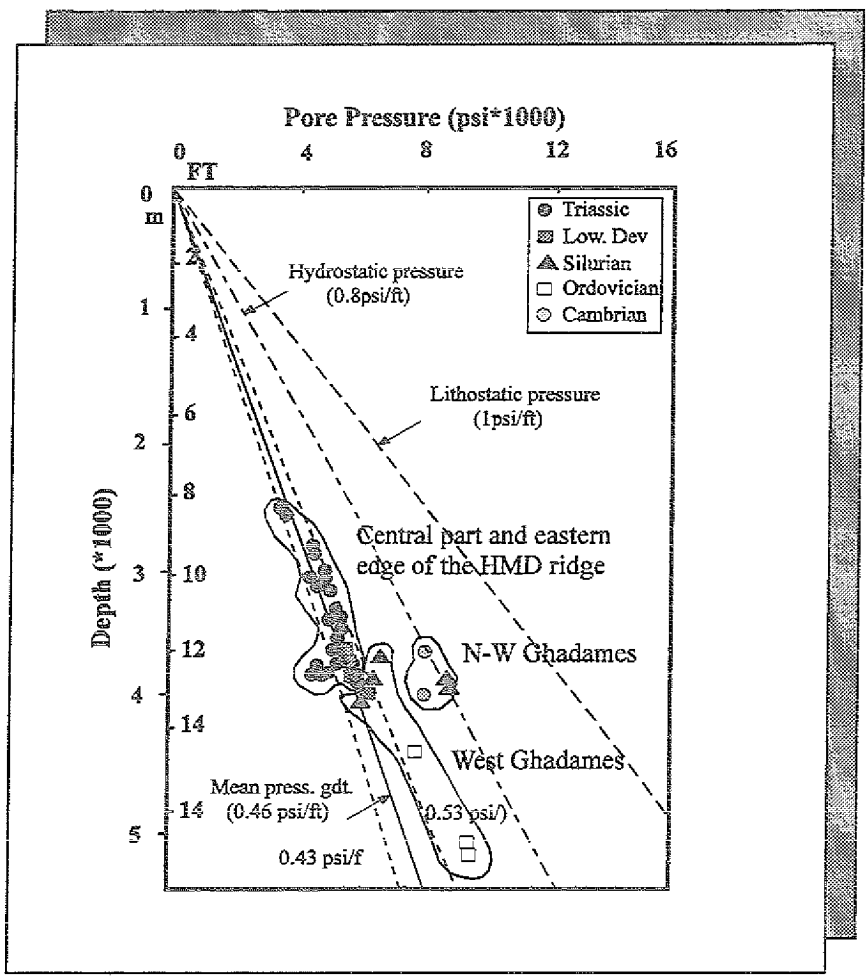


Fig. 11: Pore pressure versus depth for selected wells of the Berkine Basin. 0.8 and 1.0 psi/ft are fracture and lithostatic pressure, respectively.

In order to give an overview on the distribution of pressures and their possible geological significance, pressure data from 14 wells from the study area and adjacent parts were evaluated here. This is particularly important in basin modelling for the simulation of the mechanical processes involved during compaction.

Figure 11 shows a plot of formation pressure (in psi) versus aquifer depth for the main reservoirs in the study area. The figure reveals that the Triassic and Early Devonian

(Gedinnian) reservoirs are hydrostatically pressured with a mean pressure gradient of 0.46 psi/ft (it is considered for the present evaluation that reservoirs with pressure gradient greater than 0.53 psi/ft are overpressured; Hunt, 1996). The lowest pressure data are generally recorded in the region situated to the East of the Amguid El Biod-Hassi Messaoud ridge. For the other reservoirs (Silurian F6, Ordovician and Cambrian), pressure data from the western part (Silurian and Ordovician) and north-western part (Silurian and Cambrian) show moderately pressured Silurian and Ordovician reservoirs in the West and highly overpressured Silurian and Cambrian reservoirs in the Northwest.

From these observations three different pressure systems can be defined:

1- An open system which consists of hydropressured reservoirs communicating with the regional aquifer system (i.e. Triassic and Lower Devonian).

2- A restricted system which consists of moderately geopressured reservoirs. Excess pressure can be the result of an incomplete dissipation towards the platform (i.e. the open system).

3- A closed system which characterises particularly the north-western part of the basin. This domain is considered to be isolated from the open system.

These observations fairly correlate with the conclusions of Chiarelli (1978). Indeed, the author has showed, on the basis of stratigraphic, hydrochemical (water salinity and chemical content) and hydrodynamic criteria, that the pressure gradient in the north-eastern Sahara basins increases in a roughly SE-NW direction from the Illizi Platform towards the Oued Mya basin. However, from the observations of the author, the Triassic sandstones in the Berkine Basin were also defined as being a part of the high pressure regime. The related overpressures have been interpreted as being the results of: 1) the Triassic sandstones pinch out below the thick Liassic salt bearing strata, cutting off direct communication with the low pressure domain of the Illizi Platform, 2) the south Atlas fault, which makes the northern boundary of the Oued Mya basin to the North, act as a permeability barrier for the dissipation of excess pressures.

As well illustrated in Figure 11, the available pressure data do not support such hypothesis, at least in the central Berkine Basin. Geological considerations such as, for example, pinch out at a major unconformity (i.e. Hercynian) leading to a direct communication of some Palaeozoic reservoirs with the Triassic reservoir, as well as the vertical communication of fluids along major faults might be an explanation of the relative low pressure regime in the Triassic sandstones. Such aspects are discussed in Chapter VI with respect to basin modelling.

4. Samples and Geochemical Methods

This chapter deals with the methods used to asses the quality, the quantity and the maturity of organic matter in the sediments. It includes screening, petrographic and detailed analyses. Screening analyses comprise the measurements of the total organic carbon (TOC or C_{org}) and sulfur content, and the Rock-Eval pyrolysis. Detailed analyses, on the other hand, include molecular geochemical investigations such as capillary gas chromatography of saturates, capillary gas chromatography of aromatics and capillary gas chromatography/mass spectrometry of saturates. Petrographic analyses deal mainly with the maceral identification and vitrinite reflectance measurements.

The methods applied in this study are described in detail in the following.

4-1 Samples and Sample Documentation

The selection of high quality samples for geochemical analyses is a fundamental requirement. Bad quality and sparse samples very often lead to meaningless data. The sample set of this study consists of whole rock core and drill cutting samples belonging mainly to the Silurian and the Upper Devonian (Frasnian-Famennian) shale sequences. Seven wells were selected for sampling, providing a total of about 100 samples. Geochemical investigations on both rock units were performed to determine not only their present organic carbon content, but also the rock attributes such as lithology, depositional environment, kerogen type, the extent to which these rocks were depleted of hydrocarbons as a result of thermal processes, and their possible biological markers. The sample set was completed with four crude oils and two gas-condensates from Triassic reservoirs. The location of the sampled wells and fields is shown in Figure 1.

Additionally, SONATRACH provided unpublished screening and petrographic (vitrinite reflectance) data from other wells in the study area. These data were used in order to obtain a regional overview of the kerogen quality and maturity of the source rocks.

4-2 Screening Analysis

4-2-1 Total Organic Carbon and Sulfur content

Total organic carbon (TOC or C_{org}) analyses were performed on unextracted, dried and crushed sediments. Sulfur, total carbon (TC) and total organic carbon (C_{org}) were determined quantitatively by combustion using a CS 225 Leco instrument. For this purpose, a known weight of sediment (100-120 mg) is heated to 1700°C in a continuous stream of pure oxygen. The carbon dioxide (CO_2), carbon monoxide (CO, trace amounts) and other constituents (i.e., water and sulfur gases) produce a flow through a „gas train" which converts the carbon monoxide to carbon dioxide and removes the other constituents. Resultant pure carbon dioxide and sulfur dioxide flow to the calibrated detector which provides a digital and hardcopy read-out of the content of total organic carbon and sulfur in the sediment (both in percent). To determine organic carbon (C_{org}) rather than (TC), this procedure is performed after removal of its inorganic carbon content (i.e., carbonate carbon) with hydrochloric acid (HCl) and hydrofluoric acid (HF) treatment. The carbonate carbon content of the samples is calculated by difference according to the formula: $CaCO_3 = 8.33\ (TC\text{-}C_{org})$.

4-2-2 Rock- Eval Pyrolysis

For Rock-Eval pyrolysis, a Delsi Rock-Eval II pyrolysis instrument was used for the determination of free hydrocarbons, residual (genetic) potential, maximum pyrolytic temperature (T_{max}), and hydrogen and oxygen indices. The sediment is weighted into small stainless crucibles (up to 48), loaded into a sample rack which automatically positions each crucible so that it can be lifted onto the piston. The technique involves then a stream of helium passing through 100 to 120 mg of crushed rock, heated very rapidly to a temperature of 300 °C which is held for 3 minutes. The temperature of the

oven is then programmed to increase at about 25 °C/min, up to 550 °C. The first stage volatilizes any bitumen present, while during the second stage kerogen decomposes to form hydrocarbons and carbon dioxide. Hydrocarbons from both steps are swept into a hydrocarbon sensitive flame ionization detector (FID) and two peaks (S_1 and S_2 in mg HC/g of rock) are collected. The S_1 peak represents hydrocarbons released at 300 °C believed to be that fraction of the original genetic potential which has already been transformed into hydrocarbons. Between 300 and 550 °C, hydrocarbons (S_2) are generated by thermal cracking of the kerogen until only non-generating carbon (i.e., the refractory fraction) remains. In addition, any free high-molecular-weight bitumen, namely asphaltenes, that were not mobilized into S_1 is cracked and added to the S_2 peak. Most carboxyl groups in the kerogen decarboxylate between 300 and 390 °C, yielding CO_2 (S_3 in mg CO_2/g of rock) which is trapped and analysed later during a short cooling period, using a thermal conductivity detector (TCD). The temperature of the maximum S_2 yield is known as T_{max} and can be used as a maturity parameter. During natural generation, weak kerogen bonds are broken first, leaving only stronger bonds and yielding hence higher temperatures (T_{max}) of the pyrolysis curves.

Additional indirect Rock-Eval parameters are the HI (S_2*100/C_{org}) in mg HC/g C_{org} , the OI (S_3*100/ C_{org}) in mg CO_2/g C_{org} and the production index (PI). This later is calculated by using the formula S_2/ S_1+ S_2. HI and OI are strongly correlated to the atomic H/C and O/C of the Van Krevelen diagram and are therefore interpreted in a similar manner (Espitalié et al., 1977). Rock-Eval data interpretation guidelines are provided e.g. by Espitalié et al. (1985, 1986), Katz (1983) and Peters (1986).

4-3 Petrographic analyses

For microscopical analyses, 30 whole rock samples representing four key wells situated along the transect used for 2D simulation in this study were selected (Fig.1).The procedure involves, first, the preparation of a resin block containing dry slabs of the rock samples. One side of the resultant block was then polished using different abrasive sizes and finally by using a 0.05 µm alumina powder dispersed in water. Vitrinite reflectance measurements (R_o) were performed on the polished samples in oil immersion and at a wavelength of 546 nm. The equipment used for this

is a Zeiss photomicroscope III equipped with a 8 μm diameter measuring blind. For the necessary calibration a glass standard was used. The data were processed by HP 9816S hardware combined with Zeiss Coflex software. Identification of macerals was performed both in reflected white light and in a fluorescence mode induced by violet and ultraviolet light. Selected samples were photographed. It should be noted that in order to get maximum information about the maturity stage of the organic matter in each sample, the process of measuring vitrinite reflectance was repeated as often as possible. The number of the measured particles depends on the organic richness of each sample. For instance, a small number of measured particles in dispersed organic matter will significantly increase the uncertainty. The results are expressed in percent of reflected light (relative to the incident light) and represented in a distribution where the mean value for each sample is quoted. More information on the petrographic analysis of organic matter is found in Taylor et al. (1998).

4- 4 Molecular Geochemical Analyses

Molecular geochemical analyses on oils and rock extracts in combination with the geological background provide more information about lithology and depositional environment, organic facies and maturity (Peters and Moldowan, 1991; Peters and Moldowan, 1993, Radke, 1988). Accordingly, such analyses form the basis for correlating source rocks with petroleum.

4- 4- 1 Solvent Extraction and Sample Preparation

Significant information on organic input, depositional environment and maturity can be obtained from the free liquid or bitumen which is referred to as the extractable organic matter (EOM) contained in source rocks. For such analyses, 24 powdered samples are extracted at ambient temperature with a mixture of dichloromethane and methanol (99:1 v/v), using a high speed homogenizer (flow blending technique; Radke et al., 1978). To this end, a preweighted crushed sediment is placed with the solvent into a cylindrical flask in which a high speed mechanical blender is inserted in order to severely agitate the sample for about five minutes. After extraction, the EOM containing solvent is separated from the sediment using a standard Buchner filtration flask and a funnel. The solvent is removed first at room temperature and then by using

a rotary evaporator. The EOM is weighted and reported as either a percentage or in parts per million (ppm) of the weight of the dry sediment used for the extraction procedure.

From the oil samples, volatiles were removed at ambient temperature and the residue was dissolved in benzene. Precipitation of asphaltenes was carried out using n-hexane which were collected on a preweighed filter.

4- 4- 2 Liquid Chromatography

The extracts and the remaining oil filtrate were separated by medium pressure liquid chromatography (MPLC; Radke et al., 1980) into saturated hydrocarbons, aromatic hydrocarbons and NSO compounds (resins and asphaltenes). Silica gel and n-hexane were used during the separation procedure of the three groups as a stationary and mobile phase, respectively. The aromatic compounds were further separated into carbon ring classes by using high performance liquid chromatography (HPLC, Radke, 1981). Such a procedure was necessary because of the high amounts of the mono-aromatic compounds which occluded the naphthalene and phenanthrene peaks.

4- 4- 3 Capillary Gas Chromatography

Capillary gas chromatography (commonly abreviated GC) is a very widely used method in analytical chemistry in general, and in petroleum geochemistry in particular. Following liquid chromatography, both the saturate and the aromatic hydrocarbon fractions are each separated further by gas chromatography.

GC analyses of the saturated hydrocarbons were carried out on a Hewlett Packard 5890 series II instrument equipped with an „Ultra1" fused silica capillary column (50 m * 0.20 mm internal diameter), coated with phenyl (5%)-vinyl (1%)- methyl (94%)-polysiloxane of 0.33µm film thickness. Helium was used as a carrier gas. The temperature of the GC oven was programmed to rise linearly from 120 to 310°C at 3°C/min. Selected n-alkanes and iso-alkanes (isoprenoids) were quantified by 5α–androstane, applied prior to extraction, as internal standard.

The analyses of aromatic hydrocarbon fractions were carried out on the same GC type instrument used for the saturated fraction (i.e., HP 5890 series II). A fused silica capillary column of 50m length, 0.20 mm internal diameter and coated with cross-

linked methyl (95%) -phenyl (5%)- polysiloxane of 0.33 µm film thickness was used with helium as a carrier gas. The temperature of the GC oven was programmed to rise linearly from 90°C (hold 4 min) to 120°C at 50°C/min and from 120 to 310°C at 3°C/min. Selected naphthalenes and phenanthrenes, and various alkyl substituted compounds, such as methyl- and ethylnaphthalene, di-and trimethylnaphthalenes, and methyl- and dimethylphenanthrenes, were quantified by adding 1-phenylhexane, 1-phenylheptane, 1,8-dimethylnaphthalene, 1-phenylnaphthalene, 1-ethylpyrene, and 1-butylpyrene before extraction as internal standards. The compounds are identified by multiple ion detection (MID) using a GC/MS system (see below). A review of aromatic compound analyses is provided by Radke (1986).

4-4-4 Gas Chromatography/Mass Spectrometry (GC/MS)

GC/MS is a technique which enables to identify complex compounds existing in very low concentrations. Most of the compounds identified by this method are referred to as biomarkers or biological markers because their structural skeleton was derived from molecules produced by living organisms (Tissot and Welte, 1984).

The instrumentation used for GC/MS analyses is a Hewlett Packard 5890 series II gas chromatograph coupled with a VG 7070E mass spectrometer exchange for a flame ionisation detector (FID). The GC instrument was equipped with a temperature programmed injector system (KAS-3, Gerstel GmbH) and a multiple ion detector (MID). A fused silica capillary column (50 m, 0.22 internal diameter, 0.25 µm film thickness) was used with helium as carrier gas. The temperature of the GC oven was programmed to rise from 110 to 340°C (hold 77 min) at 3°C/min and at a constant temperature of 340°C (hold 13 min). The injector temperature was programmed to rise from 120 to 300°C at 3°C/min. More information on biomarkers and biomarker analyses is published, e.g., by Peters and Moldowan, 1993.

5. Results of Geochemical Analyses

5-1 Characterisation of the Solid Organic Matter

The characterisation of the solid organic matter (i.e., abundance and quality) of the main source rock intervals (Silurian and Frasnian-Famennian sequences) was assessed

by using screening analyses (Chapter. 4.2) as well as by petrographic analyses (Chapter 4.3) performed in the present study. The screening analyses obtained in this study are enclosed in Table 1. Additionally, unpublished available C_{org} and Rock-Eval data from Sonatrach oil company are used here in order to give a regional source rock quality overview. Such data are, for confidential reasons, presented graphically and are not listed here.

The data are discussed for each individual unit (described in Chapter 3.1) and extended, for some parameters, for individual wells in order to provide both a temporal and a spatial overview.

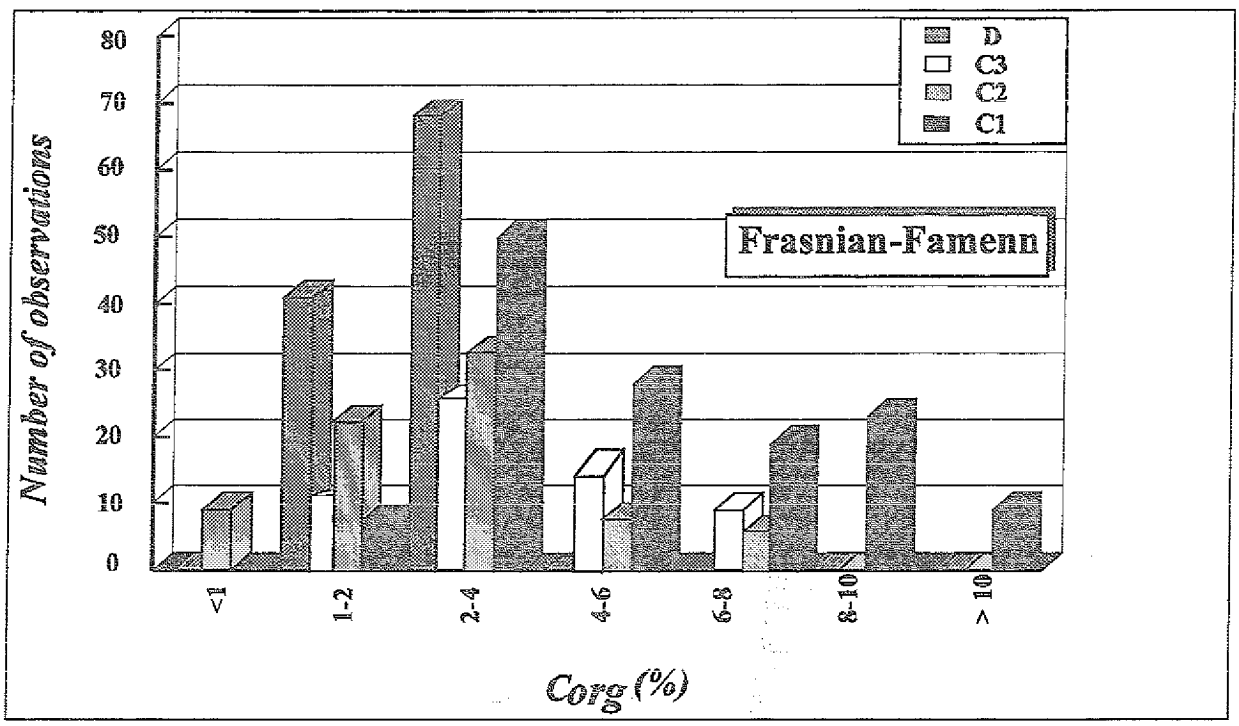


Fig. 12: Histogram of total organic carbon (wt% C_{org}) of the Frasnian-Famennian formation samples (includes data from SONATRACH). C1, C2, C3 and D refer to those members described in Chapter 3.1 and Figure 9.

5-1-1 Organic Matter Abundance and Sulfur Content

Total organic carbon contents are always expressed as weight % TOC or $C_{org.}$ The measurement of TOC is the most fundamental way of expressing the organic richness of a single sedimentary section. If sediments contain less than some minimum amount of organic carbon, there is no likelihood that they have been or could be responsible for the generation and expulsion of petroleum (Tissot and Welte, 1984). However, if a sediment contains more organic carbon, this fact alone does not make it necessarily a

source rock because of much the material can be inert. Therefore, the organic matter must meet other minimum criteria of quality (i.e., type and maturity) in order to generate hydrocarbons in amounts sufficient to form commercial oil and gas accumulations (Dow, 1978). The results derived from the C_{org} measurements (enclosed Table 1) confirm the high organic richness of the Frasnian-Famennian and Silurian formations.

Figures 12 and 13 display the distribution of organic carbon as histograms for both source rock units, and for the main subfacies described in Chapter 3.1. The entire C_{org} data set varies from slightly less than 1% to more than 10%. The Frasnian-Famennian interval exhibit a relatively narrow distribution envelope with average C_{org} values between 2 and 4%. For instance, the highest C_{org} values, as expected, are observed within the radioactive Frasnian zone (subfacies C1 in Fig. 9), i.e. the interval with high gamma ray response.

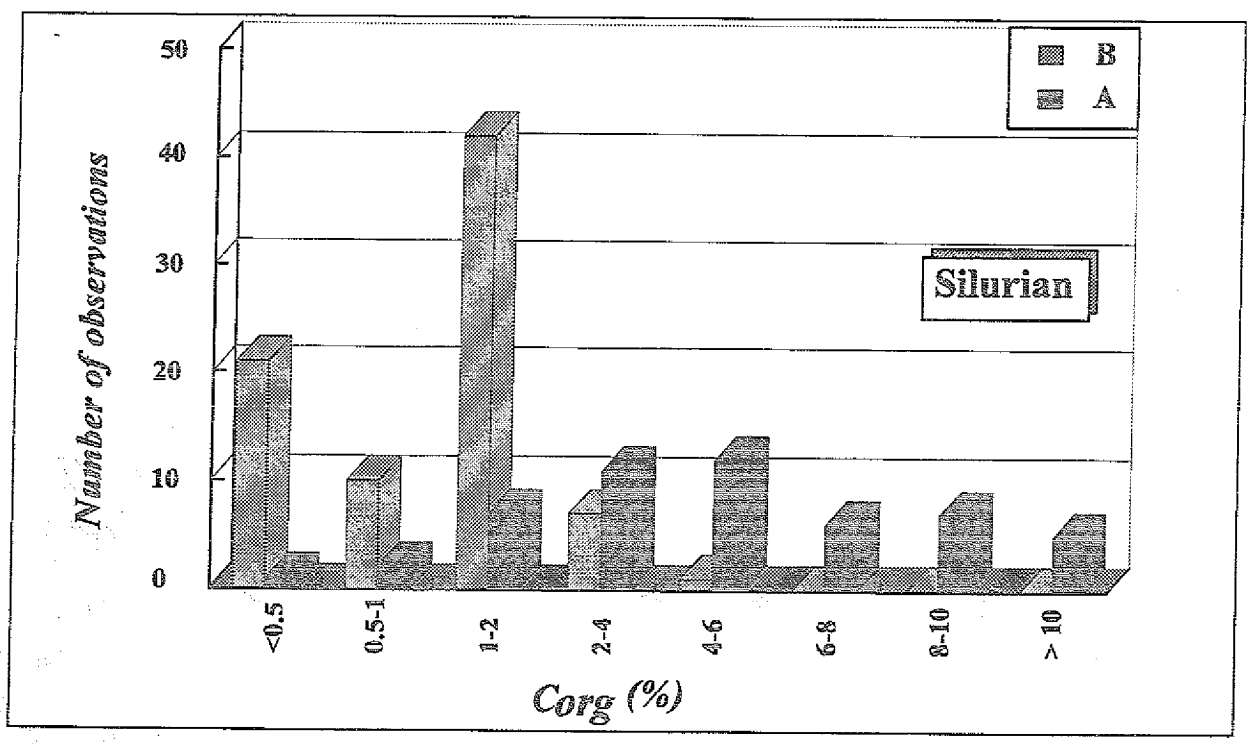


Fig. 13: Histogram of total organic carbon (wt% C_{org}) of the Silurian formation samples (includes data from SONATRACH). A and B refer to those members described in Chapter 3.1 and Figure 9.

The Silurian shale formation exhibits in general two mean distribution modes. High frequencies in the range of 1-2 % are found within the thick upper Silurian member

(subfacies B, Fig. 9), whereas C_{org} values of the radioactive Silurian zone (subfacies A) are in the range of 2-6 wt% C_{org}.

In summary, the majority of the samples reveal an above average level of organic carbon content (C_{org} > 1%, Bissada, 1982). Such a high level of organic richness is considered one of the necessary prerequisites for a rock to be considered as a possible hydrocarbon source rock (Tissot and Welte, 1984).

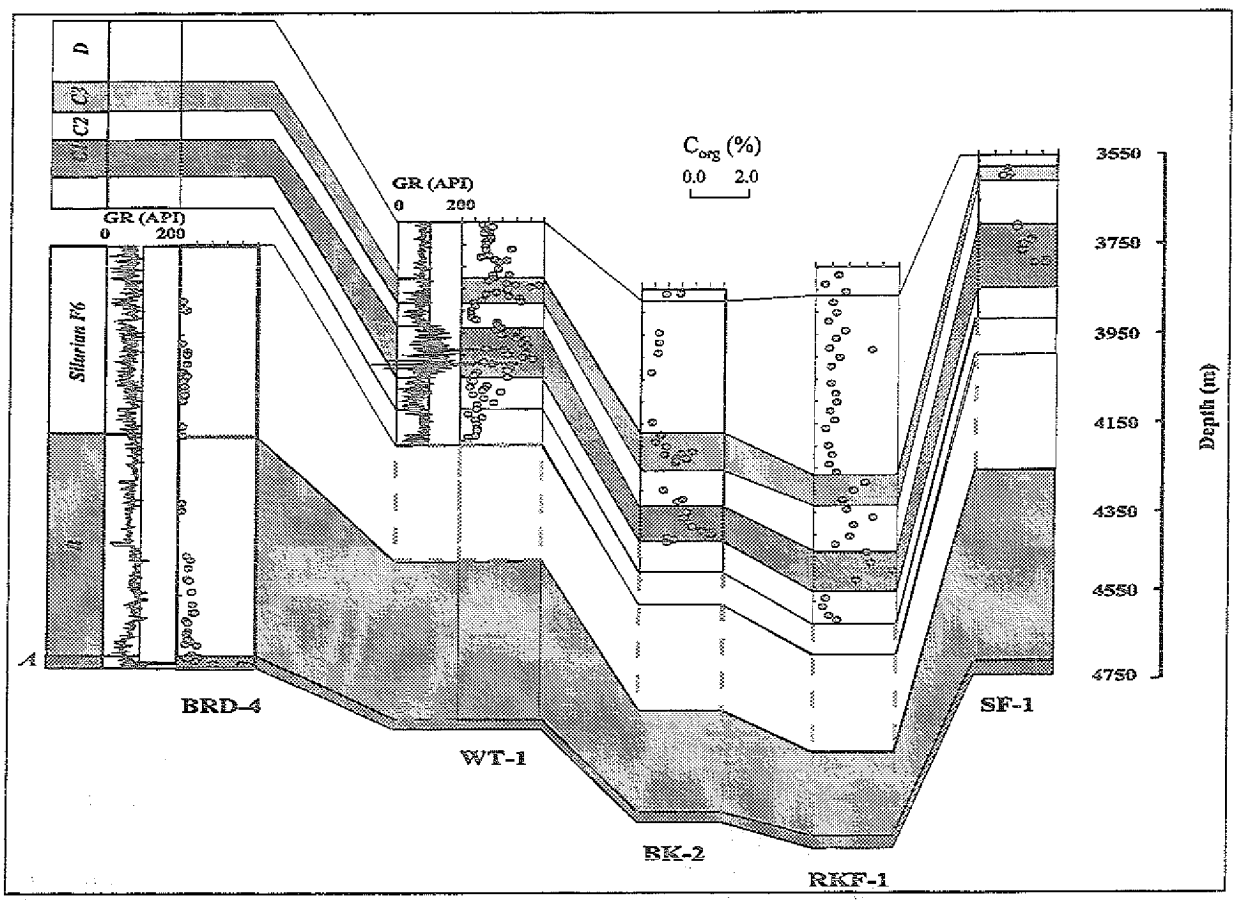


Fig. 14: Vertical and lateral organic carbon distribution along a West-East transect through the basin. A, B, C1, C2, C3 and D refer to those members described in Chapter 3.1 and Figure 9

The observed variations in organic richness from one unit to another are probably the results of the different degre of preservation of organic matter under specific local conditions. Indeed, the original concentration of organic matter depends primarily on: (1) the rate of productivity in the water column and the amount of organic matter washed in from land sources, (2) dilution effects by mineral matter, and (3) dissolved oxygen content of the water which depends on water depth and circulation (Tissot and Welte, 1984; Waples,1985; Littke et al., 1997).

Figure 14 shows the vertical and lateral organic carbon distribution along an East-West transect through the basin. The figure reveals the existence of vertical organic carbon recurrent patterns throughout a single marine sequence. This is particularly valid for the Frasnian-Famennian sequence which seems to be related to wide sea level variations during the initial phase of deposition. The highest C_{org} values belong to the basal Frasnian radioactive member (subfacies C1), as previously shown, and to the transition zone between the Frasnian and the Famennian (subfacies C3). The richness in organic carbon of members C2 and D are markedly lower. The former is generally characterised by rather low C_{org} values of less than 1%, whereas a general decrease of the organic content characterise the latter upwards.

For the Silurian of which much less data are available because the sequence was drilled less frequently, the basal radioactive member (subfacies A) shows the highest values (up to 9% in the western part of the basin). For instance, these „hot shales" showed values of up to 17% in the north-eastern part of the basin (Malla et al., 1997) C_{org} values are decreasing upwards throughout the subfacies B reaching minimum values of less than 0.5% at the top of this formation.

The C_{org} "highs" could have resulted either from high biological productivity within the water column or from the enhanced preservation of organic matter in the basin, or from both processes, and probably correlate to the maximum flooding surface.

Preservation of organic matter may have been enhanced under oxygen-deficient conditions (dissolved oxygen in water < 0.2 ml/l) during the initial phase of deposition, resulting from restricted water circulation and density stratification (Kepferle, 1983). The organic-rich laminae-nature observed in the Silurian and Frasnian-Famennian formations, particularly in the A, C1 and C3 members indicate a lack of bioturbation and provide lithological evidence for oxygen-depleted depositional conditions. The relatively organic-lean C2 subfacies which is sandwiched between two organic-rich members (i.e. C1 and C3 members) could indicate that the organic matter was predominantly decomposed in oxygenated water and, therefore, enhanced the efficiency of near-surface microbial degradation, resulting in low C_{org} values. However, one can observe that the mean organic carbon content increases with

increasing thickness, implying that rapid sedimentation allowed more organic matter to become buried before it could be oxidized (Ibach, 1982).

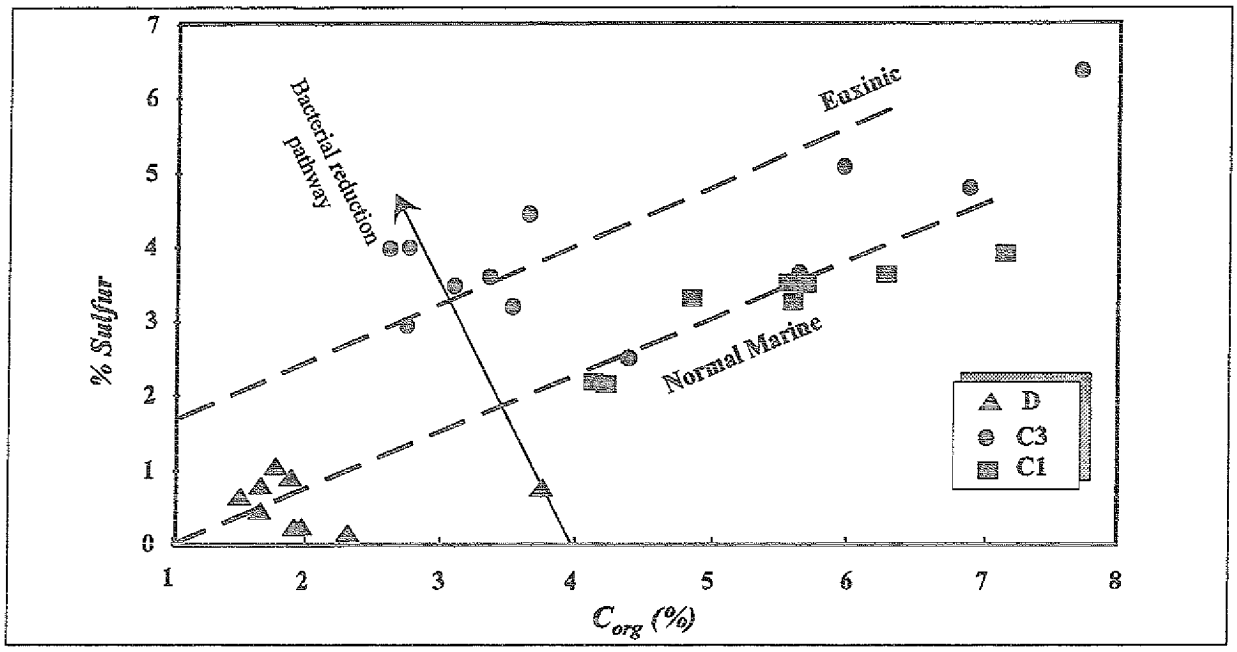


Fig. 15: Comparison of organic richness and sulfur content for samples from the Frasnian-Famennian formation. C1, C3 and D refer to those members described in Chapter 3.1 and Figure 9. Bacterial reduction pathway from Littke et al. (1991, 1997 a,b).

The decrease in upwards direction of the C_{org} content throughout the thick subfacies B and D suggests deposition under regressive conditions. Silty siliceous sediments, in generally fine-grained, become more predominant upwards, and could have diluted the organic matter. Indeed, Ibach (1982) has demonstrated that above a critical sedimentation rate, C_{org} typically decreases with increasing sedimentation rate owing to clastic dilution of the organic input. The author suggested, however, that near-surface microbial reworking is less efficient at higher burial rates.

It should be pointed out that such observations are not new; Cox and Gallois (1981) and Creany and Passey (1993) described a similar cyclicity of organic carbon in marine organic- rich shales by using well log, core and cuttings analyses. For instance, Creany and Passey, 1993, suggested that marine organic-rich shales can occur in all system tracts, depending on basinal position, and that the peak C_{org} values probably correlate with the maximum flooding surface, leading to the deposition of more marine organic matter with, therefore, increasing oil prone characters.

Total sulfur content for both formations range, respectively, from 0.1 to 6.3 % and from 0.9 to 12% (Figs. 15 and 16) . This fact suggests that bottom waters varied from normal marine to euxinic marine conditions at the time of deposition (Leventhal, 1983; Berner and Raiswell, 1983). High S/C_{org} ratios characterise in general the B and C3 members, indicating more bacterial sulfate reduction, both at and below the sediment-water interface (Kaplan, 1980). As a consequence, more organic matter is consumed by sulfate reduction than in the case where normal marine conditions prevailed (A, C1 and D members; Littke et al., 1997b).

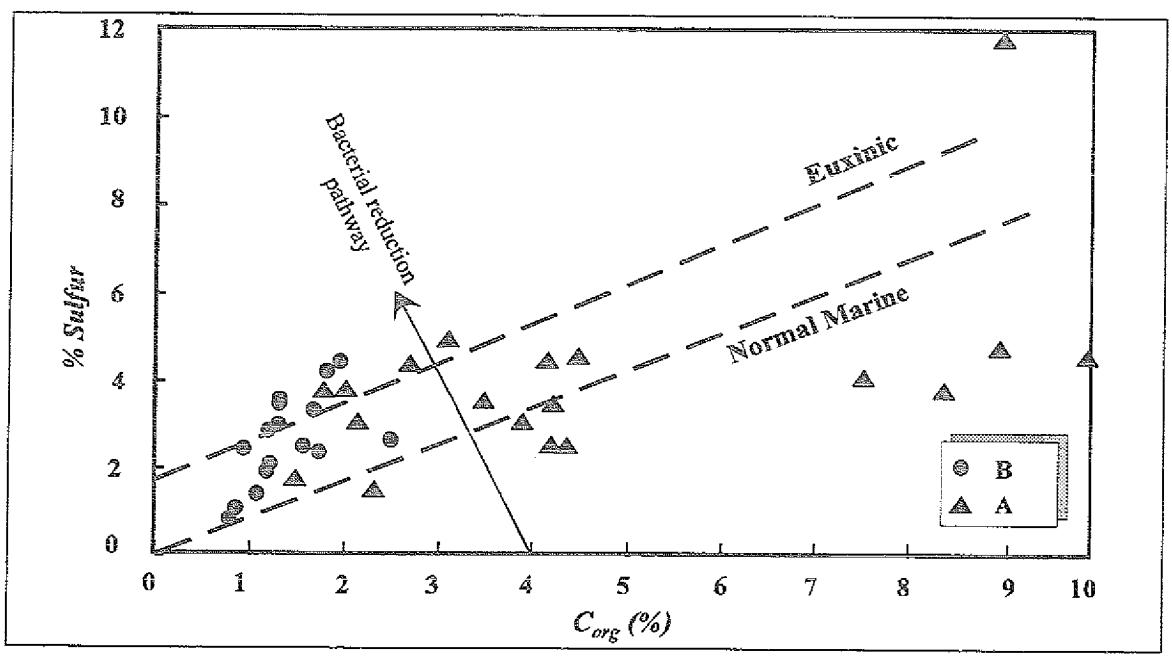


Fig. 16: Comparison of organic richness and sulfur content of samples from the Silurian formation. A and B refer to those members described in Chapter 3.1 and Figure 9. Bacterial reduction pathway from Littke et al. (1991, 1997 a,b)

Visual analyses indicate that both Silurian and Frasnian-Famennian formations contain significant amounts of pyrite framboids (common to abundant in subfacies B and D) derived from bacterial sulfate reduction and organic matter oxidation (Littke et al., 1991). This indicates that sufficient iron was available to fix most of the sulfur in the form of iron sulfide. Littke et al. (1991, 1997 a,b) showed that the consumption of part of the metabolisable organic matter during early diagenesis greatly influences the quality of organic matter in shallow marine sediments.

5-1-2 Kerogen Type and Generation Potential

The origin of organic matter in the Frasnian-Famennian and the Silurian source rocks was determined both indirectly by chemical analyses (pyrolysis) and directly by optical analyses.

a/ Rock-Eval Data

Bulk hydrocarbon pyrolysis is the major method used for the assessment of source rock quality (hydrocarbon potential), and also provides preliminary information on maturity. Rock-Eval pyrolysis (Espitalié et al., 1977, 1985, 1986) has become the industry standard for such analyses. For instance, a modified Van Krevelen diagram comparing HI (mg HC/g C_{org}) and OI (mg CO_2/g C_{org}) is commonly used for kerogen typing (Espitalié et al., 1977). Figures 17 and 18 show such diagrams in which the data for the Frasnian-Famennian and the Silurian formations are compared, and where the different subfacies described in Chapter 3.1 are discriminated.

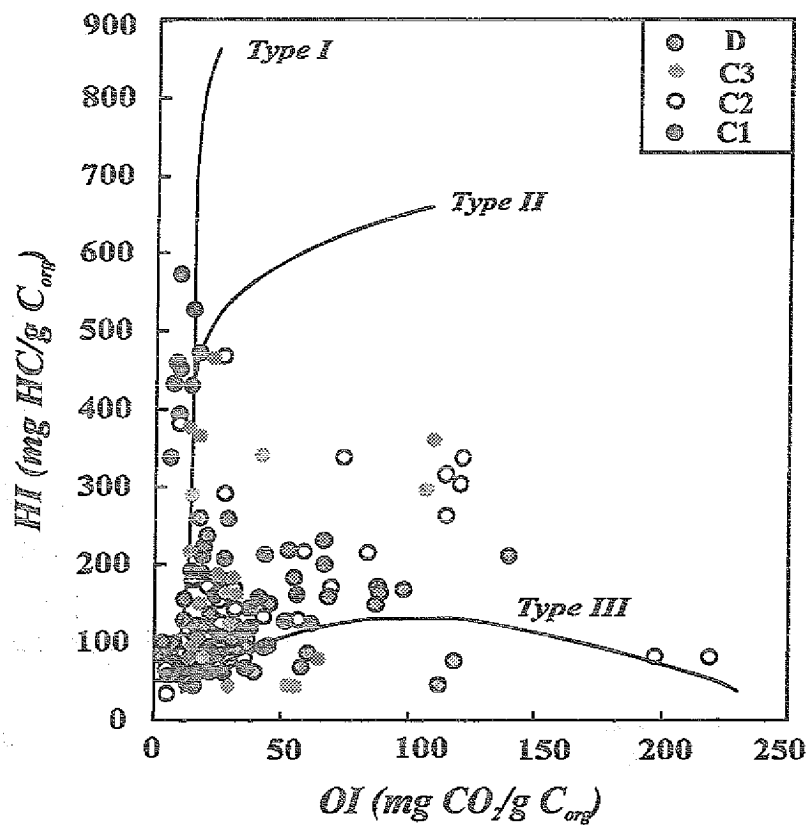


Fig. 17: Modified Van Krevelen diagram (HI vs OI) derived from Rock-Eval analyses of the Frasnian-Famennian formation samples (includes data from SONATRACH). C1, C2, C3 and D refer to those units described in Chapter 3.1 and Figure 9.

For the Frasnian-Famennian formation, the most prolific source rock samples display hydrogen indices of more than 550 mg HC/ g C_{org} and are plotted in the vicinity of the type II/I reference curve (Fig. 17). The data might also indicate that the shaly calcareous lower member (subfacies C1) has a higher generative capability for petroleum than the other units (C2, C3 and D). However, the location of samples along the evolution paths on the van Krevelen diagram-like hydrogen idex/ oxygen index (HI-OI) plot is influenced by thermal maturation and early diagenitic oxidation of organic matter (Espitalié et al., 1977; Demaison and Bourgeois, 1984). The occurrence of relatively high free hydrocarbons in some samples (Tab. 3) supports and proves that hydrocarbons have been generated and the initial HI values must have been higher. In any case, the high hydrogen index values are the imprint of a lipid-rich kerogen, predominantly of type II/I kerogen (Tissot and Welte, 1984). The highest OI values are registrated within the relatively organic-lean C2 subfacies and to a lesser extent in the subfacies D. Peters (1986) suggested that the pyrolytic generation of organic acids would generate carbon dioxide from carbonate. Consequently, the inorganic carbon dioxide can result in anomalously high oxygen index values, particularly for samples containing less than 0.5% wt% C_{org}. It is, therefore, likely that the high oxygen index values registrated are, to a certain extent, the effect of carbonate carbon decomposition rather than due to the presence of highly oxygenated organic matter. It is also possible that during some Late Devonian, less distal (nearshore or deltaic) conditions could have prevailed allowing more terrestrial input.

Figure 18 provides some insight into variations in the kerogen quality within the Silurian source rock as expressed by the differences in hydrogen index values between the basal radioactive member (Subfacies A) and the upper member (subfacies B). The former exhibits a higher hydrocarbon generation potential with HI values of up 500 mg HC/g C_{org}, mainly registrated in the northern part of the Berkine Basin (ANR-1, ZK-1), hence indicating a hydrogen-rich organic matter, i.e., predominantly type II/I kerogen (Tissot and Welte, 1984). Subfacies B in contrast, shows low HI values which a bias towards more terrigeneous material. Therefore, its facies can be considered to result in a low quality source rock. However, maturity data, as discussed later, show that the highest HI values are associated with moderately mature samples, whereas

most of the samples from the subfacies B are overmature with respect to oil generation and lost their original hydrocarbon generation potential. It is also likely that the high OI values are rather the effect of carbonate carbon decomposition; a hypothesis which is supported by geological and other geochemical evidences. It is, therefore, apparent that the organic matter of the Silurian black shales as a whole can be considered as type II kerogen (Tissot and Welte, 1984).

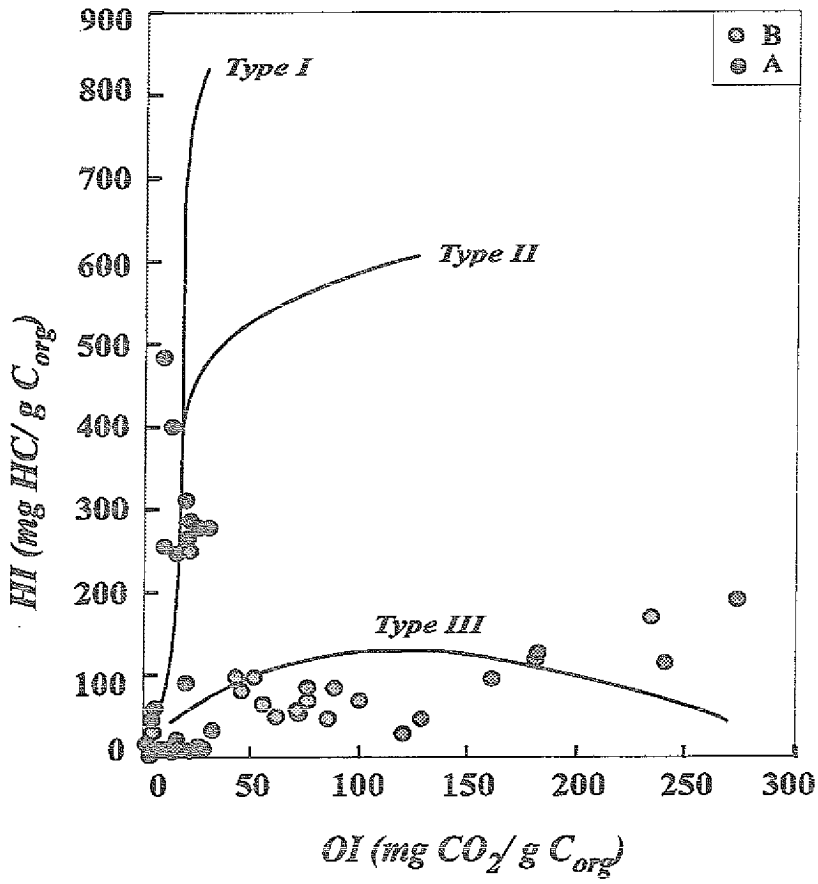


Fig. 18 : Modified Van Krevelen diagram (HI vs OI) derived from Rock-Eval analyses of samples from the Silurian formation (includes data from SONATRACH). A and B refer to those units described in Chapter 3.1 and Figure 9.

b/ Organic Petrology

The composition of the organic matter in the source rock formations was further analysed by micropetrographic methods (Taylor et al., 1998). Microscopic examination of polished sections of Frasnian-Famennian shales revealed that, predominantly, the organic matter is finely dispersed throughout the rock without being locally concentrated. The organic matter is made up of unrecognised amorphous material within a predominantly clay-rich matrix. The amorphous organic matter,

frequently termed sapropelic in contrast to humic material, is considered to result from alteration of original constituents composed mainly of plankton and similar lipid-rich precursors (Tissot and Welte, 1984). Well preserved (structured) liptinitic macerals are also present. These macerals were fluorescing in yellow-orange and are similar to alginite A or telalginite (Hutton and Cook, 1980; Taylor et al., 1998). Oil prone alginitic material composed mainly of Tasmanites was already observed by Chaouche (1991) in the case of the RE-1 well. This is supported by the good to excellent generative capability of the related basal Frasnian radioactive member as determined by Rock-Eval data (Fig. 17). Individual lipid-rich marine organisms such as acritarch and dinoflagellates are also embedded in the groundmass. The good preservation of relatively unstable macerals such as amorphous organic matter and alginite and the nearly absence of any signs of oxidation could indicate that the organic matter was deposited and conserved under reducing conditions. However, with increasing depth or maturation maceral properties change. Well defined fluorescing structured particles are common features of the moderately mature samples only. With increasing burial, and therefore maturity, the fluorescing particles progressively disappear. For instance, maturity-related changes in organic matter have also been reported by Littke et al. (1988) for the Toarcian Posidonia Shale in Northwest Germany.

Macerals of the vitrinite group, which were abundant in the samples from the Carboniferous, are also observed in variable amounts in the Frasnian-Famennian formation. The terrigeneous macerals are, however, present as small particles only. It was also observed that with increasing depth and C_{org}, there is a considerable decrease in the material attributed to higher plant bodies, indicating more oil prone organic matter downwards. This fact might indicate that the contribution of terrestrial organic matter is more prevalent in the upper section of this predominantly marine sequence.

For the Silurian source rock, visual analyses of samples from the northern Berkine Basin reveal mainly yellow-orange, fluorescing, well-preserved elongated tasmanales which are typical for oil shales and oil prone source rocks (Tissot and Welte,1984; Taylor et al., 1998).

In addition to the organic facies analyses, the reflectivity of the vitrinite macerals was determined for four key wells (Chapter 4.3). Vitrinite reflectance measurements were made mainly on samples from the Frasnian-Famennian source rock. Furthermore, the

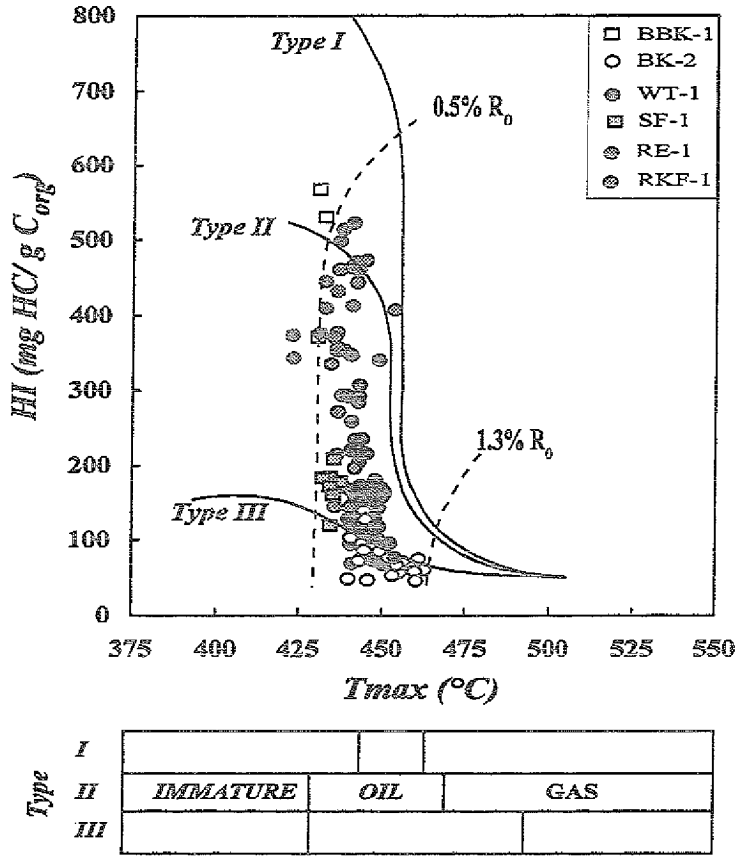


Fig. 19: Diagram comparing HI and T_{max} values derived from Rock-Eval pyrolysis of the entire Frasnian-Famennian sample set (includes data from SONATRACH). 0.5% and 1.3% R_o are the limits of the classical oil window (Tissot and Welte, 1984).

reflectivity of vitrinite-like macerals from Silurian samples of the well BRD-4 was also measured. The values obtained in this study, as well as external data, are listed in Table 14, where average vitrinite reflectance values (%R_o) for the indigeneous populations, as well as the standard deviation are presented.

5-1-3 Maturity

Figure 19 displays the relationship between hydrogen index (HI) and maximum pyrolysis yield (T_{max}) obtained for the Frasnian-Famennian interval of different wells in the basin. A very slight maturation pathway is observed indicating a successive generation of hydrocarbons (decrease in HI) paralleled by a slight increase in T_{max}. It becomes also evident that the majority of the samples fall into the mature zone (435-460°C), where hydrocarbon generation potential is diminished to values between 200

and 50 mg/g C_{org}. The low T_{max} values (<430°C) observed in wells such as BBK-1, SF-1, RKF-1, RE-1, and even WT-1 are probably due to a specific composition known as the asphaltene effect which generally lowered the T_{max} values (Espitalie et al., 1977, 1986; Clemenz, 1979). This fact may be explained by the high free hydrocarbon content (S_1 up to 36 mg/g rock) observed in some samples (Tab. 3).

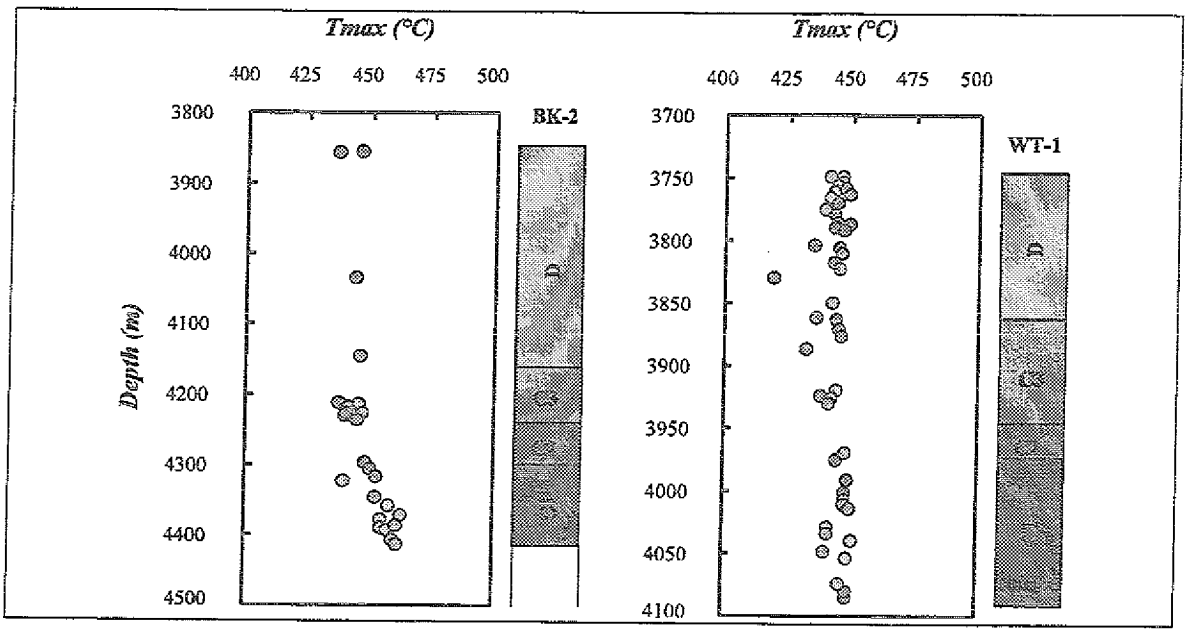


Fig. 20: Comparison of T_{max} parameter of the different Frasnian-Famennian unit samples from 2 wells (BK-2 and WT-1) located in the basin center. C1, C2, C3 and D refer to the units described in Chapter 3.1 and Figure 9. Note the scale difference for the two wells with respect to depth.

Figure 20 shows the variation of T_{max} with depth through the Frasnian-Famennian sequence within two wells in the center of the basin (BK-2 and WT-1). Since the level of organic matter maturation increases with increasing burial and since T_{max} is kerogen type dependant (Espitalié et al., 1977, 1985, 1986; Tissot and Welte, 1984), T_{max}-depth plots are used here in order to detect any major dissimilarity in the kerogen quality. The figure reveals that the maturation, as expressed by the most reliable T_{max} values, remains approximately constant for a depth interval of more than 500 m and that no changes in T_{max}, due to a strong kerogen quality variation, is observed. This indicates that, although there is an occurrence of highly organic-rich oil prone units

(e.g. the subfacies C1), predominant marine organic matter characterise the Frasnian-Famennian sequence as a whole.

The determination of vitrinite reflectance as a tool to establish the maturity level of kerogen has been used successfully in the past. In contrast to chemical methods where the kerogen as a whole is analysed, this method enables to investigate individual organic particles, i.e. indigenous vitrinite or reworked particles derived from the erosion of older sedimentary rocks. Vitrinite reflectance, in contrast to other maturity parameters (e.g. T_{max}, Espitalié et al., 1985), can be used over the entire range of maturation and is therefore considered as the most reliable and the most often used maturity indicator (Dow, 1977). Vitrinite reflectance is also applied as a major calibration tool for numerical simulation of thermal histories in sedimentary basins (Lopatin, 1971, Waples, 1980). However, vitrinite reflectance, as other maturity parameters do, is frequently influenced by variation in the original plant association and chemical composition of organic matter, and early diagenetic processes (Wenger and Baker, 1987; Buiskool Toxopeus, 1983; Durand et al., 1986; Goodarzi et al., 1992; Taylor et al., 1998). Such effects are particularly important for marine sediments where the organic matter is finely dispersed and where vitrinite is in low abundance (Tissot and Welte, 1984). Because of the proven marine nature of the Frasnian-Famennian and the Silurian source rocks as a whole and because of the difficulty to identify the indigenous vitrinite macerals, vitrinite reflectance measurements have to be compared to other maturity parameters. For instance, true maturity trends must be based on accepted calibration procedures (Chapter VI), taking into account the geological context of the basin in order to reduce possible errors. This is particularly valid for the Silurian source rock because, reflectance measurements had to be made on other particles than indigenous vitrinite (Taylor et al., 1998).

Although the reflectance values cover a broad range from 0.55% R_o (SF-1) to 1.2% R_o (BK-2), the majority of R_o values lie between 0.8 and 1.1% (Tabs. 3, 14), indicating that the Frasnian-Famennian source rock is, in most of the basin, in the main zone of hydrocarbon generation (Tissot and Welte, 1984) as already shown by most of the T_{max} values (Fig. 19). The comparison of these latter values (combined for the entire formation) with R_o values shows in general a good agreement between both maturity

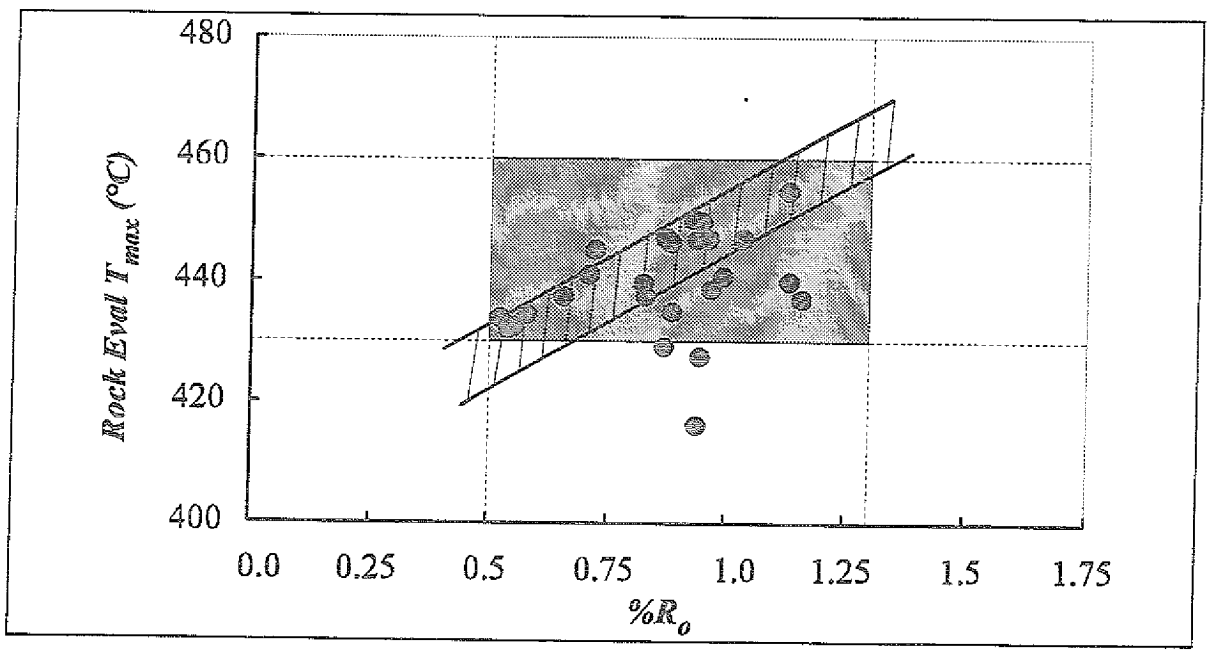


Fig. 21: Relationship between maximum pyrolytic T_{max} and vitrinite reflectance (R_o) for the entire Frasnian-Famennian formation data set. The highlighted area correspond to the classical oil window (Tissot and Welte, 1984; Espitalié et al., 1985).

parameters (Fig. 21). However, it is shown that the rather well defined relationship between R_o and T_{max} is less evident for some samples and that highest R_o is not necessarily related to the highest T_{max}. Indeed, most of the samples which are plotted below the minimum regression lines and exhibiting low T_{max} values are oil stained samples (high S_1; Tab. 3, enclosed Tab. 1). The enrichment in free bitumen of samples submitted to Rock-Eval pyrolysis is known as the asphaltenes effect, which generally lowers T_{max} values (Espitalié et al., 1977, 1986, Clemenz, 1979).

With respect to the depth-related increase of vitrinite reflectance within individual wells and correlation with other wells, it may be assumed that some documented vitrinite reflectance values are underestimated and therefore do no show the true maturity stage of the organic matter. This is well illustrated by the SF-1 well, where R_o values show a wide range (0.55 to 0.88%) in a depth interval of only 134 m (Tab. 14). This is also supported by the fact that for approximately the same depth (3788-3792 m), R_o is 0.66 % in the SF-1 well, whereas in the WT-1 well R_o is near 1.0 %. The possible causes of such low vitrinite reflectance are discussed elsewhere (e.g. Radke et

al., 1997). Practical aspects of such deviations are discussed with respect to the burial and thermal history reconstructions of the basin, provided for each individual well in the basin modelling part of this study (Chapter VI).

The Silurian source rock was drilled only in the northern, north-eastern, western, south-western and southern parts of the basin. The very low S_2 values combined, generally, with insignificant T_{max} values (around 500°C; Tabs. 3, 4 and 6), indicate an overmature stage in the western part of the basin (BRD-4). The Silurian is mature to marginally mature in the south-western part of the basin (HSN-1) with mean T_{max} values of 443°C at a depth of 2687 m. In the northern and north-eastern parts of the basin, in the ZK-1 and KA-1bis wells respectively, T_{max} values indicate a maturity within the oil generative window. T_{max} values vary between 436 and 439 °C at a depth between 3646 and 3656 m in the former, whereas in the latter, T_{max} ranges between 442 and 445°C at a depth interval of 3029-3072 m. The measured reflectance values on vitrinite-like particles correspond generally to the same maturity stages defined by the T_{max} values.

5-2 Characterisation of Bitumen (EOM) and Crude Oils

This section includes data derived from solvent extract and crude oil analyses (i.e. MPLC, GC analyses of saturated and aromatic fractions, GC-MS analyses of the saturated fraction). Detailed analyses of the extractable organic matter (EOM) was performed in order to establish the degree of thermal maturation which the organic matter has been subjected to during burial and to obtain geological and geochemical information regarding the biological contributors to the organic matter of the main source rocks. A further goal was a tentative correlation of the source rock bitumens to crude oils from adjacent fields. The results are discussed here for the boiling range which in the literature is referred to as C_{15+} compounds.

5-2-1 Total EOM Yields and Compound Class Composition

The variation in the yields of bitumens with increasing burial (i.e. maturity) is well known in the form of hydrocarbon generation curves, as illustrated by Tissot and

Welte (1984) for different sedimentary basins. For instance, the amount and composition of the extractable organic matter is mainly controlled by the nature of the organic material and its maturity. An other important factor which may have a great influence on the composition of hydrocarbons is the extent of migration which generally drains the compounds, particularly the lighter ones, towards the migration pathways and reservoirs (Tissot et al., 1973; Tissot and Welte, 1984).

The yield of volatile organic matter was determined by using Rock-Eval pyrolysis and solvent extraction (flow blending technique, Radke et al., 1978). The results are listed in Table 3.

a/ Yield As a Function of Organic Carbon Content

Because of the extent of the variation in the organic carbon content of the samples used for extraction, it is expected that the amount of the extracted bitumen will be proportional to the organic carbon content. Philippi (1956) and Baker (1962) have demonstrated positive relationships between hydrocarbons and total organic carbon content in series of shales and mudstones.

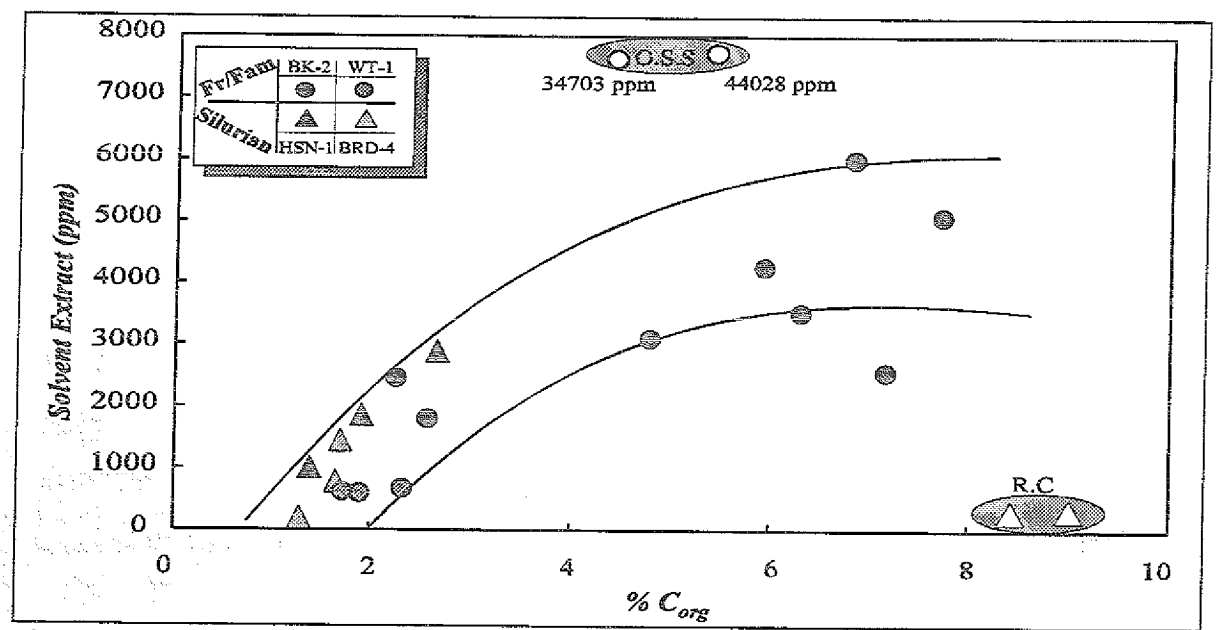


Fig. 22: Total hydrocarbon yields as a function of organic carbon content for the complete Frasnian-Famennian and Silurian samples. O.S.S, oil stained samples; R.C, residual carbon.

In Figure 22, the total hydrocarbon yields (in ppm) extracted form the different samples are plotted against organic carbon content (in wt% C_{org}). Clearly the diagram

reveals a positive relationship between the extracted hydrocarbons and the organic carbon content of the samples. As the organic carbon content increases, the amount of extractable organic matter (bitumens) increases. As already suggested by Phillipi (1957) this relationship may indicate that hydrocarbons are an indigenous part of the sedimentary rock from which they are extracted.

The obvious deviation of some samples from the Frasnian-Famennian and the Silurian formations may find explanation in the fact that the former contains migrated petroleum as evidenced by the very high free hydrocarbon content of these samples (Tab. 3). Consequently, the amount of extractable organic matter from these rocks would not be expected to bear a linear relationship to primarily trapped organic matter. The latter may be explained by the fact that the remaining kerogen constitutes a sort of carbonaceous residue in spite of the high maturity of the samples of which the generation potential is already exhausted. This is well confirmed by their very low residual potential (enclosed Table 1).

Various authors have evaluated disseminated hydrocarbons and organic carbon in ancient non-reservoir and petroliferous source rocks of various basins (Hunt, 1961; Philippi, 1965; Vassoevich, 1967; Tissot and Welte, 1984). For instance, values observed by Philippi (1965) in non-reservoir rocks are in the range of 0.53-3.67% organic carbon and 267-2360 ppm hydrocarbons, which gives an hydrocarbon to organic carbon ratio in the range of 34 to 101 mg/g C_{org}. From the evaluation of Tissot and Welte (1984), average organic carbon and hydrocarbons in shale and silts are, respectively, 1.82% and 860 ppm with an hydrocarbon to organic carbon ratio of 43 mg/g of C_{org}. For calcareous shales, the respective values are 1.9%, 1260 ppm and 66 mg/g C_{org}. This study shows that for both formations, excluding the E44280 and E44281 samples, which exceed the conventional values (Tab. 3, Fig. 21), the average values are 1.79%, 1065 ppm and 75 mg/g C_{org} in the silty shales, whereas in the calcareous shales average values are 5,6%, 2833 ppm and 59 mg/g C_{org}. The ranges commonly observed in shales, as given by Hunt (1961), are from 0 to 5% C_{org}, and from 0 to 7000 ppm hydrocarbons. The results obtained in this study extend over most of this range of distribution (Tab. 3). therefore, it can be concluded that, with respect

Tab. 3: Yield of volatilisable organic matter as derived from solvent exract (flow blending technique, Radke et al., 1978) and Rock-Eval pyrolyis of samples from the Devonian and Silurian shale sequences. The highlighted identification numbers are samples from the Silurian and the Frasnian radioactive zones. nd, not defined.

Sample ID	Well name	Depth (m)	Age	R_o (%)	T_{max} (°C)	S1 (mg/g rock)	S1 (mg/g Corg)	EOM (mg/g rock)	EOM (mg/g Corg)	ppm
E44236	BK-2	3992.00	Famennian	0.94	427	0.89	33.96	1.88	71.75	1800
E44240		4212.00	Frasnian	nd	438	2.82	36.62	5.13	66.62	5100
E44241		4216.00	Frasnian	nd	446	2,38	40.00	4.20	70.58	4284
E44243		4227.00	Frasnian	1.03	447	3.22	47.07	6.00	87.71	6000
E44244		4306.00	Frasnian	nd	450	1.71	35.40	3.00	62.11	3005
E44246		4359.00	Frasnian	nd	458	2.14	34.07	3.44	54.77	3443
E44248		4371.00	Frasnian	1.13	463	1.87	26.19	2.66	37.25	2600
E44249		4412.00	Frasnian	0.96	461	1.35	32.76	2.11	51.21	2115
E44254	BRD-4	4570.00	Silurian	1.81	360	0.90	52.63	2.43	142.10	2440
E44256		4587.00	Silurian	nd	548	0.84	50.00	1.41	83.92	1441
E44260		4642.00	Silurian	nd	nd	0.89	74.16	0.88	73.33	886
E22263		4692.00	Silurian	2.09	nd	0.01	0.78	0.16	12.25	163
E44266		4712.00	Silurian	1.97	527	0.02	0.23	0.02	0.23	23
E44267		4719.00	Silurian	2.02	521	0.02	0.22	0.27	3.00	271
E44272	WT-1	3754.00	Famennian	0.88	446	0.58	17.16	0.71	30.47	710
E44274		3763.00	Famennian	nd	449	0.40	20.51	0.78	40.00	786
E44276		3792.00	Famennian	0.94	447	0.37	19.57	0.77	40.74	770
E44280		3886.00	Frasnian	nd	432	36.30	643.61	43.02	762.76	43028
E44281		3924.00	Frasnian	0.98	438	29.20	666.66	34.69	792.00	34703
E44284		4117.00	Givetian	0.98	447	0.64	36.99	0.70	40.46	706
E44288		4220.00	Emsian	0.96	441	44.35	1534.60	59.48	2058.13	4112
E44293	HSN-1	2620.00	Silurian	nd	429	0.35	26.71	1.06	80.91	1068
E44297		2660.00	Silurian	1.08	438	0.97	31.49	1.89	61.36	1893
E44299		2682.00	Silurian	nd	436	1.69	63.05	2.82	105.22	2829

to their organic carbon and hydrocarbon contents, the Frasnian-Famennian and the Silurian shale formations are quite similar to the shaly petroliferous source rocks found in other sedimentary basins.

b/ Yield as a Function of Maturity

Figure 23 shows the C_{15+} hydrocarbon concentrations (normalized to organic carbon) of both formations as a function of maturity. Excluding the oil stained samples, it clearly shows that most of the extracted samples from the Frasnian-Famennian (BK-2, WT-1) and Silurian (HSN-1) are within a narrow range of maturation (from 0.83 to 1.16%) as expressed by R_o values, and that the extract yields are in the range of 30-100 mg/g C_{org}. The diagram also reveals that as maturation proceeds, the amount of

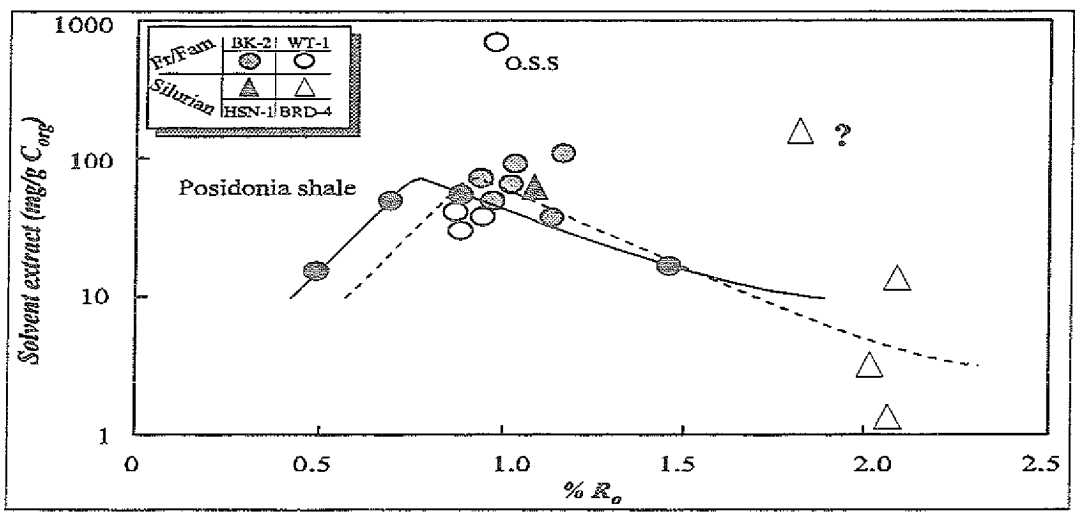


Fig. 23: Total extract yield (flow blending method) as a function of the maturity level reached by the Frasnian-Famennian and the Silurian formations. For comparison, the trend of Posidonia shale has been superimposed using data from Rullkötter et al.(1988). Note the logarithmic scale for the solvent extract. O.S.S, oil stained samples.

total hydrocarbons decreases as established by the samples from BRD-4 well which are overmature with respect to the oil generation window. Indeed, Rullkötter et al. (1988) showed for the Posidonia shales that the amount of extractable organic matter increases until a certain maturation threshold, after which the yield of hydrocarbon becomes inversely proportional to thermal maturation. In any case, the amount of hydrocarbons in the mature Silurian and Upper Devonian formations remains in the range of 30-100 mg/g C_{org}, values which are observed in other marine type II kerogens

deposited under reducing conditions (Tissot et al., 1971; Tissot and Welte, 1984; Rullkötter et al., 1988). On the other hand, Rullkötter et al. (1988) suggested that for such a kerogen type, about half of the hydrocarbon generation potential is already released at 0.7 % R_o, at least under conditions of high geologic heating rates.

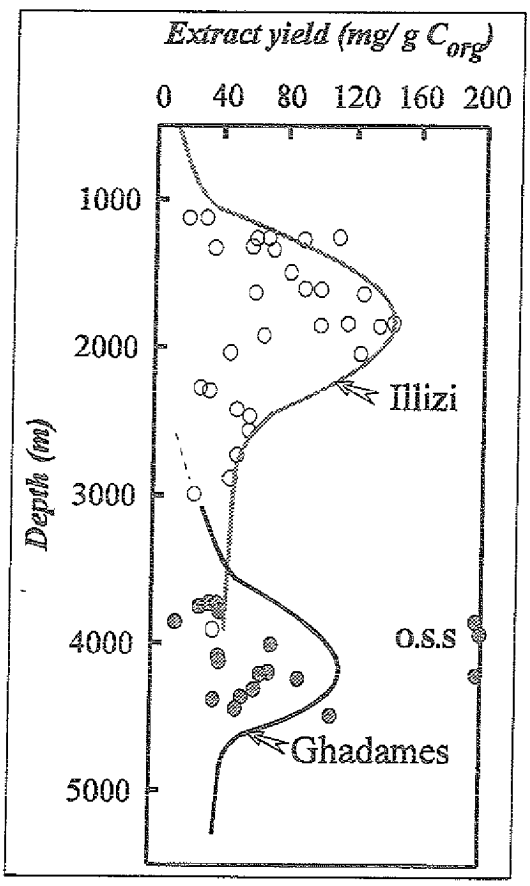


Fig. 24: Evolution of the yield of extract (normalised to C_{org}) as a function of maximum burial of the Frasnian-Famennian formation. For comparison, the trend of their equivalent in the Illizi Platform is superimposed using data from Tissot et al.(1973). O.S.S, oil stained samples

Figure 24 shows the extractable organic matter, normalized to organic carbon, as a function of maximum burial depth for the Frasnian-Famennian formation. For comparison, the hydrocarbon generation curve established by Tissot et al. (1973) for the Middle-Upper Devonian sequence of the Illizi Platform is superimposed. The data obtained in this study show an increase of the ratio of extract to total organic carbon from about 3750 m to about 4250 m where the data culminate. From 4250 m downwards, a decrease is observed, corresponding probably to the formation of lighter products (gas). In the Illizi Platform the ratios culminate at a depth of around 2000 m, hence indicating that maximum oil generation is much shallower, thought mean R_o values are in the same range as those observed in the Berkine Basin (0.8-1.0%; Malla et al.,1997). Assuming that no significant differences in the petrophysical properties of

the rocks in the two areas, only higher heat flow values in the Illizi platform can account for such differences. The possible causes which might have played a role in enhancing (Illizi Platform) or prohibiting (Berkine Basin) the maturation of kerogen are discussed in Chapter VI with respect to basin modelling.

c/ Compound Class Composition

The different compound classes of the Frasnian-Famennian and Silurian rock extracts and crude oils as derived from MPLC are listed in Table 4.

The saturated and aromatic hydrocarbons and heterocompounds (resins and asphaltenes), which are the main components of crude oils (Tissot and Welte, 1984), are presented in a ternary compositional diagram (Fig. 25). Three of the crude oil samples (GT-35, HC-102 and KA-2) show a rather similar composition with high amounts of saturates (>80 %) and low quantities of aromatics (about 20%) and heterocompounds (less than 2%). These proportions reflect their light character(41-45° API). The oil sample RNSE-3 is the heaviest one (30°API). This is evidenced by its relatively elevated heterocompounds content (15%). According to these observations, the oils can be considered as paraffinic oils (Tissot and Welte, 1984).

The extracts show a rather similar composition with high amounts of saturates and low yield of aromatics. The enrichment of some samples, such as those of the Silurian formation (Fig. 25), in polar compounds is consistent with the expulsion theory which suggests that volatile aliphatic hydrocarbons (low molecular weight paraffins) can more easily escape from a source rock than do polar compounds (Tissot and Welte, 1984). The high hydrocarbon contents of the samples located in the upper left corner of the diagram might be rock-matrix controlled (Espitalié et al., 1980, Espitalié et al., 1986). In fact, certain organic matter-rich shale intervals were probably more prone to the early blockage of the pore throat than intervals where shaly and silty laminae were more common. Furthermore, these samples show an aliphatic/aromatic ratio of less than unity in contrast to the other samples. Indeed, the differences observed in the aliphatic/aromatic ratios are not due to maturation differences, but might be related to migration efficiency by diffusion due to the low permeability of these domains. For instance, Hanebeck (1994) has shown that in the absence of an interconnected aqueous phase diffusion can still proceed in the bitumen-saturated pore space where diffusion

Tab. 4: Yield of saturate, aromatic and heterocompounds (resins and asphaltenes) fraction as derived from MPLC of Devonian and Silurian shale rock extracts (top) and crude oils (bottom). The highlighted identification numbers are samples from the Silurian and the Frasnian radioactive zones. Samples with asterisk are condensate samples. nd, not defined.

Sample ID	Well name	Age	R_o %	T_{max} (°C)	Sat	Aro	Hetero	Sat	Arom	Hetero
					mg/ g extract			% of extract		
E44236	BK-2	Famennian	0.94	427	113.87	43.56	78.42	48.28	18.42	33.24
E44240		Frasnian	nd	438	146.00	66.80	27.07	60.86	27.84	11.28
E44243		Frasnian	1.03	447	152.43	51.93	22.17	67.28	22.92	9.78
E44247		Frasnian	1.13	463	134.89	96.43	96.31	41.17	29.43	29.39
E44249		Frasnian	0.96	461	175.94	112.35	93.30	46.10	29.44	24.45
E44254	BRD-4	Silurian	1.81	360	197.86	103.96	94.36	49.94	26.24	23.81
E44256		Silurian	nd	548	141.46	63.47	143.21	40.63	18.23	41.13
E22263		Silurian	2.09	nd	151.94	37.20	193.54	39.70	9.72	50.57
E44265		Silurian	1.97	527	nd	12704.98	247.70			
E44267		Silurian	2.02	521	47.75	30.93	136.24	22.21	14.35	63.39
E44272	WT-1	Famennian	0.88	446	165.48	84.36	95.24	47.95	24.44	27.59
E44274		Famennian	nd	449	153.36	49.28	107.90	49.38	15.86	34.74
E44276		Famennian	0.94	447	183.99	57.81	92.96	54.96	17.26	27.76
E44280		Frasnian	nd	432	180.08	448.83	35.17	27.11	67.58	5.29
E44281		Frasnian	0.98	438	178.46	235.79	29.02	40.25	53.19	6.54
E44284		Givetian	0.98	447	202.34	49.00	91.09	59.08	14.30	26.60
E44288		Emsian	0.96	441	159.51	299.35	26.44	32.86	61.68	5.44
E44293	HSN-1	Silurian	nd	429	107.32	30.27	175.56	34.27	9.66	56.06
E44297		Silurian	1.08	438	127.04	51.07	170.46	36.44	14.65	48.90
E44299		Silurian	nd	436	111.29	35.59	94.07	46.18	14.77	39.04

Oils

	Fields	*Res. Age*	*°API*	*mg/g Oil*			*% of Oil*		
E44516	GT-35	Triassic	41.48	323.99	19.50	2.69	93.20	5.60	1.18
E44517	HC-102	Triassic	43.21	281.52	17.33	1.78	93.24	5.74	1.01
E44518	KA-2	Triassic	44.51	145.41	22.93	1.87	84.84	13.30	1.77
E44519	RA-8*	Triassic		176.84	30.14	0.75	85.12	14.50	0.00
E44520	RC-1*	Triassic		365.47	10.85	0.55	96.90	2.87	0.00
E44521	RNSE-3	Triassic	30.00	140.46	21.86	8.12	73.40	4.24	15.14

of saturated hydrocarbons is faster than that of aromatic compounds.

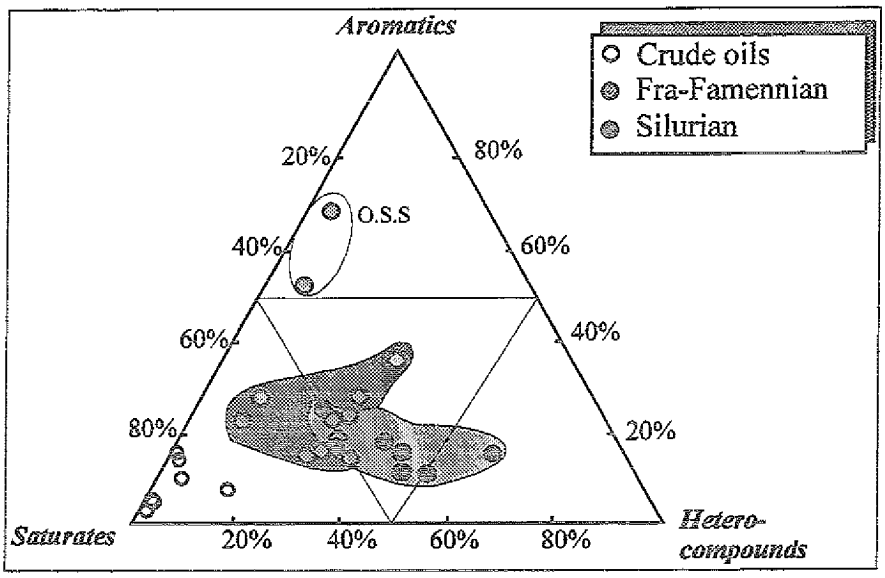


Fig. 25: Relative composition of the Frasnian-Famennian and Silurian shale solvent extracts (flow blending method) and crude oils produced from different field reservoirs, as derived from MPLC fractionation. O.S.S, oil stained samples.

5-2-2 Molecular Characterisation

a/ Aromatic Hydrocarbons

Compositional variations and amounts of the aromatic compounds in sedimentary organic matter, especially diaromatic (naphthalenes) and triaromatic (phenanthrenes) compounds with increasing maturity has gained wide acceptance in the last fifteen years (Radke et al., 1982; Radke and Welte, 1983; Radke, 1987, 1988). These maturity indicators rely either on an increase of the degree of alkylation of a given parent compound, namely ratios of quantitatively prominent 2-ring and 3-ring aromatics, with maturity, or on a change in the isomer distribution of alkyl-aromatic homologues towards thermally more stable isomers. In particular, the most widely preferred and accurate aromatic maturity parameter is the methylphenanthrene index (MPI-1), introduced by Radke et al. (1982). Based on such a parameter calibrated against vitrinite reflectance on a series of bituminous coals and type III kerogen, Radke (1988) suggested that a calculated value of vitrinite reflectance can be determined by using empirical formulas such as R_c= 0.6 MPI1+0.4 and R_c = -0.6 MPI1+2.40 for vitrinite reflectance lower than 1.35% and greater than 1.35%, respectively.

Tab. 5: Selected maturity parameters for the aromatic hydrocarbon fraction of Devonian and Silurian solvent extracts (top) and crude oils (bottom). Equations for calculations of ratios are given in the appendix. The highlighted identification numbers are samples from the Silurian and the Frasnian radioactive zones.Samples with asterisk are condensate samples. nd, not defined.

Sample ID	Well name	Depth (m)	Age	R_o (%)	R_c (%)	MNR	MPR	MPI-1
E44236	BK-2	3992.00	Famennian	0.94	0.84	1.54	0.9	0.73
E44240		4212.00	Frasnian	nd	0.88	1.61	0.97	0.80
[illegible]		4227.00	Frasnian	1.03	0.93	1.65	1.04	0.88
E44247		4371.00	Frasnian	1.13	1.03	1.95	1.25	1.05
[illegible]		4412.00	Frasnian	0.96	0.94	1.82	1.16	0.89
E44254	BRD-4	4570.00	Silurian	1.81	1.86	1.67	0.92	0.72
E44256		4587.00	Silurian	nd	1.89	1.74	0.95	0.67
E44263		4692.00	Silurian	2.09	1.83	1.61	1.15	0.78
[illegible]		4712.00	Silurian	nd	1.74	1.80	1.88	0.93
[illegible]		4719.00	Silurian	2.02	1.86	2.18	1.68	0.72
E44272	WT-1	3754.00	Famennian	nd	0.86	1.77	0.99	0.77
E44274		3763.00	Famennian	0.88	0.87	1.88	0.96	0.78
E44276		3792.00	Famennian	nd	0.89	1.98	1.05	0.81
E44280		3886.00	Frasnian	0.94	0.89	1.25	0.91	0.82
E44281		3924.00	Frasnian	nd	0.91	2.05	0.91	0.85
E44284		4117.00	Givetian	0.98	1.01	2.14	1.21	1.02
E44288		4220.00	Emsian	0.96	1.05	2.14	1.21	1.01
E44293	HSN-1	2620.00	Silurian	nd	0.83	1.44	0.85	0.72
[illegible]		2660.00	Silurian	1.08	0.82	1.44	0.85	0.72
[illegible]		2682.00	Silurian	nd	0.83	1.31	0.88	0.72
Oils								
	Fields		***Res. Age***	***°API***				
E44516	GT-35		Triassic	41.48	1.25	1.69	2.28	1.41
E44517	HC-102		Triassic	43.21	1.04	1.27	1.83	1.06
E44518	KA-2		Triassic	44.51	0.94	1.18	1.49	0.90
E44519	RA-8*		Triassic		0.49	0.64	10.00	3.02
E44520	RC-1*		Triassic		0.87	0.68	2.23	0.78
E44521	RNSE-3		Triassic	30	1.19	1.68	1.85	1.32

A set of selected maturity parameters (Tab. 5, equations given in the appendix) based on alkylnaphthalene and alkylphenanthrene ratios are plotted against measured vitrinite reflectance data for the Frasnian-Famennian shale sequence (Fig. 26). The diagram shows that a reasonable correlation exists for the methylnaphthalene ratio and the methylphenanthrene index (MNR and MPI-1). This is in particular established for vitrinite reflectance values of less than around 1%, which corresponds to the late mature hydrocarbon catagenesis zone. The variation of the methylphenanthrene ratio with maturity, however, is not clear and is likely to be inversely proportional to the maturation of organic matter.

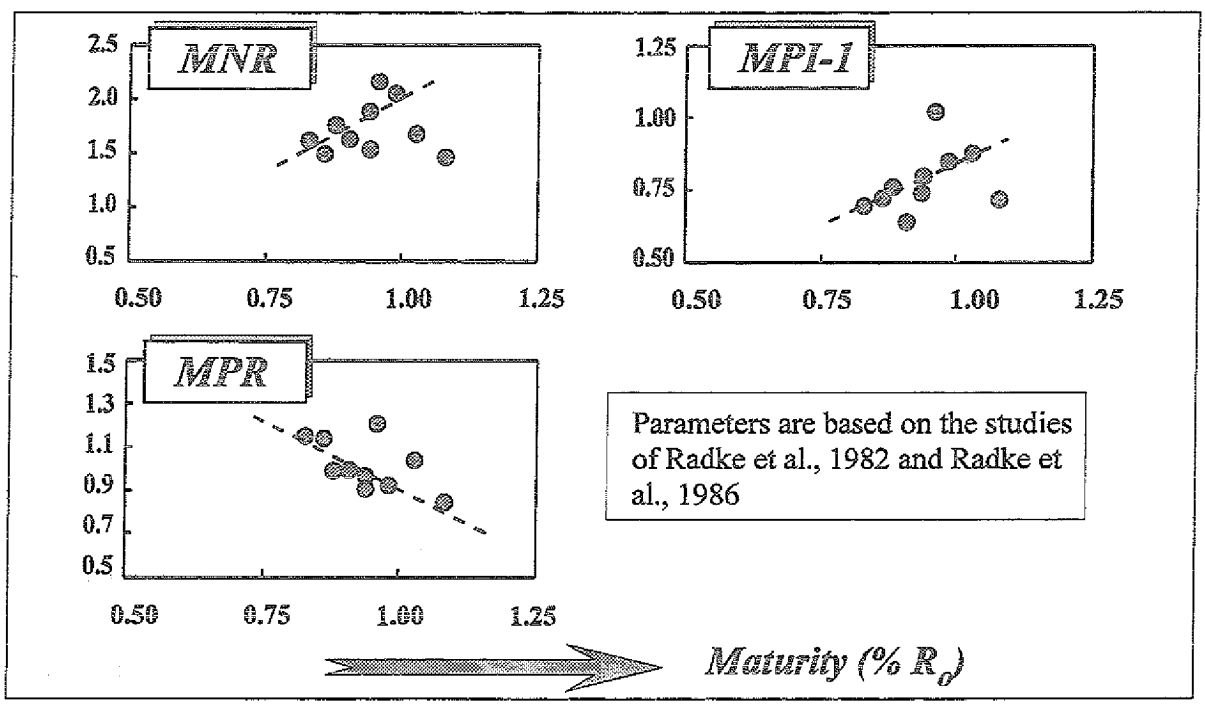


Fig. 26: Evolution of selected maturity parameters (MNR, MPI-1 and MPR) of the Frasnian-Famennian shale solvent extracts.

The alkylnaphthalene based parameter MNR outlines a positive linear trend up to around 1.1% R_o. After this threshold, the MNR is decreasing with increasing R_o. Therefore, this ratio may be useful for establishing maturity of the Devonian shales particularly in the main zone of hydrocarbon generation typically associated to vitrinite reflectance values between 0.5% and 1.1% (Tissot and Welte, 1984).

The alkylphenanthrene ratio MPI1 is known to show a good correlation for type III kerogens between 0.5% and 1.3% (Radke and Welte, 1983), corresponding to the classical oil generation window. In Figure 26 MPI1 increases as the maturity progresses up to a certain R_o limit. Because of the absence of Upper Devonian samples of higher maturity, the variation of MPI1 at higher degree of thermal alteration cannot be shown. Assuming that the organic facies associated with the Silurian source rock is similar to that of Devonian, which is mostly the case, this ratio shows low values at higher thermal maturity levels (Tab. 5, well BRD-4) indicating probably that the same effect as observed by Radke and Welte (1983) after the 1.3% R_o threshold is present here. This is illustrated by Figure 27 where R_o values are plotted against a maturity parameter based on MPI-1 (R_c) and where a linear increase of R_c with increasing R_o is observed throughout the entire maturity range observed in the complete data set (i.e. Silurian and Frasnian-Famennian shale formations).

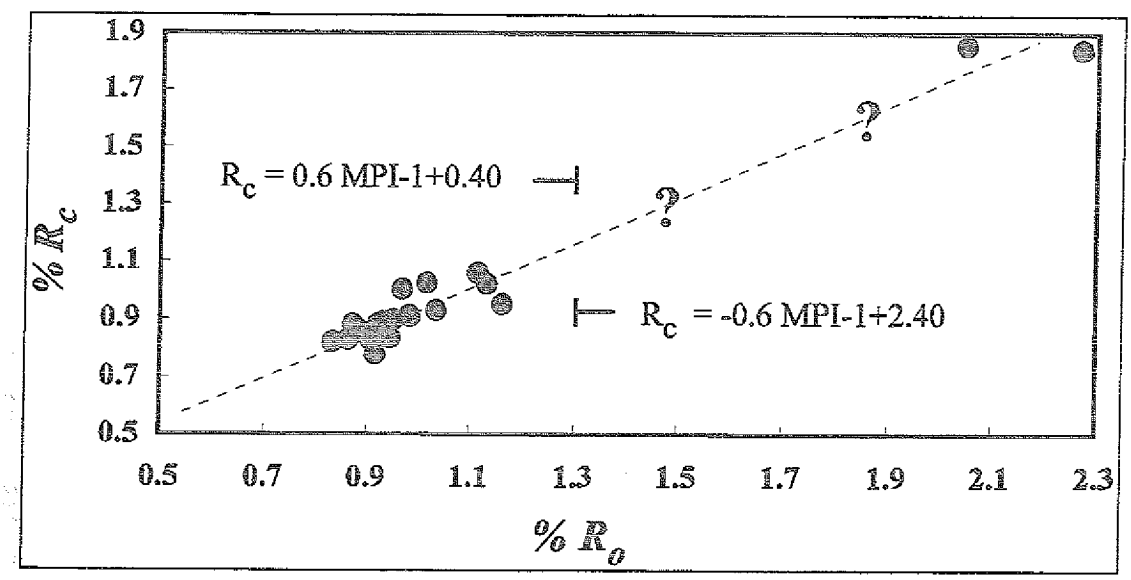


Fig. 27: Relation between measured (R_o) and calculated (R_c) vitrinite reflectance of the whole sample set. R_c is based on the study of Radke and Welte (1983).

Further geochemical investigations in this way are highly required. The confirmation of this relationship may solve maturity assessment problems generally encountered in the Palaeozoic strata and particularly for the pre-Devonian sediments where true vitrinite macerals are absent.

Figure 28 shows the variation of aromatic maturity parameters, analogous to those of Figure 26, as calculated for crude oils. The diagram shows an opposite relationship to that observed for the rock extracts. The alkylnaphthalenes and alkylphenanthrenes, namely MNR and MPI-1, are inversely proportional to the API gravity of the oils. In general, as the API gravity of the oils increases (i.e. maturity increases), the MNR and MPI-1 decrease. The methylphenanthrene ratio (MPR-1) shows more scatter with the sample GT-35 yielding values different to the others. This is distinctively pronounced in the RA-8 condensate sample where this ratio reaches the value of 10 (Tab. 5).

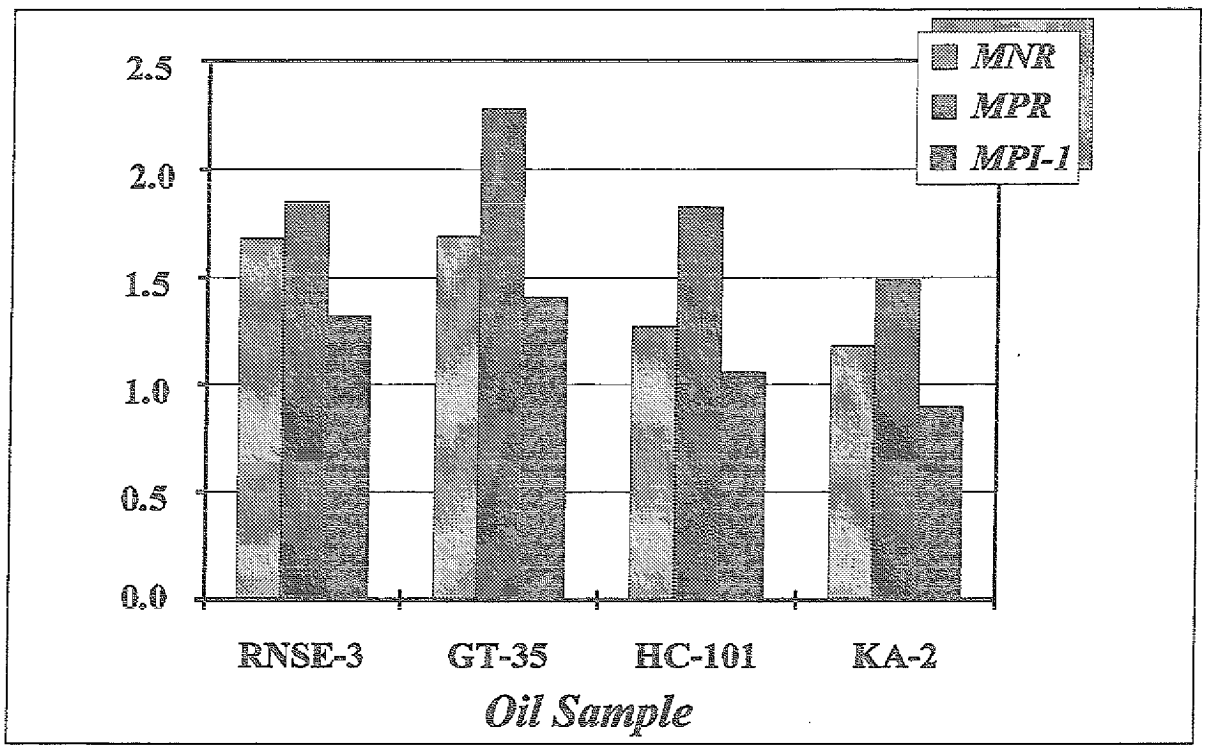


Fig. 28: Calculation of selected parameters (analogous to those of Figure 25) for crude oils from different fields (see Figure 1 for location).

b/Saturated Hydrocarbons

b-1/ Whole Rock Extracts and Oil Hydrocarbon Distributions

The chromatograms resulting from GC analyses of saturated compounds represent a molecular weight distribution of this hydrocarbon fraction. The major components are a series of *n*-alkanes which contain from ca. 10 carbon atoms to ca. 35 carbon atoms. The preservation of molecular features bearing the imprint of their biochemical precursors in ancient sediments is commonly observed. The type of data acquired from gas chromatograms providing information on kerogen type, maturity and depositional

environment include the pristane/phytane concentration ratio (Brooks et al., 1969; Connan, 1974; Powell and McKirdy, 1975). Whether there is a bias towards longer

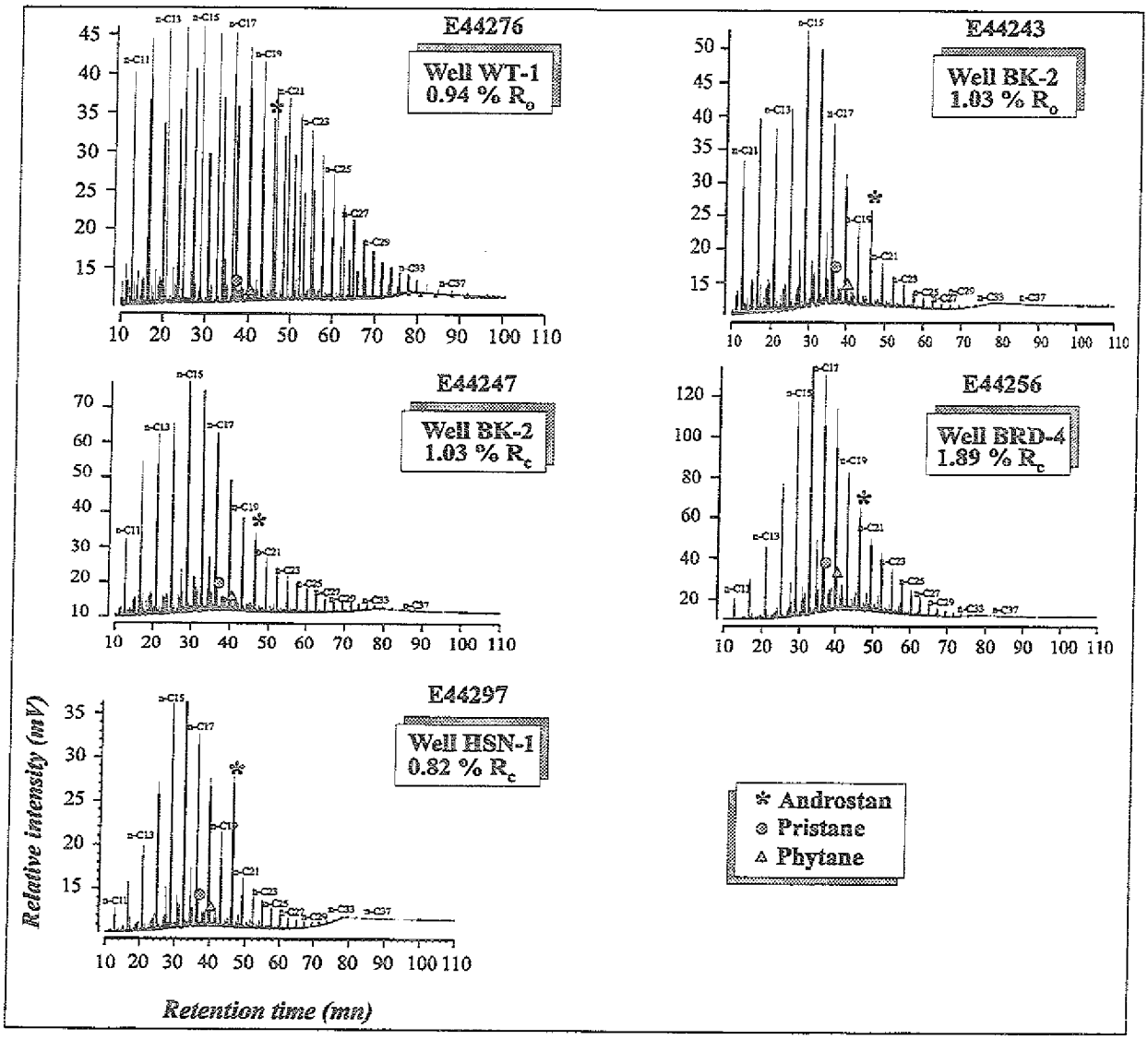


Fig. 29: Gas chromatography fingerprints of selected samples from the Frasnian-Famennian and Silurian formations of different maturity levels (as deduced from R_o and R_c). Description includes sample identification number, well name and maturity. 5α-Androstan, internal standard

(C_{27}) or shorter (C_{17}) chain lengths and whether there is a preference of either odd or even alkane chains among the normal alkanes is described by carbon preference index values (CPI; Bray and Evans, 1961; Philippi, 1975; Tissot and Welte, 1984)).

Figure 29 displays the normal paraffin (*n*-alkanes) and the isoprenoid (pristane and phytane) distributions of selected Frasnian-Famennian and Silurian rock samples as inferred from gas chromatographic analyses. The most striking molecular feature is

their uniformity in distribution patterns and their virtual maturity independence on a molecular level (e.g. samples E44243 and E44256). The saturated hydrocarbon distributions are dominated by low molecular weight *n*-alkanes with maximum peak areas occurring between *n*- C_{14} H_{30} and *n*- C_{18} H_{38}. Heavier *n*-alkanes bearing more than 20 carbon atoms are low in concentration and a steady decrease of *n*-alkanes concentration with increasing chain length is observed. Such distribution patterns are typical for solvent extractable organic matter and crude oils of marine origin (Tissot et al., 1971, 1977). Because of the confirmed marine nature of the organic matter, the predominance of low molecular weight *n*-alkanes might reflect that kerogen break-down reactions of lipid-rich long-chain components, such as waxes, resinites and exinites, occurred, hence yielding low molecular weight hydrocarbons (Connan et al., 1975, Powell et al., 1982, Powell and McKirdy, 1973). Generally, processes leading to a shift in *n*-alkanes distribution from heavy to light components are attributed to a final stage of catagenesis, after the peak of hydrocarbon generation has already been surpassed (Tissot and Welte, 1984). Therefore, this feature might be related to enhanced thermal alteration of the soluble organic matter in both petroleum systems, which is well confirmed by the established maturity data.

Compositional uniformity is also reflected by selected compound parameters, such as odd- over even-numbered n-alkanes (CPI), pristane/phytane ratio (Pri/Phy) and isprenoids/*n*-alkanes ratios (pristane/*n*- C_{17} H_{36}, phytane/*n*- C_{18} H_{38}), listed in Table 6. The carbon preference index, introduced by Bray and Evans, 1961, for the carbon atom range 23 to 25 are close to or slightly less than 1. CPI values significantly greater than 1 and generally attributed to low mature organic matter of terrestrial origin (Louis and Tissot, 1967, Albrecht et al., 1976) are absent in the *n*-alkane fraction of samples from the present study. However, the use of the CPI as organic source input indicator is problematic because most of the aquatic organisms synthesize odd-carbon numbered chains in the low molecular weight range, but not in the C_{25}- C_{33}, which defines generally the continental contribution. Moreover, sediments composed only of marine source material have a CPI of 1 at the surface and their CPI values do not change with depth (Tissot and Welte, 1984; Hunt, 1996). The *n*-paraffins are subjected to secondary processes including biodegradation, thermal maturation and migration (Tissot and Welte, 1984; Peters and Moldowan, 1991) and even over odd predomin-

Tab. 6: Molecular maturity parameters for the saturate hydrocarbon fraction of Devonian and Silurian solvent extracts (top) and crude oils (bottom). Equations for calculation of ratios are given in the appendix. Samples with asterisk are condensate samples. nd, not defined.

Sample ID	Well name	Depth (m)	Age	T_{max} (°C)	R_o (%)	CPI-1 (23...25)	CPI-5 (25...31)	LHCPI	Pr/ n-C_{17}	Ph/ n-C_{18}	Pri/Phy
E44236	BK-2	3992.00	Famennian	427	0.94	1.02	1.07	4.30	0.37	0.26	1.69
E44240		4212.00	Frasnian	440	nd	1.00	1.03	13.81	0.35	0.28	2.10
E44243		4227.00	Frasnian	447	1.03	1.02	1.04	8.80	0.27	0.22	1.80
E44247		4371.00	Frasnian	463	1.13	0.96	1.02	27.70	0.32	0.26	1.94
E44249		4412.00	Frasnian	461	0.96	0.97	1.02	64.97	0.35	0.28	2.21
E44254	BRD-4	4570.00	Silurian	360	1.81	0.96	1.04	25.37	0.41	0.35	1.70
E44256		4587.00	Silurian	548	nd	1.01	1.07	19.55	0.32	0.32	1.26
E22263		4692.00	Silurian		2.09	1.04	1.02	11.61	0.37	0.29	1.93
E44267		4719.00	Silurian	521	2.02	0.93	1.00	2.03	0.33	0.26	1.79
E44272	WT-1	3754.00	Famennian	446	nd	1.06	1.10	3.46	0.16	0.07	2.79
E44274		3763.00	Famennian	449	0.88	1.03	1.07	3.69	0.26	0.22	1.31
E44276		3792.00	Famennian	447	nd	1.05	1.08	3.70	0.13	0.08	1.76
E44280		3886.00	Frasnian	432	0.94	0.95	1.25	220.71	0.46	0.41	1.23
E44281		3924.00	Frasnian	438	nd	0.99	1.35	85.97	0.45	0.41	1.16
E44284		4117.00	Givetian	447	0.98	1.01	1.07	8.71	0.25	0.22	1.09
E44288		4220.00	Emsian	441	0.96	0.97	1.24	143.16	0.45	0.41	1.25
E44293	HSN-1	2620.00	Silurian	429	nd	1.03	1.04	13.04	0.41	0.32	1.51
E44297		2660.00	Silurian	438	1.08	1.00	1.04	18.96	0.33	0.24	1.92
E44299		2682.00	Silurian	436	nd	1.05	1.03	14.35	0.40	0.33	1.83
Oils											
	Fields		*Res. age*	*°API*							
E44516	GT-35		Triassic	41.48	1.01	1.02	4.92	0.24	0.24	1.50	
E44517	HC-102		Triassic	43.21	1.02	1.03	5.17	0.24	0.24	1.46	
E44518	KA-2		Triassic	44.51	1.01	1.04	4.78	0.35	0.35	1.61	
E44519	RA-8		Triassic		1.05	1.05	19.78	0.19	0.19	1.85	
E44520	RC-1		Triassic		0.96	1.05	19.68	0.26	0.26	2.41	
E44521	RNSE-3		Triassic	30	1.01	1.03	3.92	0.38	0.38	1.40	

ance, if it existed, was mostly lost due to maturity effects. For example, hydrocarbons from high wax spores which have been reported, particularly in Silurian source rock (Richardson and Ioannides,1973), are probably diluted by hydrocarbons

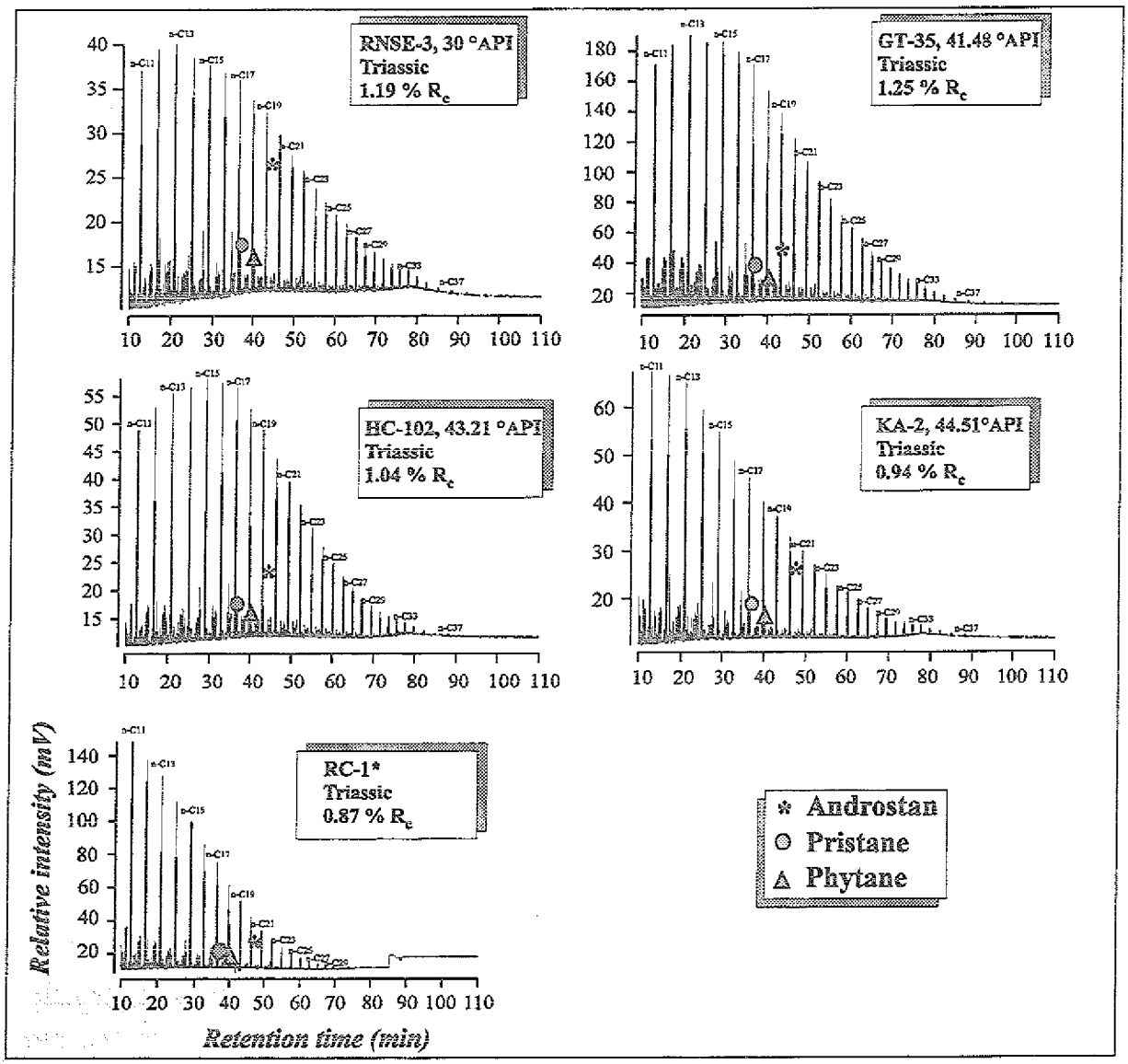


Fig. 30: Gas chromatography fingerprints showing distribution patterns of *n*-alkanes and isoprenoids (pristane and phytane) of selected crude oil and condensate(*) samples. Description includes well name, productive reservoir and oil gravity. 5α-Androstan, internal standard

resulting from kerogen degradation. Pristane and phytane which are commonly considered to be mainly derivatives of the phytyl side-chain of the chlorophyll molecule (e.g. Maxwell et al., 1972; Illich, 1983), and of which the abundance is local-environment dependant (Tissot and Welte, 1984) are present in all the samples, suggesting that the biological source did use chlorophyll to synthesize cellular carbon.

In coal and terrestrial organic matter, the oxidation of phytol into phytanic acid occurs to a large extent during the initial aerobic stage of plant decay, thus resulting into a progressive generation of pristane by decarboxylation of phytanic acid and therefore, in an increase of the pristane/phytane ratio (e.g. Connan, 1974; Powell and McKirdy, 1975). However, when catagenesis proceeds, the acyclic isoprenoids are progressively generated and an increase of the pristane/phytane ratio is observed. Therefore, the pristane/phytane ratio is also used as a maturity indicator (Tissot and Welte,1984). Pristane/phytane ratios range somewhere between 1 and 3 in the samples studied here and never exceed this latest value, as typical for marine source rocks with some terrestrial input (McKirdy et al., 1983). As has been suggested by Alexander et al. (1981), maturity can cause an increase of pristane/phytane ratios and might be quite high as a result of source material not depending so much on the nature of the depositional environment. Pristane/n- C_{17} H_{36} and phytane/n- C_{18} H_{38}, to a certain extent influenced by maturity effects (Peters and Moldowan, 1991), are all below 0.5 suggesting deposition under marine conditions.

Figure 30 depicts the *n*-alkane distribution patterns of crude oil and condensate samples from fields located in the basin. The *n*-alkane fraction of all the samples revealed patterns with short chain components, generally encountered in normal mature oils with maximum peak heights situated between C_{11} and C_{15}. It should be pointed out that due to the light character of the samples, their molecular composition might have been slightly affected by evaporation losses, particularly of the lightest compounds. In fact, after precipitation of the asphaltene fraction, the crude oil samples were exposed to evaporation for 24 hours at room temperature. In all the samples CPI values are around 1 and there is a limited abundance of hydrocarbons in the C_{25}-C_{33} range. Pristane/phytane ratios are greater than 1, and range from 1.4 to 2.41. Such features might prove that hydrocarbons have been originated from source rocks deposited under marine conditions. Obviously, they originate from a siliciclastic source rock. There are no indications for a source of carbonate and/or evaporite facies which commonly result in pristane/phytane ratios below unity.

In summary, the observed predominance of low molecular-weight material in the source rock extracts as well as in the oil samples may be a result of thermal alteration, rather than an imprint of the original organic input. The high concentration of low

molecular weight *n*-alkanes in the soluble organic matter and crude oil could be interpreted as the result of thermal cracking reactions which generally dilute the higher molecular weight n-alkanes due to additional hydrocarbon formation (Tissot and Welte, 1984). This hypothesis of an overall high degree of thermal alteration of the saturated fraction, as suggested by their *n*-alkane distribution fingerprints, might also be derived from selected compound ratios such as CPI and pristane/phytane (Tab. 6).

b/2 Steranes and Triterpanes (Biological Markers)

Biomarkers are lipid-derived compounds that can be linked to particular biological precursor molecules found in recent, as well as in ancient sediments. The most stable biological marker molecules are preserved over geological time even at great depth (Tissot and Welte, 1984). The less stable molecules suffered degradation in response to increasing depth and temperature (Tissot and Welte, 1984). Furthermore, biological marker molecules are increasily diluted by newly formed hydrocarbons without biological fingerprint. The biomarker molecules are synthesized by plants or animals of which much of their carbon skeleton is preserved, and which are linked to some major structural types such as cyclic or acyclic terpenoids and steroids (Tissot and Welte, 1984).

The differentiation and assessment of rock extracts and crude oils with respect to source rock attributes (lithology, depositional environment, kerogen type and maturity) increased greatly in the recent years (Seifert and Moldowan, 1978, 1980; Peters and Moldowan, 1991; Peters and Moldowan, 1993). Ratios of certain saturated and aromatic biomarker compounds are some of the most commonly used thermal maturity indicators. These maturity parameters result from two types of reactions involving cracking reactions (including aromatisations) or isomerisations at certain „asymmetric" carbon atoms. Isomerisations are more commonly used (Peters and Moldowan, 1993). The most commonly used isomerisation reactions are those involving hydrogen atoms at the C-22 position in hopanes and at the C-20 position in steranes.

GC-MS data (tricyclics, polycyclics and steranes) were used to conduct a more detailed characterisation of the source rock intervals and crude oils. In general, all the samples have shown very low biomarker concentrations relative to the *n*-paraffins (Fig. 28). A comparison between the relative abundance of hopanes and steranes reveals a

Tab. 7: Peak identification of the hopane (m/z 191) and sterane (m/z 217) compounds.

Hopanes
a, 18α(H)-Trinorneohopane
b, 17α(H)-Trinorhopane
c, 17α(H)-Norhopane
d, Normoretane
e, 17α(H)-Hopane
f, 17α(H)-Homohopane (22S)
g, 17α(H)-Homohopane (22R)
i, j, 17α(H)-Bishomohopane (22S and 22R)
k,l, 17α (H)-Trishomohopane (22S and 22R)
m,n, 17α (H)-Tetrakishomohopane (22S and 22R)
o,p, 17α (H)-Pentakishomohopane (22S and 22R)
Steranes (m/z 217)
A, 13β,17α-Diacholestane (20S)
B, 3β,17α-Diacholestane (20R)
F, 14α, 17α-Cholestane (20R)
G, 14β, 17β-Cholestane(20R)+ 24-Ethyl-13β, 17α-Cholestane (20S)
H, 14β,17α-Cholestane (20S)+ 24-Methyl-13α, 17β-Diacholestane (20R)
I, 14α,17α-Cholestane (20R)
J, 24-Ethyl-13β,17α-Diacholestane (20R)
M, 24-Ethyl-14α,17α-Cholestane (20S)
N, 24-Ethyl-13α,17β-Diacholestane (20R)+24-Methyl-14β,17β-Cholestane (20R)
P, 24-Methyl-14α,17α-Cholestane (20R)
Q, 24-Methyl-14α,17α-Cholestane (20S)
R, 24-Ethyl-14β,17β-Cholestane (20R)
S, 24-Ethyl-14β,17β-Cholestane (20S)

slightly greater abundance of hopanes. Low amounts of steranes and low sterane/hopane ratios are thought to be indicative of non-marine material and/or microbial activity (Tissot and Welte, 1984; Peters and Moldowan, 1993). Conversely, high amounts of steranes combined with high sterane/hopane ratios are considered to be typical of marine organic matter; planctonic and or benthic algae being the major contributors (Moldowan et al., 1985).

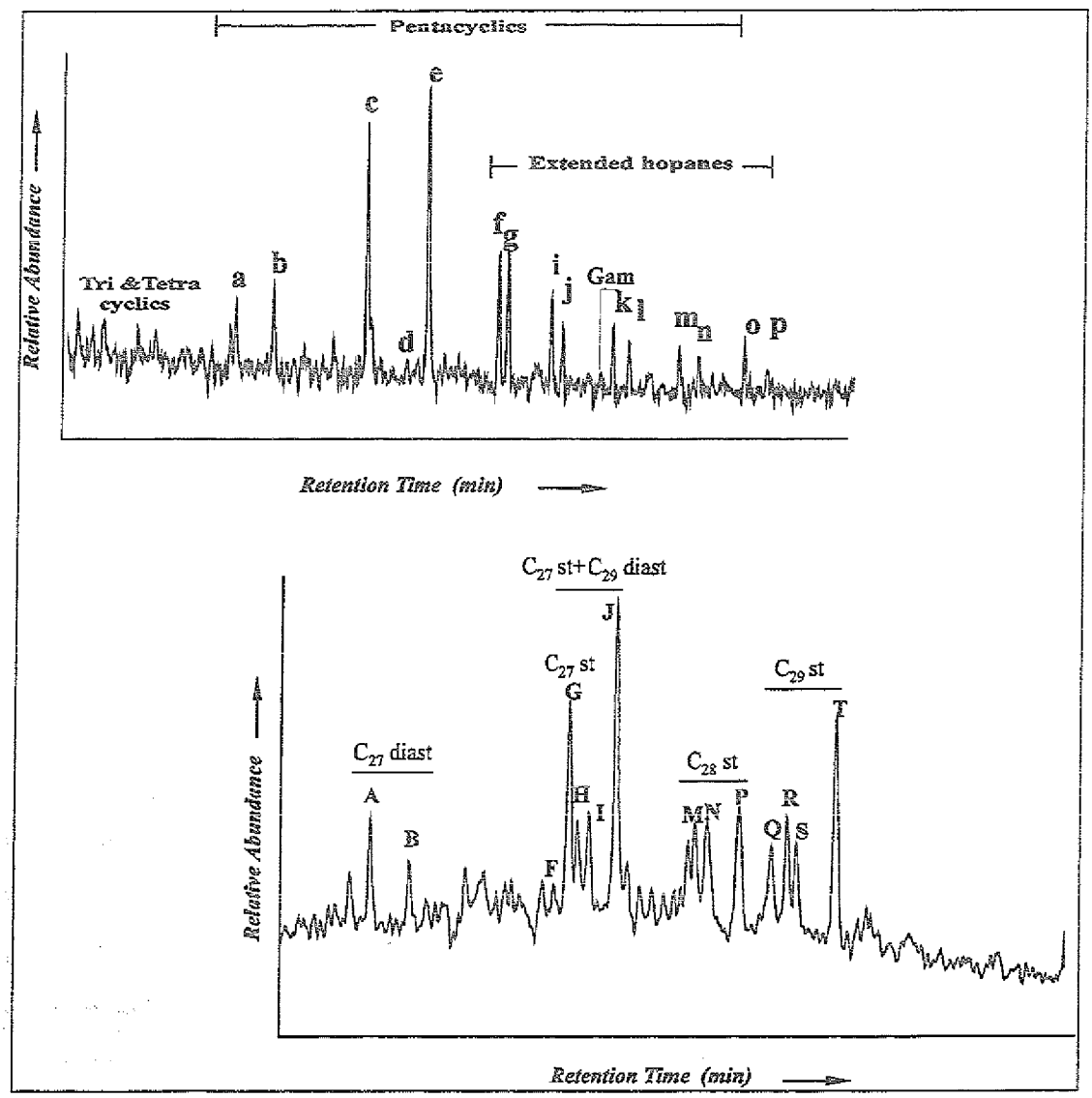


Fig. 31: Hopane (above) and sterane (below) distribution patterns of Frasnian sample (E 44247, well BK-2, 4371 m). See Table 7 for peak identification. Gam, Gammacerane. st and diast are steranes and diasteranes, respectively.

The identification of the terpanes and tentatively of the regular steranes are given in Table 7, whereas Table 8 summarizes the biological marker compound ratios for rock extracts and oils. It should be noted that the low biological marker concentrations,

particularly those of the steroids, prohibited unfortunately the calculation of the complete set of compound ratios. The maturity, as expressed by hopane isomerisation ratios (22S/22S+22R) of all the samples are around 0.6 (Tab. 8), showing an „equilibrium value" and thus indicating that the oil window has been reached or surpassed (Seifert and Moldowan, 1978). Two samples (E44274 and E44276), however, exhibit a C_{32} 22S/22S+22R ratio of less than 0.5. This is strange because extended hopanes have generally reached their equilibrium.

Figures 31 and 32 show the terpane and sterane distribution of selected organic-rich samples from the Frasnian and the Silurian radioactive zones, as determined from GC-MS analysis, and represented, respectively, by the m/z 191 and m/z 217 ions. Almost the same fingerprints are observed. The tricyclic terpanes in the range of C_{20} to C_{28} which are thought to represent evidence for the contribution of higher plant material (Tissot and Welte, 1984) are nearly absent. Pentacyclic terpanes which belong to the hopane series, and including molecules from C_{27} to C_{35} are dominated by C_{30} hopane and a full range of C_{31} to C_{35} homohopanes. The distribution and occurrence of C_{31} to C_{35} homohopanes, derived from bacteriohopanetetrol, are paleoenvironmental indicators (Peters and Moldowan, 1991). The C_{31}- C_{35} homologues show a regular stair-step progression, typical for source rocks deposited under marine shelf conditions (Peters and Moldowan, 1991, 1993). The resulting very small homohopane indices (C_{35}/C_{31}-C_{35}, Tab. 8) suggest that anoxic conditions did not occur at the time of deposition (Peters and Moldowan, 1991). However, suboxic to dysoxic bottom water may have existed (Tyson and Pearson, 1991). The occurrence of hopanes reflects the contribution of prokaryotic membranes present in bacteria and blue-green algae (Ourisson et al., 1979; Tissot and Welte, 1984; Peters and Moldowan, 1993). Gammacerane, which is indicative of hypersaline environments (Ten Haven et al., 1988), is present in all the samples, but in low to very low concentrations indicating a shaly rather than a highly saline calcareous or evaporitic source rock.

The norhopane (C_{29})/ hopane (C_{30}) ratio is less than 1 and the C_{33}- C_{35} extended hopanes are relatively low in concentration. High concentrations of C_{29} norhopane and a considerable enrichment in C_{33}- C_{35} extended hopanes, as a result of preferential preservation in the presence of sulfur, are frequently observed in sediments with limited iron availability such as carbonates and evaporites (Peters and Moldowan,

Tab. 8: Hopane biological marker compound ratios for selected Devonian and Silurian solvent extracts (top) and crude oils (bottom). The highlighted identification numbers are samples from the Silurian and the Frasnian radioactive zones. Samples with asterisk are condensate samples. nd, not defined.

Sample ID	Well name	Depth (m)	Age	22S/ 22S+22R	Ts/ Ts+Tm	Hop/ Hop+Mor	C35/ C31-C35	Ga/ Ga+Hop	Ga/ Hop
E44243	BK-2	4371.00	Frasnian	0.62	0.45	0.95	0.10	0.00	0.00
E44249		4412.00	Frasnian	0.57	0.51	0.87	0.14	0.12	0.14
E44256	BRD-4	4587.00	Silurian	0.61	0.53	0.90	0.11	0.06	0.06
E22263		4692.00	Silurian	0.54	0.50	0.89	0.09	0.13	0.16
E44267		4719.00	Silurian	0.61	0.51	0.90	0.13	0.14	0.16
E44272	WT-1	3754.00	Famennian	0.52	0.85 ?	0.82	0.08	0.21	0.27
E44274		3763.00	Famennian	0.47	0.85 ?	0.72	0.12	0.23	0.30
E44278		3830.00	Famennian	0.42	0.86 ?	1.00	0.00	0.15	0.17
E44280		3886.00	Frasnian	0.61	0.48	0.90	0.13	0.13	0.15
E44281		3924.00	Frasnian	0.62	0.55	0.88	0.08	0.14	0.16
E44284		4117.00	Givetian	0.59	0.53	0.88	0.13	0.11	0.13
E44288		4220.00	Emsian	0.56	0.53	0.86	0.13	0.08	0.09
E44305	HSN-1	2620.00	Silurian	0.60	0.48	0.91	0.12	0.10	0.11
E44307		2660.00	Silurian	0.60	0.39	0.91	0.12	0.10	0.11
Oils									
	Fields		*Res. Age*						
E44516	GT-35		Triassic	nd	nd	nd	nd	nd	nd
E44517	HC-102		Triassic	0.69	0.58	0.85	0.09	0.23	0.30
E44518	KA-2		Triassic	0.61	0.66	0.90	0.07	0.07	0.08
E44519	RA-8*		Triassic	0.54	0.48	0.86	0.09	0.16	0.19
E44520	RC-1*		Triassic	0.49	0.54	0.85	0.08	0.21	0.27
E44521	RNSE-3		Triassic	0.63	0.49	0.91	0.07	0.1	0.11

1993). Oleanane which indicates the influx of angiosperms is absent. This is not surprising, since angiosperms only developed in the Cretaceous.

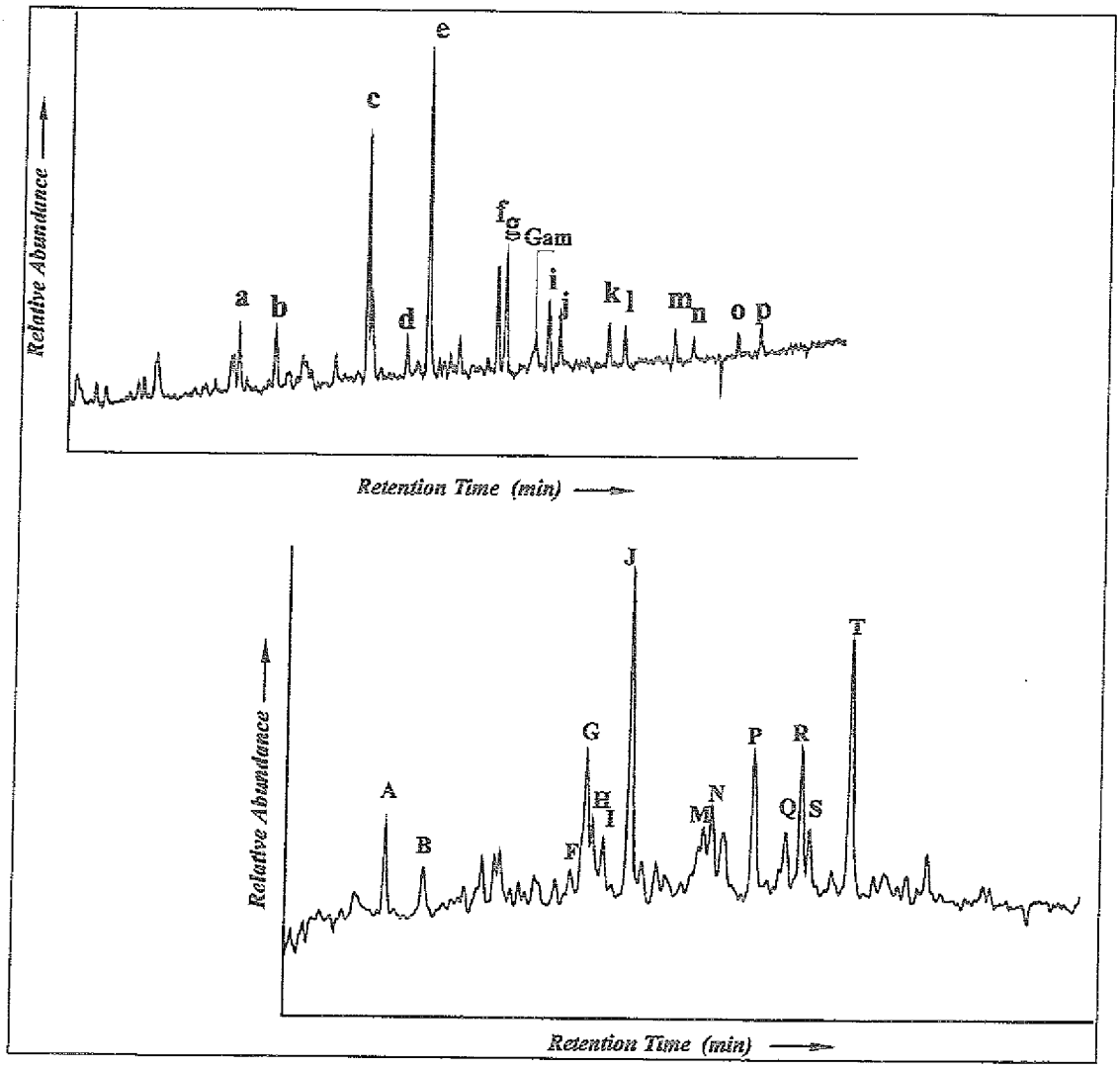


Fig. 32: Hopane (above) and sterane (below) distribution patterns of a Silurian sample (E 44267, well BRD-4, 4719 m). See Table 7 for peak identification. Gam, Gammacerane

The steranes which are thought to be mainly sourced from eukaryotic organisms in sedimentary organic matter (e.g. Ourisson et al., 1979) are dominated by C_{29} regular steranes, especially the ααα20R epimers, with high concentrations relative to the C_{27} and C_{28} regular steranes. High concentrations of C_{29} steranes originally were proposed to be associated with a terrestrial contribution of organic matter to sediments and crude oils (Huang and Meinschein, 1979; Robinson, 1987). However, it was subsequently noted that such distributions are typical for Palaeozoic strata in general, particularly for those deposited prior to the development of higher plants (Rullkötter et al., 1986;

Tissot and Welte, 1984). Therefore, the terrestrial origin of the C_{29} steranes has lately been questioned. Especially, the occurrence of C_{29} sterols in lower Palaeozoic and Precambrian sedimentshas lead to the conclusion that there must be unknown marine

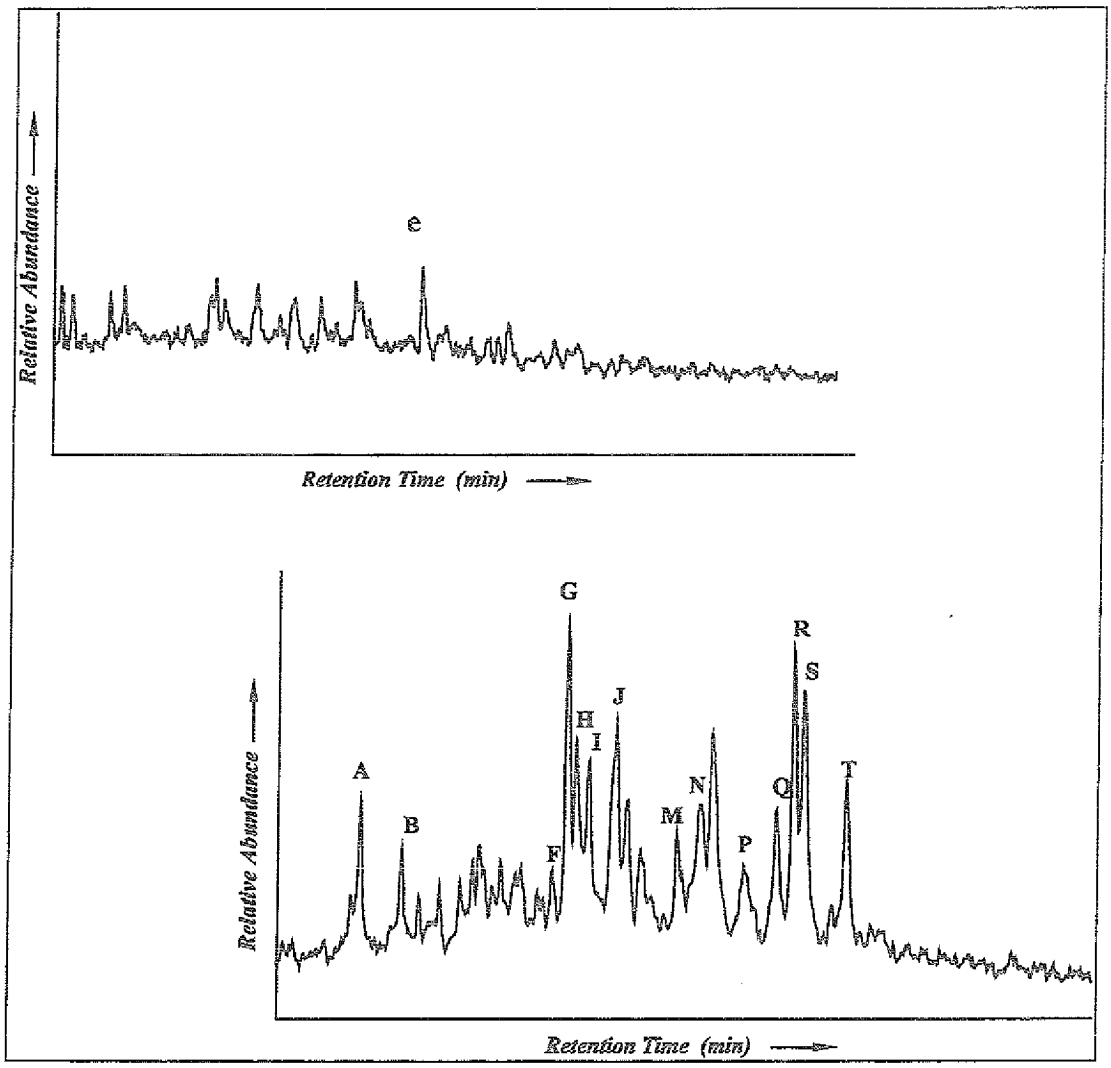


Fig. 33: Hopane (above) and sterane (below) distribution patterns of a crude oil sample from well RNSE-3 (E44521). See Table 7 for peak identification.

organisms which do contribute to such carbon-skeleton precursor molecules (Volkman, 1986, 1988). In addition, Nichols et al. (1990) showed that large amounts of C_{29} sterols are produced by marine diatoms during the spring bloom in cold Antarctic waters. Cyanobacteria (blue-green algae) could also contribute to the C_{29} steranes as suggested by Matsumoto et al. (1982) and Fowler and Douglas (1987). C_{30} sterane, a dinoflagellate algal marine indicator is present in all sample but in very low concentrations. Although their presence in Palaeozoic sediments was confirmed by microscopic analyses of some of the Devonian samples, this fact is not surprising

because the bloom of dinoflagellates occurred during Mesozoic and Tertiary time (Tissot and Welte, 1984). All the samples contain variable amounts of C_{27} and C_{29} diasteranes, indicating clay catalysis in their source rocks (Sieskind et al., 1979).

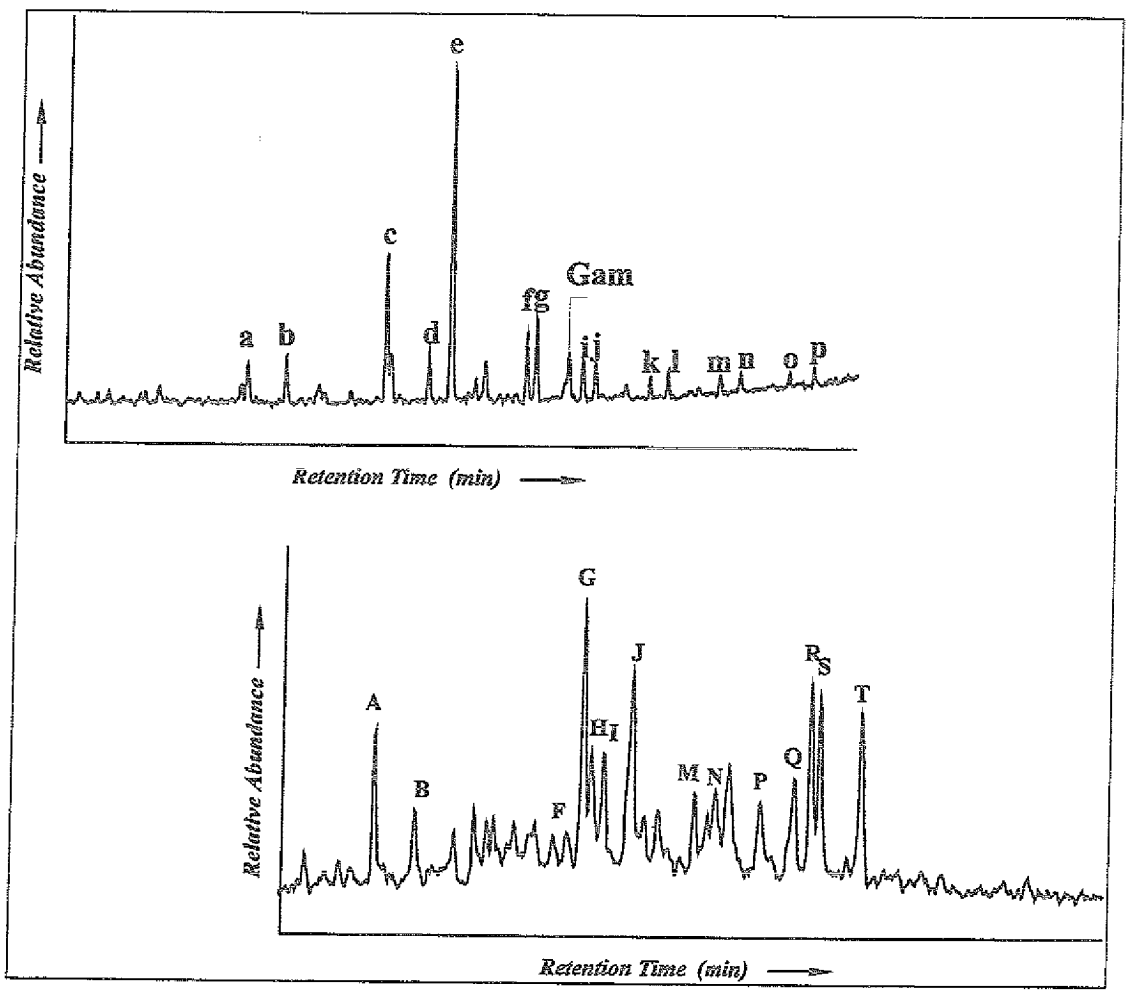


Fig. 34: Hopane and sterane distribution patterns of a condensate sample from well RA-8 (E44519). See Table 7 for peak identification. Gam, Gammacerane

Based on these observations it can be concluded that both the Frasnian-Famennian and Silurian source rock formations contain mainly marine organic material deposited under suboxic to dysoxic marine shelf conditions. Remains of bacteria are also common . In fact, extracts do not have high hopane /sterane ratios which are common in terrestrial organic matter.

Figures 33 and 34 depict the terpane and the sterane distribution patterns of the crude oil and condensate samples analysed in this study. All the samples have reached equilibrium as expressed by the C_{32} 22S/22S+22R ratio of about 0.6. Such values are also observed in the source rock extracts (Table 6). An important geochemical feature

observed here is that in almost all the oil samples, except the KA-2 oil from the north-eastern part of the basin, the concentration of biomarkers, particularly the triterpanes, is very low or near the detection limit. Biological markers are more abundant in the condensate samples. This is surprising and the opposite should be observed, if we do consider that precursor molecules suffer thermal degradation (Tissot and Welte, 1984). Possibly, this condensate is the result of physical separation (migration) processes rather than due to a generation feature.

The most representative oil samples are generally characterised by similar biological distribution patterns and show great analogies with the Frasnian-Famennian and the Silurian rock extracts. The m/z 191 chromatograms are dominated by C_{30} hopanes and extended C_{31} to C_{35} homohopanes. On the other hand, the C_{29} regular steranes dominate the m/z 217 mass spectra. The fingerprints revealed that all the samples were sourced from aquatic organic matter.

By a detailed examination certain distinctive features can be observed and the samples can be classified in two groups. The first group includes the oil samples GT-35, HC-102, and RNSE-3 (Fig.1). Group 2 includes an oil and 2 condensates represented, respectively, by the samples KA-2, RC-1 and RA-8. The difference between the two groups is due to the fact that group 1 contains much lower terpane concentrations than group 2. This effect is obvious and is shown by the defocusing caused by the high concentration of paraffins compared to biomarkers (Peters and Moldowan, 1993). This observation was also reported for some source rock extract samples, particularly those from the Upper Devonian formation. The sterane fingerprints do not clearly separate the samples into distinct genetic type families, although there is a tendency that group 2 is slightly enriched in steranes. In view of the present observations and in the light of the geology of the area, group 2 is likely to have a Silurian source rock. This group correlates well with the group 3 oils defined by BHP Petroleum in the Illizi Platform and attributed to the same source rock. The group 1 oils, on the other hand, correlates with group 2 defined by the same company. A contribution of both Silurian and Upper Devonian has been proposed. However, if the latter source rock did contribute to the group 2 oils, a long-distance lateral migration should have occurred, because the presumed source rock is eroded in this part of the basin, where only the Silurian is preserved (Fig.7). It is more likely that these oils have also a, yet unproved, Silurian

origin. Phenomena such as crude oil alteration tend do obscure the original character of the oils, and affect, therefore, crude oil correlation studies.

5-3 Summary

Based on geological considerations and the geochemical results, it follows that:

- The organic-rich units of the Silurian and Frasnian-Famennian formation were deposited under dysaerobic to anaerobic conditions, developed within a continental shelf environment during maximum transgression of an epicontinental sea. Fine-scale laminations in the organically-rich members are very common and suggest a restricted low energy environment associated with isolated bathymetric lows. Fully euxinic conditions may have occurred in the organic-rich basal radioactive members of both formations (subfacies A and C1 of Figure 9) making them the most important source rock horizons. The Silurian radioactive member is characterized by a complete absence of any benthos or nectobenthos (ammonoid) species, and by the presence of pelagic organisms such as graptolithes which are tolerant in extreme marine conditions. In the absence of benthos, sulfur bacteria mats coated the sediments until fully anoxic conditions were established (Wignall, 1994). The presence of some benthos species in the Frasnian radioactive member, on the other hand, indicates a deposition in partly oxygenated water. An episodic colonisation may have reduced the anoxia, although several bivalve species can also withstand dysoxic conditions (Pearson and Rosenberg, 1978). Terrestrial organic matter is low in abundance, suggesting low continental run-off at the time of deposition. High planktonic productivity in the surface water and restricted circulation resulted in a deposition of organically-rich oil prone source beds. The relatively high hopane to sterane ratio indicate extensive reworking of the primary organic matter during early diagenesis by anaerobic bacteria. The regressive sequences (i.e. Famennian and Upper Silurian) are less organic-rich units, although measured C_{org} values may underestimate the original organic carbon content of a given formation. Those effects are particularly pronounced for mature formations that have generated and expelled hydrocarbons.

- The Frasnian source rock is in the main zone of hydrocarbon generation (oil/wet gas zone) in most of the Berkine Basin. Except for the northern part of the basin, the

Silurian hot shale formation, on the other hand, is overmature with respect to oil generation, i.e. in the gas generation zone.

- Aromatic maturity parameters such as the alkylnaphthalenes and the alkylphenanthrene ratio (MNR and MPI-1) may be useful for the assessment of the maturity of the Devonian and and post-Devonian stratigraphic units. For the pre-Devonian sediments, due to the small set of samples analysed, further geochemical investigations could not be carried out in the context of the present work. Future investigations would be very helpful.

- Although some small distinctive features can be observed, the rock extracts and oils exhibit insufficient variability in their molecular composition that would allow assignements of genetic relationships between the oil samples and the Frasnian and the Silurian source rocks. Phenomena such as organic facies similarities and alteration as well as maturation effects tend to obscure the original character of the bitumen and oils and affect, therefore, accurate correlations. Nevertheless, based on geological considerations, it is possible to speculate that most of the oils analysed in this study have a Silurian source rock as origin. The contribution of the Frasnian source rock to the hydrocarbon pools situated along the Amguid El Biod-Hassi Messaoud structural trend would necessitate a long distance lateral migration which implies the absence of any permeability barriers (i.e. lithological and structural seals). The 2D basin modelling study (Chapter 6.4) should validate or invalidate such a speculation.

6. Basin Modelling

6-1 Principles of Computer-Aided Basin Modelling

Integrated geological modelling, using mathematical models is a fundamental technique in petroleum exploration. In particular, deterministic (as opposite to probabilistic) models attempt to quantify the formation and development of sedimentary basins based on the best input parameters including sedimentology, stratigraphy, paleogeography, hydrodynamics, geothermics and organic geochemistry (Ungerer et al., 1984; Yalcin et al., 1988; Poelchau et al., 1997). Once the geologic evolution of the basin is optimized by minimizing differences between computed and measured data, the simulation tries to quantify generation and expulsion, migration and areas of hydrocarbon charges by coupling the equations which describe the compaction history and subsequent overpressure development and the thermal history and subsequent hydrocarbon generation history.

In basin modelling, organic maturity parameters such as vitrinite reflectance are used to optimize temperature histories. Models for vitrinite reflectance prediction using chemical kinetic approaches were provided by Larter (1989), Burnham and Sweeney (1989) and Sweeney and Burnham (1990). The geochemical aspects are provided by Tissot and Espitalié (1975), Tissot et al. (1987), Burnham and Sweeney (1988), Ungerer (1990) on the kinetics of petroleum generation and expulsion; Ungerer et al. (1990) on basin-scale modelling of fluid flow, and Welte (1987), England et al. (1987), Durand (1988) and Schowalter (1989) on the physics of petroleum migration.

The techniques of basin modelling concepts and approaches are well described by Poelchau et al., 1997 and Yalcin et al., 1997 which can be taken as references for further information.

6-1-1 Application and Material

One of the fundamental tasks in basin modelling is to investigate subsidence and erosional periods and their relationship to temperature, the most critical parameter (Tissot and Welte, 1984), and hence hydrocarbon generation. It is widely accepted that the reliability of migration and hydrocarbon charge depends on the reliability of the modelled hydrocarbon generation history.

A total of eight key wells from different parts of the Berkine basin were subjected to 1D numerical simulations in the present study. These are respectively BK-2, WT-1, SF-1, BBK-1, BRD-4, HAD-1, TZM-1 and KA-1bis (Fig. 1). Most of these wells were drilled on compressional and inversion anticlines or on extensional fault block structures. Four of these wells (BRD-4, WT-1, BK-2 and SF-1) were used for the reconstruction of the 205 km cross-section for which detailed stratigraphic and structural interpretation was established. The cross section was subjected to a 2D modelling study, notably for the reconstruction of sedimentation, paleopressures and those factors related to hydrocarbon generation and migration.

The reconstruction of the geological cross section used for the 2D basin modelling was based on the interpretation and analysis of combined seismic lines and a data set of 11 wells distributed along the transect (Fig.35). Despite the thick Mesozoic section (more than 3500 m), the penetration energy was good and an Ordovician reflector was observed locally at up to 4000 ms two-way travel time. Major seismic events (Fig. 8) were identified by correlating formation tops in the wells to seismic data. Two-way travel time values were read from the seismic data and then converted to depth and thickness, respectively, by using mean well velocity-depth relationships. The interpolation between the wells was achieved by using static velocity data which provide reasonable information about the geometry of the basin.

PDI/1D (Pre Drilling Intelligence, version 2.2) and PetroMod/2D (version 3.1) numerical programs developed by IES (Integrated Exploration Systems, Jülich, Germany) were applied in this study. The 1D results are quantified for a single sedimentary section (i.e. well) using a finite difference method (Wygrala, 1989). The PetroMod program, on the other hand, quantifies parameters in basin evolution for a finite element grid (FEM) that is established for a series of defined grid points (i.e. wells or pseudo-wells) and layers (or events).

A detailed description of the theoretical backgrounds of both programs is given in the reference user manuals.

6-1-2 The Conceptual Model

The conceptual model in basin modelling is defined as the description of the formation and evolution of a given sedimentary basin (Welte and Yükler, 1881). The conceptual

model is, therefore, based on the geological framework of the study area. Ist eleaboration requires at a first basic step a stratigraphic analysis of the basin sedimentary fill. In this manner, the sedimentation history is subdivided into a series of stratigraphic units which were deposited during a certain period and refered to as events. Hence, each event represents a time span during which either deposition (sediment accumulation), non- deposition (hiatus) or sediment removal (erosion) takes place. In the same way, structural and tectonic events, such as faulting, fracturing, salt doming and intrusion of volcanic bodies can be assigned in the conceptual model.

The basic geological model used in the present study is summarized in Table 9. The model briefly described here, segregates the major phases which characterise the basin development and evolution. After the peneplanation of the Precambrian igneous and metamorphic basement, widely clastic, both marine and continental Cambrian to Carboniferous sedimentation occurred (Figs. 8 and 35). During this first sedimentation cycle, no substantial interruption in sedimentation occurred, except for some minor erosional events during the Late Ordovician and Late Givetian-Early Frasnian.

After the Hercynian movements, which took place during Late Carboniferous time, the basin was subjected to erosion for a period of more than 50 my during Permian-Triassic time. Post-Hercynian and Triassic subsidence led to the development of a new sedimentation cycle from Upper Triassic (Keuper) to Neogene (Chapter II). This second sedimentation cycle is also characterised by some minor erosional events occurring after the Alpine (Eocene) and Pliocene uplift movements, and locally by substantial erosion after the Austrian orogenic phase, which occurred at Pre-Aptian time.

Detailed chronostratigraphic discretization led to a maximum of 49 events used in 1D models. Because of some limitations of PDI/1D, the 1D models were constructed only for the time from the earliest Silurian (435 Ma) to recent.

Except for some minor differences the same geological conceptual model was used with respect to 2D modelling. However, pre-Silurian sedimentation is considered. Furthermore, certain erosional events which are considered to be of minor importance to the overall thermal history of the basin (i.e. erosions 1, 2 and 6 in Table 9) are omitted in order to provide simplification. In the same way, certain geological events

are aggregated or generalized in order to reduce computation time. The resulting 2D models contain a total of 60 events, including the erosional events.

Tab. 9: Basic geological conceptual model used in the present study. The identification name, importance, and the duration of the different erosional events are indicated. The events in-between erosions correspond to continuous sedimentation cycles.

Cycle	Events	Erosion Id. name	Age (Ma)	Relative intensity
MESO-CENOZOIC	Quaternary			
	Erosion 6	Pliocene	4-2	Minor
	Oligo-Pliocene			
	Erosion 5	Alpine	42-35	Minor
	Aptian-Eocene			
	Erosion 4	Austrian	124-117	Minor
	Trias-Barremian			
PALAEOZOIC	Erosion 3	Hercynian	286-231	Major
	Frasnian-Carbon			
	Erosion 2	Frasnian	376-373	Minor
	Silurian-Givetian			
	Erosion 1	Taconic	411-409	Minor
	Cambro-Ordovician			
	Basement			

The basic input data, described later in more detail, include absolute age for each event, thickness, lithologies and their physical and thermal properties (e.g. density, compressibility, heat conductivity and heat capacity), paleobathymetric and eustatic change estimates (SWI, sediment water interface temperature), as well as heat transfer (conduction and convection). For the simulation of petroleum generation and the dynamics of petroleum through time in the basin, further input data are required and include the hydrocarbon generation potential (C_{org}, HI) of each source unit, the kinetic model for petroleum generation, and fluid properties (e.g. composition, density, viscosity, heat conductivity and heat capacity).

The calibration of the geological model is achieved by comparing measured parameters with the simulation results (i.e. computed data). Data which are used as calibration parameters include present temperatures, pore pressure and vitrinite reflectance. Parameters which do not offer a direct measure such as heat flow, duration of each event and eroded sediments and their lithology are difficult to constrain. Their

modification during the calibration procedure must be considered as a „ trial and error" until a good match (maximum agreement) is observed between predicted and observed data.

6-1-3 The Horizontal Discretization and the Generation of the Grid Net (2D)

After a well defined geologic time framework has been generated, the 2D profile is further discretized into a series of grid points or pseudo-wells. The horizontal discretization is initially performed by the program. The number of the grid point depends primarily on the length of the section as well as on some important geological features such as truncations, pinch-out, faults and facies changes. The modification of the grid is a user's decision and is a function of the expected objectives of the study. Consideration with respect to computation times have also to be taken into account.

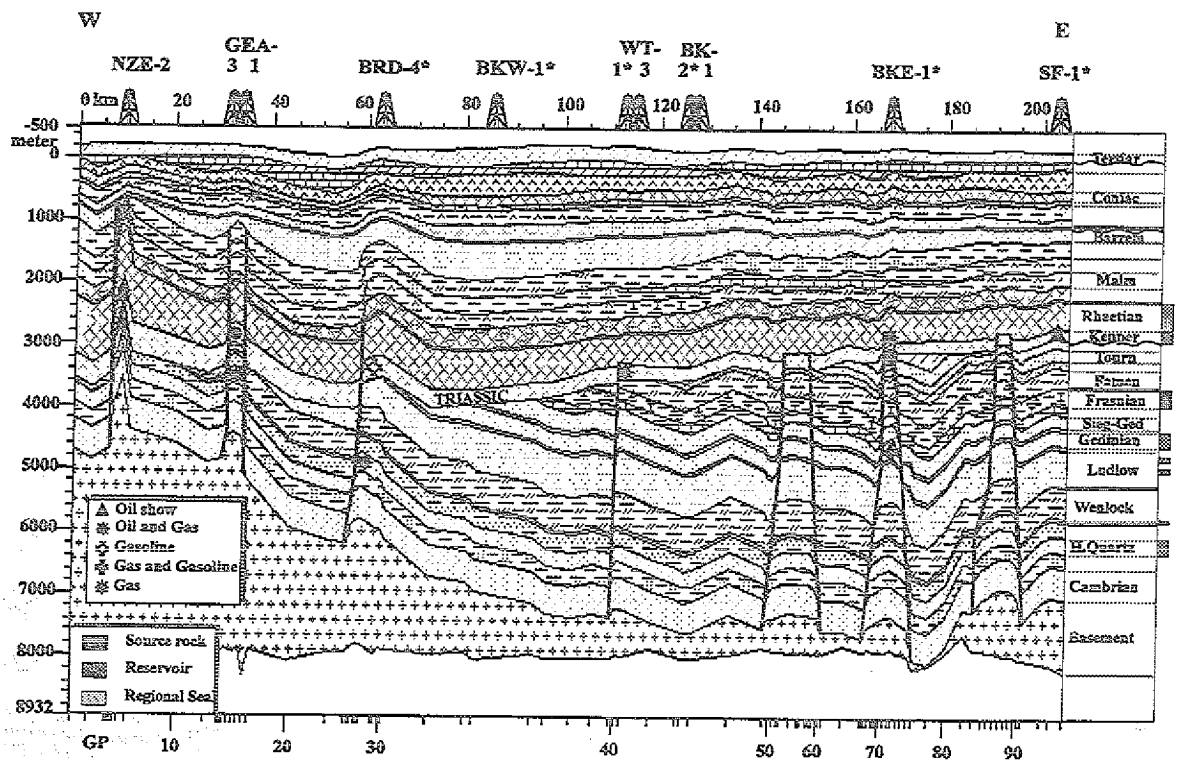


Fig. 35: Geology op the modeled section showing actual hydrocarbon pools and the different plays. Note that the pre-Jurassic sediments are completely sealed by thick salt deposits of Liassic (Hetangian) age.The wells used for calibration (temperature and/or compaction) are designated by an asterisk. Numbers 1-60 identify events used during modelling. Rock types can be find out in Table 17. The position of the section is shown in Figure 1.

The vertical and horizontal discretization resulted here in a 60*95 mesh of finite elements (Fig. 35). The PetroMod finite elements subdivide this geologic framework into a grid net of triangular element cells. Large cells are associated with low resolution; therefore, less computation time is required and vice versa. The input data are incorporated as a function of time and space and stored within each finite grid or triangular element. The numerical quantification of these data allow the interaction between sediment subsidence (i.e. compaction and pressure), heat transfer, temperature evolution with burial and organic matter maturation, generation of hydrocarbons, migration as a consequence of pressure build-up, and accumulation.

6-1-4 Petrophysical Properties of Rocks

The most important physical parameters affecting the basin fill during the basin evolution and leading to the formation of hydrocarbon pools are temperature and pressure and related parameters. Such parameters have a great control on hydrocarbon generation, the dynamic of oil and gas and water circulation (Tissot and Welte, 1984; Doliguez et al., 1986). The numerical simulation of thermal history in sedimentary basins consists of 2 basic processes: 1) the simulation of the mechanical processes of compaction including pressure development, and 2) the simulation of thermal processes. The numerical treatment of pressure and temperature requires the quantification of many basic mechanical and thermal properties such as porosity, permeability, compressibility, thermal conductivity and heat capacity.

a/ Thermal Conductivity and Heat Capacity of Rocks and Fluids

Generally, temperature profiles are not linear and show important variations with depth (Tissot and Welte, 1984). These variations are related mainly to thermal conductivity which depends on the physical and chemical properties of rocks such as lithology, porosity, temperature and pore filling fluids (Blackwell and Steele, 1989; Tissot and Welte, 1984, Poelchau et al., 1997). The variation of temperature with depth is well established by linking heat flow (Q), thermal conductivity (k) and temperature gradient (dT/dz): Q (mW/m^2) = k (W/(m /K))* dT/dz (°K/ km). From this formula, it becomes

evident that thermal conductivity of sediments has a great control on temperature gradients in sedimentary basins as the lower boundary condition (heat flow) is virtually constant with depth. In addition to the rock matrix, another important controlling factor on thermal conductivity is the conductivity of the pore space which is determined by the pore space configuration and its filling fluids (Poelchau et al., 1997, Yalcin et al., 1997). Pore filling fluids characterised by their lower thermal conductivity values compared to those of minerals drastically affect the bulk (or effective) thermal conductivity.

Tab. 10: Petrophysical properties of the main lithotypes used during the 1D simulation procedure (PDI/PC). Data are from IES (1995). φ_o, k and C_w are initial porosity, thermal conductivity and heat capacity, respectively.

Lithology	Density	φ_o (%)	Comp (1E-7/kPa)		k (W/m/K)		C_w (kJ/kg/K)	
	kg/m³		Min	Max	20°C	100°C	20°C	100°C
SHALE	2680	65	60000	10	1.98	1.91	0.213	0.258
SHALEevap	2630	47	7000	10	2.93	2.61	0.210	0.247
SHALEcalc	2688	52	5000	10	2.22	2.09	0.208	0.248
SHALEsilty	2677	46	25000	10	2.05	1.94	0.210	0.254
SHALEsandy	2674	57	9000	10	2.32	2.12	0.205	0.248
SHALE&SAND	2669	52	2800	10	2.65	2.38	0.197	0.236
SANDSTONE	2660	42	2660	10	3.12	2.64	0.178	0.209
SANDsilty	2664	46	1200	10	2.97	2.64	0.188	0.223
SANDshaly	2666	48	1400	10	2.78	2.37	0.190	0.226
SANDcalc	2675	42	600	10	3.35	2.59	0.179	0.209
SAND&LIME	2685	42	400	15	2.93	2.54	0.186	0.215
LIMESTONE	2710	24	300	25	2.83	2.56	0.195	0.223
LIME&EVAP	2625	21	200	20	4.69	3.95	0.193	0.213
LIME&SHALE	2695	53	1500	20	2.39	2.24	0.208	0.246
LIMEshaly	2700	37	550	10	2.51	2.31	0.203	0.237
LIMEmarly	2707	33	300	10	2.63	2.41	0.201	0.235
LIMEdolo	2750	26	180	10	3.18	2.82	0.198	0.226
DOLOMITE	2836	48	250	10	3.81	3.21	0.202	0.229
DOLOevap	2808	23	78	6	3.75	3.20	0.193	0.208
SALT	2160	6	4	1	5.69	4.76	0.206	0.212
EVAPshaly	2585	20	100	10	3.87	3.31	0.200	0.221
EVAPORITE	2540	10	10	1	4.69	3.91	0.194	0.210
Water	1160	0	2	1	0.60	0.68	0.999	1.008

The specific heat capacity is another important parameter during the simulation of thermal processes in sedimentary basins. It defines the ability of a given lithotype to store heat (Yalcin et al., 1997). Together with thermal conductivity, heat capacity of rocks determines the distribution of heat in the basin and, consequently, the maturation

of organic matter and hydrocarbon generation. As temperature increases, heat capacity of rocks increases (Mongeli et al., 1982).

The main lithotypes used during the 1D (PDI/PC) and 2D (PetroMod) simulations and their petrophysical properties are presented in Tables 10 and 11. The petrophysical properties of fluids used during the 2D simulation procedures are listed in Table 11.

It should be pointed out that because of the forward modelling approach, PDI/1D and PetroMod 2D calculate effective thermal conductivities and heat capacities after each stage of burial (i.e. compaction) due to the variations in porosity and temperature. Both programs calculate thermal conductivities and heat capacities by interpolation between values at 20°C and 100°C (Tabs. 10 and 11) and extrapolation to temperatures above 100°C.

Tab. 11: Petrophysical properties of rocks and fluids used during the 2D simulation (PetroMod) procedure. Data are from IES (1995). φ_o, k, C_w, K and A are initial porosity, thermal conductivity, heat capacity, permeability and anisotropy, respectively.

Lithology	Density	φ_o	Comp (1E-7/kPa)		k (W/m/K)		C_w (kJ/kg/K)		K (Log md)		A.K	A.k	Mig	Cap. Pres. Petr (MPa)	
	kg/m³	(%)	Min	Max	20°C	100°C	20°C	100°C	at 5%φ	at 75%φ	(Log)		Sat	at 5%φ	at 75%φ
SHALE	2680	65	60000	10	1.98	1.91	0.213	0.258	-5.50	-1.00	2.50	1.50	0.05	5.00	5.00
SHALEsilty	2677	62	25000	10	2.05	1.94	0.210	0.254	-5.35	-0.70	2.30	1.40	0.05	4.00	4.00
SHALEsandy	2674	57	9000	10	2.32	2.12	0.205	0.248	-4.50	0.00	2.20	1.40	0.05	3.50	3.50
SHALE&SAND	2669	52	2800	10	2.65	2.38	0.197	0.236	-4.00	3.00	2.00	1.30	0.05	2.50	2.50
SHALEevap	2630	47	7000	10	2.93	2.61	0.210	0.247	-8.00	-4.00	2.00	1.40	0.05	10.00	10.00
SHALEcalc	2688	52	5000	10	2.22	2.09	0.208	0.248	-2.50	8.50	2.10	1.40	0.05	4.00	4.00
SHALE&LIME	2695	53	1500	20	2.39	2.24	0.208	0.246	-5.00	6.00	1.90	1.30	0.05	3.00	3.00
SANDSTONE	2660	42	500	10	3.12	2.64	0.178	0.209	-2.00	0.00	1.50	1.10	0.02	0.01	0.01
SANDshaly	2666	48	1400	10	2.78	2.37	0.190	0.226	-4.00	0.00	1.80	1.30	0.03	1.50	1.50
SANDsilty	2664	46	1200	10	2.97	2.64	0.188	0.223	-3.00	0.00	1.70	1.20	0.03	0.50	0.50
SILTSTONE	2672	56	8000	10	2.14	2.03	0.201	0.242	-5.00	0.00	2.00	1.30	0.05	1.50	1.50
SILTsandy	2666	52	3000	10	2.55	2.33	0.192	0.230	-4.50	1.50	1.80	1.20	0.05	1.00	1.00
LIMEshaly	2700	37	550	10	2.51	2.31	0.203	0.237	-4.25	13.25	1.50	1.20	0.05	2.20	2.20
LIMEmarly	2707	33	300	10	2.63	2.41	0.201	0.235	-4.25	13.25	1.20	1.10	0.05	1.00	1.00
LIMEdolo	2750	26	180	10	3.18	2.82	0.198	0.226	-3.25	14.25	1.10	1.10	0.05	1.00	1.00
DOLOevap	2808	23	78	6	3.75	3.20	0.193	0.208	-6.19	6.94	1.07	1.07	0.05	3.76	3.76
SALT	2160	6	4	1	5.69	4.76	0.206	0.212	-16.00	-16.00	1.00	1.00	0.05	199.00	199.00
EVAPshaly	2585	20	100	10	3.87	3.31	0.200	0.221	-13.00	-12.00	1.50	1.10	0.05	20.00	20.00
BASEMENT	2750	5	2	1	2.72	2.35	0.188	0.223	-16.00	-16.00	1.00	1.00	0.05	99.00	99.00
Water	1160	0	2	1	0.60	0.68	0.999	1.008	1.00	1.00	1.00	1.00	0.05	0.01	0.01

	Density (Kg/m³)			Viscosity (mPa*s)			k (W/m/K)	C_w (kJ/kg/K)
	50°C	100°C	150°C	50°C	100°C	150°C	(100-150°C)	
Oil	650	500	450	0.50	0.20	0.10	0.50	0.50
Gas	230	400	450	0.20	0.12	0.10	0.05	0.20

b/ Porosities and Permeabilities

Compaction due to the progressive overburden loading during basin evolution is another important factor in basin modelling, particularly for the simulation of compaction processes. The mechanical processes involved during compaction play an important role not only due to their effect on thermal conductivity and heat capacity, but also as the main driving force for fluid flow (Magara, 1979, Tissot and Welte, 184). Compaction can be described primarily as a function of pore space reduction during the burial of sediments (i.e. %porosity reduction) .

Permeability is the additional controlling parameter in compaction processes. In sediments, permeability is controlled by the effective porosity, the number and type of interconnected pores, and by the nature of the permeating fluid or gas. Permeability generally decreases with decreasing porosity during burial. The porosity- permeability relationship is controlled by primary depositional factors such as grain size, distribution, shape, orientation, packing and surface area (Riecke and Chilingarian, 1974), as well as by secondary factors such as fracturing, cementation and other mineralogical processes (Poelchau et al., 1997).

It should be pointed out that both PDI/1D and PetroMod programs do not use the inverse, isostatic simple backstripping method which decompact layers using porosity versus depth relationships and assuming that porosity reduction with depth is a physical process of water expulsion. In contrast, the observed thickness, lithology and porosity of each sedimentary layer are input data of the program. By forward (past to present) modelling, the evolution of thickness, pore pressure, permeability and water flow velocity are predicted, taking into account the initial porosity, compressibility and the rates of deposition and erosion. The observed and predicted layer thicknesses are then compared, and for simulation runs in which more than 1% difference is observed, the model is re-run in order to optimize the simulation results of the larger thicknesses.

6-1-5 Input Parameters

a/ Thickness and Lithological Data

The thickness and lithology of the different Palaeozoic and Mesozoic units were defined by using well log and seismic data. 23 lithotypes characterize the Berkine

basin sedimentary fill (Tabs. 10 and 11). Generally, the Palaeozoic series are largely clastics, both marine and continental and comprise mainly alternations of clay and sandstone (Figs. 8 and 35). For sediments which are penetrated neither by the wells nor by seismic data, such as the Cambrian, lithologies were defined by correlation with nearby sections.

Another critical point in basin modelling is the definition of lithologies of the eroded formations. Not only the thicknesses of the eroded overburden, but also their lithologies can be of great importance to the overall thermal history of the basin (Littke et al., 1994).

b/ Estimation of the Amount of Eroded Sediments

The estimation of the thicknesses of eroded sediments is another critical point in basin modelling, particularly where large-scale erosion occurred. The stratigraphic sequence of the Berkine basin contains several unconformities which occurred during the evolution of the basin (Fig. 8, Tab. 9). Sediment removal during the Late Ordovician and Middle -Upper Devonian (see Table 9) took place during very short periods (2 and 3 Ma, respectively) and is therefore considered of minor importance to the overall thermal maturity. Because of ist long duration (286-231 Ma) and because the sediments were near their maximum Palaeozoic burial prior to the erosion, sediment removal during the Hercynian orogeny is the most important one. Sediment removal started after the general uplift which began in the middle Carboniferous (Visean) and reached its climax during the Stephanian as a result of the Variscan orogeny. The importance of the Hercynian orogeny is evidenced by many geological observations. The first evidence is provided by seismic data which show many Palaeozoic horizons pinching out below a major unconformity (Figs.10 and 35). The presence of up to 1500 m of Carboniferous (Tournaisian to Stephanian) sediments in the south-eastern part of the basin (Fig. 8) might be another evidence. It should be pointed out that neither the precise thickness nor the lithologies of the eroded overburden, particularly for the area of deepest erosion (Amguid El Biod-Hassi Messaoud ridge) are known exactly. The estimation of the eroded amount of sediments by using the break in shale porosity-sonic transit time obtained from porosity and velocity logs (Magara, 1978) was not possible because of the great present-day depth of the Hercynian unconformity

(up to 4 km at some locations). Also, there is no "jump" in vitrinite reflectance values (Dow, 1977; Littke et al., 1994; Katz et al., 1988) which would provide also such an opportunity. Consequently, the amount of eroded overburden could only be estimated from data on units present in nearby sections and from numerical simulations.

Three erosional events occurred during the Meso-Cenozoic cycle. These are respectively, the Austrian (pre-Aptian), the Alpine (Eocene-Oligocene) and the Pliocene unconformities (erosions 4, 5 and 6 in Table 9). These erosional events are of no or very minor importance with respect to organic matter maturation.

c/ Absolute Age

Except for the Cambro-Ordovician sediments which are not always easy to correlate due to a lack of faunal associations, consistent chronostratigraphic correlations are available for eastern Algeria and adjacent parts of Libya and Tunisia.

In the absence of specific age data in any given basin, the choice of the appropriate time scale becomes problematic and subjective. This is mainly due to the existence of many different time scales (e.g. Harland, 1982, 1990; Palmer, 1983; Haq et al., 1987). In the case of the present study, the composite time scale of Harland (1990) which includes the geologic record from Cambrian to the present time, was used.

d/ Heat Flow Density

The Hoggar swell in southern Algeria (Figs. 2, 3 and 6), a basement uplift due to a density reduction of the African upper mantle during the Late Cretaceous-Tertiary, has the imprint of Cenozoic alkali eruptions (Lesquer et al., 1988; Dautria and Lesquer, 1989). According to these observations, Takhrist and Lesquer (1989), based on the evaluation of a large number of logging data (bottom hole and drill stem test temperatures, and rock porosities) studied the present heat flow variations in the different Sahara basins. Although no recent volcanic activity has been reported, except for some narrow volcanic structures in the Illizi district (Megartsi, 1972; Bossiere and Megartsi, 1982), the study showed that the Sahara basins are characterized by higher than normal average heat flow values (80 mW/m^2 and more) with maximum values (90-130 mW/m^2) registered in the Illizi Platform. These thermal anomalies are thought to be the result of a Tertiary (30-40 Ma) thermal perturbation of the upper mantle

(Lesquer et al. (1990). This is particularly important in the present study because a direct link is expected to occur between these hot spots and the maturation of organic matter.

As outlined by Yalcin et al., 1997, not only the present heat flow but also the paleoheat flow must be known for the reconstruction of thermal history of sedimentary basins. However, although basal heat flow is considered as an input parameter in basin modelling, it is often difficult to define this value and its behaviour in the past based. Because no measurable maturity parameter is directly converted to paleotemperatures, the heat flow used in the reconstruction of the thermal history of sedimentary basins is always simplified and calibrated against maturity profiles such as vitrinite reflectance.

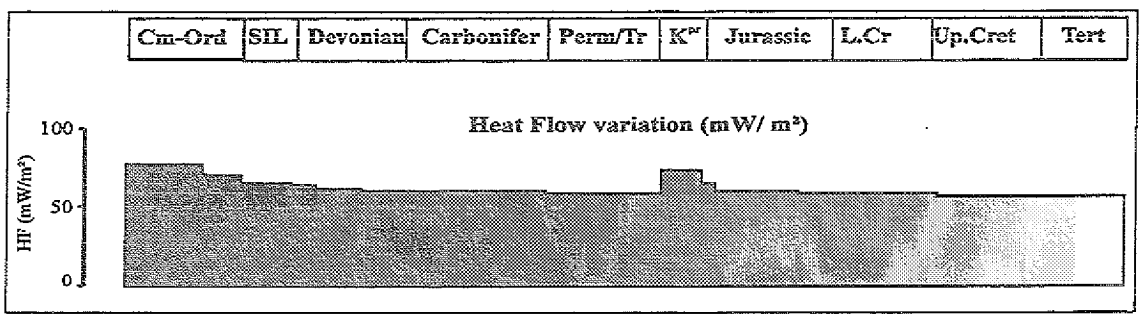


Fig. 36: Heat flow scenario used for the Berkine Basin. This model represents the best fit to tectonic events.

The heat flow assumption used in the present study attempts to match heat flow variations to geological events. It is based on the theory of Mackenzie (1978) which suggests that the period of stretching and thinning of the lithosphere and the uprising of the asthenosphere is associated with a relative increase of heat flow and that the period following the basin formation (post-rift thermal subsidence) is characterised by a decrease of heat flow over time due to the relaxation of the isotherms.

The heat flow model used in the present study is shown in Figure 36. The heat flow maxima of the model are used to describe the Cambro-Ordovician and the Late Triassic-Early Jurassic rifting phases. Consequently, the Cambro-Ordovician period was characterised by a heat flow value of 75 mW/m^2 which is close to the mean value observed in active rift or passive margin basins (Allen and Allen, 1990). For the Triassic-Liassic rift phase, a maximum value of 70 mW/m^2 is assumed. Because of the

amount of extension and the magnitude of volcanic activity (Boudjema, 1987), it is believed that higher heat flow might characterise the region situated farther to the North of the study area (i.e. Oued Mya basin). These heat flow maxima are assumed to decrease with time during the Palaeozoic and Mesozoic subsidence cycles as a consequence of the post-rift cooling.

f/ Sediment-Water Interface (SWI) Temperature

Another important parameter which has a significant effect on temperature history, refered to as the upper boundary condition, is the sediment/water or sediment/air interface temperature (Yalcin et al., 1997). By using data such as paleo-latitude and paleo-water depth (Wygrala, 1989), PDI/PC and PetroMod programs predict the SWI temperature through geologic time.

In the case of the present study, the calculated default values were used, except for the Late Ordovician glaciation during which a value of 4°C is assumed. Because no great variations in terms of lithology were observed, the paleo-water depth of each event is assumed to be constant over the 2D profile. The paleogeography of each event is inferred from lithological and palynological observation.

g/ Organic Carbon Content and Kerogen Type (Hydrocarbon Generation Potential)

The characterisation of potential source rocks is required for the reconstruction of hydrocarbon generation in sedimentary basins. Therefore, parameters such as the organic richness (C_{org}) and hydrocarbon generation potential (HI) which depend on the kerogen type are needed in order to calculate mass balances of generated hydrocarbons.

Tab. 12: Geochemical characteristics (C_{org} and HI) used during 2D simulation. The Silurian and Frasnian correspond to the subfacies A and C of Figure 9.

Source Rock	C_{org} (%)	HI mg/g C_{org}
Frasnian	10	492
Silurian	15	630

One of the advantages that is given by the application of the PetroMod/ 2D program is the concept of multiple source rocks (Mann et al., 1997). The concept allows to handle different source units, each with its specific geochemical properties (i.e. C_{org}, kerogen type). In this order, the petroleum generated from each source rock is traced separately through its entire migration history in order to ensure that the properties of mixed petroleum are determined correctly. It is, therefore, always possible to reconstruct which and how much petroleum is generated from each source rock unit.

Although different source rocks were identified and can contribute to hydrocarbon generation in the Berkine basin (Chapter V), only the best source rocks of the radioactive "hot" shales of the Frasnian and Silurian (subfacies A and C of Figure 9) are considered for the simulation of hydrocarbon generation and migration. The geochemical characteristics (C_{org} and HI) used during the simulation of hydrocarbon generation and migration are summarized in Table 12.

6-1-6 Calibration Parameters

Bottom hole temperature (BHT), drill stem test temperature (DST) and vitrinite reflectance data (R_o, R_c) are used in the present study for the calibration of the temperature history of the basin. The present-day compaction model is further calibrated by using field pressure data obtained during RFT and DST operations.

Unstable bottom hole temperatures should be corrected to circulation of cooler drilling completion fluids. These temperatures are generally lower than the real present temperatures and therefore are not in equilibrium. Corrections were corrected based on drilling depth using the chart of Kehle (1973). This method can be used when data limitations prohibit the construction of horner plots to determine equilibrium temperatures (Dowdle and Cobb, 1975; Poelchau et al., 1997). Furthermore, DST temperatures are used, where available, for the calibration of the present-day geothermal gradient. Temperature measured during testing have been demonstrated to be more accurate than temperatures recorded during logging (Hermanrud et al., 1991b) and are, therefore, used to reduce errors.

The temperature history, on the other hand, is calibrated against maturity profiles using vitrinite reflectance data. The calculated vitrinite reflectance (R_c, Radke, 1987) are

used in some key wells in order to provide more reliabilities for the models. The different data used for calibrations are listed in Tables 13 and 14.

Tab. 13: Formation temperature and pressure data used for the calibration of the present-day temperature and pressure. Temperature values with asterisk are recorded during testing.

Well	Depth (m)	BHT/DST Temp (°C)	Pore Pressure (psi)	Well	Depth (m)	BHT/DST Temp (°C)	Pore Pressure (psi)
BK-2	3480		5940	BBK-1	3555	104.4*	
	3492		5951		3600	110.7*	
	3558		5613		3605	110.7*	
	3569		5632		3627	107.8*	
	3695	118			3671	104*	
	3832	122			4569	104*	
	4762	143		BRD-4	3192	115	
	4889	148			3388		6076
WT-1	1500	55			3399		6076
	3487		6721		3420		6110
	3494		6686		3768		7196
	3512		6668		4660	155.6	
	3527		6518		5001	178	
	3742	116.7*			5050		10748
	3748	116.7*			5130		10967
	3798	116.7*			5132	177	
	3798	117*		TZM-1	1870	72	
	3798	120*			3370	115	
	3998	116.1*			3570	140	
	4227	130		BKE-1	2780		5248
	5500	170			2812		5248
HAD-1	1732	64			2842		5248
	3232	101			2876		5349
	6200	180			3112		5717
SF-1	2160	82.7*			4587		8494
	2863	92.6*					
	2930	95*					
	3082	101*					
	4279	121*					
	4286	124*					
	4350	134*					

The reflectance values were compared to the calculated reflectance following the Easy% R_o algorithm of Sweeney and Burnham (1990). The Easy R_o model is based on the more sophisticated approach of Burnham and Sweeney (1989) called Vitrimat. The Vitrimat is based on a chemical kinetic model that use Arrhenius rate constants to calculate vitrinite elemental composition as a function of temperature and time.

Tab. 14: Vitrinite reflectance data used for the calibration of the temperature history of the basin. Values followed by an asterisk are from this study. Those followed by (+) are from Sonatrach. 24 other measurements are for confidential purpose not listed here. The different data sources are symbolized in the 1D modelling by closed circles, rectangles and open circles, respectively. Calculated reflectance (R_c) are represented by closed triangles.

Well	Depth (m)	A	Type (Ro or Rc)	Value (%)	SD (%)	Well	Depth (m)	A	Type (R_o or R_c)	Value (%)	SD (%)
BK-2	3737	Tourn	R_o	0.86	0.15	BRD-4	4461	Silurian	R_o	1.81	0.15
	3737	Tourn	R_o	0.83			4570	Silurian	R_c	1.86	
	3744	Tourn	R_o	0.83	0.19		4587	Silurian	R_c	1.89	
	3745	Tourn	R_c	0.82			4642	Silurian	R_o	2.09	0.16
	3856	Strunian	R_o	0.91	0.18		4692	Silurian	R_o	1.97	0.20
	3856	Strunian	R_c	0.78			4692	Silurian	R_c	1.83	
	3992	Famennian	R_o	0.94	0.19		4719	Silurian	R_c/R_o	1.86/2.02	/0.20
	3992	Famennian	R_c	0.84		HAD-1	2609	Namurian	R_o	0.92+	0.12
	4176	Famennian	R_o	0.96	0.18		2886	Visean	R_o	1.01+	0.13
	4212	Frasnian	R_c	0.88			2992	Visean	R_o	1.09+	0.10
	4227	Frasnian	R_o	1.03	0.16		3080	Visean	R_o	1.21+	0.10
	4227	Frasnian	R_c	0.93			3180	Visean	R_o	1.29+	0.20
	4371	Frasnian	R_o	1.13	0.17		3240	Visean	R_o	1.34+	0.25
	4393	Frasnian	R_o	1.11	0.20		3308	Visean	R_o	1.17+	0.15
	4412	Frasnian	R_c	0.94			3433	Visean	R_o	1.27+	0.15
	4461	Givetian	R_o	1.16	0.12		3567	Visean	R_o	1.34+	0.15
	4643	Sie	R_o	1.13	0.09		3755	Strunian	R_o	1.34+	
WT-1	3738	Triassic	R_o	0.90	0.10		3813	Strunian	R_o	1.56+	0.20
	3749	Famennian	R_o	0.92	0.30	TZM-1	2797	Strunian	R_o	0.70+	
	3754	Famennian	R_c/R_o	0.86/0.88	/0.20		2925	Frasnian	R_o	0.85+	
	3758	Famennian	R_o	0.87	0.20		2962	Sie	R_o	0.90+	
	3763	Famennian	R_c	0.87			3647	Cambrian	R_o	1.30+	
	3792	Famennian	R_o	0.94	0.30	KA-1bis	500	Cenomanian	R_o	0.71+	
	3793	Famennian	R_c	0.89			1100	Malm	R_o	0.31+	
	3862	Famennian	R_o	0.95	0.18		1220	Malm	R_o	0.33+	
	3924	Frasnian	R_o	0.98	0.15		1390	Do	R_o	0.42+	
	4117	Givetian	R_o	0.98	0.25		1490	Malm	R_o	0.38+	
	4117	Givetian	R_c	1.01			2580	Triassic	R_o	0.57+	
	4220	Givetian	R_o	0.96	0.20		2725	Silurian	R_o	0.45+	
	4250	Sie	R_o	1.20	0.04		2750	Silurian	R_o	0.55+	
SF-1	3075	Tourn	R_o	0.77	0.15	BKW-1	2005	Barremian		0.37+	
	3092	Tourn	R_o	0.71	0.15		2237	Neocomian	R_o	0.37+	
	3114	Tourn	R_o	0.81	0.15		4125	Triassic	R_o	1.37+	
	3324	Famennian	R_o	0.77	0.14		4200	Sie	R_o	1.26+	
	3584	Famennian	R_o	0.86	0.20		4250	Silurian	R_o	1.40+	
	3618	Frasnian	R_o	0.83	0.13		4300	Silurian	R_o	1.46+	
	3728	Frasnian	R_o	0.88	0.16		4350	Silurian	R_o	1.45+	
	3760	Frasnian	R_o	0.82	0.13						
	4159	Sie	R_o	0.73	0.16						

A reaction scheme for vitrinite reflectance evolution is used in which the loss of water, carbon dioxide, higher hydrocarbons and methane are considered as four independent

first order parallel reactions. The resulting composition is used to calculate vitrinite reflectance values via correlations between elemental composition (H/C and O/C) and vitrinite. This approach provides the basis for the Easy% R_o model, in which a single distribution of activation energies is considered for the four reactions.

The Easy% R_o model is widely used. It is valid for a broad range of vitrinite reflectance values ranging from 0.25% to 4.6% and is considered to be the best model for the calibration of thermal history in sedimentary basins. Although it is thought to overestimate the importance of time and underestimate that of temperature (Quigley et al., 1987; Sweeney and Burnham, 1990), the TTI approach of Lopatin (1971) and Waples (1980) is also still used. However, it is now accepted that the Easy% R_o method provides more reliable results in practical cases (Leischner et al., 1993; Sachsenhofer and Littke, 1993).

6-2 Petroleum Generation and Migration

One of the aims in basin modelling is to assess the amount and type of hydrocarbons that could have been generated from typical source rocks and accumulated in reservoirs. Maturation reconstruction requires the kinetic parameters (activation energy distributions, pre-exponential factors) since the conversion of kerogen to oil and gas is controlled by reaction kinetic processes which are temperature and time dependant (Tissot and Welte, 1984).

The modelling of petroleum migration is another extension of the thermal modelling. For this purpose tools are provided to analyse the processes following the generation of hydrocarbons in source rocks: primary migration (expulsion), secondary migration and accumulation.

6-2-1 Kinetics of Petroleum Generation

Generated petroleum compounds are thought to be a result of a multitude of quasi-irreversible, assumed first order thermal cracking reactions. The rate is mainly governed by kerogen structure and the evolution of temperature over time (Schenk et al., 1997). In this order, several chemical kinetic models (e.g. Tissot and Espitalié, 1975; Tissot et al., 1987; Ungerer et al., 1988; Ungerer, 1990b) were established. The

kinetic law used here is the Arrhenius law which states that the reaction rate increases exponentially with temperature, and is written as: $K = A \exp^{(-E/RT)}$; where K, A, E, R and T are the reaction rate, the frequency factor or Arrhenius constant, the activation energy, the gas constant and the absolute temperature (K), respectively.

The most commonly used kinetic model was developed by Tissot and Espitalié (1975) and later redefined by Ungerer and Pelet (1987). This model assumes that oil is formed from kerogen by a series of parallel first order chemical reactions. Each reaction has its own kinetic parameters (E and A) and their relative importance is defined in terms of the weight of hydrocarbons produced per gram of organic carbon once the kerogen has lost all reactivity. It also assumes that gas is formed only from oil by secondary cracking; a process which is described by a single reaction.

PetroMod allows the use of hydrocarbon generation kinetics such as those established by Tissot and Espitalié (1975), Espitalie et al.(1987), Tissot et al.(1987) and Quigley et al.(1987).

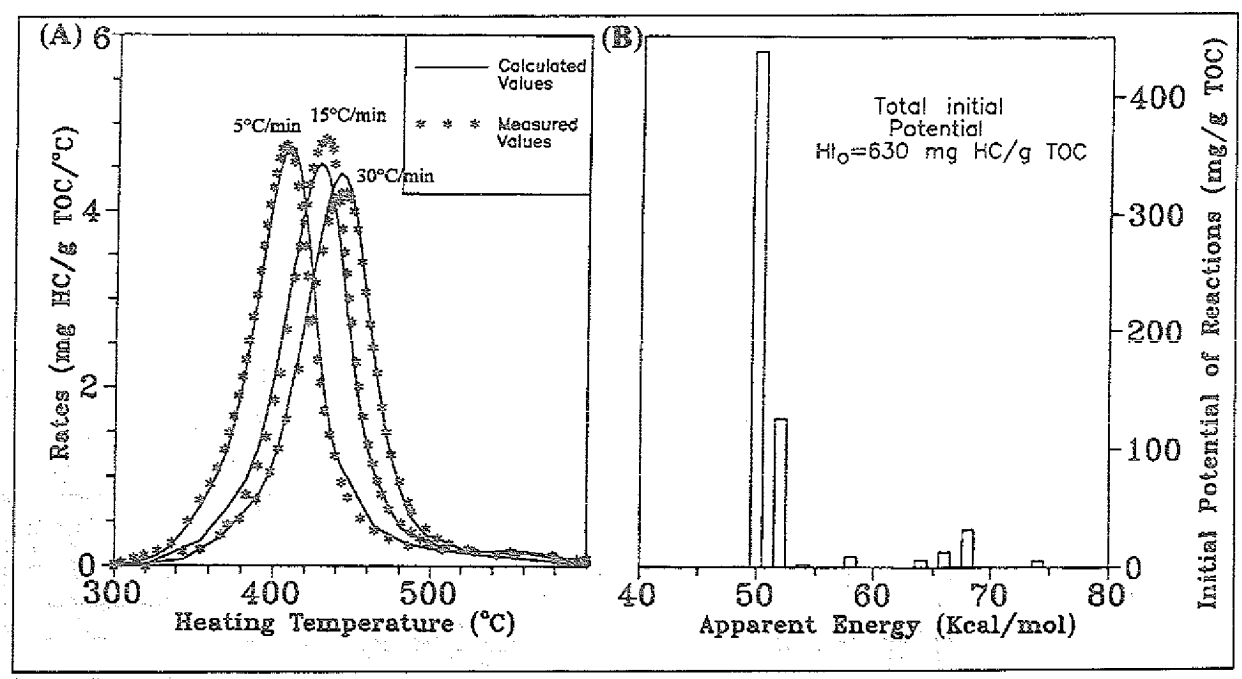


Fig. 37: Gross hydrocarbon formation rates (mg/g C_{org} /°C) as a function of temperature (°C) and distribution of activation energy of a Silurian sample from the northern Oued Mya basin (after Makhous et al., 1997). Hydrocarbon formation rates are derived from open system pyrolysis at heating rates of 5, 15 and 30°C/min.

PetroMod allows the use of hydrocarbon generation kinetics such as those established by Tissot and Espitalié (1975), Espitalie et al.(1987), Tissot et al.(1987) and Quigley et al.(1987).

The kinetics used for both the basal Silurian and Frasnian radioactive shales, which are highly similar with respect to their organic facies composition, is that of Tissot et al.(1987) for type II kerogens. Open system pyrolysis have been used by Makhous et al.(1997) in order to specify the kinetic parameters controlling maturation for an immature Silurian sample from the north-eastern part of the Triassic province in eastern Algeria. The energy spectrum shown in Figure 37 is rather typical for marine type II kerogen (Tissot et al.1987). Activation energy distribution, pre-exponential factors and the activation energy for oil-gas cracking for such kerogen are given in Table 15.

Tab. 15: Kinetic parameters of kerogen Type II (after Tissot et al., 1987). E, activation energy; TGP, total hydrocarbon generation potential; Xio, hydrocarbon generation potential of the kerogen fractions; A, Arrhenius constant.

E (Kcal/mol)	Freq. Factor	TGP mg/g Corg	Xi0 (%)	A 1/my
	$2.87* 10^{27}$	492		
40			0.014	1.00
48			0.010	1.00
50			0.057	1.00
52			0.555	1.00
54			0.293	1.00
56			0.045	1.00
58			0.012	1.00
60			0.008	1.00
62			0.006	1.00
	Oil/Gas cracking			
57	$9.47* 10^{27}$			

6-2-2 Fluid Flow in Sedimentary Rocks

The dynamics of fluid flow is commonly determined from Darcy's law originally established to describe the monophasic flow of a fluid. It was adapted to describe pressure driven two phase fluid flow in porous media (see Ungerer et al., 1990a).

The dominant mechanisms for both primary and secondary migration is a discrete phase flow driven by pressure gradients, gravity forces and capillary pressures (e.g. Welte, 1987; Durand, 1988). Because such phenomena can be predicted by basin

modelling softwares, the PetroMod 2D program is used in the present study for addressing migration problems in the Berkine Basin. The model allows expulsion to occur when a pre-set value (i.e. 5%) of hydrocarbon saturation is exceeded. The model gives also the possibility for the simulation of three phase fluid flow (oil, water and gas) and diffusion.

6.3 1D Simulation Results

The 1D numerical modelling results obtained for each locality and individual well are based on the input data matrix enclosed in Appendix (Tabs. 2 to 9). In the following, the burial, thermal and generation histories will be discussed based on the results of the best (optimum) calibrated models. The modelling was carried-out in two interrelated steps. First, burial and thermal histories of distinct units were reconstructed; second, hydrocarbon generation history of the thermally mature source rock horizons was computed using the previously determined thermal history and a kinetic model for hydrocarbon (oil and gas) generation. The thermal history was calibrated by comparing measured (R_o, R_c) and calculated vitrinite reflectance using the Easy% R_o algorithm of Sweeney and Burnham (1990). Present-day geothermal gradients were calculated by using BHT and/or DST temperatures and a mean surface temperature of 25°C. If these data are combined with present-day thermal conductivity for each sedimentary layer, present-day heat flow values can be calculated.

6.3.1 Geothermal Gradient in the Berkine Basin

Present-day subsurface temperatures within the stratigraphic sequence can be used to approximate the depth range of hydrocarbon generation (Tissot and Welte, 1984) in a given sedimentary basin. Plotting subsurface temperature can be a very useful method of determining whether present-day temperatures are the highest which the sediments experienced (Robbins, 1979).

Figure 38 shows a plot of present-day temperature data Vs depth for the different wells submitted to 1D modelling. The data reveal that large differences in the general thermal gradients do not exist between the different wells. The graphic shows a systematic increase in temperature with depth, indicating for the upper crust an average

geothermal gradient of 2.5 °C/ 100 m with a surface temperature intercept of 25°C. The lithologies, which due to their thermal properties (i.e. conductivity, heat capacity) can modify the thermal gradient are fairly similar across the basin.

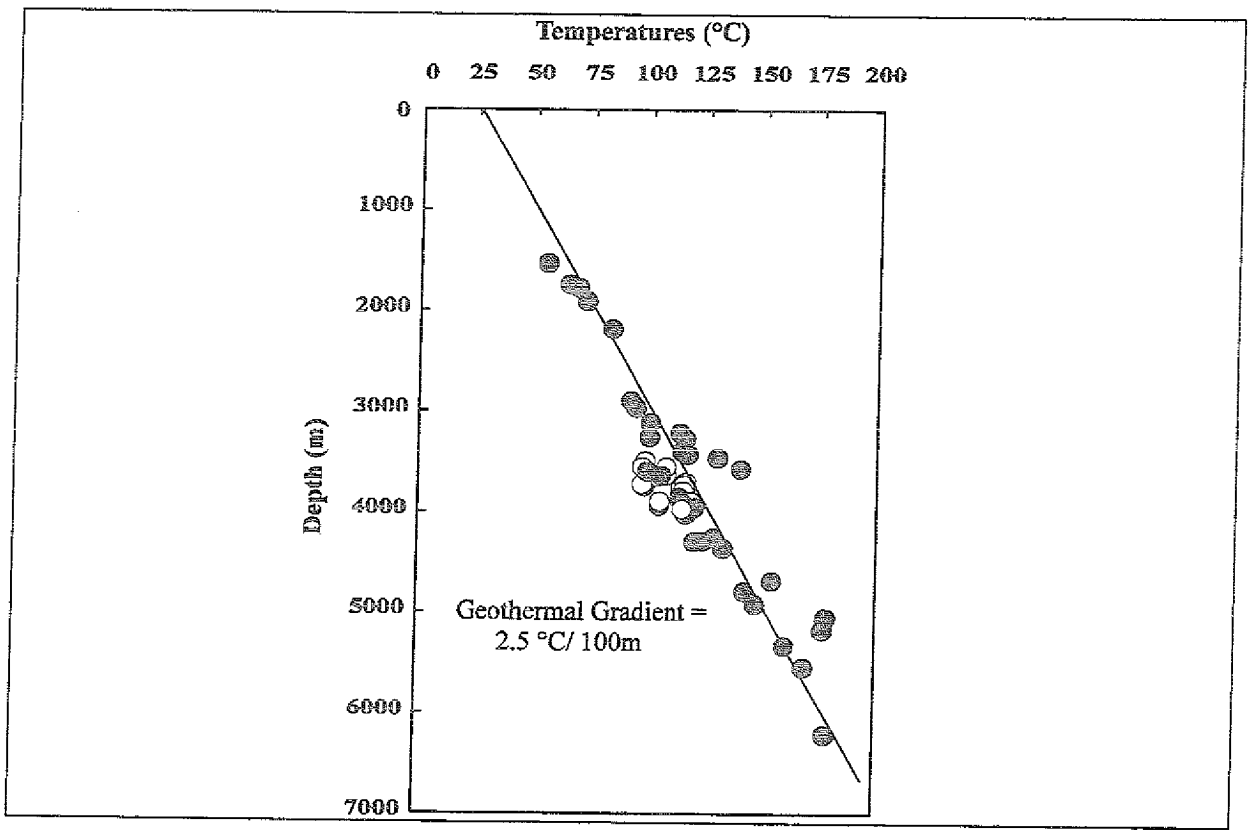


Fig. 38: Selected temperature data versus depth of burial from wells in the Berkine Basin. Solid symbols are BHT data; open symbols are DST data.

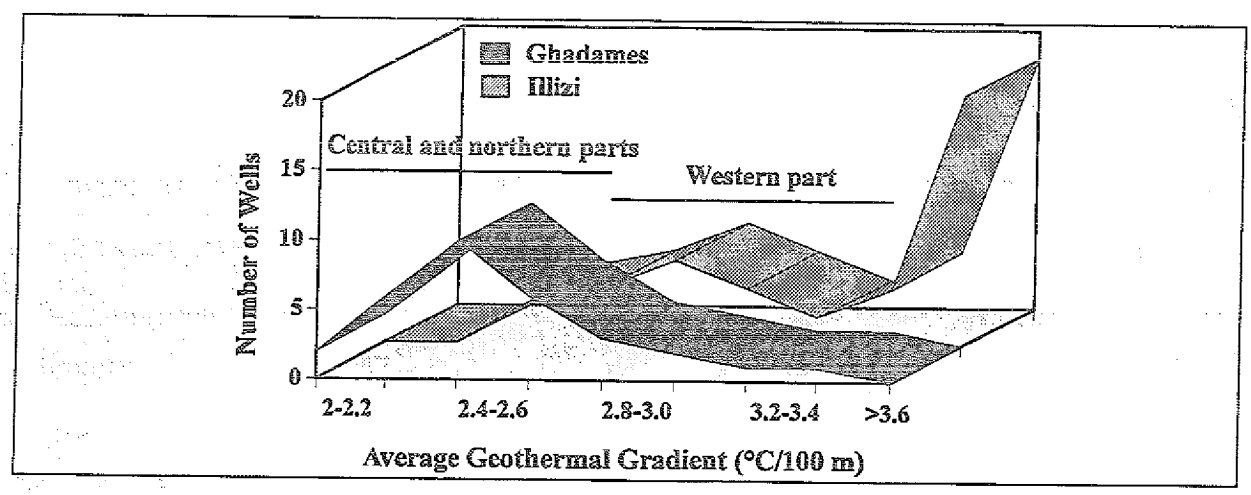


Fig. 39: Average geothermal gradients for the upper crust as a function of the number of observations. High geothermal gradients are generally associated with the highly structured zone of the basin (i.e. Amguid El Biod-Hassi Messaoud area). For comparison the distribution of geothermal gradients in the Illizi Platform are superimposed.

Figure 39 shows the general variation of the present-day thermal gradients for the upper kilometres within the Berkine Basin . The figure reveals that the central and northern part of the basin are characterised by low geothermal gradients (2.2-2.5°C/100 m). Geothermal gradients are higher in the western part of the basin and increase along the Amguid El Biod-Hassi Messaoud ridge. A comparison between the Berkine Basin and the Illizi Platform shows that the Illizi Platform is characterised by higher geothermal gradients.

6.3.2 Burial and Thermal History

Depositional and thermal histories are discussed in the following by plotting curves of depth of burial versus geological age for each stratigraphic unit and for each individual well. The right side of the figures shows the calibration obtained between the measured and calculated maturity data (i.e. vitrinite reflectance). Additional information about the heat flow value at the time of maximum burial as well as the amounts of eroded overburden used in order to get the optimum calibrated models are also indicated.

a/ Central Berkine Basin

Five wells from different parts of the central Berkine Basin were used for burial and temperature history reconstructions. These are BK-2 and WT-1 in the south-west, HAD-1 in the south-east, BBK-1 in the north and SF-1 in the north-east (Fig.1).

Well BK-2

Berkine 2 is one of the Central Berkine Basin wells for which burial and temperature history were reconstructed. The drilled Palaeozoic section is 1159 m thick and includes sediments from Early Devonian (Siegenian-Gedinnian) to Lower Carboniferous (Tournaisian). These sediments are unconformably overlain by 3731 m of various sediments ranging in age from Upper Triassic (Keuper) to Neogene.

Random mean vitrinite reflectance values increase in a regular way from 0.4% at a depth of 1275 m to 1.13% at 4643 m. Calculated vitrinite reflectance (R_c) data based on the aromatic maturity parameter (MPI-1) range from 0.78 to 0.84% between 3737

and 3992 m and are in good agreement with R_o data (Tab. 14, Fig. 40). These data are well explained by calculating with a heat flow value of 55 mW/m² at the time of maximum burial (i.e. Late Cretaceous-Tertiary) and a Hercynian erosion of 1420 m. A present heat flow of 55 mW/m² was sufficient to match present-day formation temperatures.

The burial and thermal history of the well is shown in Figure 40. The restoration of the sedimentation in the Berkine area shows two subsidence cycles separated by an uplift phase during Permian-Triassic. The first subsidence cycle took place during the Palaeozoic and is shown to be characterised by a continuous and rapid burial. The oldest sediments reached a burial depth of more than 4000 m in the Late Carboniferous with temperatures higher than 160°C.

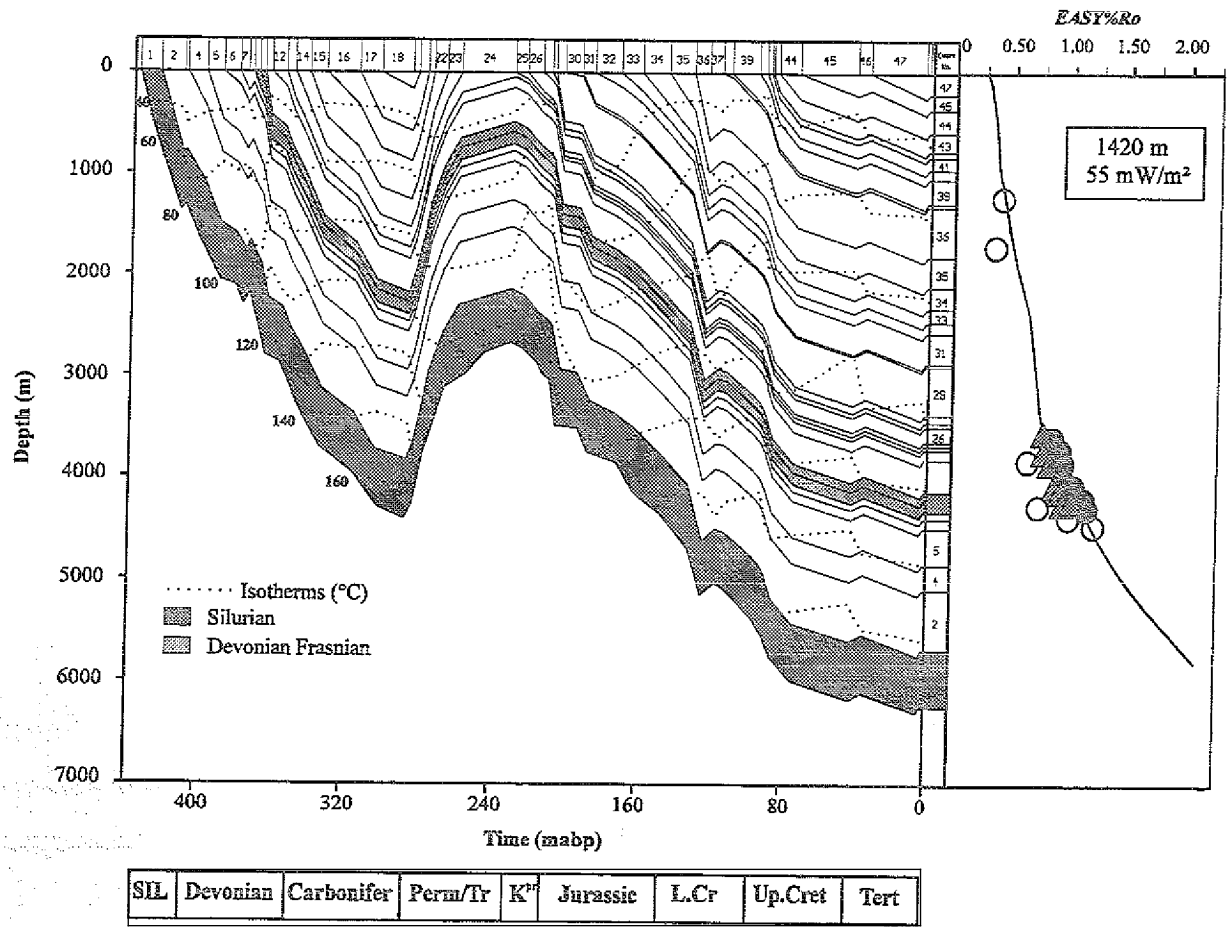


Fig. 40: Simulated burial and temperature history of well BK-2. The right side of the figure shows measured and calculated vitrinite reflectance. The different symbols correspond to the data sources defined in Table 14.

The Palaeozoic subsidence cycle ended at the Late Carboniferous time (Stephanian) as a consequence of the Hercynian inversion movements and subsequent uplift and

erosion. Stephanian to Tournaisian sediments are estimated to have been eroded between 286 and 231 Ma. The calibration of the model suggests an uplift which is slightly in excess of 1400 m. Consequently, the burial curve take a "V-like shape" for the successive subsidence, uplift and erosion (Fig. 40). This fact suggests that the Berkine area has been an eroding dome prior to the Late Triassic-Early Jurassic rift phase as indicated by the Palaeozoic subcrop pattern of the basin (Fig. 7).

Thermal activation of the lithosphere in the Berkine Basin began during the Late Triassic, or probably earlier. The presence of Triassic basalt in the northern part of the basin is an evidence for high thermal gradients during the Triassic-Jurassic. Consequently, the Late Triassic and Early Jurassic were characterised by high heat flow (Fig. 36).

Mesozoic burial was rapid during the Late Triassic-Early Jurassic, then slowed down from the Middle Jurassic to the Late Cretaceous (Coniacian). From the Late Cretaceous to the present time, the subsidence rate was relatively slow. The Late Triassic-Early Jurassic subsidence of the basement is a consequence of thermal re-equilibration (cooling) of the lithosphere. Rapid deposition of thick salt and anhydrite sediments and their high thermal conductivities contributed to the subsequent temperature evolution.

Regardless of these variations, it is clear from the model that the maximum burial (i.e. maximum heating) of the sediments occurred during the Late Cretaceous-Tertiary time. Any assumption of higher heat flows during that time would lead to an overestimation of the maturity data.

Well WT-1

The burial and thermal history of the Wed Teh area was assessed by using the WT-1 well. This well is situated approximately 24 km to the south of the BK-2 well (Fig.1). The stratigraphy consists of 1068 m of Palaeozoic sediments from Gedinnian to Famennian in age. The Palaeozoic sequence is overlain by 3746 m of Meso-Cenozoic (Keuper to Neogene) sediments. Measured vitrinite reflectance values range from 0.4 % at a depth of 1585 m to 1.21% at 4250 m. The calculated vitrinite reflectance from MPI-1 ranges from 0.86 to 0.89% between 3754 and 3792 m and is in good agreement with measured vitrinite reflectance. Results of the calibrated model, supported by

present-day temperatures and vitrinite reflectance data suggest that present-day heat flow and the paleo heat flow value at the time of maximum burial both do not exceed 55 mW/m².

Except for some minor differences, this area provided similar simulation results with respect to the burial paths of the different statigraphic units as well as the variation of the depth of the isotherms (Fig. 41). At the end of the Carboniferous time, prior to the Hercynian uplift, the burial depth of the oldest Palaeozoic strata reached 4500 m. The Hercynian orogeny and subsequent cooling resulted in an erosion of about 1800 m of Devonian and Carboniferous sediments. Like the BK-2 well, this area which constituted an uplifted dome submitted to erosion during the Permian-Triassic time, was the center of extensional tectonic movements during the Triassic-Early Jurassic that caused intense subsidence. During the Late Cretaceous-Tertiary, the subsidence slowed down. The present-day burial depth reached by the oldest sediments is more than 6000 m at a temperature of more than 160 °C.

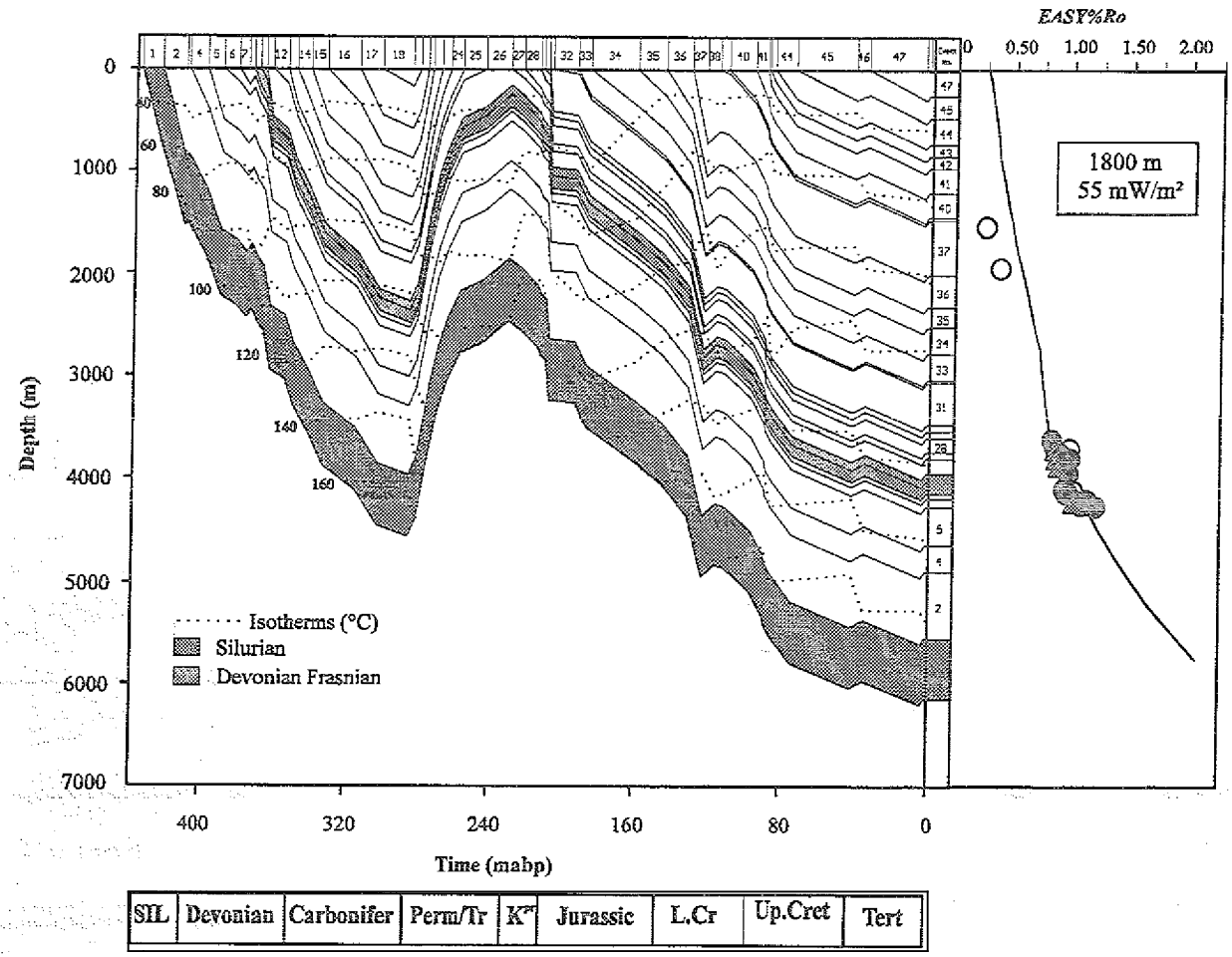


Fig. 41: Simulated burial and temperature history of well WT-1. The right side of the figure shows the measured and calculated vitrinite reflectance. The different symbols correspond to the data sources defined in Table 14.

Well HAD-1

The well HAD-1 (Hiad-1) is situated approximately 90 km south-east of the WT-1 well (Fig. 1). Palaeozoic sediments penetrated by the well are 2349 m thick and range from lower Devonian to Westphalian. The burial history is similar to those described for the two previous wells, with maximum burial occurring during the Late Cretaceous-Tertiary time. However, some major differences can be observed (Figs. 42, 43 and 44). Here, the Hercynian erosion does not seem to extend significantly since the Late Carboniferous (Westphalian) sediments are preserved. Furthermore, the Triassic-Jurassic period is characterised by a slower subsidence. This fact is mainly due to the reduced total thickness of these sediments which is about 700 m in contrast to the 1500 m observed in the Berkine and Wed Teh areas. Another important difference is that the rapid isotherm sinking observed during the Late Triassic-Early Jurassic time in the previous wells is not observed here. This effect is mainly due to the reduced thickness of sediments of high thermal conductivity (i.e. salt and anhydrite) in that part of the basin.

With respect to the thermal history reconstruction and due to the scatter shown by the vitrinite reflectance values, the calibration of the model was achieved by considering different heat flow scenarios. These heat flow assumptions are based on populations of vitrinite reflectance generating different coalification trends. Vitrinite reflectance data are either sourced from different laboratories or are simply provided from the same laboratory, but showing big scatter in their values. Consequently, different models, which are discussed in the following, were established.

Model A

This model assumes that vitrinite reflectance data, represented by open circles (Fig. 42), correspond to the true vitrinite population, and are therefore more representative. In this case, the calibration of the model requires a heat flow value of 55 mW/m^2 at the time of maximum burial. Because the Hercynian erosion was not significant in that part of the basin, it is presumed a priori that the total amount of Carboniferous sediments eroded was only 200 m. The present-day heat flow value calculated using formation temperatures is similar to that observed during the time of maximum burial (i.e. 55 mW/m^2).

It is clear that such assumed vitrinite reflectance data and the associated thermal history model would indicate that no major heat flow event during the Late Cretaceous-Tertiary was responsible for the temperatures reached by the sediments; a result which was established for the previous simulated wells.

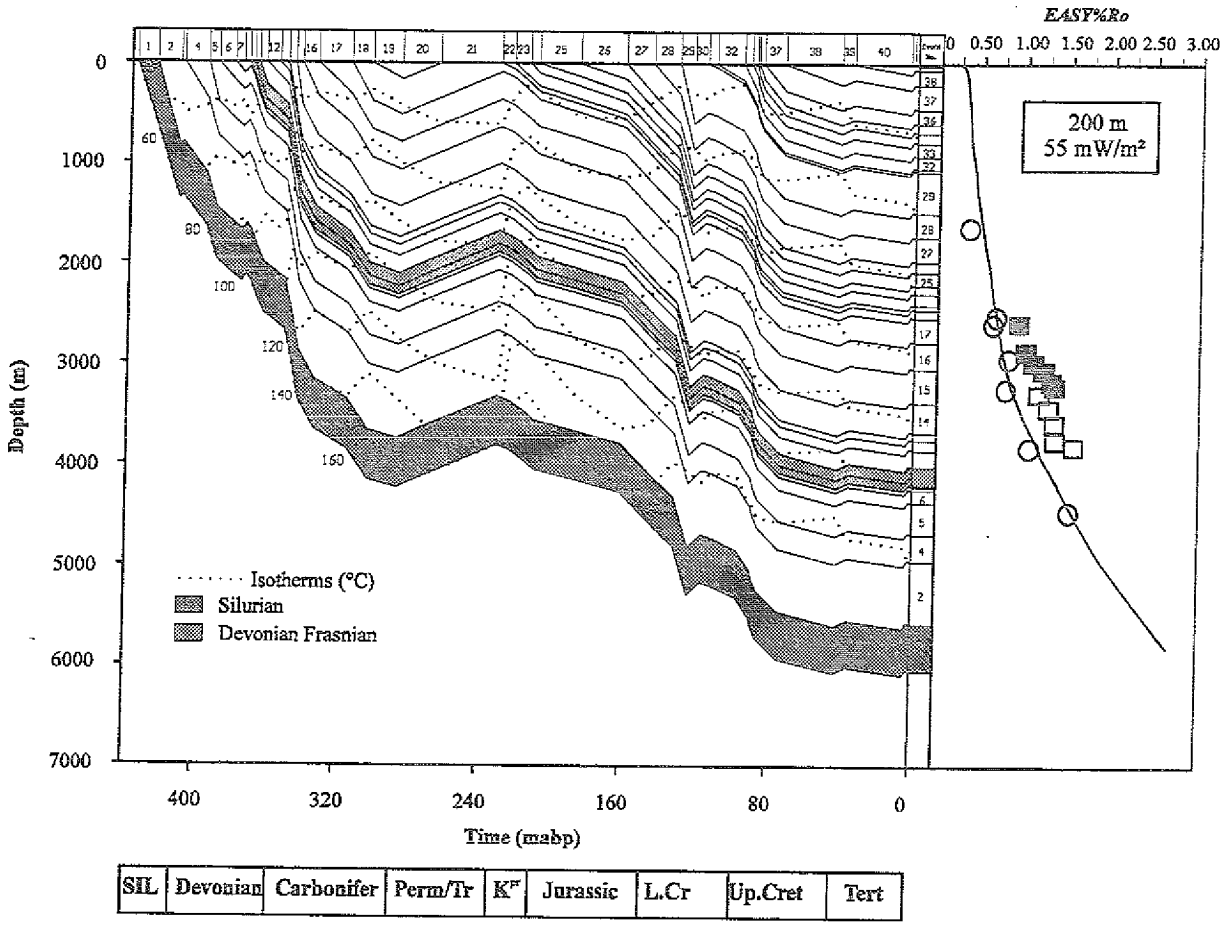


Fig. 42: Simulated burial and temperature history of HAD-1 well. The right side of the figure shows the measured and calculated vitrinite reflectance (model A). The different symbols correspond to the data sources defined in Table 14.

Model B

Model B assumes that vitrinite reflectance data represented by open rectangles are true vitrinite populations. Because the calibration of the model cannot be achieved by assuming additional eroded overburden, the simulation must be based on an assumption of greater heat flow during maximum burial. The assumption that the Late Cretaceous-Tertiary time was characterised by a heat flow value of 73 mW/m² led a satisfactory agreement between the observed and calculated maturity trends. Such high heat flow is reflected by the rising of the isotherms during the Cenozoic time (Fig. 43)

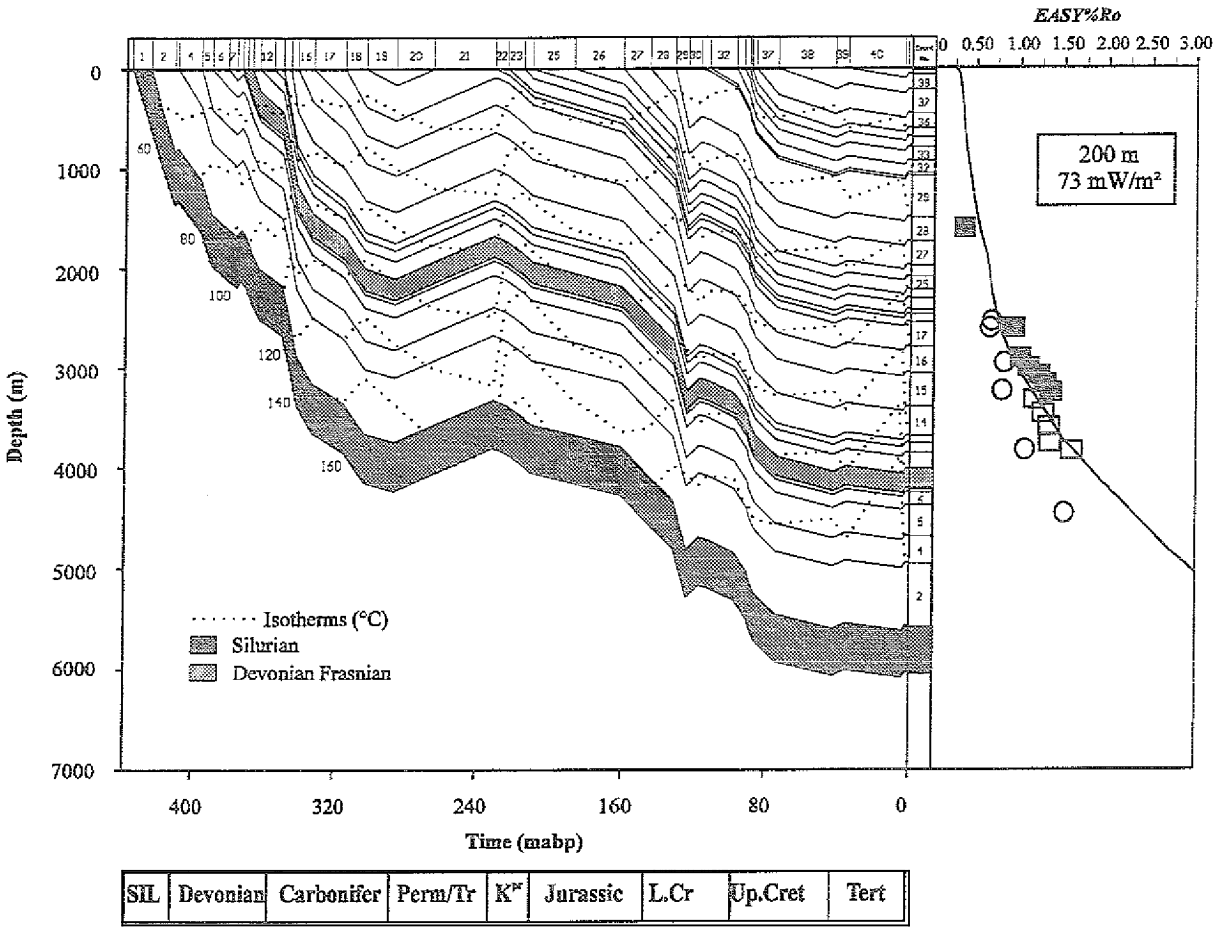


Fig. 43: Simulated burial and temperature history of well HAD-1. The right side of the figure shows the measured and calculated vitrinite reflectance (model B). The different symbols correspond to the data sources defined in Table 14.

Model C

If we do consider that the vitrinite population represented by closed rectangles is indigenous, a heat flow of 80 mW/m² during the Late Cretaceous- Tertiary is necessary to fit the model. As already shown in the case of Model B, the depth of the isotherms is reduced during that time implying high geothermal gradient (Fig. 44)

Regardless of the results given by the two latter models, only a stretching phase accompanied by a thermal activation of the lithosphere during the Cretaceous-Tertiary time could explain the rather high heat flows. However, from the geological knowledges, there is no indications of strong magmatic activity or rifting during Cretaceous-Tertiary. Furthermore, high heat flow during Cretaceous-Tertiary would bear some effects on the kerogen in terms of the conservation of the palynomorph as well as on hydrocarbon generation potential of the source rocks. This was not observed

in the present study (Chapter V). Therefore, it is believed that the first alternative (i.e. Model A) is the best possible assumption to describe the temperature evolution for the source rocks.

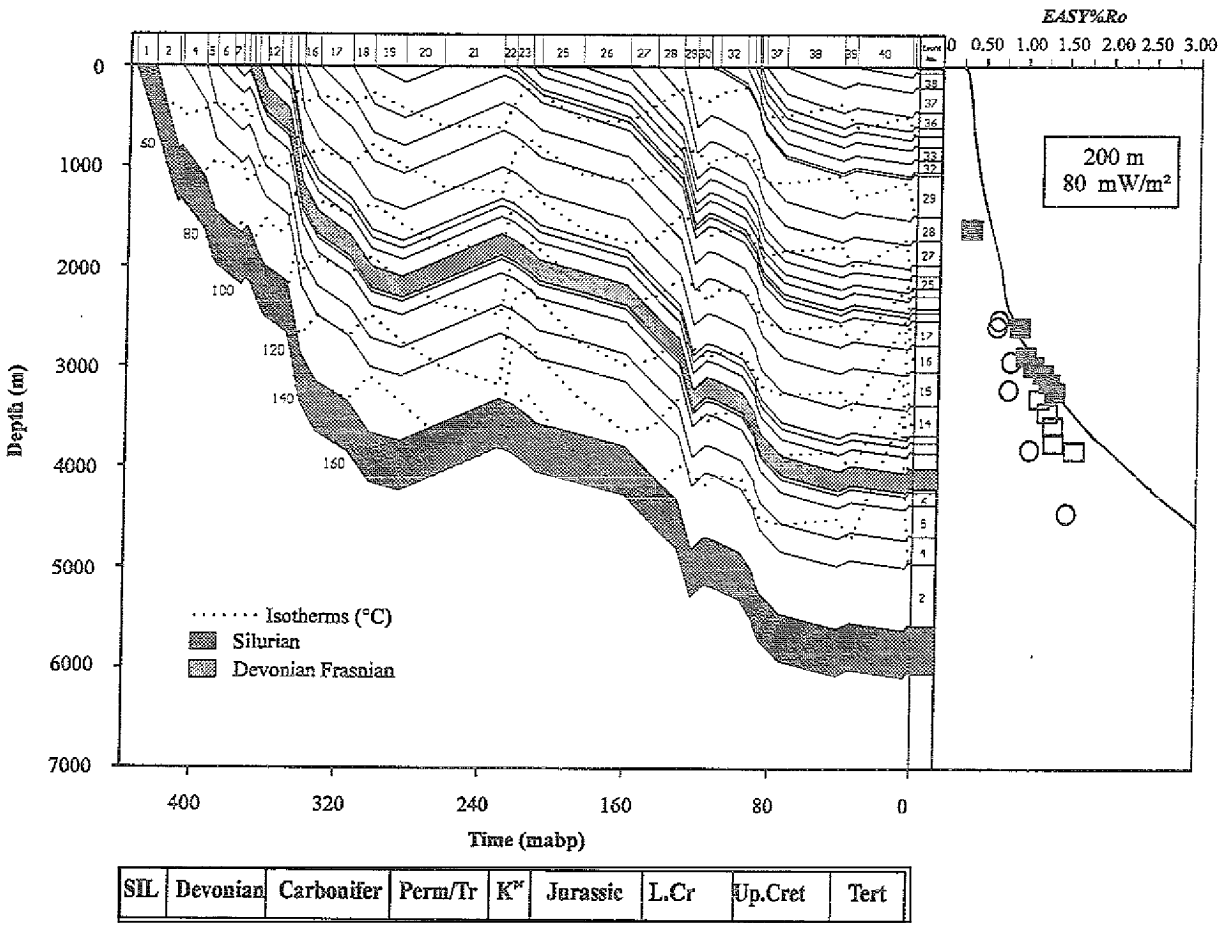


Fig. 44: Simulated burial and temperature history of well HAD-1. The right side of the figure shows the measured and calculated vitrinite reflectance (model C). The different symbols correspond to the data sources defined in Table 14.

Well SF-1

The Sif Fatima 1 (SF-1) well is located approximately 70 km to the north-east of the BK-2 well. The drilled sediments consist of 1308 m of Palaeozoic rocks from Gedinnian to Tournaisian in age. The Palaeozoic section is unconformably overlain by about 3000 m of sediments ranging in age from Upper Triassic to Neogene.

In contrast to the BK-2 and WT-1 wells, vitrinite reflectance data from this well are fairly sparse. Unpublished vitrinite reflectance values vary from 0.38% at 1572 m to 0.65% at 4159 m, indicating a rather low maturity stage of the sediments and associated organic matter even at great depths of burial.

Vitrinite reflectance measurements from this study vary from 0.71% to 0.82% and show in general a regular increase at a depth interval between 3092 and 3760 m.
The burial history model established for this part of the basin (Figs. 45 and 46) does not show great differences to those of the previous modelled wells and reflect roughly the geological evolution of the basin. As in the case of the HAD-1 well, the scatter shown by the vitrinite reflectance data allowed the calibration of the model by considering different thermal history assumptions.

Model A

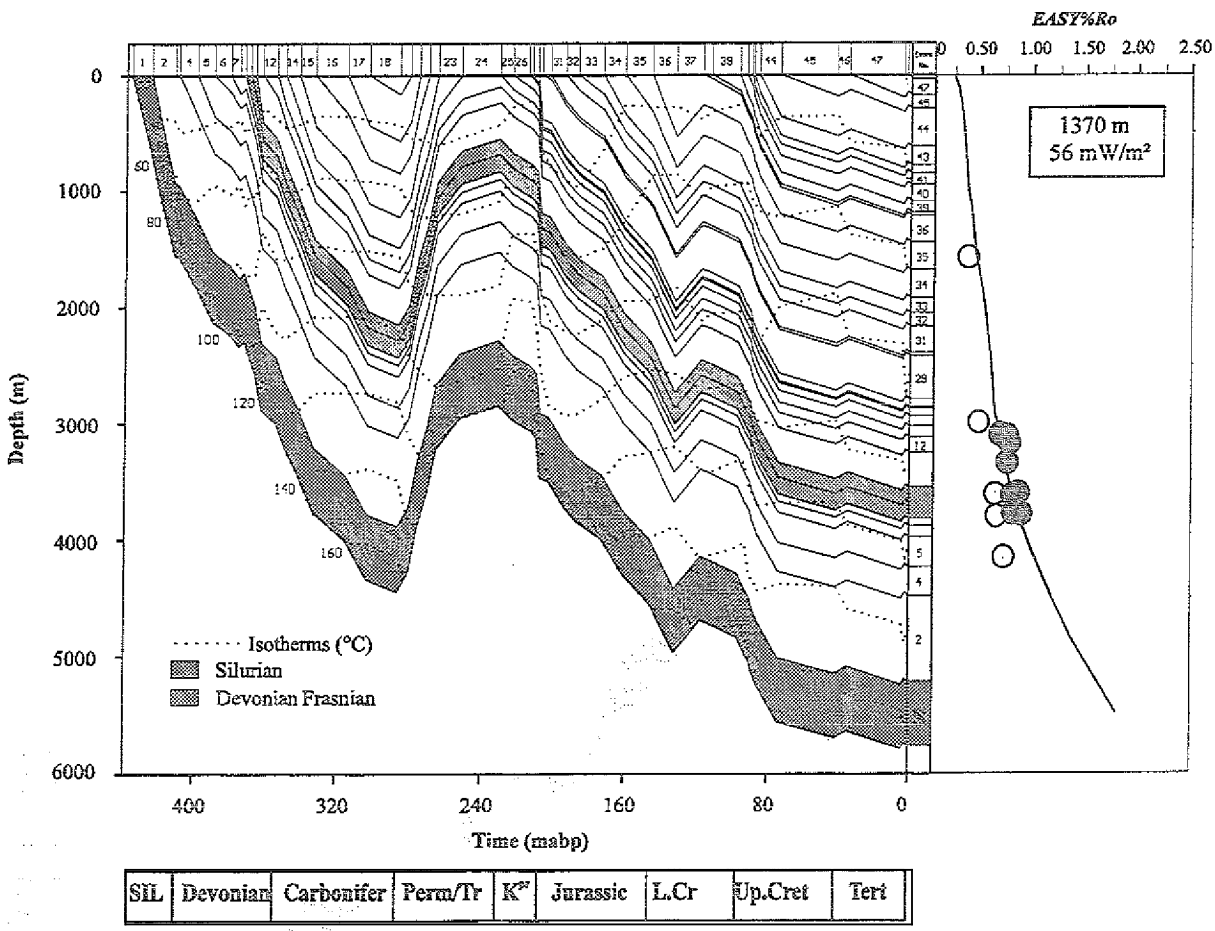


Fig. 45: Simulated burial and temperature history of well SF-1. The right side of the figure shows the measured and calculated vitrinite reflectance (model A). The different symbols correspond to the data sources defined in Table 14.

The first simulation run which leads to a good fit between the measured (closed circle data) and the calculated maturity trends is based on the assumption that a total of 1370 m of Tournaisian to Stephanian sediments has been removed during the Hercynian

orogeny, and that a heat flow of 56 mW/m² persisted at Late Cretaceous-Tertiary times (Fig. 45). The simulation results with respect to temperature history are quite similar to those obtained for the BK-2 and WT-1 wells situated further to the East. The present-day heat flow of about 58 mW/m² is in agreement with the temperature data of the SF-1 well.

Model B

This model assumes that vitrinite reflectance values represented by open circles are more reliable maturity data (Fig. 46). Assuming that the same amount of sediments has been removed between 231 and 186 Ma, a good fit between the measured and calculated reflectance values is obtained only if heat flow values of 35 mW/m² are assigned to the Cretaceous-Tertiary events (i.e., between 112 and 4 my).

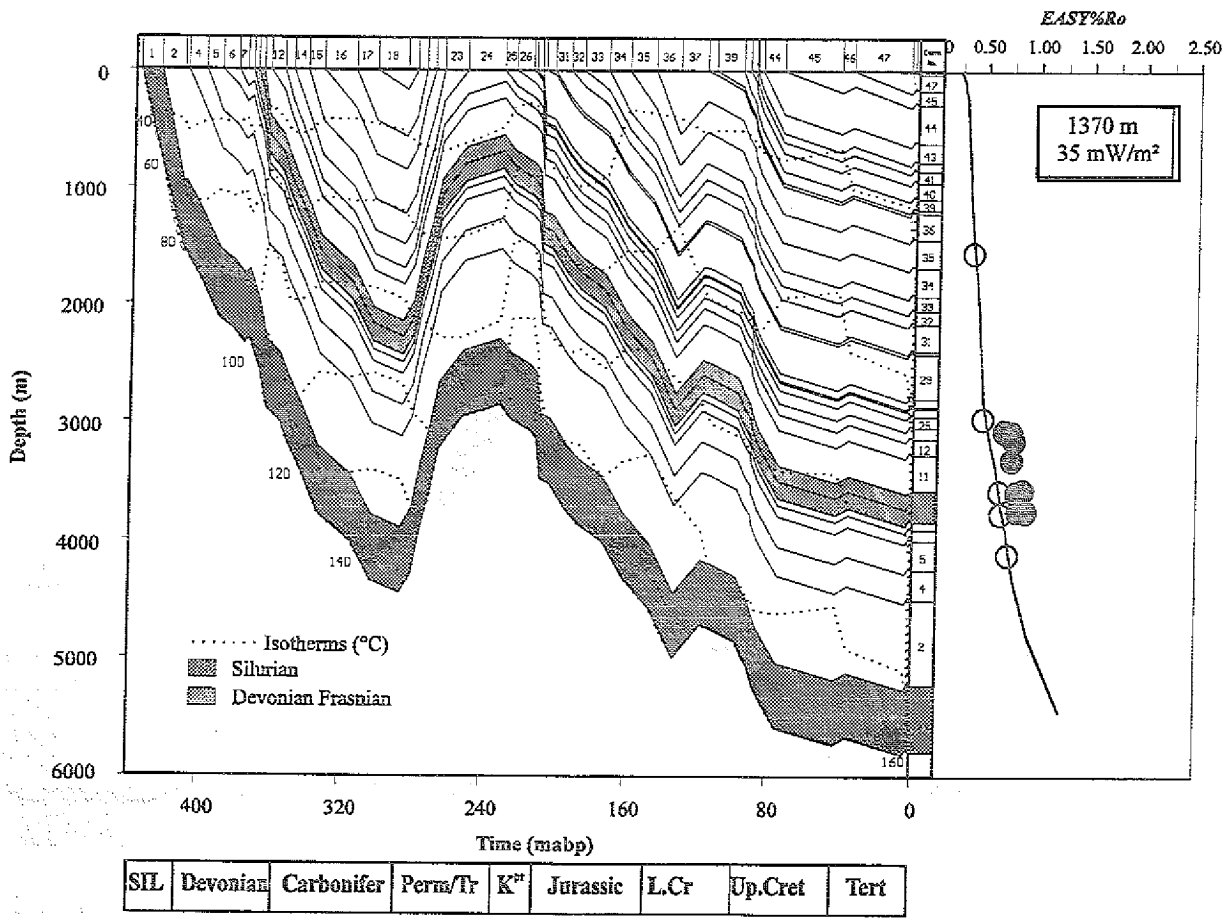


Fig. 46: Simulated burial and temperature history of well SF-1. The right side of the figure shows the measured and calculated vitrinite reflectance (model B). The different symbols correspond to the data sources defined in Table 14.

Not only low heat flow values during the Mesozoic characterise this coalification trend, but heat flow values of around 50 mW/m² must also characterise the Carboniferous period in order to get an agreement between the observed and calculated maturity trend. With respect to the depth of the isotherms, a rapid sinking accompanied by a widening is observed during the Mesozoic time, that is between around 146 and 4 Ma. An extreme uprising of the isotherms which reflect the present-day geothermal gradient is observed during the last 4 Ma. Such local and even particular evolution would indicate a cooler than normal thermal regime during the Cretaceous and Tertiary. It would be extremely difficult to explain this abrupt increase in heat flow from 35 mW/m² to 58 mW/m² during the last 4 Ma. Therfore, Model A is the acceptable model.

Well BBK-1

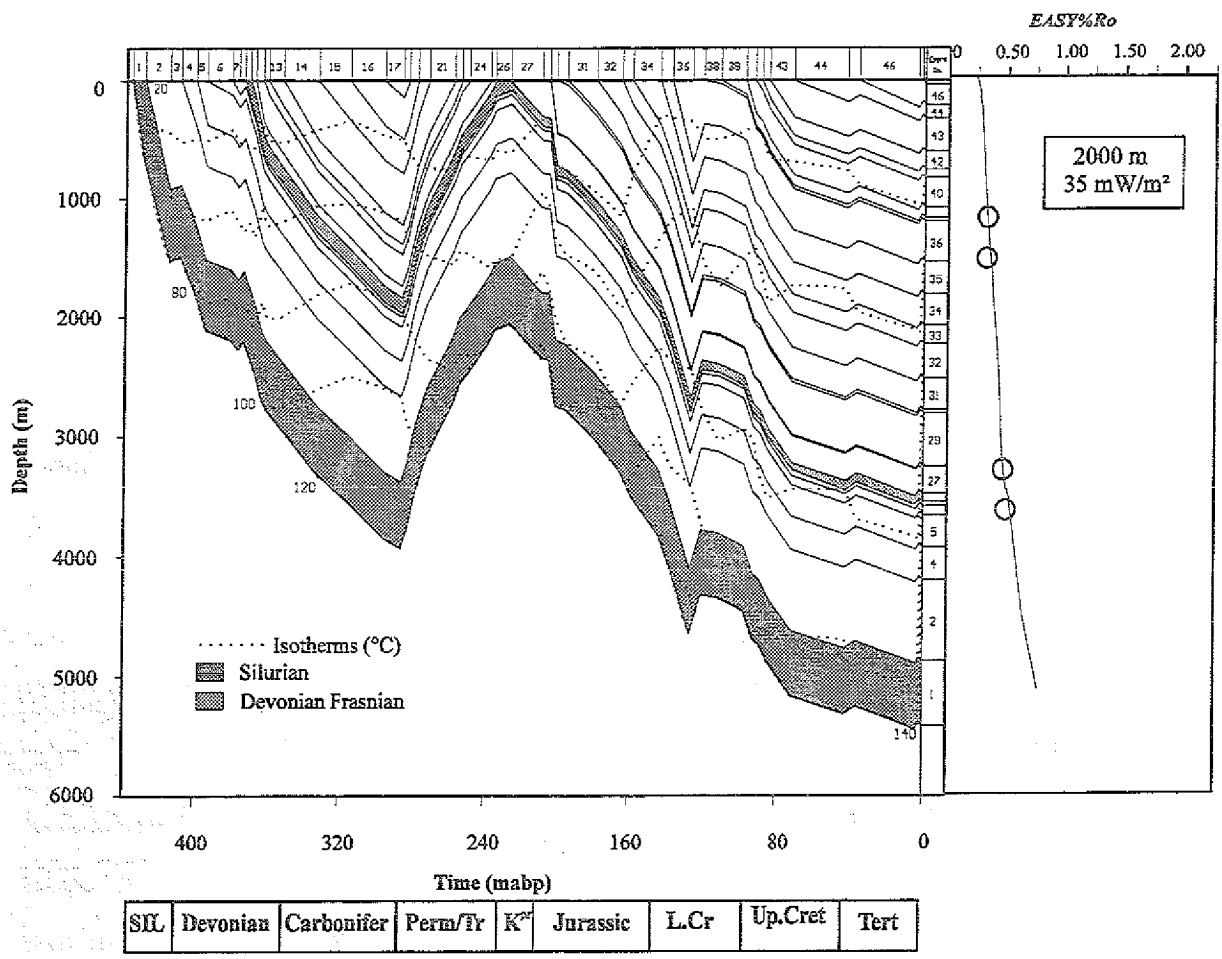


Fig. 47: Simulated burial and temperature history of well BBK-1. The right side of the figure shows the measured and calculated vitrinite reflectance.

Bir Berkine 1 well is situated between BK-2 and SF-1 wells at approximately 44 km to the north-east of BK-2 and 40 km to the West of SF-1. The Palaeozoic sediments penetrated in this well are from Late Silurian (Ludlow) to Late Devonian (Frasnian) in age and are 876 m thick. The Palaeozoic sequences are overlain by approximately 3300 m of Meso-Cenozoic sediments.

Vitrinite reflectance values obtained in this well vary from 0.37% to 0.58%, indicating a low maturity stage of the in-situ organic matter. The vitrinite reflectance profile (Fig. 47) shows that R_o is about 0.58% at a depth of 3627 m. The sublinear shape of the curve indicates an abnormally low geothermal gradient (heat flow) during the Late Cretaceous-Tertiary (i.e. maximum subsidence).

Assuming that approximately 2000 m of sediments were removed after the Hercynian orogeny, a heat flow value of 35 mW/m^2 has to be assigned to most of the Mesozoic events in order to obtain a good fit between measured and calculated vitrinite reflectance. The subsequent burial and thermal models show that the near-present maximum heating temperature reached by the oldest sediment (i.e. Silurian) did not exceed 140°C even at a burial depth of around 5500 m (Fig. 47). Such combined data would indicate a cooler than normal (hypothermal) basin, a case which was already observed in Model B of the SF-1 well. It is likely that such too low values are unrealistic in post-rift thermally subsiding basins. Present-day heat flow value calculated by using drill stem test temperatures is 56 mW/m^2. This value is much higher than the value indicated by the calibration of the model to vitrinite reflectance data.

b/ Western Berkine Basin

The western part of the Berkine Basin constitutes the eastern flank of the Amguid El Biod-Hassi Messaoud ridge and is therefore of particular interest. This area, in contrast to the central part which remained tectonically more stable, was subjected to most of the tectonic movements which affected the basin. For instance, the area under discussion was gently tilted and folded during the Carboniferous time by intense crustal shortening with the development of reverse faults with displacement of up to 1500 m (Chapter II). The main problem of this area, with respect to basin modelling, is the amount of sediments removed during and after the Hercynian orogeny. This is

important because sediment compaction affects directly or indirectly the modelling of thermal and hydrocarbon generation histories. It is, therefore, of great importance to know if the coalification process occurred prior to the Hercynian movements or during Mesozoic times.

The reconstruction of the burial and thermal history of that part of the basin was assessed using the Brides 4 well (BRD-4) drilled on a Cretaceous and Tertiary inversion structure, located at approximately 60 km West of WT-1 (Fig.1). The Palaeozoic sediments encountered by the well are of Ordovician to Late Silurian (Ludlow) age and are 1410 m thick. The Palaeozoic sediments are unconformably overlain by 3690 m of Meso-Cenozoic sediments of Late Triassic to Tertiary. Vitrinite reflectance values range from 0.57% at a depth of 1953 m to 2.02% at 4719 m. Calculated vitrinite reflectance (from MPI) ranges from 1.83 to 1.86 between 4587 to 4692 m.

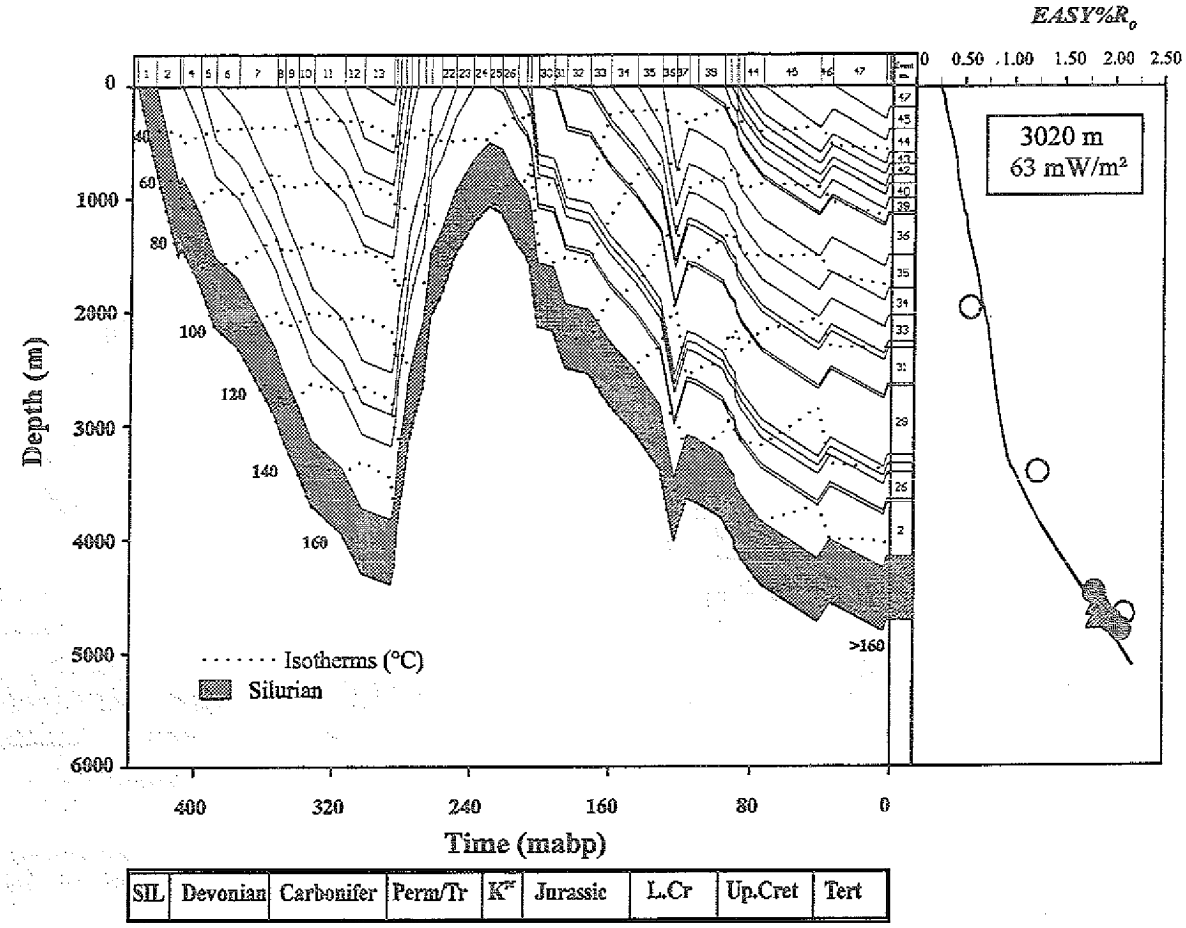


Fig. 48: Simulated burial and temperature history of well BRD-4. The right side of the figure shows the measured and calculated vitrinite reflectance (model A). The different symbols correspond to the data sources defined in Table 14.

Regardless of the position of the Hercynian unconformity, which cuts down as deep as the Late Silurian, the observed high maturity levels of the sediments and associated organic matter might be related to significant amounts of eroded overburden which seems to be in accordance with the paleogeography. In fact, Figure 7 shows that the areas which might be subjected to intense erosion are the areas which were tilted during the Hercynian orogeny (Amguid El Biod-Hassi Messaoud arch, Fig. 6). However, this remains hypothetical because the sediments which were deposited may be also reduced in their thickness due to specific and local geologic conditions.

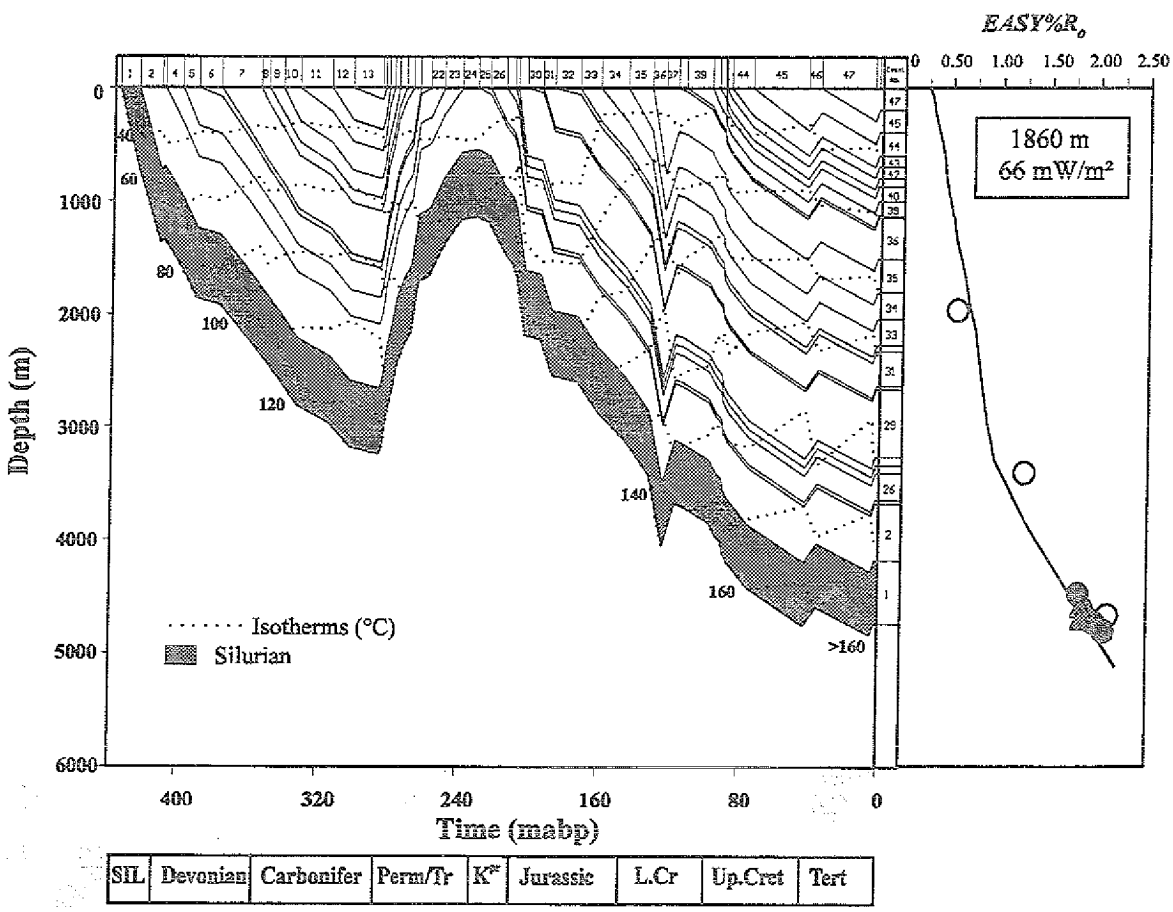


Fig. 49: Simulated burial and temperature history of well BRD-4. The right side of the figure shows the measured and calculated vitrinite reflectance (model B). The different symbols correspond to the data sources defined in Table 14.

Although Palaeozoic sediments in the central part of the basin are likely to be homogeneous in their thickness, as inferred from seismic observations, post-Devonian sedimentation might be reduced in the western part of the basin. Such an hypothesis might be supported by the fact that the early pulses of the compressive Hercynian movements took place during the Early Carboniferous (Visean) time. Unfortunately,

the calculation of a thinning rate was not possible because of the absence of completely preserved Carboniferous layers. Therefore, the profiles of measured and calculated vitrinite reflectance are brought into maximum agreement by adjusting heat flow and by changing the burial paths, by adjusting the thickness of eroded sediments.

In spite of the previous geological observations, two different burial and thermal models, which achieve the same present-day results, are proposed. The first model, namely A (Fig. 48) assumes that a large scale Hercynian erosion occurred. The data on thickness and lithology of the various stratigraphic units which were eroded between 286 and 231 Ma were derived from locations where they are preserved (i.e. central and eastern parts of the basin) below the Hercynian unconformity. A good agreement between measured and calculated maturity trends was achieved for a heat flow of 63 mW/m^2 during the Late Cretaceous/Tertiary. Associated with this, about 3000 m of Late Silurian to Carboniferous sediments are estimated to have been removed with an erosion rate of about 55 m/my. Present-day heat flow derived from temperature data of the BRD-4 well is 63 mW/m^2 and is similar to the „critical" heat flow value.

It should be pointed out that the mismatch observed when assuming lower heat flow values during the Cretaceous/Tertiary time could not be compensated by a reasonable increase of heat flow prior to and during the Hercynian movements (i.e. time of maximum Palaeozoic burial).

Model B on the other hand (Fig. 49) assumes that the sediments deposited on the western edge of the basin, particularly those of the Carboniferous age, were thinner. Following this, only 1860 m of sediments are estimated to have been removed during the Hercynian orogeny. Consequently, the conceptual model used in this case is quite similar to that used for other wells from the central part of the basin with respect to the rate of erosion which is only about 39 m/Ma. This scenario led to a good fit between measured and calculated reflectance values in combination with a heat flow of 66 mW/m^2 at maximum burial times. In the case of Model B, a rapid burial is observed from the initiation of the basin up to about 390 Ma (Middle-Late Devonian). The subsidence from that time on and up to the Late Carboniferous is rather slow, as a consequence of slower sedimentation rates. Another distinctive feature is that maximum temperature values reached by the basal Silurian source rock during the Late

Carboniferous are moderate (120°C), in contrast to more than 160°C observed in Model A..

c/ Southern Berkine Basin (Northern Illizi Platform)

1D numerical simulation was also performed on the southern edge of the Berkine Basin (northern Illizi Platform) by considering the well TZM-1. This well is located on the Ahara ridge, at around 80 km South of HAD-1 well (Fig. 1). The well penetrated 3920 m of Palaeo-Mesozoic sediments. The Palaeozoic sedimentation (2301 m) was continuous and nearly complete because sediments of Stephanian age were encountered in this area. In contrast to the deepest zones of the basin, this area shows reduced thickness of most of the Palaeozoic units with many unconformities, particularly during Early Palaeozoic times (Fig. 8). Non-deposition events are also characteristic of this area (e.g. during the Emsian and Middle Devonian, BEICIP/SH, 1991). In this sequence, the Late Devonian units are transgressive over Early Devonian (Gedinnian) sediments. Furthermore, Caledonian movements seem to be more pronounced since the Early Devonian sediments unconformably overly the Late Silurian (B1 unit partly or totally eroded). This area is also characterised by a reduced total thickness of the Mesozoic section which is only 1600 m thick in spite of more than 3000 m observed in other parts of the basin. Another important feature in that particular area is the complete absence of sediments of high thermal conductivity (i.e. the Liassic salt and anhydrite).

Measured vitrinite reflectance values vary from 0.58% at 1740 m to 1.30% at 3674 m. Taking into account the above-cited geological observations, a burial and thermal history model was constructed (Fig. 50). Maximum agreement between measured and calculated vitrinite reflectance data was obtained by assuming a heat flow of 56 mW/m^2 at the time of maximum burial. Only about 370 m of Carboniferous sediments are estimated to have been eroded during the Hercynian orogeny. The calibration of the present-day geothermal gradient was achieved by assuming a heat flow value of 56 mW/m^2.

It is important to note that the maximum burial which the sediments have experienced prior to the Hercynian uplift is relatively small compared to the other parts of the basin. Another distinctive feature is that the rapid deepening of the isotherms observed

during the Late Triassic- Liassic time is not observed here. This effect is mainly due to the absence of deposits of high thermal conductivity such as salt and anhydrite.

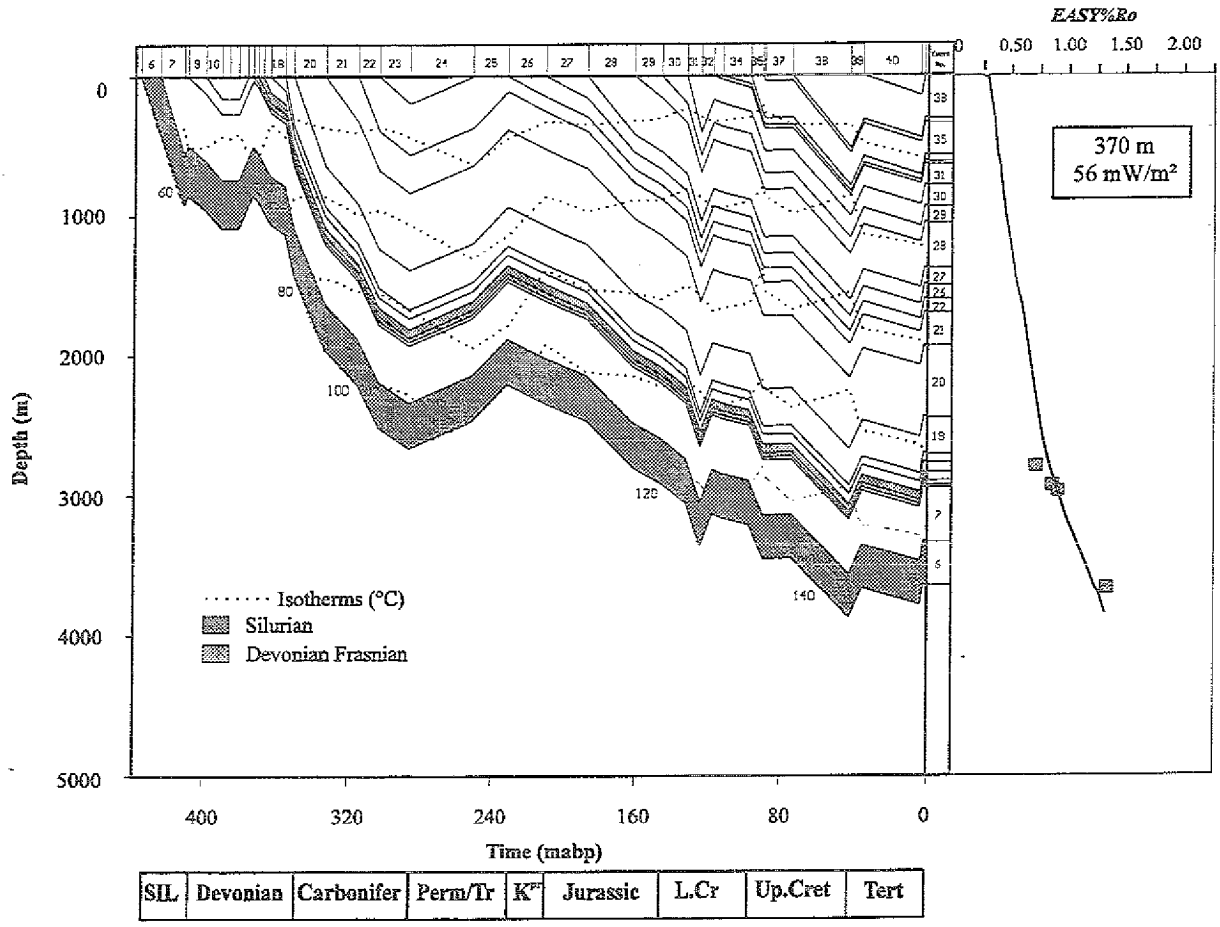


Fig. 50: Simulated burial and temperature history of well TZM-1. The right side of the figure shows the measured and calculated vitrinite reflectance.

d/ North-Eastern Berkine Basin

Available vitrinite reflectance data form the KA-1bis in the north-eastern part of the Berkine Basin allowed the simulation of the burial and thermal history of this area. The well is located on the Dahar ridge near the Tunisian border (Fig.1) and penetrated 513 m of Palaeozoic sediments from Ordovician to Late Silurian. These sediments are unconformably overlain by 2600 m of Mesozoic and Tertiary sediments.

Vitrinite reflectance values vary from 0.3% at a depth of 500 m to 0.71% at 2725 m (Table 14, Fig. 51).

The Palaeozoic sediments are likely to be deeply eroded since the Late Silurian sediments are truncated by the Hercynian unconformity. However, this area may have developed under different tectonic conditions as evidenced by many stratigraphic gaps and unconformities during the Cambro-Ordovician time. Indeed, this area, as the Ahara

ridge does, could present an early elevated zone resulting from Caledonian movements. The sedimentary rocks could be of reduced thickness here; an hypothesis which might be supported by observations of BEICIP/SH (1991) concerning the Silurian rocks for which a thickness of only 70 m in the northern extension of the Dahar mole was determined. This contrasts with thick Silurian in the Central part of the basin. This fact might suggest that the present area has probably been an elevated zone during that time and that all of the post-Silurian sediments were reduced in thickness as well. However, the absence of Late Silurian and Devonian sediments make the role played by this region during these epochs difficult to evaluate.

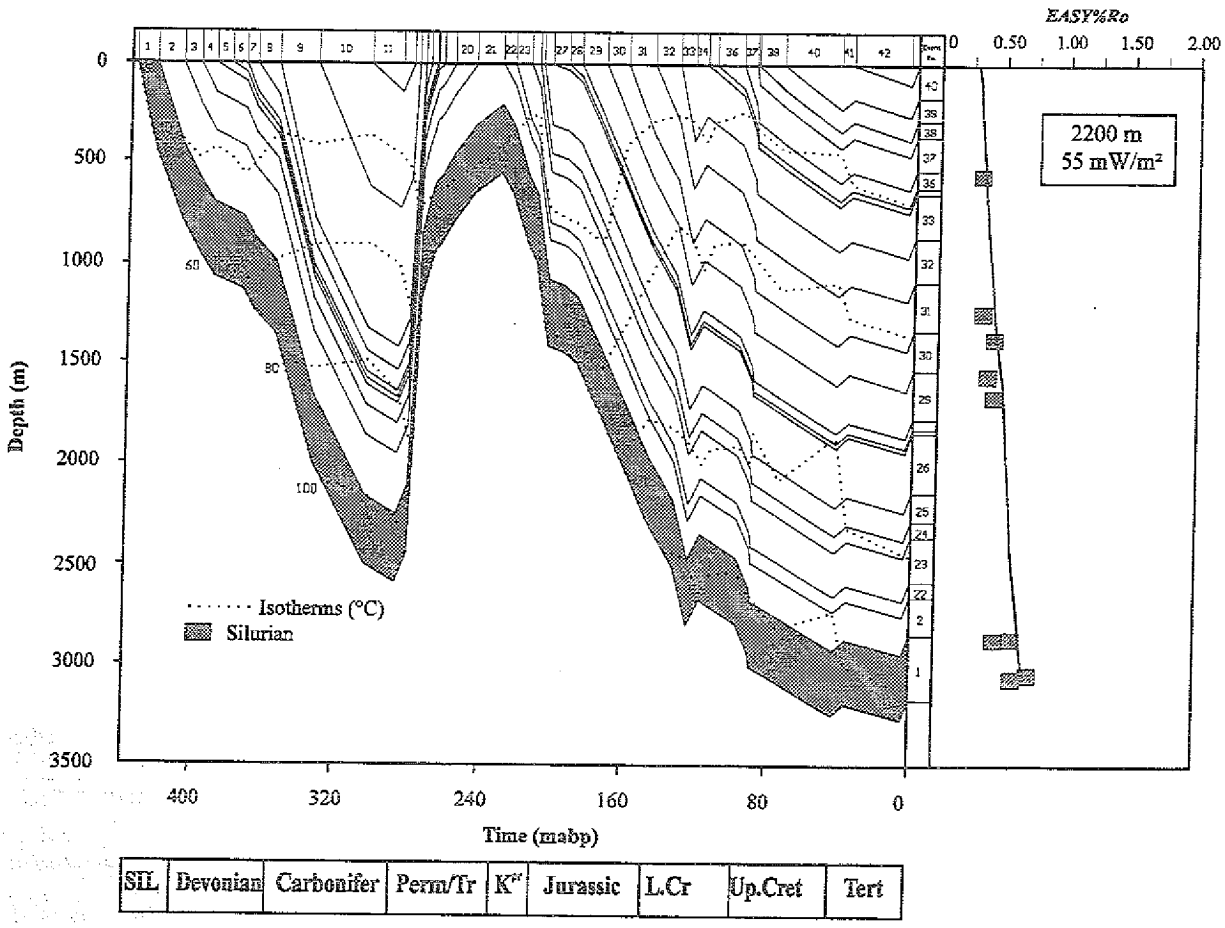


Fig. 51: Simulated burial and temperature history of well KA-1bis. The right side of the figure shows the measured and calculated vitrinite reflectance.

In the absence of information on the exact sediment thickness which has been removed during the Hercynian orogeny, it was assumed for the calculations that post-Silurian sedimentation occurred continuously up to the Stephanian time and that sediment thicknesses were the same as those of the TZM-1 well. Then, about 2200 m of Palaeozoic sediments are estimated to have been eroded. A close fit between measured

values and the reflectance calculated by the Easy%R_o algorithm was achieved if a heat flow value of 55 mW/m² was used during the time of maximum burial. Maximum temperature reached by the Silurian source rock did not exceed 120°C, a temperature close to the oil expulsion threshold.

6.3.3 Maturation History

Although the maturation development in terms of vitrinite reflectance was computed for the whole considered sequence (i.e. Silurian-Quaternary), the maturation history in the study area is discussed only for the basal Silurian and Frasnian source rocks.

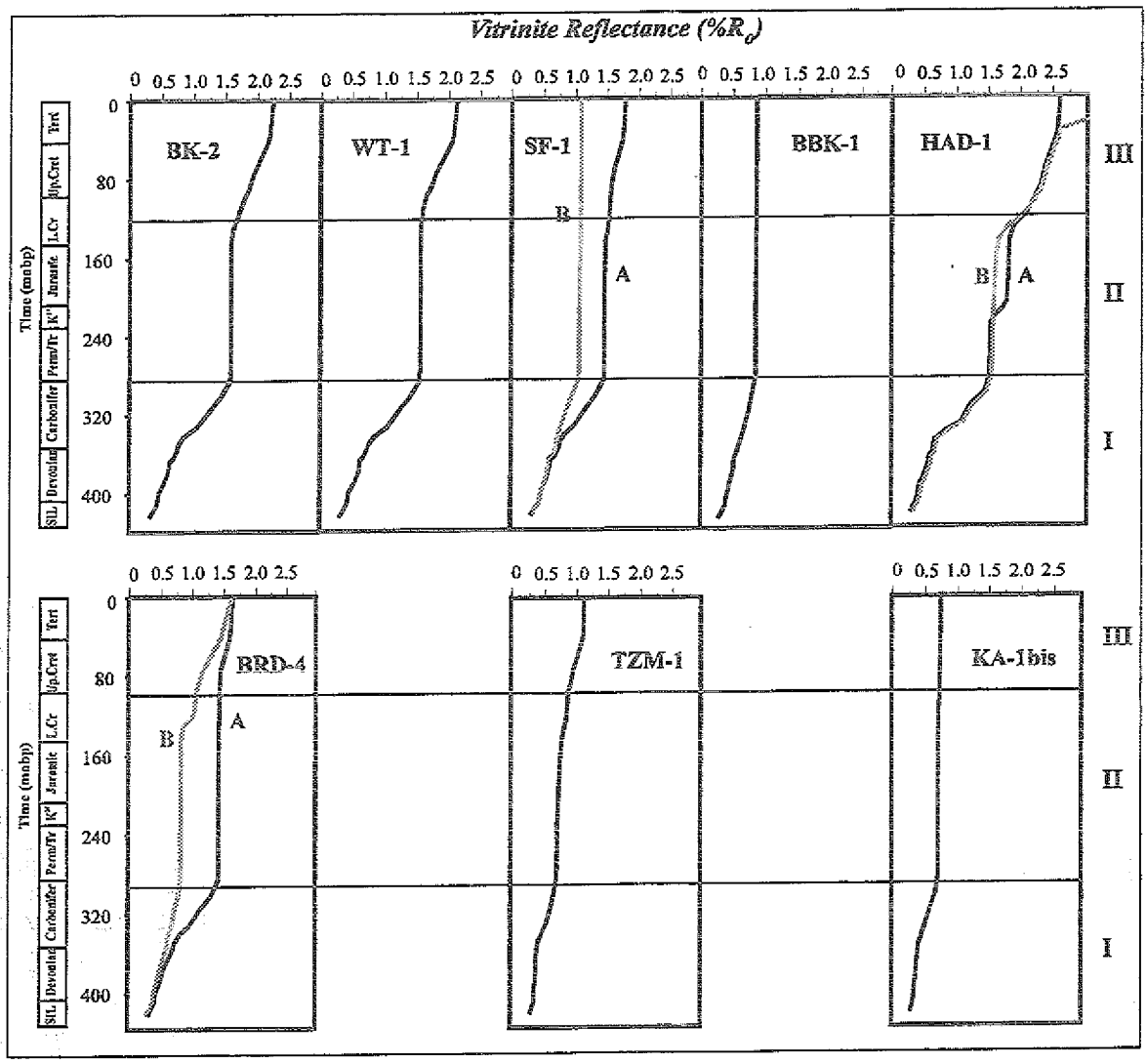


Fig. 52: Maturity (vitrinite reflectance) evolution for the basal Silurian „hot" shales at seven locations within the study area. A and B refer to the models discussed in the previous chapter.

Respective maturity (vitrinite reflectance) versus time diagrams for the different wells (and models) for both source rocks are shown in Figures 52 and 53. Their maturation history closely reflect the trends of the temperature history discussed in the previous chapter and emphasized later with respect to hydrocarbon generation. It is apparent from these diagrams that all areas have reached the highest maturity only in the recent geological past. Exceptions are BBK-1 and KA-1bis. Maturation profiles are generally composed of three distinct evolution „segments". Each segment represents a maturity evolution period.

The first segment (I, in Figures 52 and 53) represents a regular increase of maturation as a function of increasing burial and depth which occurred during the Palaeozoic, prior to the Hercynian uplift and erosion. The level of organic maturity reached during the Late Carboniferous is directly proportional to the depth of burial reached by the sedimentary rocks during that time. The second evolution segment (II) shows no increase in the maturation level reached by the source rocks although high heat flow occurred during Triassic-Early Jurassic time. This effect is mainly due to the Hercynian uplift and subsequent erosion which brought the sediments to shallower depths, and hence lower temperatures. The third maturation segment (III), which is slightly parallel to the first one, occurs during the Late Cretaceous-Tertiary as a consequence of the maximum Meso-Cenozoic burial.

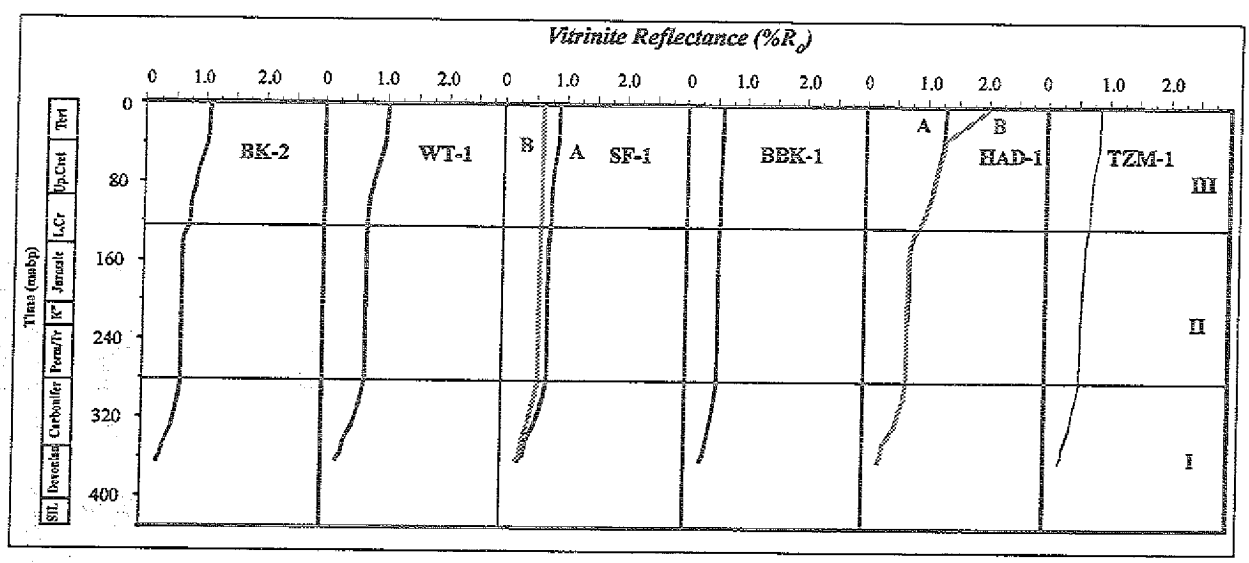


Fig.53: Maturity (vitrinite reflectance) evolution for the Frasnian shales at six locations within the study area. A and B refer to the models discussed in the previous chapter.

Assuming that the onset of oil and gas generation are respectively 0.5% and 1.2% R_o, it is apparent from these plots that the Silurian source rock has surpassed the oil generation window except in the north-eastern part of the basin where the Silurian still shows high capability for generating oil. The Frasnian source rock, on the other hand, is in the main phase of oil generation or at the threshold of gas generation in all of the studied wells.

It is notable that in models which required a higher than normal heat flow value during the time of maximum burial in order to achieve the calibration of their corresponding vitrinite reflectance data (e.g. HAD-1, models B and C), a drastic increase in the maturation during the Tertiary time is observed. Furthermore, hypothermal models such as those observed in BBK-1 and SF-1(Model B) show no increase of the degree of maturation during that time although sediment burial proceeded.

6.3.4 Hydrocarbon Generation History

The timing of hydrocarbon generation is one of the most important factors in exploration play evaluation. In organic geochemical reactions, temperature (magnitude and duration) is one of the most important factors that determine the rate of a particular chemical reaction. Hence, the conversion of kerogen into hydrocarbons (oil and gas) can be determined rather accurately once the principal reaction mechanism of this conversion and the temperature history of a given source rock is known (Tissot and Welte, 1984; Yalcin and Welte, 1988). When the temperature history is coupled with a kinetic model for hydrocarbon generation (Chapter 6.2), a better understanding of timing, quality (oil and/or gas) and amount of generated hydrocarbons can be achieved.

In the present study, modelling results on hydrocarbon generation history will be discussed with the help of temperature, transformation ratio and hydrocarbon (oil and gas) generation curves Vs time at each modelled location. The hydrocarbon generation modelling results are evaluated for the basal Silurian and Frasnian source rocks by using the type II kerogen kinetics (Chapter 6.2).

6.3.4.1 Silurian Source Rock

a/ Central Berkine basin

Because no substantial differences in terms of hydrocarbon generation were observed as inferred from the simulation results of the different wells of the Central part of the basin, the results of the Silurian source rock are discussed for the BK-2, taken as a reference well.

The temporal development of the temperature for the Silurian source rock and the results of numerical simulation of petroleum generation are presented in Figure 54 along a time axis between 435 and 0 Ma. The gradual increase of temperature between 435 and 286 Ma with a maximum value of around 170°C is a result of the successive deposition of layers and subsequent increasing burial of the source rock. Between 286 and 231 Ma temperature dropped from 170 to 120°C as a result of the Hercynian erosion and subsequent cooling. It becomes also apparent that the Triassic-Jurassic subsidence was such that, even with higher paleoheat flow values (Fig.36), the temperatures during and immediately after the rifting phase were insufficient to cause any great increase in the maturity of the source rock.

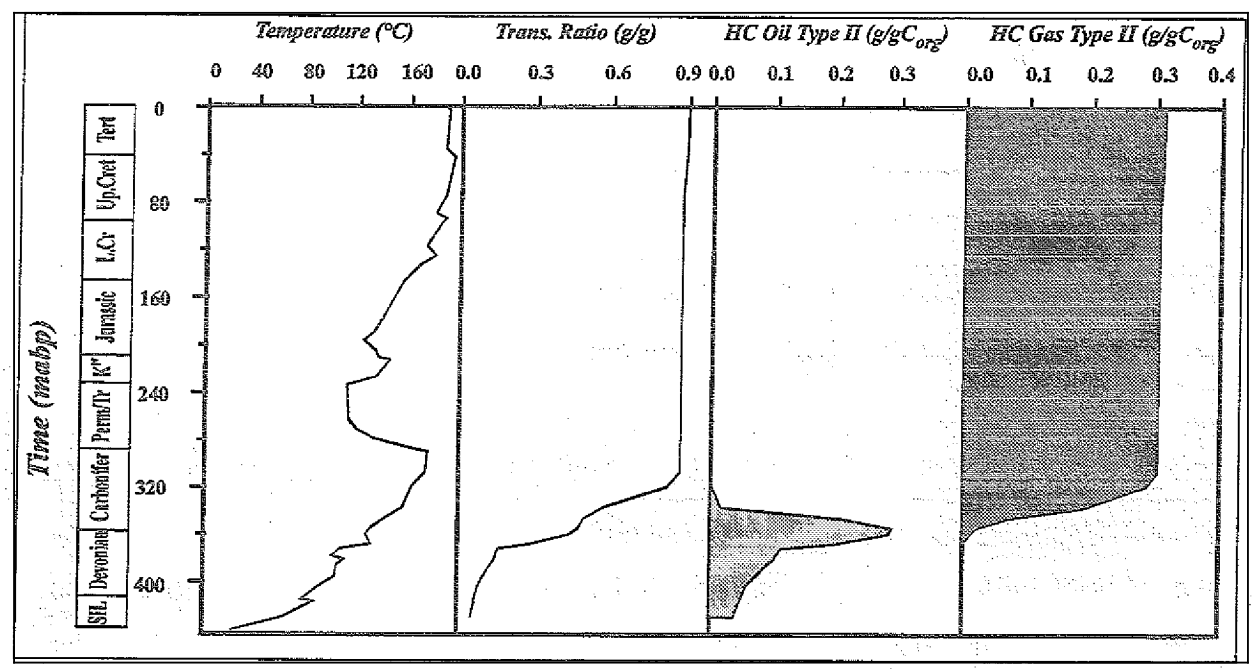


Fig. 54: Evolution of temperature, transformation ratio, oil generation and gas generation for the basal Silurian „hot shales" at the Berkine site (BK-2), Central Berkine basin.

From 210 and 0 Ma, the temperature increased gradually as a result of increasing burial. A maximum value of 190 °C was reached in the Late Cretaceous and maintained up to the present time.

According to Figure 54, the Silurian oil potential was reached already during the Palaeozoic time. Oil began to be generated during the Middle Palaeozoic with peak oil generation attained between 363 and 350 Ma (Tournaisian). The calculated transformation ratio during that time is 0.45 g/g, implying that 45% of the initial hydrocarbon potential was already generated. From 350 Ma and up to the Late Carboniferous time, the Silurian source rock generated gas with some amounts of oil. The transformation ratio reached by the source rock is at around 0.90 at the Stephanian time, implying that 90 % of the initial generation potential was realized prior to the Hercynian uplift. From that time and until the present, the Silurian source rock generated only gas.

b/ Western Berkine Basin

Since the temperature is the most sensitive parameter in hydrocarbon generation and since the burial and thermal history of the western part of the basin was assessed by assuming two different scenarios, the hydrocarbon generation history is discussed here for each individual model.

Model A

This model assumes that the sediments in the Brides area were subjected to a high burial depth during the Palaeozoic time with high Hercynian erosion amplitude (Fig.48). The subsequently modelled hydrocarbon generation histories are shown in Figure 55. One can observe that the simulation results for the basal Silurian source rock are quite similar to those of the central part of the basin. Paleotemperature calculations indicate that the Silurian source rock generated hydrocarbons as early as during the Early Carboniferous with peak oil generation occurring during the Visean.

Maximum temperatures of around 180°C were achieved during the Late Carboniferous implying that 90 % of the initial hydrocarbon potential was already realized prior to the Hercynian cooling.

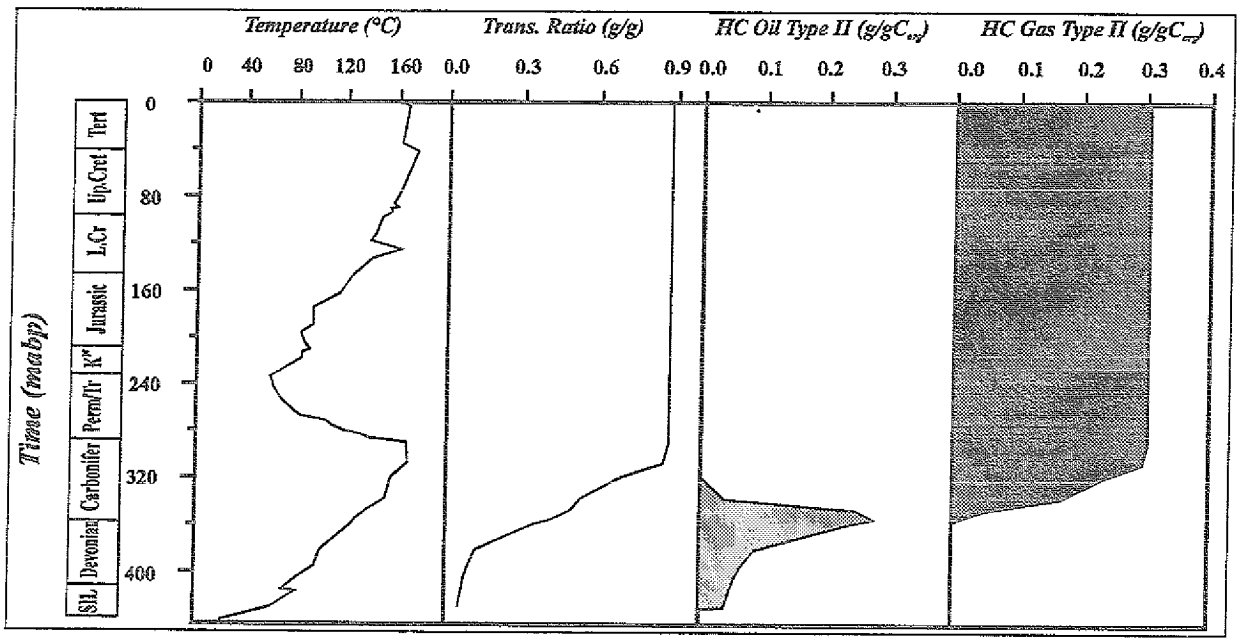


Fig. 55: Evolution of temperature, transformation ratio, oil generation and gas generation for the basal Silurian „hot shales" at the Brides site (BRD-4, Model A), western Berkine basin.

Model B

Model B assumed, in contrast to model A, that the sediments in the Brides area were subjected to a higher thermal regime in the Mesozoic time with reduced erosion amplitude during the Permian (Fig. 49). Great differences in terms of temperature and hydrocarbon generation can be observed here. Model B shows that the temperature reached by the basal Silurian source rock during late Carboniferous time does not exceed 120°C and that the Late Cretaceous-Tertiary temperatures are the highest which the associated organic matter was subjected to. In contrast to model A which implied that the Silurian oil potential was realized during the Late Carboniferous, the Silurian still owns high capabilities for generating oil during the Mesozoic. Indeed, oil generation began in the Early Carboniferous and persisted up to the Barremian time, although at smaller rates. According to Figure 56, the transformation ratio reached by the Silurian source rock prior to the Hercynian orogeny is 0.5 g/g implying that only 50 % of the initial hydrocarbon generation potential was realized. Since the temperature reached by the sediments prior to the Hercynian movements was moderate as a consequence of the associated reduced amount of eroded overburden, the appropriate conditions for liquid hydrocarbon generation were not greatly influenced.

After the Barremian time the Silurian source rock started to generate gas with minor amounts of oil. One can also observe that the 0.9 g/g transformation ratio, which was reached during the Late Carboniferous in the case of Model A, was only achieved at the present time for this case.

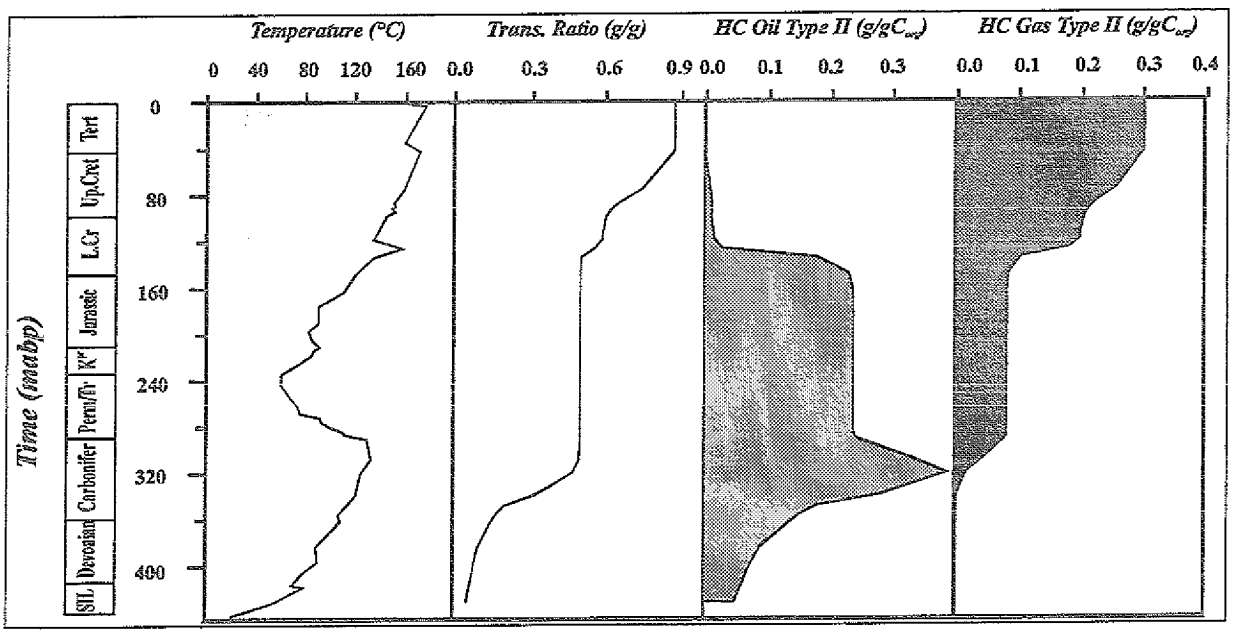


Fig. 56: Evolution of temperature, transformation ratio, oil generation and gas generation for the basal Silurian „hot shales" at the Brides site (BRD-4, Model B), western Berkine basin.

c/ Southern Berkine Basin (Northern Illizi Platform)

The timing of peak oil generation for the Silurian source rock in the southern part of the basin varies significantly compared to the central part. The variation of temperature as a function of time and the results of numerical simulations of petroleum generation for the Silurian source rock in the southern part of the basin are presented in Figure 57. The graphic shows that the Silurian temperature increases gradually with time, reaching maximum values of around 140°C during the Late Cretaceous-Tertiary. No substantial drop in temperature is observed here. As the Hercynian erosion was minor, the proceeding of the maturation of the Silurian source rock was only slightly affected. Therefore, the appropriate conditions for hydrocarbon generation were not interrupted. With respect to hydrocarbon generation history, the Silurian radioactive shales started to generate oil in the Visean time after the 10% transformation ratio was reached. The generation of liquid hydrocarbons proceeded throughout the Mesozoic

with peak oil generation occurring during the Middle Jurassic (between 187 and 146 Ma). During that time only 50 % of the initial hydrocarbon generation potential was realized. From the Middle Jurassic, Silurian shales started to generate gas, and while the amount of gas increased, that of oil decreased.

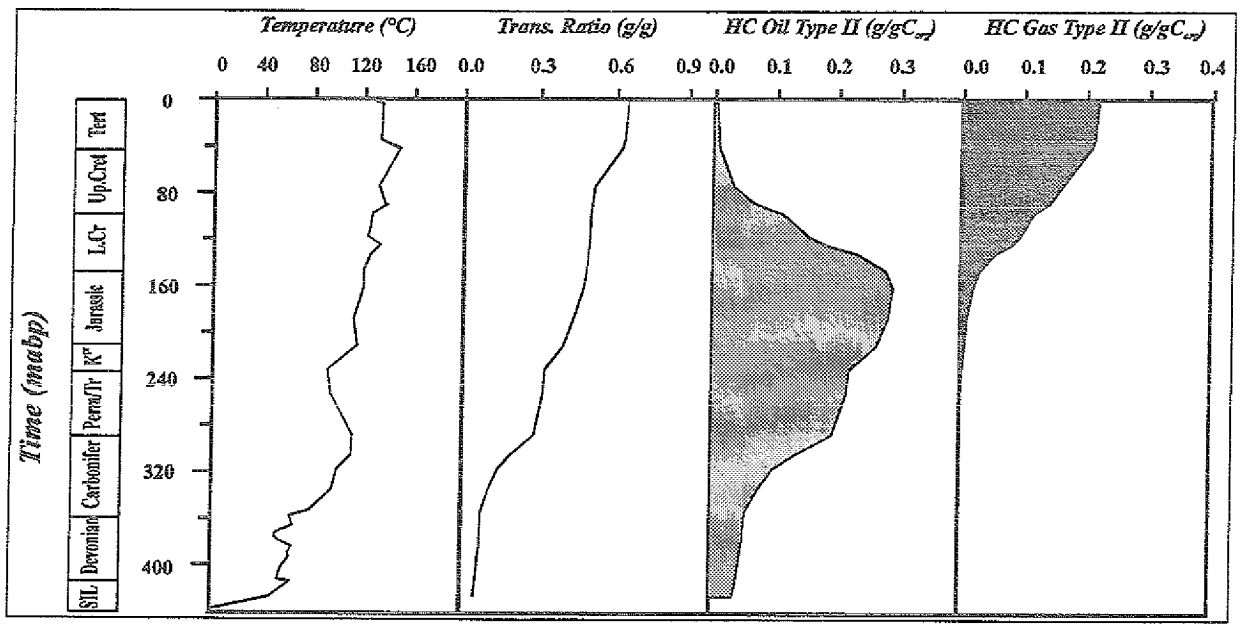


Fig. 57: Evolution of temperature, transformation ratio, oil generation and gas generation for the basal Silurian „hot shales" at the Tin Zemane (TZM-1), southern Berkine basin.

At the present time the Silurian is in the wet gas generation window and still shows capabilities for generating further hydrocarbons. This fact is indicated by the present-day residual hydrocarbon generation potential which is approximately 35 %.

d/ North-Eastern Berkine Basin

Modelling results for the Silurian shales in the north-eastern part of the basin are presented in Figure 58. Active oil generation occurred between 333 and 286 Ma at a temperature range between 90 and 120 °C. Hydrocarbon generation rate remained constant between the Late Carboniferous and the Barremian. Since the maturation of the Silurian was affected by the Hercynian erosion and subsequent cooling, the generation of oil slowed-down. Maximum oil generation occurred between the Barremian and the present time when appropriate temperature conditions re-appeared again. However, the Silurian shales are still in active oil generation in that part of the

basin. The present residual potential of the source rock is about 55% of the initial hydrocarbon potential indicating that only 45% was generated during its evolution.

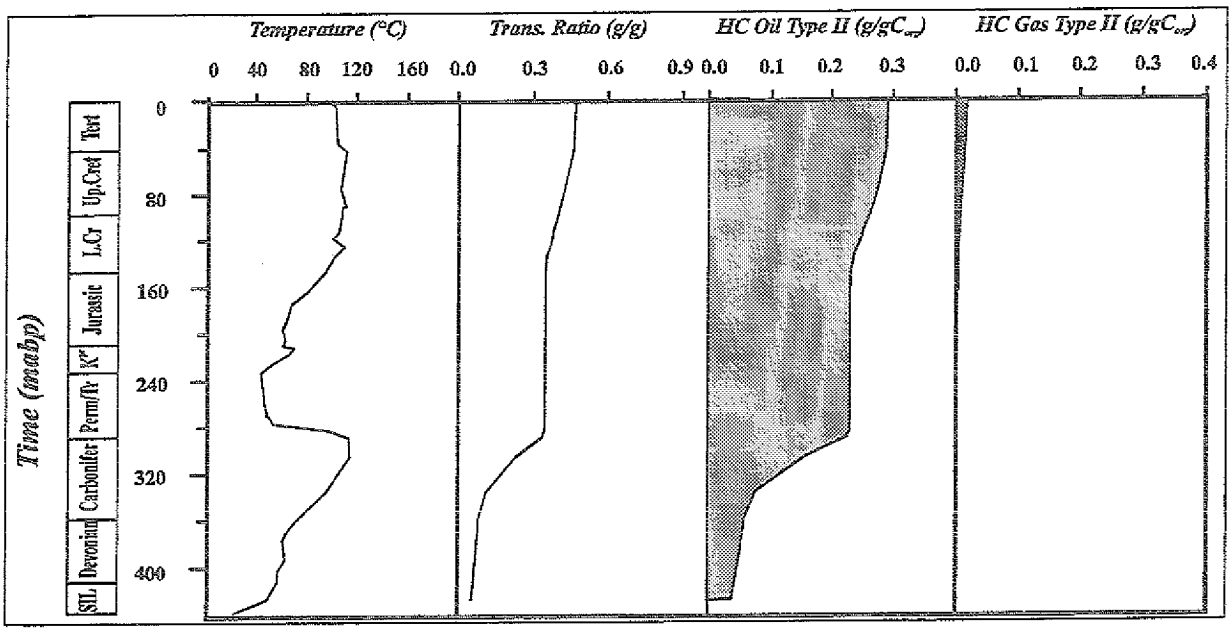


Fig. 58: Evolution of temperature, transformation ratio, oil generation and gas generation for the basal Silurian „hot shales" at the Keskassa site (KA-1bis), north-eastern Berkine basin.

6.3.4.2 Frasnian Source Rock

The development of temperature for the Frasnian shales and the results of numerical simulation of petroleum generation are discussed for three sampling locations represented by the BK-2 well, the HAD-1 well, and the TZM-1 well. For the other wells of the central part of the basin, the results are quite similar to those of the BK-2 well. The relatively limited extent of the Devonian source rock did not allow, unfortunately, investigations in the northern and western part of the basin.

a/ Central Berkine basin

Well BK-2

The temporal development of the temperature for the Frasnian source rock in the sampled well and the corresponding results of petroleum generation are presented in Figure 59 along a time interval between 373 and 0 Ma.

The graphic shows that maximum heating occurred at maximum burial. Temperatures reached by the Frasnian source rock during the Late Cretaceous-Tertiary did not

exceed 140 °C. Liquid hydrocarbon generation started in the Early Carboniferous and slowed-down during the Permian-Late Jurassic, as a consequence of the Hercynian erosion and subsequent cooling.

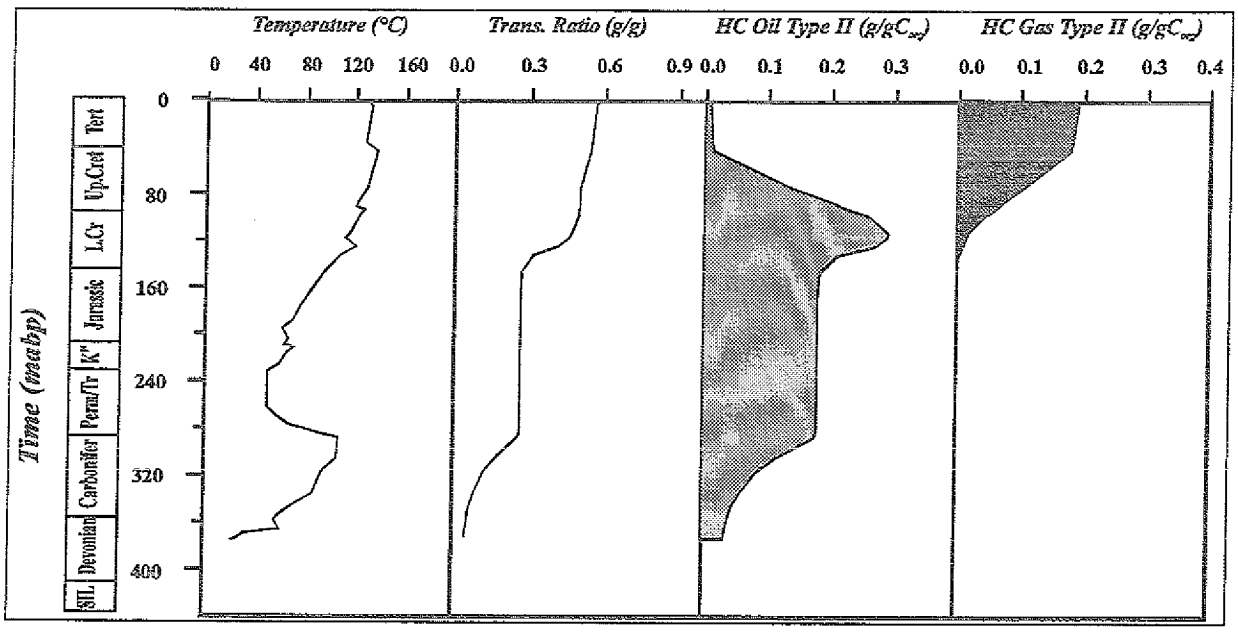


Fig. 59: Evolution of temperature, transformation ratio, oil generation and gas generation for the Devonian Frasnian at the Berkine site (BK-2), Central Berkine basin.

It is also apparent from the graphic that active hydrocarbon generation occurred during the Early Cretaceous-Tertiary with peak oil generation occurring during the Albo-Aptian. During the last 42 Ma very little oil generation has occurred and the Frasnian source rock generated mainly gas. The transformation ratio curve also indicates that only 60% of the initial hydrocarbon generation potential of the source rock was realized, and hence, still good capabilities for further gas generation exist.

Well HAD-1

The three assumptions used for the reconstruction of burial and thermal history of the Hiad area did not show any differences with respect to the timing of oil generation. The great difference which can be mentioned is related to the maximum temperature reached by the source rock at the time of maximum burial during which a sudden increase of temperature is observed when assuming higher heat flow (Figs. 43 and 44). For the other modelled parameters (i.e. transformation ratio and amount of gas

generated) only very slight differences can be observed. These differences are related to the increase in the transformation ratio and gas generation rates caused by the high heat flow assumptions. Regardless of the above-cited observations, the results are discussed here for Model A which assumed that no significant thermal event occurred at the time of maximum burial.

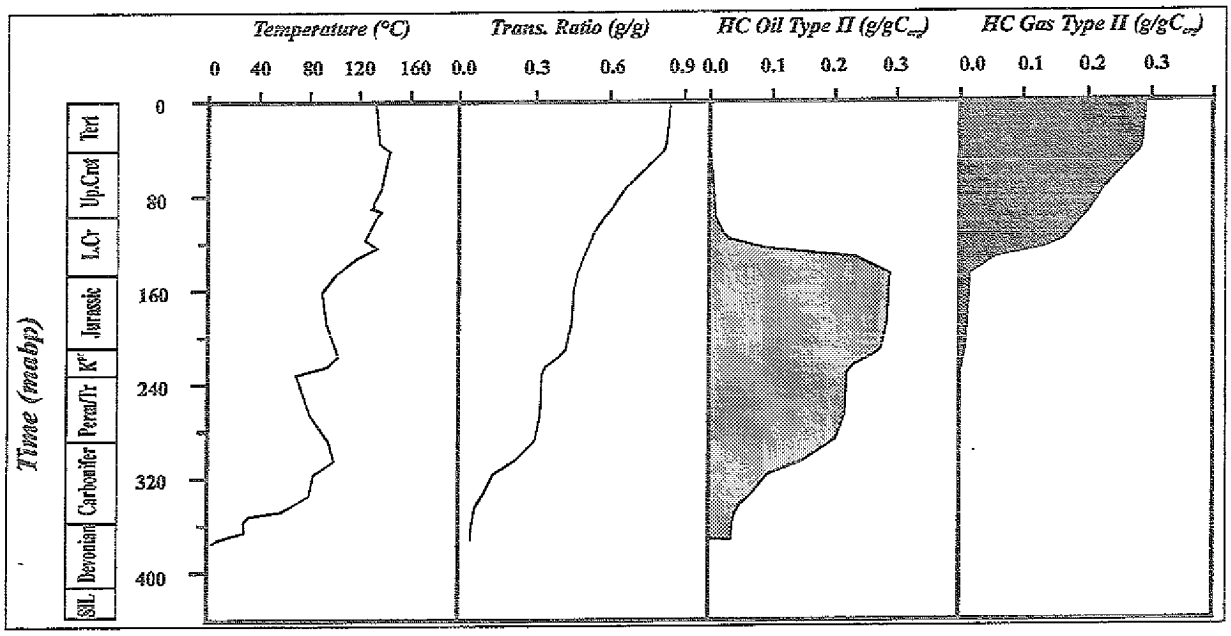


Fig. 60: Evolution of temperature, transformation ratio, oil generation and gas generation for the Devonian Frasnian at the Haiad site (HAD-1), Central Berkine basin.

Figure 60 shows a general increase of temperature during basin evolution. As previously mentioned, the small amount of eroded Carboniferous overburden did not allow any substantial interruption in temperature proceeding. Therefore, the maturation progress was not interrupted. Liquid hydrocarbons started to be generated in the Late Palaeozoic. Although at slower rates during some periods, the generation of liquid hydrocarbon continued up to the Late Jurassic time, a threshold after which only gas was generated. The graphic also reveals that the Frasnian shales reached almost 90 % of their initial hydrocarbon generation potential at the present time and have, therefore, a lower capability for further hydrocarbon generation than their equivalents in the Berkine area (BK-2 well).

The main results obtained for the Frasnian at the other sites of the Central part of the basin are shown in Figure 61.

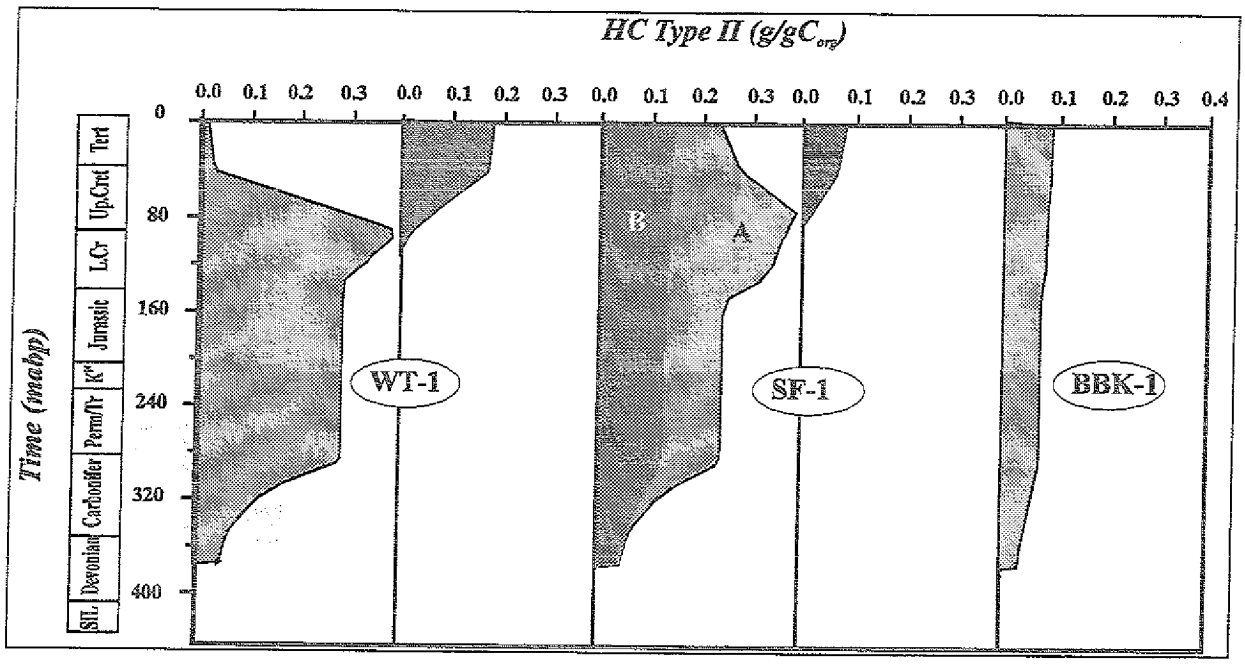


Fig. 61: Hydrocarbon (oil and gas) generation curves Vs time in the WT-1, SF-1 and BBK-1 sites, respectively. A and B refer to the Models described in Chapter 6.3.2. Light and dark areas are oil and gas, respectively.

b/ Southern Berkine Basin (Northern Illizi Platform)

The temporal variation of temperature for the Frasnian shales in the Tin Zemane area and the results of the numerical simulation of petroleum generation are shown in Figure 62.

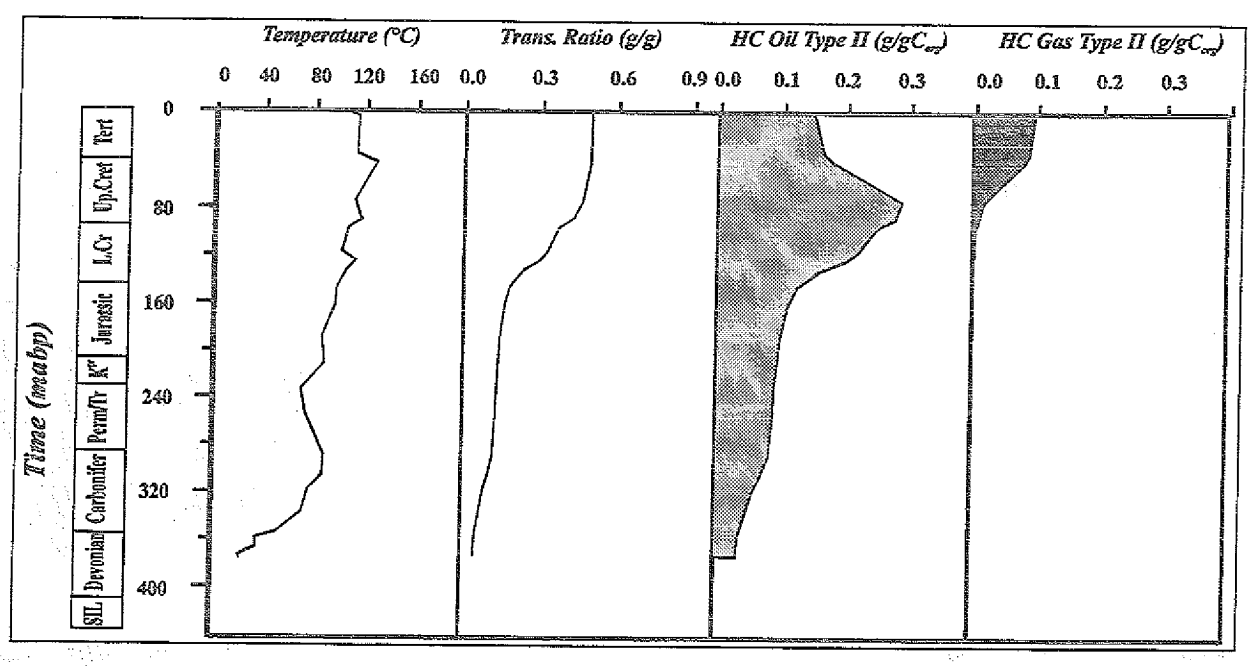


Fig. 62: Evolution of temperature, transformation ratio, oil generation and gas generation for the Frasnian at the Tin Zemane site (TZM-1), southern Berkine basin.

A general increase of temperature with increasing burial and time is also observed here. As in the Haiad area, no substantial interruption in temperature increase is observed and the maturation history of the Frasnian source was not affected by the Hercynian erosion, due to its small amount. Liquid petroleum started to be generated in the Palaeozoic. This generation continued throughout the Mesozoic and was mainly active during the Late Cretaceous. The generation of oil slowed-down during the Tertiary when small amounts of gas were generated. The graphic reveals also that approximately half of the initial hydrocarbon potential was not yet realized indicating that the source rock still has capabilities for generating further gas.

The principal results obtained in all the simulations with respect to temperature calibration and hydrocarbon generation for the Silurian and Frasnian are summarized in Table 16.

Tab. 16: Heat flow density and temperature at the time of maximum burial (Late Cretaceous/Tertiary), estimated total eroded thickness and peak oil generation for the basal Silurian and Frasnian as inferred from numerical simulations at the different sites. A and B are those models described in Chapter 6.3.2.

Well	HF density (mW/m²) at maximum burial	Eroded sediments	Total Erosion (m)	Present-day HF (mW/m²)
BK-2	55	Tournaisian-Stephanian	1420	55
WT-1	55	Famennian-Stephanian	1800	55
HAD-1	55 (A), 73(B), 80 (C)	Westphalian-Stephanian	200	55
SF-1	56 (A), 35 (B)	Tournaisian-Stephanian	1370	58
BBK-1	35	Frasnian-Stephanian	2000	56
BRD-4	63 (A), 66 (B)	Late Silurian- Stephanian	3000 (A), 1860 (B)	63
TZM-1	56	Westphalian-Stephanian	370	56
KA-1bis	55	Late Silurian-Stephanian	2200	55

	Hydrocarbon Generation					
	Silurian			Frasnian		
	depth (m)	T(°C) max burial	Peak oil generation (Ma)	depth (m)	T(°C) max burial	Peak oil generation (Ma)
BK-2	6536	190	350	4414	140	120
WT-1	6168	190	350	4091	140	110
HAD-1	6049	205 (A), >240 (B)	345	3812	150	200
SF-1	5982	180 (A), 120 (B)	350 (A), 320 (B)	4210	125 (A), 90 (B)	80 (A)
BBK-1	5251	80?	320?	3989	80?	Not reached
BRD-4	4723	180	350 (A), 320 (B)	Eroded		
TZM-1	2982	150	200	2650	130	80
KA-1bis	3167	120	0	Eroded		

6.3.5 Significance of the Triassic-Liassic Thermal Anomaly to Hydrocarbon Generation

The rift basins are generally characterised by high heat flow values, depending on the amount of extension (stretching factor of McKenzie, 1978). For instance, heat flow can reach values of 125 mW/m² in present-day active rift basins such as the Red Sea (Allen and Allen, 1990). As the Triassic basin was characterised by crustal extension with igneous activity during the Triassic-Liassic and because the determination of the relative paleoheat flow variation by interpreting regional tectonic processes is possible, it is assumed that the Berkine basin was characterised by higher than normal heat flow during that time (see also Chapter 6.1.5). For the objectives of the present study, it is important to know the contribution of such high heat flow to the maturation of organic matter and hence, hydrocarbon generation. This was illustrated for the Frasnian source rock by using the BK-2 well for which the modelling results for two extreme heat flow hypotheses were compared.

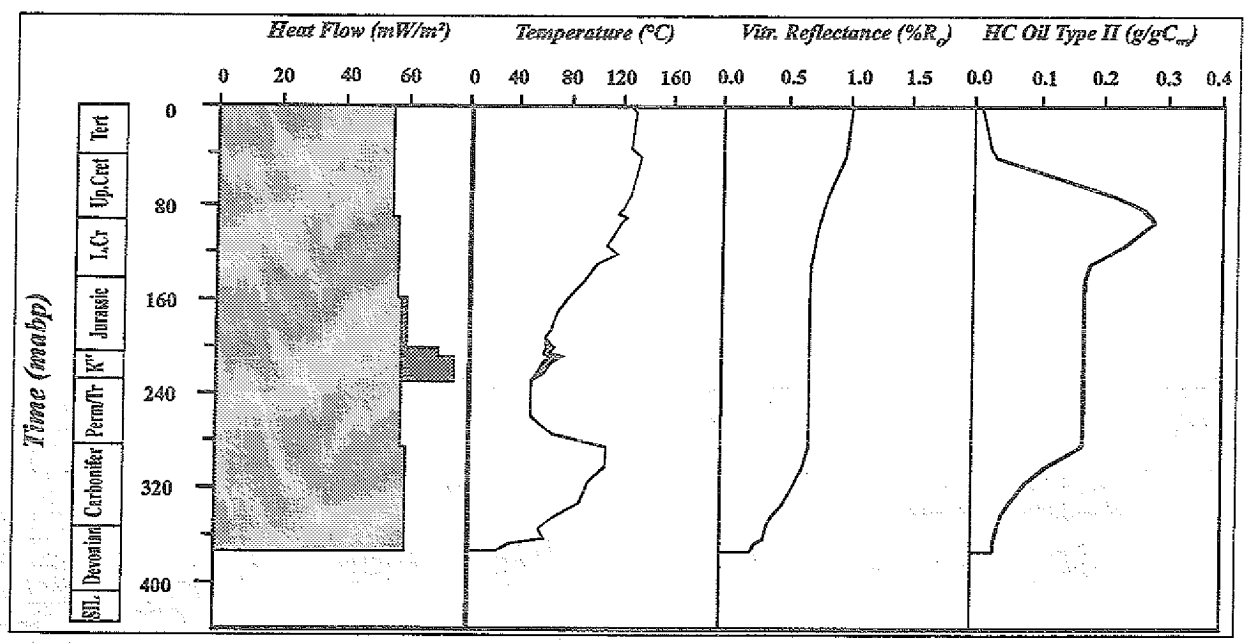


Fig. 63: Diagrams illustrating the effect of the Triassic-Liassic thermal event to hydrocarbon generation.

First, it is was assumed that the Late Triassic-Early Jurassic rifting was characterised by an average heat flow value of 60 mW/m². In a second case a heat flow value of 75 mW/m² which is close to the mean value given by Allen and Allen (1990) for present-

day active synrift or passive margin basin is considered. The modelling results with respect to temperature, vitrinite reflectance and hydrocarbon generation by considering the hypotheses cited above are superimposed on Figure 63.

Although, temperature is slightly affected by considering the second and more accurate hypothesis, the graphic reveals that neither vitrinite reflectance nor the timing of hydrocarbon generation were affected. This effect is interpreted as being the effect of the extent of the Hercynian orogeny and cooling. The considerable drop in sediment temperature as a result of the Hercynian erosion could not be compensated by assuming a high heat flow. It was subsequently noted that hydrocarbon generation is slightly affected in areas where the Hercynian erosion was minor (e.g. HAD-1, TZM-1). However, great differences with respect to the peak hydrocarbon generation were not observed.

6.3.6 Significance of Thermal Properties of Rocks to Hydrocarbon Generation

Regardless of the apparent role of the depth of burial in hydrocarbon generation from the basal Silurian and Frasnian source rocks, thermal properties of rocks such as thermal conductivity and heat capacity are of major importance to the overall temperature distribution in sedimentary basins (Chapter 6.1.4). The effect of thermal properties of rocks are illustrated in the present study by comparing sequences where sediments such as salt and anhydrite (evaporites) are either present or absent. Because their higher thermal conductivities (low heat capacities) salt and anhydrite tend to dissipate the produced thermal energy and can, therefore, act as conductive pipes (Neunzert et al., 1996; Poelchau et al., 1997; Neunzert, 1998). This phenomenon is well illustrated in the Berkine basin. The presence of sediments of relatively higher thermal conductivity such as salt, anhydrite and even carbonate in the Mesozoic section led to a general widening of the isotherms during that time. The isotherms within the Mesozoic section are also spread wider than those observed in the Palaeozoic section. Because of the shaly and sandy nature of most of the Palaeozoic sediments, the observed depth of the isotherms in all the modelled wells of the basin are in contrast narrower (Figs. 40 to 51). Furthermore, comparisons between maximum temperature development for the Frasnian section in field where high thermal conductivity sediments are either present (Berkine) or absent (Illizi) reveals that

specific high temperatures are attained by the sediments in the second case at much shallower depth (Tab. 16). This could explain why the Illizi Platform is characterised by higher geothermal gradients (Fig. 38) and why a relatively shallow hydrocarbon generation window characterises the Illizi Platform (Fig. 24). Therefore, the possibility of higher heat flow as the cause of the exhausted generation potential of organic matter in the Illizi Platform has to be reconsidered.

It is clear that the assumed temperature history of the Tin Zemane area as illustrated by the TZM-1 well cannot be generalized to all the Illizi Platform. Other literature data have to be taken into account for the regional evaluation of the results. For instance, Tissot et al. (1987) and Makhous et al. (1997) observed the same temperature range (100-130°C) for the Devonian source rock, respectively, in the north-eastern and eastern Illizi where many oil fields are located. Furthermore, the presence of any heat flow anomaly at the time of maximum burial should have also some effects on the kerogen in terms of reduced hydrocarbon generation potential, as well as on the present hydrocarbon distributions. This was not observed on the Illizi Platform or in the Berkine Basin.

6.3.7 Data Limitations

This present modelling study is based on the assumption that measured maturities reflect roughly the thermal history of the different fields analysed. However, it is recognised that this type of measurement is prone to errors which could adversely affect the accuracy of the modelling scenarios presented here. Vitrinite reflectance measurements lead to less uniform data if the measurements are performed on dispersed organic matter (Scheidt and Littke, 1989). Hence, it is always important to keep the possibility of errors in mind and not to accept blindly the data (e.g. vitrinite reflectance is even measured in Cambrian, Table 14) particularly if only one kind of organic maturity parameter is used.

Although it is not unusual that different conceptual models are within limits consistent, true maturity trends must be based on reasonable geological considerations. In view of the basin modelling results of this study, three thermal features (all were conduct to fit the present maturity data) emerge by using vitrinite reflectance measurements of different sources. These are:

1/ An hypothermal regime as inferred from the modelling results of BBK-1 and SF-1 (Model B), where heat flow values at times of maximum burial do not exceed 35 mW/m^2.

2/ A normal or near normal thermal regime as inferred from most of the maturity data.

3/ an hypothermal regime with higher than normal heat flow values (up to 80 mW/m^2) as inferred from the coalification trends observed in the HAD-1 well (Models B and C).

In view of the tectonic evolution of the basin, lower than normal heat flow values seem to be unrealistic. Hypothermal basins are generally associated with crustal shortening in tectonically active zones, such as oceanic trenches, foreland and outer fore-arc basins unrelated to arc magmatism and not in post-rift thermally subsiding basins (Allen and Allen, 1990). It is believed that the second alternative is the best possible model in terms of the thermal and generation history of the Silurian and Frasnian source rocks. This fact can be supported by visual analysis of kerogen from the Frasnian-Famennian interval which revealed yellow-orange fluorescing particles and suggesting a maturity stage of about 0.7-0.8% R_o which is analogous to the measured values in this study. The heat flow history of the SF-1 (Model B) and BBK-1 is believed to be incorrect. One possible reason of the low reflectance values could be the poor quality of the polished sections measured by the laboratory. In addition, an unusual composition of vitrinite precursors might offer an explanation for the low reflectance values. In other words the fraction may have a different composition according to the source and conditions of deposition and could, therefore, constitute different plant associations or a variety of gelification (Tissot et al., 1987). Another possibility is that the analysed particles are hydrogen-enriched, inhibiting aromatisation. In fact Rock-Eval data from both wells (SF-1 and BBK-1) reveal highly bituminous samples with free hydrocarbon contents of up 6 mg/g rock.

The cause of high vitrinite reflectance values in the Haiad area (HAD-1) could be the measurement of particles wrongly defined as vitrinite due to the small size and dispersed nature of the kerogen. An hyperthermal regime implying an updoming of the mantle or plutonism during the Cretaceous-Tertiary time, as shown by models B and C

for HAD-1, is unlikely because there are no indications of strong magmatic activity or rifting.

6-3-8 Summary

- The tectonic events which affected the Berkine basin as inferred from subsidence analysis repeat basically the sequence of tectonic movements determined from seismic interpretation (Boudjema, 1987, BEICIP- SH 1991):

- Crustal extension through the Cambro-Ordovician time associated with volcanic activity.
- Subsidence from Late Ordovician to Stephanian time as a consequence of thermal contraction of the lithosphere.
- Late Carboniferous crustal shortening with the development of reverse faults defining the Amguid-El Biod fault zone of the western part of the Berkine basin.
- Basement stretching during the Late Triassic-Early Jurassic associated with volcanic activity.
- Post- rift subsidence up to the present time as a consequence of thermal contraction.

- As the present-day or near present-day burial is the greatest which sediments have experienced, any increase of the heat flow during that time would overestimate the maturity data.

- Most of the maturity data bear no imprint of any high temperature event during the time of maximum burial. The associated heat flow range ranges from 66 to 55 mW/m^2. The highest values were registered for the western edge of the basin (Amguid El Biod-Hassi Messaoud ridge) and are in good agreement with the associated geothermal gradients. Tectonically less stable, this part of the basin could have experienced higher than normal heat flow. Furthermore, present-day temperature data indicate that heat flow values range between 63 and 55 mW/m^2 and that the average geothermal gradient for the upper crust is 25°C/km.

- The extent of Hercynian erosion, present-day burial depth and thermal conductivity of rocks are main factors enhancing or inhibiting the maturation of the in-situ organic matter and hence hydrocarbon generation.

- With respect to hydrocarbon generation, the modelling results show two periods of generation. Both Palaeozoic and Mesozoic generation are shown in the study area and concern the Silurian source rock, whereas hydrocarbon generation from the Frasnian source rock occurred mainly during the Mesozoic time.

For the Silurian source rock, oil generation was achieved during the Palaeozoic in most of the study area. Exceptions to this rule are the north-eastern and the southern parts. In the former the Silurian is still actively generating petroleum, whereas in the latter peak oil generation occurred at Jurassic time at around 180 Mabp. One should not ignore that the Silurian oil potential in the western Berkine basin was probably achieved during the Mesozoic as deduced from the modelling results of BRD-4 well, Model B. This hypothesis seems to be in agreement with the timing of trap formation and the observed hydrocarbon distribution in that particular area of the basin (Fig. 1).

From the Frasnian source rock, oil was generated mainly in Mesozoic between Jurassic and Tertiary time. The earliest time of peak oil generation was 200 Ma; the latest is the present.

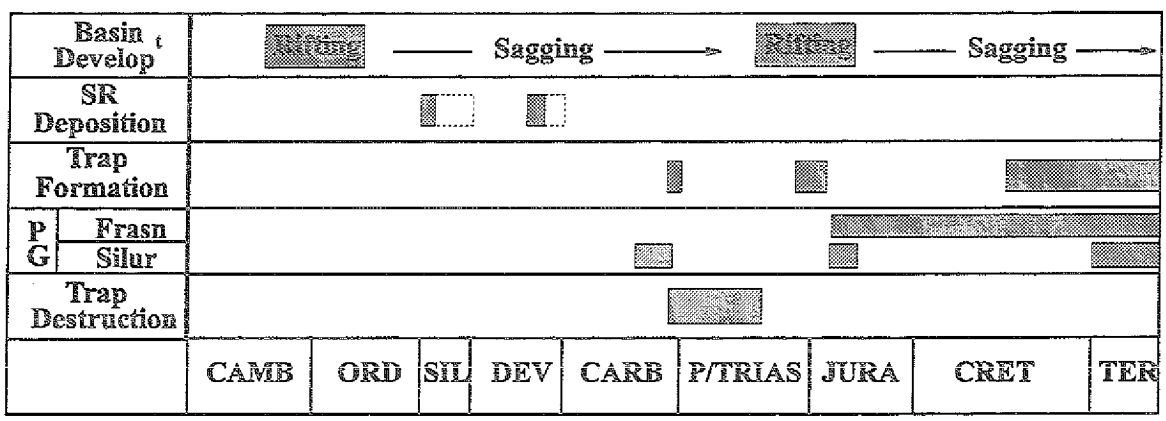


Fig. 64: Simplified tectonic and petroleum system history of the Berkine basin. The Meso-Cenozoic petroleum cycle appears to be more consistent as Late Palaeozoic traps are expected to be largely destroyed during the Hercynian movements. PG, petroleum generation.

Based on the structural development of the basin and the modelling results described before, a simplified tectonic and generation history model can be generated for the Berkine basin with the key events related to two main cycles controlled primarily by plate tectonic movements (Fig. 64). It is generally emphasized that the relationship between the events greatly controls the success or failure of exploration at a basin scale.

6-4 2D Simulation Results

In addition to the 1D numerical simulations performed for different sites of the basin (Chapter 6.3), a 2D numerical modelling study was carried out in order to understand the geological and thermal evolution of the basin, to quantify this information and to derive the history of hydrocarbon (oil and gas) generation. A further important goal was to investigate the history of hydrocarbon migration and entrapment along the 205 km long transect across the Berkine Basin. This transect crosses major petroleum areas where oil, gas and condensate were accumulated in different trap types and reservoir levels (Figs. 1 and 35). To the West, the folded area of the Amguid El Biod-Hassi Messaoud hydrocarbon bearing trend includes, from West to East, the structures of Nezla, Gassi El Adem and Brides. These structures are bounded by basement faults which were reactivated during Cretaceous and Tertiary times. Gas has been recovered in deep Ordovician (Hamra Quartzites) reservoirs. The Triassic reservoir in these structures is heterogeneous with respect to the type of hydrocarbon that it contains. Gas and oil were recovered in Nezla, oil in Gassi El Adem and condensate in the Brides structure. To the East, there are the fault block structures of the Berkine area (Wed Teh, Berkine East and Sif Fatima). The structural style in the central part of the basin as illustrated by the cross section (Fig. 35) reflects mainly the Triassic-Liassic rifting phase. The fault blocks contain, on the other hand, light oil (40-45°API) and gas in a reservoir of Triassic age. Gas and condensate are also recovered from Carboniferous (Visean) and Early Devonian (Gedinnian) reservoirs in the Berkine East structure.

In this study the 2D finite element numerical model PetroMod (version 3.1) was used. Necessary modelling and calibration data are described in Chapter 6.1. Regardless of the burial, thermal and hydrocarbon generation histories, two important aspects of petroleum geology, with respect to the factors controlling generation, migration and accumulation of hydrocarbons, are not yet discussed:

1- Overpressures and the transmissibility of the major faults to fluid movements.

2- The contribution of each source rock to the present oil and gas accumulations within the basin.

The present chapter deals with the 2D numerical modelling results pertaining with the above-cited aspects.

It should be pointed out that the results presented here are derived from a model where the thicknesses of the eroded overburden is extrapolated from nearby sections. In other words, it is assumed that the thickness of the different eroded layers in the western part of the basin are similar to their equivalents preserved from erosion elsewhere (i.e. central and south-eastern parts of the basin). For comparison, a model assuming sediment thickness reduction for the Carboniferous layers at the western edge of the basin, as the result of the early pulses of the Hercynian orogeny, is discussed with respect to hydrocarbon generation and migration as an alternative model.

6-4-1 Present-Day Temperature Distribution

When the thermal properties of the different rocks making up the sedimentary fill and the present-day average surface temperature is known (here set to 25°C), the modelling of the present-day temperature distribution depends on the present-day heat flow. This latter is calculated by calibration of the temperatures obtained during logging and/or testing (BHT and/or DST) within five wells situated along the cross-section at the grid points 29, 42, 45, 72 and 94 and representing the BRD-4, WT-1, BK-2, BKE-1 and SF-1 wells, respectively. Temperature data used for calibration are listed in Table 13. The present-day temperature distribution is obtained by tuning the present-day heat flow until a good match between the measured and calculated values is observed. It was consequently observed that the western part of the basin (i.e. in the vicinity of the anticlines) is warmer than the region situated farther away from the folded area represented by the central and eastern parts of the profile (Fig. 65). The calculated respective present-day heat flow values are 60 and 50 mW/m^2. The latter value is lower than the average continental value proposed by Allen and Allen (1990) for thermally subsiding (post-rift) and passive margin basins. The rising of the depth of the isotherms in the western part of the basin is the result of the higher heat flow which caused higher temperature gradients. Another feature is the temperature contrast observed in the Palaeozoic and Mesozoic sediments. This is obvious by the fact that the isotherms in the Mesozoic section are wider than those observed in the Palaeozoic sediments (Fig. 65). This effect arises from the contrast in the mineralogical composition of the sediments making-up the fill of both sections. The presence of

sediments of relatively higher thermal conductivity such as salt, anhydrite and carbonates in the Mesozoic section is the direct cause of such differences.

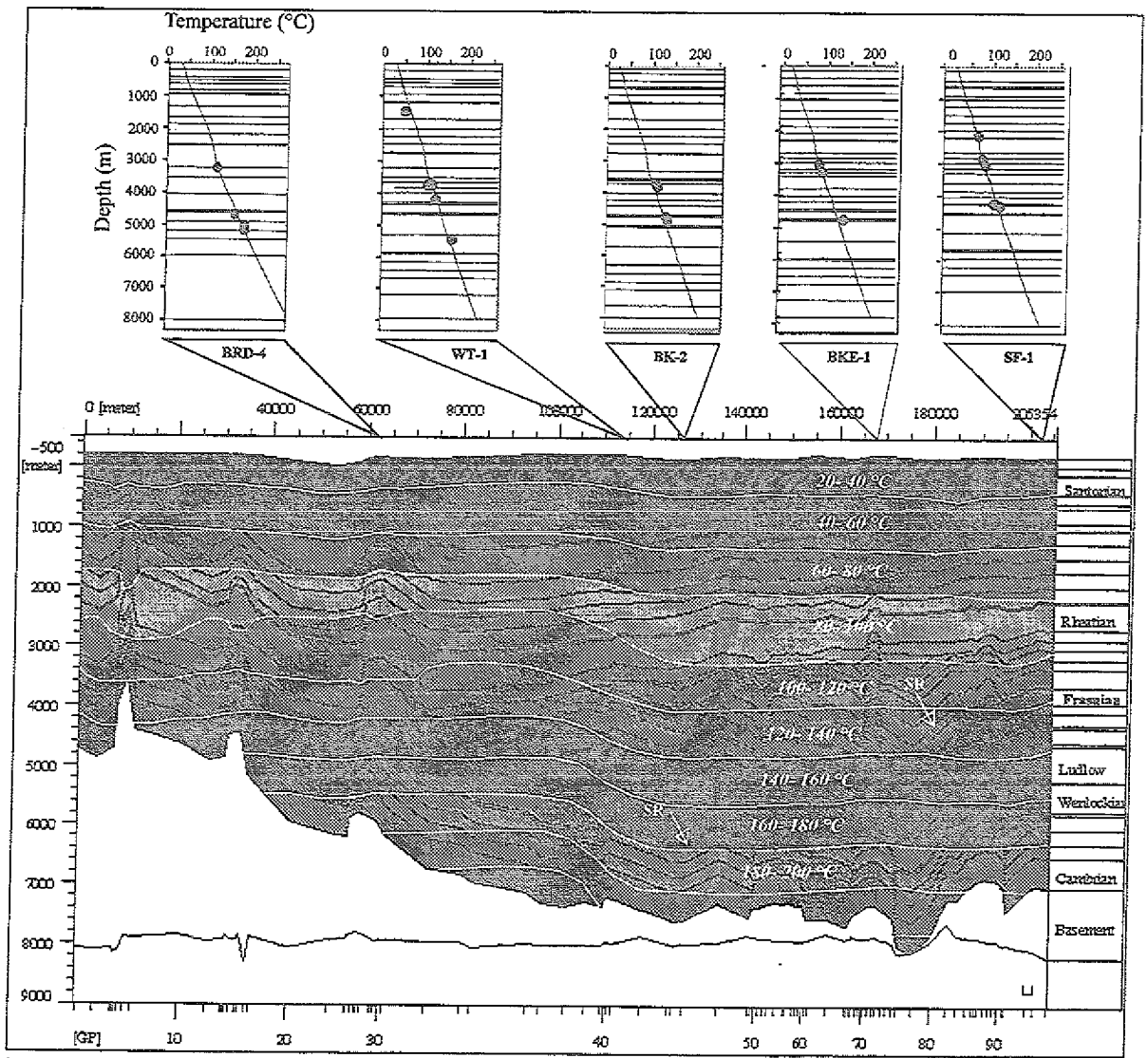


Fig. 65: Simulated present-day temperature distribution along the cross-section and the achieved match with the bottom hole and/or drill stem test temperatures of the calibration wells. SR, source rock.

6-4-2 Maturity Distribution and Evolution

The computation of paleotemperature as a consequence of conductive and convective heat transfer and of the geodynamic evolution of the basin was obtained by calibrating heat flow against vitrinite reflectance profiles obtained from 5 wells situated along the 2D investigated profile at the grid points 29, 33, 42, 45 and 94. These grid points are represented by BRD-4, BKW-1, WT-1, BK-2 and SF-1 wells, respectively (Fig. 35). Necessary calibration data are listed in Table 14. During the simulation procedure, the vitrinite reflectance distribution along the 2D profile that was calculated according to

Tab. 17: Lithology, sediment thickness (m) and heat flow (mW/m^2) for calibration wells along the simulated cross section. The highlighted values are sediments which were totally (-9999) or partly eroded during the Hercynian orogeny.

Event N°	Event Name	Time (Ma)	Lithology	BRD-4 (GP29) Thick	HF	BKW-1(GP33) Thick	HF	WT-1 (GP42) Thick	HF	BK-2 (GP45) Thick	HF	SF-1(GP94) Thick	HF
60	Tertiary	35	SAND,silty	192	60	288	60	253	50	210	50	172	50
59	Alpine	42	LIME,dolo	-150	60	-140	60	-50	50	-50	50	-50	50
58	Maes-Eoc	74	LIME,dolo	345	60	270	60	274	50	216	50	171	50
57	Santonian	86	DOLO, evap	208	60	348	60	252	50	232	50	329	50
56	Coniacian	89	SALT	97	60	155	60	122	50	180	50	161	50
55	Turonian	90	LIME,marly	100	60	78	60	111	50	58	50	67	50
54	Cenoman	97	SHALE,evap	205	60	242	60	241	50	223	50	238	50
53	Albian	112	SAND,shaly	125	60	268	60	237	50	219	50	99	50
52	Aptian	117	LIME,dolo	25	60	30	60	30	50	30	50	25	50
51	Austrian	119	"	0	60	0	60	0	50	0	50	0	50
50	Austrian	121	"	0	61	0	61	0	53	0	53	0	53
49	Austrian	124	SAND,silty	-350	61	-124	61	-100	53	-150	53	-150	53
48	Baremm	132	SAND,silty	705	61	705	61	620	53	653	53	381	53
47	Neocom	146	SHALE,sandy	306	62	316	62	309	55	313	55	247	55
46	Malm	161	SHALE&LIME	248	62	248	62	209	55	218	55	242	55
45	Dogger	187	SHALE,calc	309	63	238	63	259	58	243	58	246	58
44	Pliensb	194	EVAP,shaly	310	63	320	63	257	58	299	58	230	58
43	sinemur	203	LIME,shaly	25	63	25	63	25	58	25	58	25	58
42	Rheatian	210	SALT	673	65	637	65	470	60	553	60	441	60
41	Tr.Keuper	231	SAND,shaly	344	75	232	75	266	70	231	70	175	70
23-40	Hercynian	286		See the table below									
22	Stephan	303	SHALE,evap	120	60	120	60	120	60	120	60	120	60
21	Westphal	315	LIME,shaly	300	60	300	60	300	60	300	60	300	60
20	Namurian	333	SHALE,calc	250	60	250	60	250	60	250	60	250	60
19	Visean-C	342	SILTSTONE	350	60	350	60	350	60	350	60	350	60
18	Visean-B	350	SAND&SHALE	250	60	250	60	250	60	250	60	250	60
17	Tournias	355	SAND,shaly	200	60	200	60	200	60	200	60	191	60
16	Strunian	363	SILT,sandy	106	60	106	60	106	60	106	60	134	60
15	Famenn	367	SHALE,silty	349	60	349	60	349	60	350	60	313	60
14	Frasnian	377	SHALE,calc	200	60	200	60	196	60	230	60	270	60
13	Emsian	390	SHALE&LIME	136	60	136	60	136	60	180	60	156	60
12	Gedi-Sieg	397	SAND&SHALE	320	62	320	62	321	62	309	62	206	62
11	Intra G-Sieg	399	SHALE	50	62	50	62	50	62	50	62	50	62
10	Gedinian	409	SANDSTONE	270	62	282	62	260	62	270	62	250	62
9	Pridolian	411	SHALE	50	63	50	63	50	63	50	63	50	63
8	Ludlow	424	SAND&SHALE	600	63	600	63	650	63	650	63	600	63
7	Wenlock	433	SHALE,silty	510	65	550	65	550	65	550	65	500	65
6	Llandov	435	SHALE,calc	50	65	50	65	50	65	50	65	50	65
5	Llanvirn	780	SAND&SHALE	293	70	293	70	260	70	260	70	250	70
4	Arenigian	493	SANDSTONE	280	70	250	70	250	70	250	70	250	70
3	Tremadoc	510	SHALE,sandy	273	75	273	75	250	75	250	75	250	75
2	Cambrian	570	SANDSTONE	500	75	500	75	500	75	500	75	500	75
1	Basement	650	BASEMENT	2000	40	1132	40	761	40	407	40	1082	40

Event N°	Event Name	Time (Ma)	BRD-4 (GP29) Thick	HF	BKW-1(GP33) Thick	HF	WT-1 (GP42) Thick	HF	BK-2 (GP45) Thick	HF	SF-1(GP94) Thick	HF
40	Hercynian	233	0	58	0	58	0	58	0	58	0	58
39	Hercynian	236	0	58	0	58	0	58	0	58	0	58
38	Hercynian	240	0	58	0	58	0	58	0	58	0	58
37	Hercynian	244	-75	58	0	58	0	58	0	58	0	58
36	Hercynian	248	-9999	58	0	58	0	58	0	58	0	58
35	Hercynian	253	-9999	58	0	58	0	58	0	58	0	58
34	Hercynian	257	-9999	58	-9999	58	0	58	0	58	0	58
33	Hercynian	261	-9999	58	-9999	58	0	58	0	58	0	58
32	Hercynian	264	-9999	58	-9999	58	0	58	0	58	0	58
31	Hercynian	267	-9999	58	-9999	58	0	58	0	58	0	58
30	Hercynian	270	-9999	58	-9999	58	-200	58	0	58	0	58
29	Hercynian	273	-9999	58	-9999	58	-9999	58	0	58	0	58
28	Hercynian	276	-9999	58	-9999	58	-9999	58	-150	58	-100	58
27	Hercynian	278	-9999	58	-9999	58	-9999	58	-9999	58	-9999	58
26	Hercynian	280	-9999	58	-9999	58	-9999	58	-9999	58	-9999	58
25	Hercynian	282	-9999	58	-9999	58	-9999	58	-9999	58	-9999	58
24	Hercynian	284	-9999	58	-9999	58	-9999	58	-9999	58	-9999	58
23	Hercynian	286	-9999	58	-9999	58	-9999	58	-9999	58	-9999	58

the conceptual model is compared to measured vitrinite reflectance data until a good agreement between both values is obtained. The input data set of the calibration wells is listed in Table 17. The complete data set for the simulated cross section, expressed by some of the important input parameters such as sediment thickness and heat flow are listed in the enclosed Tables 10 and 11.

From the 1D simulation results, it was observed that the sediments in the basin reached their maximum burial and temperature only recently. Therefore, vitrinite reflectance data reflect mainly the Late Cretaceous-Tertiary burial. The calibration of the model was achieved by assuming heat flow values of 60 mW/m² in the vicinity of the anticlines and 50 mW/m² in the region situated farther away from the folded area. The estimated amount of eroded overburden during Permian-Triassic times increases from the East to the West along the profile (Fig. 66).

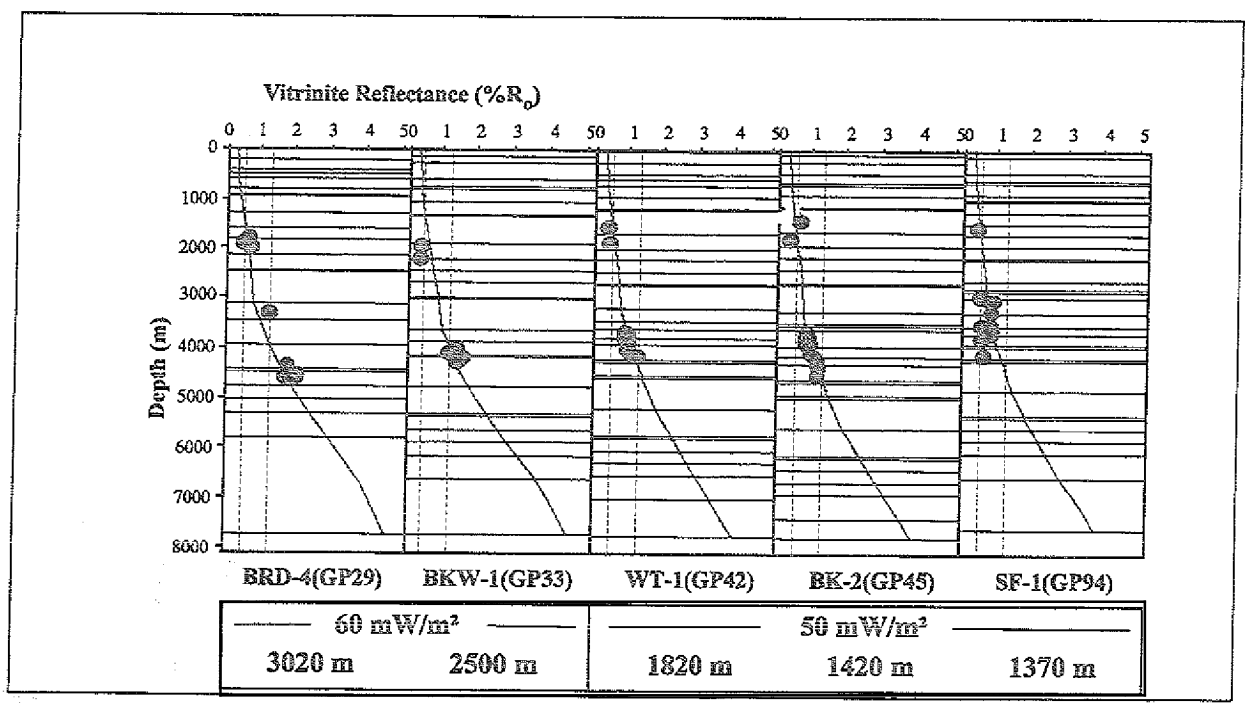


Fig. 66: Achieved match between measured and calculated vitrinite reflectance of the calibration wells. Additional information about the heat flows during maximum burial and the amounts of eroded Palaeozoic sediments are indicated. Black and grey symbols are measured and calculated (from MPI 1) vitrinite reflectance, respectively.

Figure 67 shows simulated maturity distributions and evolution, as expressed by vitrinite reflectance, at the end of the Carboniferous (286 Ma), during the Early Cretaceous (124 Ma), and at the present time. The calculated vitrinite reflectance at the Late Carboniferous time (Fig. 67a) for the Silurian and Frasnian source rocks range

from 1.6 to 1.8% R_o and from 0.6 to 0.8% R_o, respectively, along the whole transect. Being the result of the maximum Palaeozoic burial, these maturity data are in good agreement with the respective calculated temperatures (150-175°C and 100-125°C). Considering that oil expulsion occurs in the 100-120°C temperature window while gas is largely expelled in the 150-230 °C temperature range (Mackenzie and Quigly, 1988), the Silurian source rock has surpassed the oil expulsion threshold, whereas the Frasnian source rock was at the optimum temperature for expulsion.

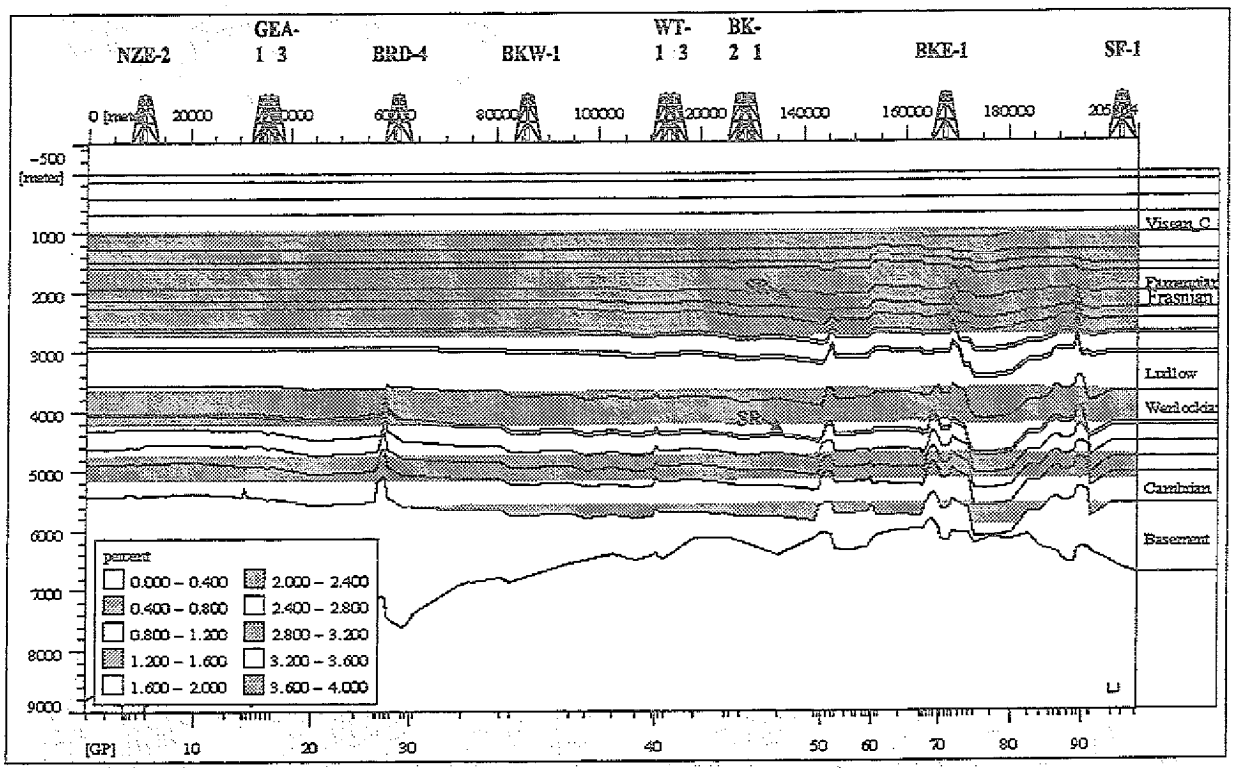


Fig. 67a: Computed maturity (vitrinite reflectance) at 286 Ma (end of Stephanian) for the modelled profile. SR, source rock.

Figure 67b reveals that, although higher heat flow values existed during the Late-Triassic-Early Jurassic rift phase, the maturation of organic matter did not proceed since the maturation levels observed within both source rocks during the Early Cretaceous (124 Ma) are similar to those observed during the Late Carboniferous. This evolution step is expressed as the maturation evolution segment 2 defined in Chapter 6.3.3 and interpreted as being the result of the Hercynian movements and subsequent cooling.

Figure 67c shows the present-day maturity distribution along the simulated cross section. From this figure, it becomes evident that present or near present-day maturities

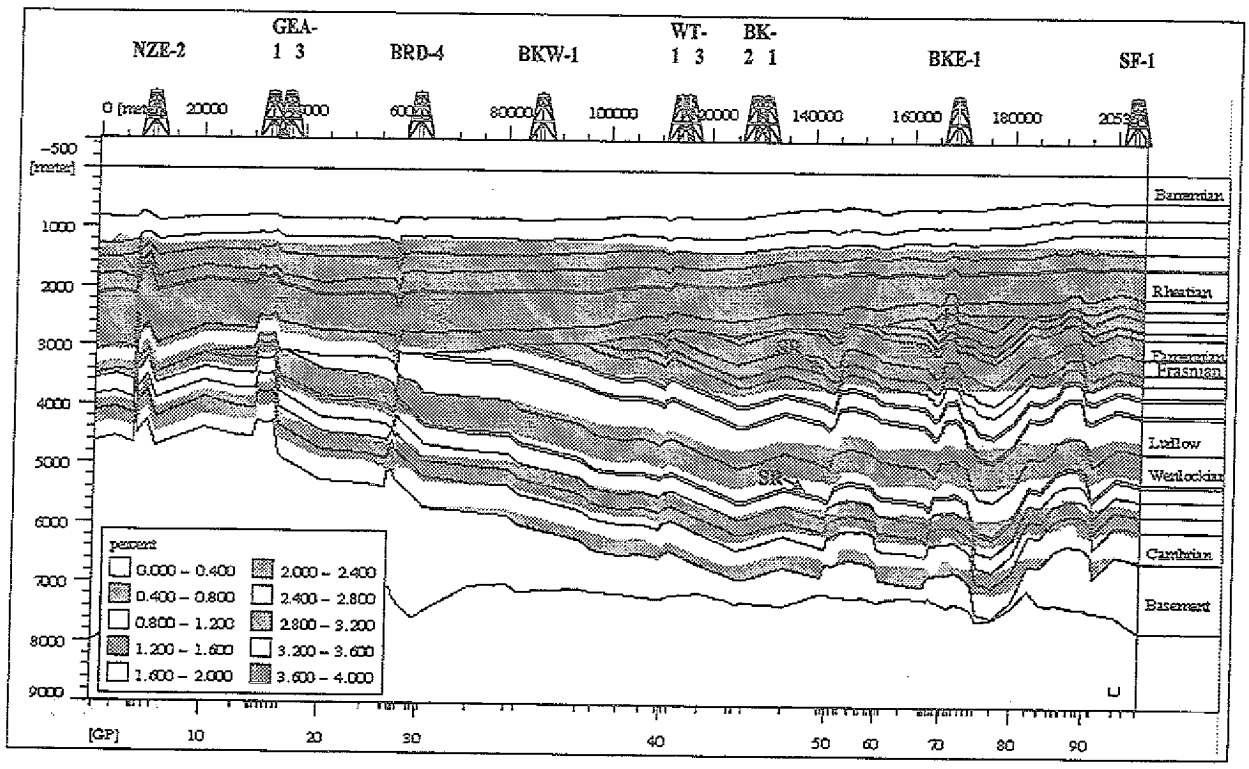


Fig. 67b: Computed maturity (vitrinite reflectance) at 124 Ma (end of Barremian) for the modelled profile. SR, source rock.

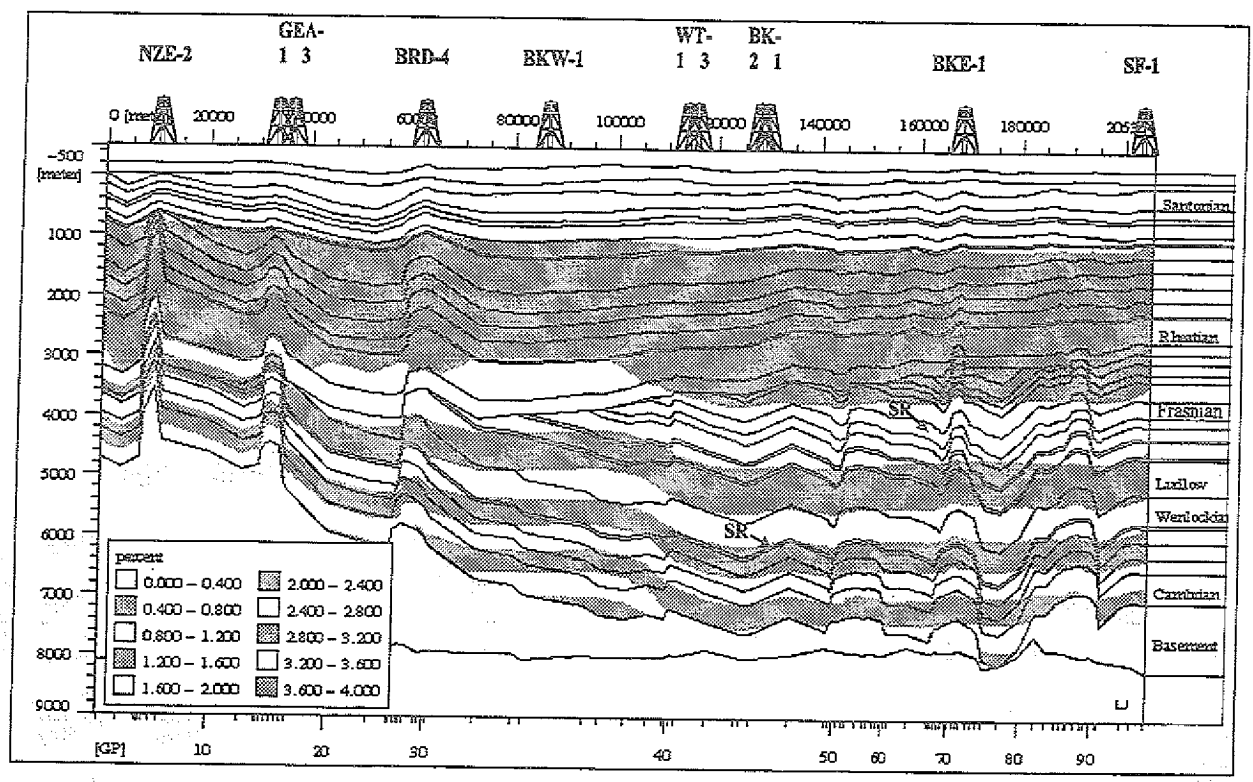


Fig. 67c: Computed present-day maturity (vitrinite reflectance) for the modelled profile. SR, source rock.

are the greatest ever experienced throughout the burial history of these rocks. Calculated vitrinite reflectance values for the Silurian and the Frasnian source rocks are more than 2% R_o and around 1% R_o, respectively, and are in accordance with the calculated temperatures (Fig. 65). Consequently, it is expected that only gas can be expelled by the Silurian source rock, whereas oil and some gas can be expelled by the Frasnian source rock. The generally westward rising of the isoreflectance lines is due to a westward increase of heat flow during maximum burial times. Furthermore, it can be observed that the isoreflectance lines are much tighter downwards in the stratigraphy because of the sandy and shaly nature of the Lower Palaeozoic series.

The relatively low heat flow values observed in the central and eastern parts of the profile (i.e. central and eastern Berkine Basin) might be due to the fact that the underlying crust is thicker and more stable. Tectonically less stable, the folded area of the Amguid El Biod-Hassi Messaoud axis could have experienced higher heat flows.

6-4-3 Compaction Induced Overpressures and Fault Transmissibility

As alrady discussed in Chapter 3.4, the reservoirs in the study area are characterised by different pressure regimes. An important question in the present study relates to the contribution of the major faults to overpressure development and fluid movements. For this purpose, computed overpressures at different locations along the modelled profile are checked against pressure data observed during testing of the different reservoirs. The pressure data used for calibrations are listed in Table 13.

It should be noted that the data are generally recorded at either aquifer or hydrocarbon bearing reservoirs. It is well known that there is always some amount of overpressure wherever a column of oil or gas is present. The amount of overpressure is a function of the density contrast between petroleum and water and the height of the hydrocarbon column (e.g. Osborne and Swarbrick, 1997). The data correction due to the effect of the hydrocarbon column was not necessary because oil- bearing reservoirs are of low net pay. Furthermore, it is well known that the oil trapped in the Triassic reservoirs has a high gas content. Therefore, the pressure correction may be small or zero. The effect of the hydrocarbon column might be significant in gas-bearing reservoirs of high net pay (e.g. Burhig, 1989) such as the Ordovician (Hamra quartzites).

The faults are described in PetroMod as having volume properties and can be modelled as preferred highly permeable migration paths that conduct flow along and/or across the fault planes, or as low permeability domains that restrict flow along and/or across the fault planes, creating pressure seals (Jones et al., 1998).

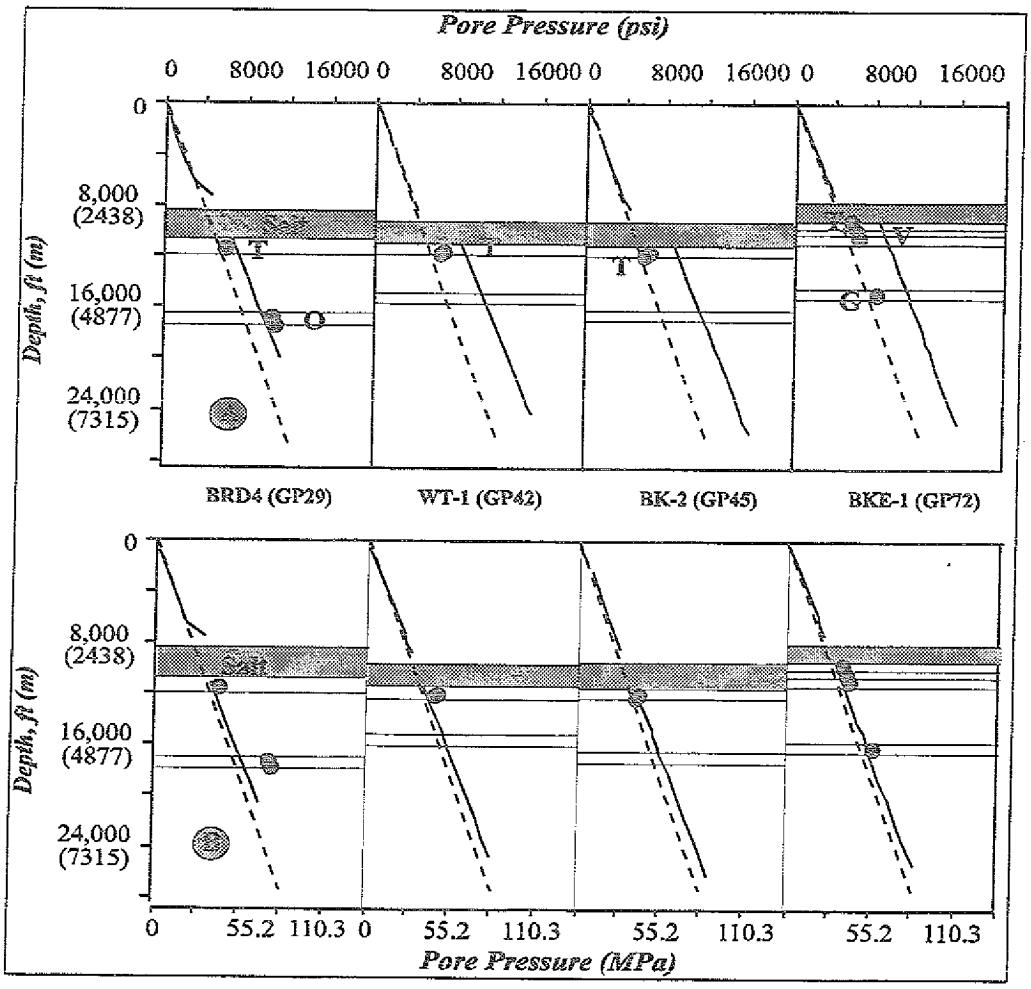


Figure 68: Comparison between measured (dots) and calculated (solid lines) pore pressures for two extreme hypotheses of fault transmissibility: A, impermeable faults and B, permeable faults. T, V, G and O are Triassic, Visean, Gedinnian and Ordovician reservoirs, respectively. The dashed line correspond to hydrostatic pressure (i.e. 0.46 psi/ft or 10.4 KPa/m).

Figure 68 shows the calculated overpressures (assuming hydrocarbon generation) obtained with two extreme hypotheses for fault transmissibility: all the faults were assumed to be „impermeable", and all faults were assumed to be „permeable" to fluid movements. It should be pointed out that because of some limitations of the program which does not take into account pressure dissipation, and because it is known that the Lower Devonian units are open systems, an artificial opening of the model was

performed such that dissipation is taken into account during calibrations. The omission of such a dissipation would imply too high overpressures in the Palaeozoic reservoirs. Figure 68 (A) shows that with the impermeable hypothesis the observed pressure data in the region situated farther away from the anticlines, as illustrated by the grid points 42, 45 and 72, are overestimated leading to a higher pressure regime below the salt deposits (i.e. the regional seal). This fact may indicate that the Triassic is laterally confined by the faults. For the Gedinnian reservoir, which is considered as a part of the gravity flow system which begins at the Hoggar massif in the South, the computed data are also in disagreement with the observed data (GP 72). The computed pressure profile for both the Triassic and the Palaeozoic reservoirs is in good agreement with the measured one only in the Brides area (GP 29) situated farther to the West. By contrast, for the permeable hypothesis (Fig. 68, B) the Triassic reservoirs are found to communicate laterally and are not overpressured anywhere from Gp 29 to GP 72. The calculated pressure data in the Brides area (GP 29) are underestimated indicating that the Ordovician reservoir is not overpressured.

From the above-cited observation, it becomes obvious that:

1. The Triassic and Lower Devonian reservoirs in the central and eastern parts of the profile are found to be hydrostatically pressured implying that fluids can be exchanged through the permeable sandstones and faults. According to modelling results, overpressures cannot dissipate easily enough towards the Illizi Platform only across the Hercynian unconformity where the Triassic and Lower Devonian reservoirs are communicating.

2 The Triassic (except that of the Brides structure) and the Ordovician reservoirs within the folded area (i.e. western part of the basin) are overpressured. The relatively high pressure observed may be interpreted as the result of the low permeability of the faults bounding the anticlines, hence prohibiting fluid movements, the high pressure regime in the North-West (see also Chapter 3.4) and the presence of permeability barriers to the South.

In the following migration reconstruction, all the normal faults situated in the central and eastern part of the profile were assumed to be permeable. The faults located at the western edge of the basin were, in contrast, assumed to be impermeable.

6-4-4 History of Hydrocarbon Generation and Migration

Following the reconstruction of the dynamic geological framework including the computation of burial and temperature history, hydrocarbon generation and migration history was investigated in the Berkine Basin along the 205 km profile. One of the main objectives of such reconstruction is to understand the oil and gas distribution in the basin and to assess the contribution of each source rock to these accumulations.

Figures 69 to 73 show the evolution of petroleum saturation and direction of hydrocarbon flow (arrows) at different stages of basin formation (i.e. 367 Ma, 333 Ma, 244 Ma, 97 Ma and at the present time. The simulation results are based on the kinetics of hydrocarbon generation, hydrocarbon generation potential and fluid properties described in Chapters 6.1 and 6.2. The faults bounding the anticlines were maintained closed (like shale dykes) during the whole time of the basin evolution. The extension faults of the central part of the basin were, on the other hand, kept open (like sand dykes) during the Triassic-Liassic (210-197 Ma) and during the Late Cretaceous-Tertiary (97-0 Ma). The default permeability values given by the PetroMod 2D program were used (i.e. 10^{-12} md for the closed faults and 10^{8} md for the open faults).

The simulation results show that hydrocarbon generation and expulsion out of the basal Silurian source rock had already started in the Frasnian time (Fig. 69). One of the important features that can be observed here is that the expulsion of oil occurred preferably downwards towards the underlying sandy horizons of the Late Ordovician (Llanvirnian) and particularly the Middle Ordovician (Arenigian). Because of the heavy nature of the oil (it is expected that the first oil expelled from the source rock is composed of heavy compounds), and because the synrift sequences are considered to be more permeable than the overlying shales which act as a cap rock, the oil migrated downwards.

In Namurian time (333 Ma), an increase in hydrocarbon generation and saturation is observed (Fig. 70). At that time, oil is migrating both upwards towards the overlying Late Silurian sandstone and downwards towards the underlying Ordovician sandstone. The upwards directed oil is probably due to the pressure build-up in the deepest horizons as a consequence of the successive deposition of layers and due to the

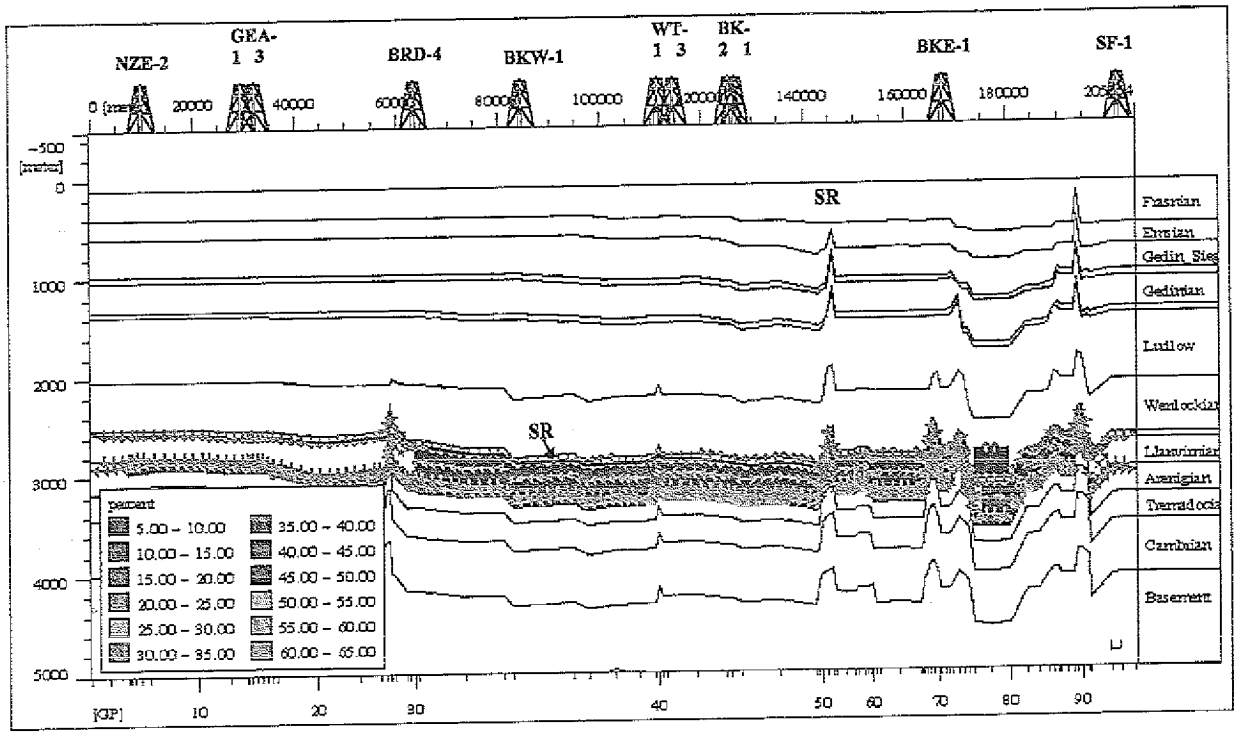


Fig. 69: Computed petroleum saturation (in %) and migration at 367 Ma (Late Devonian). Green arrows show the direction of migration of oil. SR, source rock.

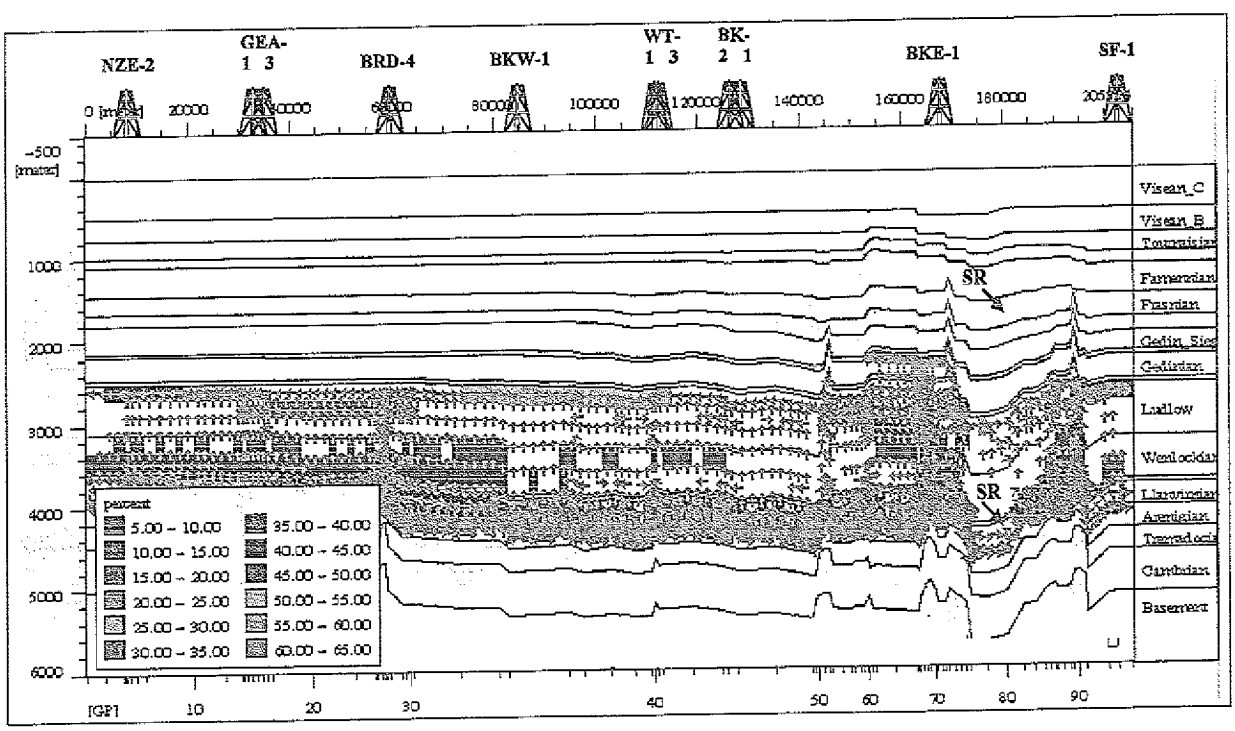


Fig. 70: Computed petroleum saturation (in %) and migration at 333 Ma (Namurian). Green and red arrows show the direction of migration of oil and gas, respectively. SR, source rock.

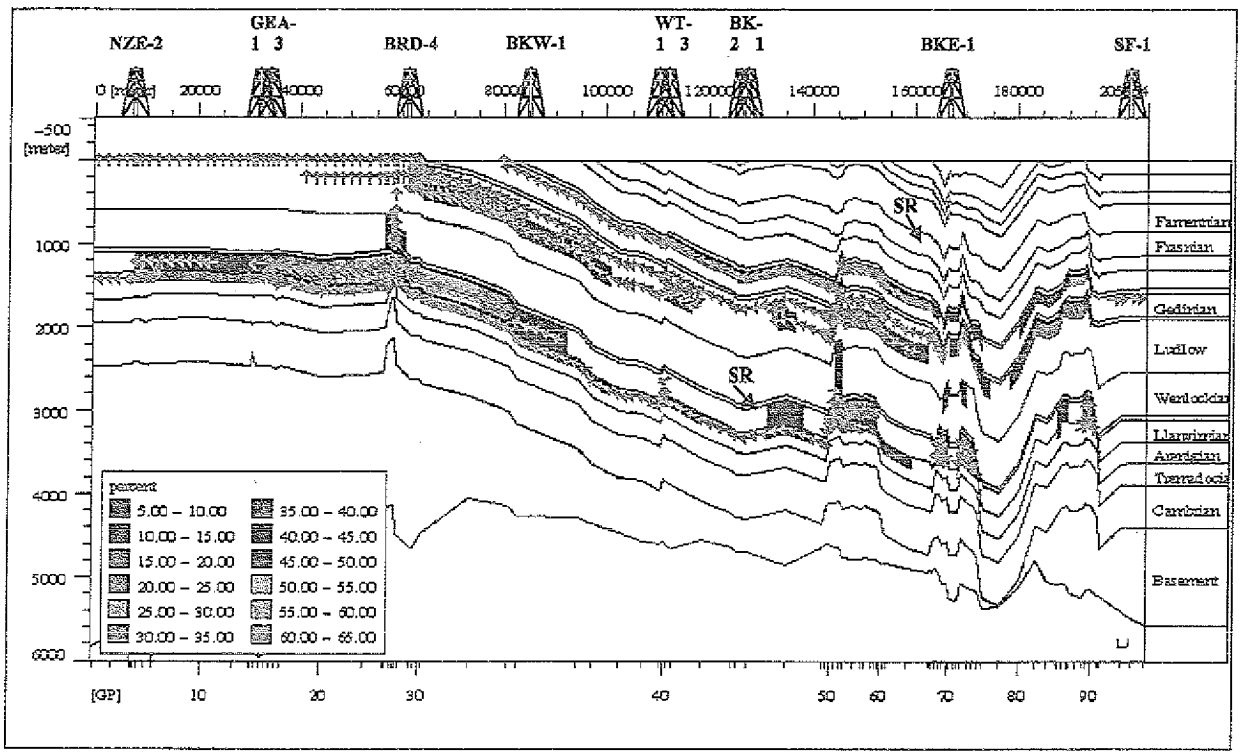


Fig. 71: Computed petroleum saturation (in %) and migration at 244 Ma (Early Triassic). Green and red arrows show the direction of migration of oil and gas, respectively. SR, source rock.

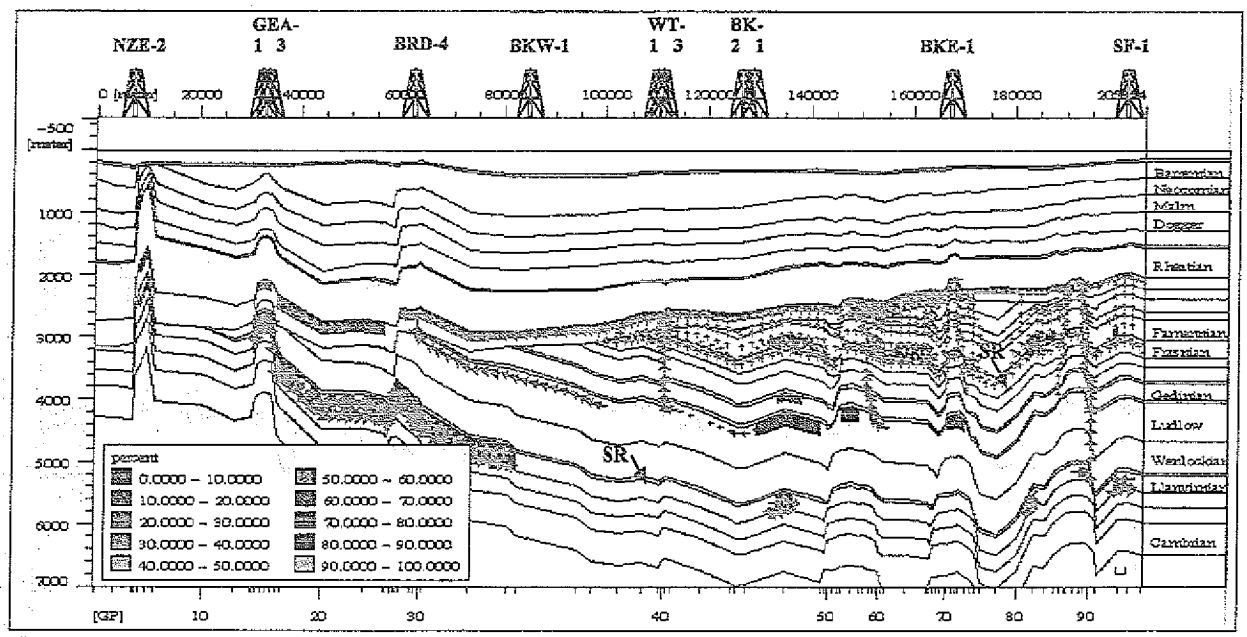


Fig. 72: Computed petroleum saturation (in %) and migration at 97 Ma (end of Albian). Green and red arrows show the direction of migration of oil and gas, respectively. SR, source rock.

progressive maturation of the oil (gas started already to be generated in the deepest parts of the basin).

During the Late Carboniferous (Hercynian) movements, the basin was tilted and hydrocarbons migrated in an up-dip direction. Due to the pressure release caused by the Hercynian movements, hydrocarbons migrated outside the center of the basin along carrier beds and filled the structures probably created during that time along the Amguid El Biod-Hassi Messaoud axis. However, as well illustrated in Figure 71, it is likely that hydrocarbons which were probably trapped in the anticlines were destroyed by the Hercynian uplift/erosion movements. The different Upper Palaeozoic reservoirs were progressively exposed to the atmosphere during the Permian-Triassic as a consequence of the Hercynian erosion. Therefore, hydrocarbons were destroyed by weathering. Another possible destructive movement (not shown here) is the Triassic-Jurassic rift phase. It has been predicted that before the deposition of the Liassic regional seal, hydrocarbons generated during the Palaeozoic and trapped in the center of the basin seeped to the surface along the major faults.

After the pre-Aptian compressive movements, new structures were generated in the western part of the basin. It was predicted that these structures were filled with hydrocarbons during the Albian (Fig. 72). It was subsequently noted that the Triassic reservoirs of these structures were filled progressively by the redistribution of gas pre-accumulated in the deepest reservoirs (i.e. Ordovician) and thought to be of secondary cracking origin. From Figure 72, it is also concluded that the Triassic fault block structures of the central part of the basin started to be saturated with oil generated by the Frasnian source rock during the Cretaceous. The structures are filled by vertical migration along faults and to a lesser extent at the Hercynian unconformity (i.e. where the source rock is pinching out below the unconformity). It is also observed that the extent of lateral migration along the Triassic carrier bed is not as long as the Brides structure.

At the present time (Fig.73), it can be observed that the Frasnian oil (and probably wet gas) is still showing an upwards direction of migration along faults. An increase of the petroleum saturation in the Triassic reservoirs is also observed.

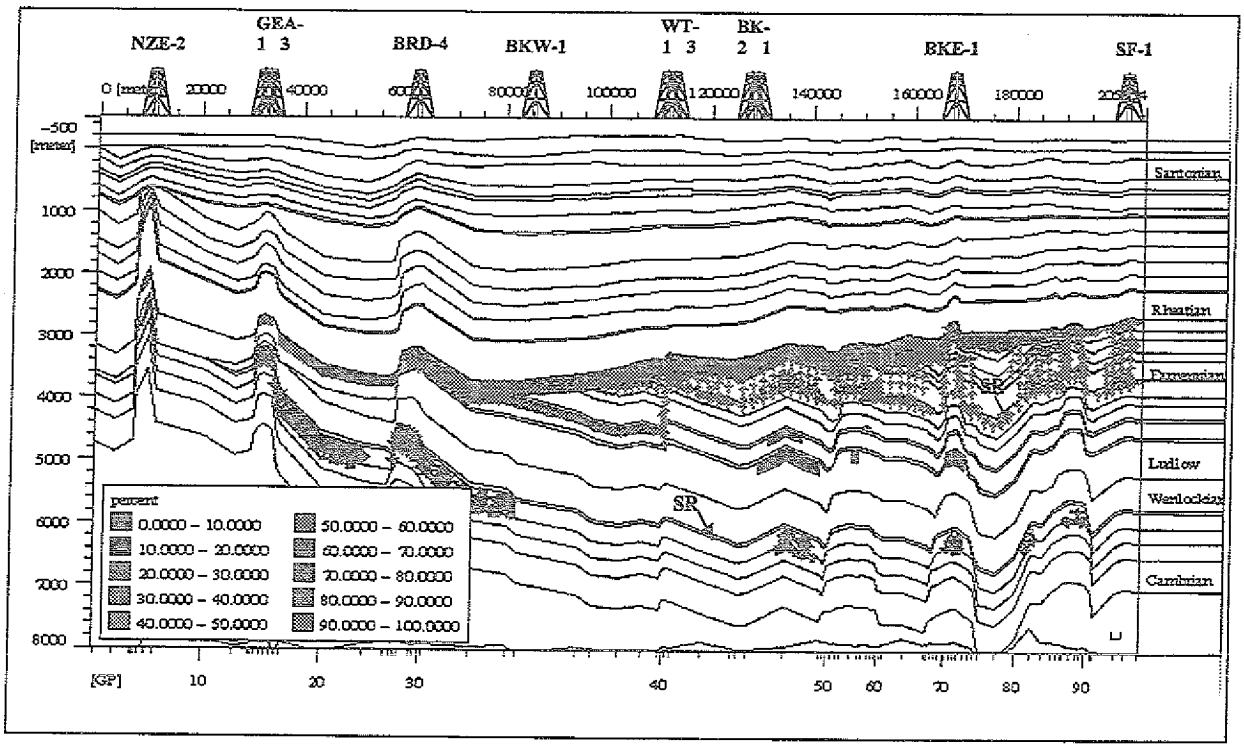


Fig. 73: Computed petroleum saturation (in %) and migration at the present time. Grey and dark grey arrows show the direction of migration of oil and gas, respectively. SR, source rock.

These quantifications allow a comparison between the model results and what is realy observed in nature. The Frasnian sourced oil accumulations are restricted in the model to the Triassic-Jurassic extensional blocs of the central part of the Berkine Basin (i.e. Wed Teh, Berkine East and other undrilled structures). From the simulation results and taking into account the timing of oil and gas generation for each source rock as well as other geological considerations, it can be concluded that the hydrocarbon discoveries in fields such as Rhourd Messaoud, Rhourd Khrouf and Rhourd El Rouni (see Figure 1) were filled mainly by the Frasnian source rock. Good drainage capabilities are attributed to major faults. The results show also some differences from the observed data. Among others, the presence of a huge gas accumulation (270 000 m^3/day gas) in the Hamra quartzite (Middle Ordovician) in the Brides structure cannot be produced by the model. The necessary downward migration of gas towards the reservoir which is situated 300 m below the source rock could not be modelled. Furthermore, the model could not predict the oil accumulation in the Triassic of the Gassi El Adem structure to the west of Brides (only gas accumulation in the model). This is mainly due to the timing of hydrocarbon generation. The Silurian source rock realized its oil

potential during the Palaeozoic and the Frasnian source rock is of limited extension (Figs. 1 and 7). Based on these observations it is still very difficult to explain nearby oil fields such as those of Gassi Touil and Nezla North situated on the same structural trend.

6-4-5 The Alternative Hydrocarbon Generation and Migration Model

The previous hydrocarbon generation and migration simulations showed some inconsistencies with what is observed in nature. According to the data available in this study, it can be argued that some of these inconsistencies are mainly related to the Silurian hydrocarbon generation timing. Therefore, it was judged useful, though biased, to test within geologically reasonable limits possibilities which allow younger hydrocarbon generation.

The alternative model presented here assumes that the Hercynian erosion was not as srong as assumed in the original model and that the Carboniferous sedimentation in the vicinity of the anticlines was reduced in thickness due to early pulses of the Hercynian orogeny. The main input data for a calibrated well (i.e. BRD-4) and two other wells located to the west of the Brides structure (i.e. GEA-3 and NZE-1) are listed in Table 18. Sediment thickness and heat flow used along the whole simulated transect are given in the enclosed Tables 12 and 13.

It should be pointed out that large differences in the computed pressure gradient were not observed. Nevertheless, the predicted pressure gradient in the Palaeozoic series of the western part of the profile, as illustrated by the BRD-4 well, was slightly lower than that observed in the previous model (Fig.68, A) and a mismatch between the calculated and measured pressure data in the Ordovician reservoir was observed. However, it should be kept in mind that the effect of the gas column on pressure is greater in reservoirs of high net-pay and that possibly the observed data must be corrected.

For the calibration of the temperature history, the same agreement as for the previous model (see Figure 66) between the measured and calculated vitrinite reflectance was obtained in the Brides field when assuming a slightly higher heat flow value (i.e. 63 mW/m^2 instead of 60 mW/m^2) at maximum burial times and eroded overburdens of

Tab. 18: Input data set used for the alternative model of three wells located in the western part of the basin (cf. Table 17). The highlighted values correspond to sediments which were totally (-9999) or partly eroded during the Hercynian orogeny.

Event N°	Event Name	Time (Ma)	Lithology	NZE-2(GP7) Thick	NZE-2(GP7) HF	GEA-3 (GP16) Thick	GEA-3 (GP16) HF	BRD-4 (GP29) Thick	BRD-4 (GP29) HF
60	Tertiary	35	SAND,silty	184	63	168	63	192	63
59	Alpine	42	LIME,dolo	-168	63	-164	63	-150	63
58	Macs-Eoc	74	LIME,dolo	210	63	379	63	345	63
57	Santonian	86	DOLO, evap	144	63	185	63	208	63
56	Coniacian	89	SALT	120	63	123	63	97	63
55	Turonian	90	LIME,marly	73	63	97	63	100	63
54	Cenoman	97	SHALE,evap	148	63	174	63	205	63
53	Albian	112	SAND,shaly	139	63	140	63	125	63
52	Aptian	117	LIME,dolo	30	63	30	63	25	63
51	Austrian	119	"	-115	63	0	63	0	63
50	Austrian	121	"	-9999	63	0	63	0	63
49	Austrian	124	SAND,silty	-9999	63	-565	63	-350	63
48	Baremm	132	SAND,silty	725	64	670	64	705	64
47	Neocom	146	SHALE,sandy	345	64	296	64	306	64
46	Malm	161	SHALE&LIME	220	64	229	64	248	64
45	Dogger	187	SHALE,calc	182	65	309	65	309	65
44	Pliensb	194	EVAP,shaly	160	65	121	65	310	65
43	sinemur	203	LIME,shaly	25	65	25	65	25	65
42	Rheatian	210	SALT	1000	68	664	68	673	68
41	Tr.Keuper	231	SAND,shaly	399	75	317	75	344	75
23-40	Hercynian	286	See the table below						
22	Stephan	303	SHALE,evap	53	60	60	60	70	60
21	Westphal	315	LIME,shaly	154	60	167	60	180	60
20	Namurian	333	SHALE,calc	107	60	128	60	150	60
19	Visean-C	342	SILTSTONE	132	60	165	60	220	60
18	Visean-B	350	SAND&SHALE	124	60	137	60	150	60
17	Tournias	355	SAND,shaly	121	60	111	60	100	60
16	Strunian	363	SILT,sandy	50	60	50	60	50	60
15	Famenn	367	SHALE,silty	220	60	220	60	220	60
14	Frasnian	377	SHALE,calc	150	60	150	60	150	60
13	Emsian	390	SHALE&LIME	50	60	50	60	50	60
12	Gedi-Sieg	397	SAND&SHALE	200	62	200	62	200	62
11	Intra G-Sieg	399	SHALE	50	62	50	62	50	62
10	Gedinian	409	SANDSTONE	160	62	160	62	160	62
9	Pridolian	411	SHALE	50	63	50	63	50	63
8	Ludlow	424	SAND&SHALE	500	63	500	63	550	63
7	Wenlock	433	SHALE,silty	460	65	460	65	510	65
6	Llandov	435	SHALE,calc	50	65	50	65	50	65
5	Llanvirn	780	SAND&SHALE	206	70	206	70	293	70
4	Arenigian	493	SANDSTONE	293	70	252	70	280	70
3	Tremadoc	510	SHALE,sandy	250	75	313	75	273	75
2	Cambrian	570	SANDSTONE	500	75	500	75	500	75
1	Basement	650	BASEMENT	4327	40	3461	40	2000	40

Event N°	Event Name	Time (Ma)	NZE-2(GP7) Thick	NZE-2(GP7) HF	GEA-3 (GP16) Thick	GEA-3 (GP16) HF	BRD-4 (GP29) Thick	BRD-4 (GP29) HF
40	Hercynian	233	-9	58	0	58	0	58
39	Hercynian	236	-9999	58	0	58	0	58
38	Hercynian	240	-9999	58	-325	58	0	58
37	Hercynian	244	-9999	58	-9999	58	-100	58
36	Hercynian	248	-9999	58	-9999	58	-9999	58
35	Hercynian	253	-9999	58	-9999	58	-9999	58
34	Hercynian	257	-9999	58	-9999	58	-9999	58
33	Hercynian	261	-9999	58	-9999	58	-9999	58
32	Hercynian	264	-9999	58	-9999	58	-9999	58
31	Hercynian	267	-9999	58	-9999	58	-9999	58
30	Hercynian	270	-9999	58	-9999	58	-9999	58
29	Hercynian	273	-9999	58	-9999	58	-9999	58
28	Hercynian	276	-9999	58	-9999	58	-9999	58
27	Hercynian	278	-9999	58	-9999	58	-9999	58
26	Hercynian	280	-9999	58	-9999	58	-9999	58
25	Hercynian	282	-9999	58	-9999	58	-9999	58
24	Hercynian	284	-9999	58	-9999	58	-9999	58
23	Hercynian	286	-9999	58	-9999	58	-9999	58

1860 m instead of 3020 m. In the absence of maturity data for the other wells (i.e. GEA-3 and NZE-1), it is assumed that the same heat flow density occurred at the maximum burial time with eroded overburden of 2298 and 2637 m, respectively. These eroded thicknesses are still rather high.

It is clear that such a model allows later generation from the Silurian source rock (see Model B, BRD-4 well in Chapter 6.3). Therefore, the probability that hydrocarbons were destroyed during the Hercynian movements is much lower.

Figure 74 shows the simulated present-day oil saturation (and hydrocarbon flow). It can be seen that the Gassi El Adem oil accumulation (not shown in the previous model) is predicted here. From the simulation results, this structure is filled by vertical migration of oil originally accumulated in the Ordovician. The downward migration of oil towards the underlying more permeable sandstone occurred during the Jurassic-Cretaceous (i.e. between 161 and 124 Ma) as illustrated at 146 Ma in Figure 75. The filling of the Triassic reservoir with oil started at around 89 Ma after the Cretaceous folding and faulting (Fig. 76). This alternative explanation of the Gassi El Adem oil could also explain the origin of the oil in Nezla North an Gassi Touil. These accumulations could have occurred in different steps represented by: 1) a downward expulsion towards the underlying more permeable reservoirs, 2) up-dip direction along the carrier rocks towards structurally higher positions and 3) redistribution towards the Triassic reservoirs.

In Figure 77, the Triassic gas of the Brides structure is also predicted. The calculation results showed also that the Triassic reservoir of the Brides structure was filled by vertical migration of gas at around 112 Ma. This gas was originally accumulated in the Ordovician sandstone and redistributed later after the Cretaceous compressive movements. A partial redistribution could explain why the Triassic reservoir is not filled up to the spill point. The many gas bubbles observed during the drilling of the sediments underlying the reservoir may be an indication of the recent emplacment of this gas.

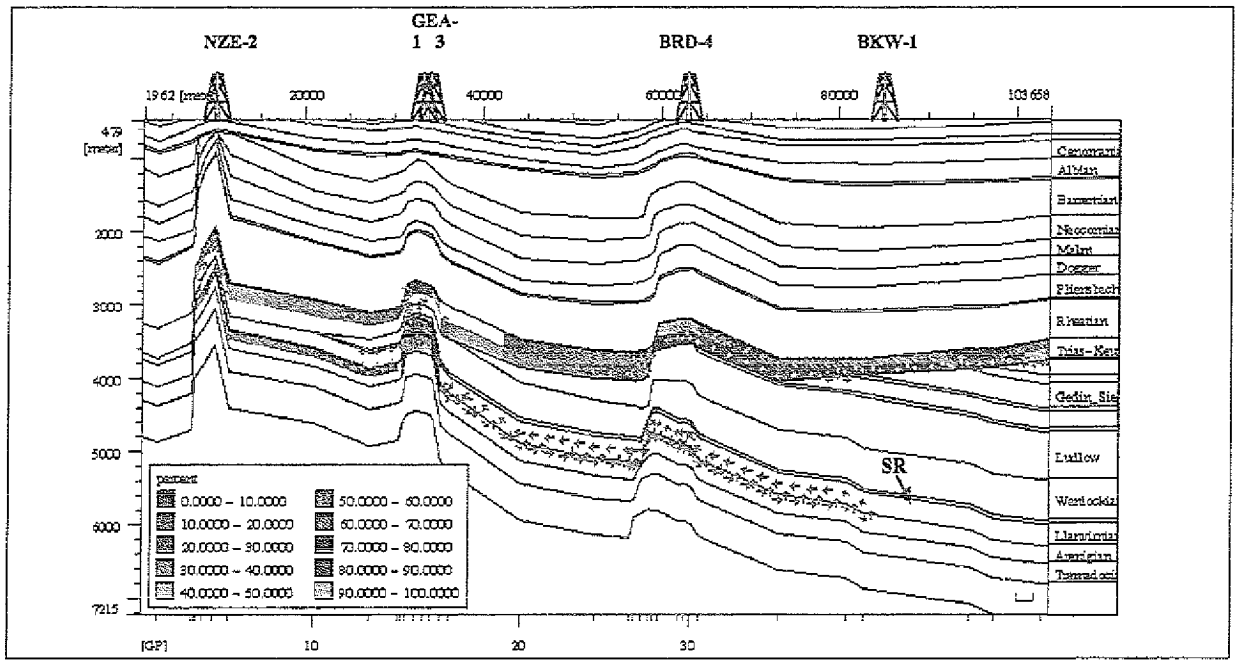


Fig. 74: Computed oil saturation (in %) and migration for the western part of the basin at the present time. Green and red arrows show the direction of migration of oil and gas, respectively, following the alternative model. SR, source rock.

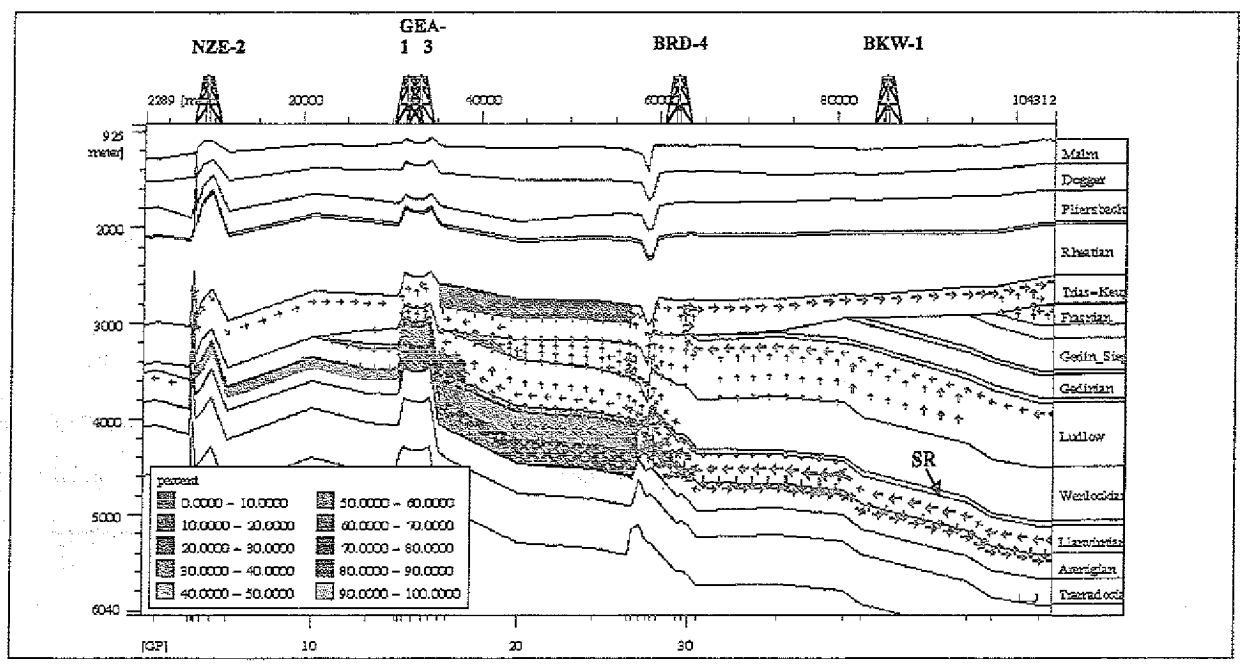


Fig. 75: Computed oil saturation (in %) and migration for the western part of the basin at 146 Ma (end of Malm). Green and red arrows show the direction of oil and gas, respectively. SR, source rock.

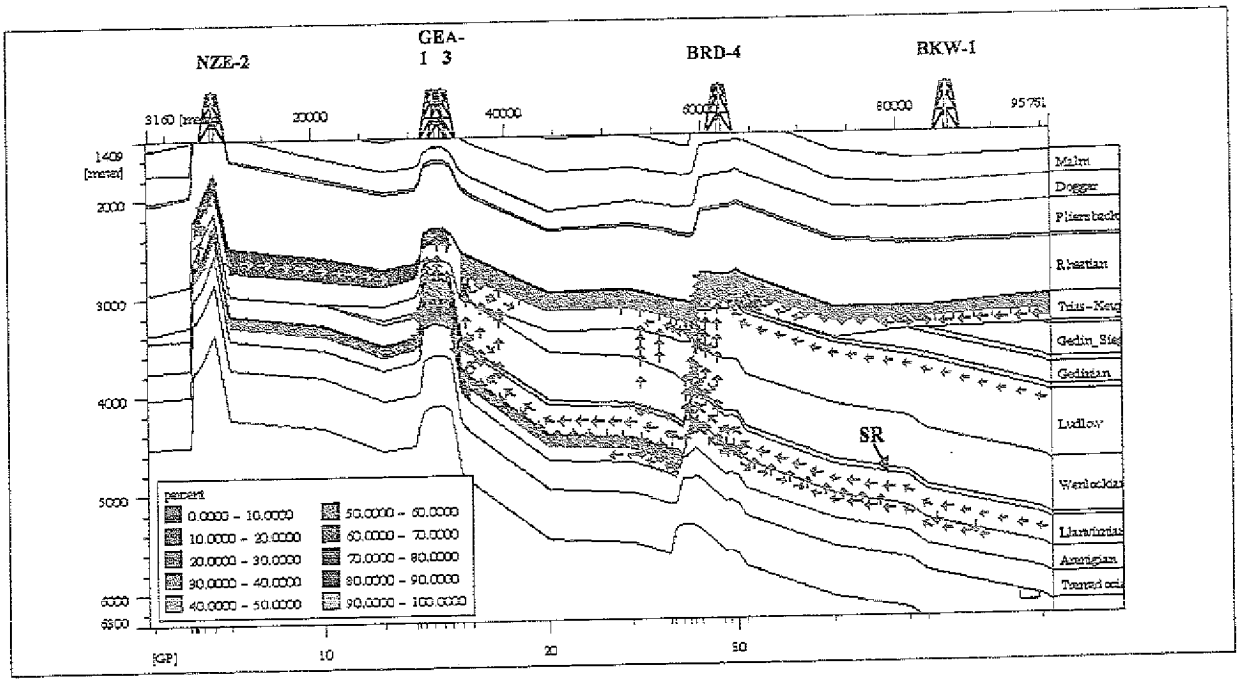


Fig. 76: Computed oil saturation (in %) and migration for the western part of the basin at 89 Ma (end of Turonian). Green and red arrows show the direction of migration of oil and gas, respectively. SR, source rock.

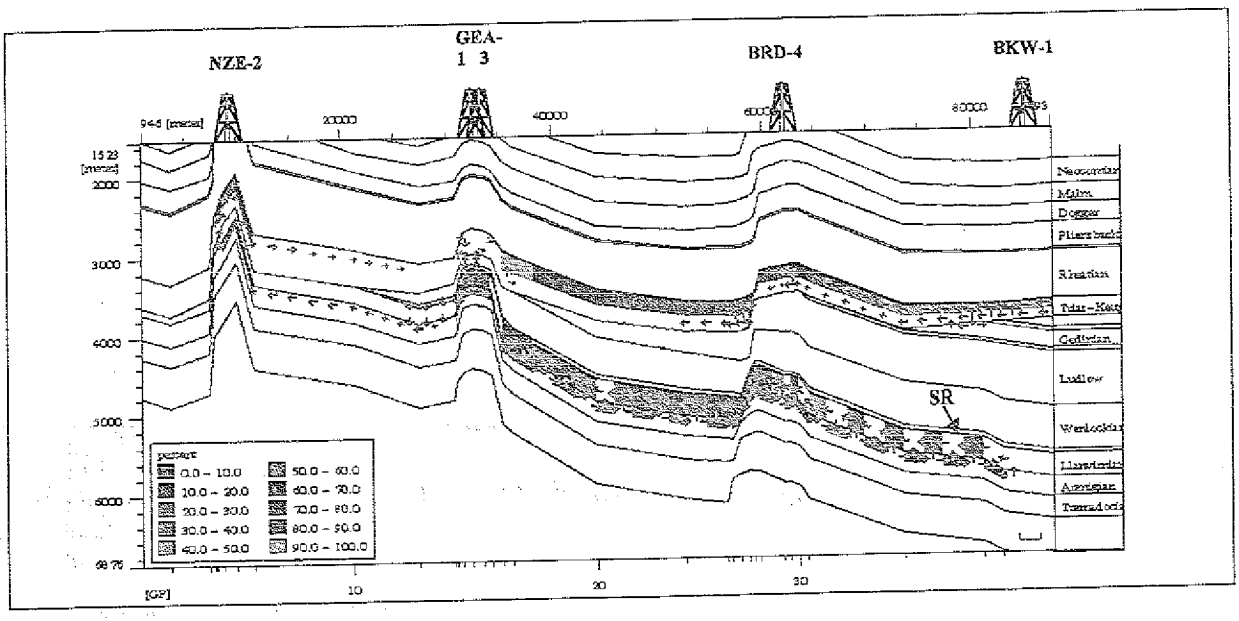


Fig. 77: Computed gas saturation (in %) and migration for the western part of the basin at the present time. Green and red arrows show the direction of migration of oil and gas, respectively. SR, source rock.

7. Conclusions

The main conclusions which can emerge from the present study can be summarized as follows:

- The most important source rocks of the basin are the organic-rich units of the Silurian and the Frasnian „radioactive" black-dark finely laminated shales. Mean organic carbon contents range between 4 and 6% for the former and between 2 and 4% for the latter. Both source rock units reach values even greater than 10% for the richest samples. Based on a number of biomarker, S/C ratios and other compositional parameters (e.g., CPI, pristane/phytane and isoprenoids/ n-alkanes ratios), these source rocks have been interpreted to be marine algal-rich rocks developed within a continental shelf environment during maximum flooding of an epicontinental sea and where dysaerobic to anaerobic bottom water conditions may have prevailed. The absence of any benthos species and the laminae nature of the Silurian „hot" shales suggest that fully euxinic conditions may have occurred. The presence of some benthos species such as goniatites and brachiopods suggests, on the other hand, that the organic-rich „hot" shales of the Frasnian were anoxic, whereas the water column above was at least partly oxygenated. Extensive reworking of the sedimentary organic matter by anaerobic bacteria, as deduced from biological marker patterns, was a common feature.

- Most of the maturity data revealed that the Frasnian source rock is at the oil and/or late oil/early gas generation stage depending upon position within the basin. The Silurian, on the other hand, is overmature (i.e. in the gas generation phase) in most of the study area. An exception is the northern part of the basin where the Silurian shows high capabilities for oil generation. Oil and gas expelled from these source rocks are trapped mainly in the Triassic (TAGI formation) reservoir which is sealed by the overlying Liassic salt.

- The oils analysed in this study showed great similarities, with respect to their molecular composition, with the source rock extracts. Obviously, they originate from a siliciclastic source rock deposited under marine conditions as deduced from

selected compound ratios. The similarities observed between the oils and the rock extracts in their biological marker fingerprints make oil to oil and oil to source rock correlations difficult to constrain. Correlations alone are, therefore, not conclusive for solving some important petroleum geology aspects such as the effective contribution of each source horizon to hydrocarbon pools observed in the basin.

- The observed maturity profiles in the basin reflect mainly the Late Cretaceous-Tertiary burial. Most of the maturity data bear no imprint of any high heat flow event during that time. According to the 1D and 2D numerical simulations, the associated heat flow values range between 60 and 66 mW/m^2 in the vicinity of the anticlines (i.e. along the Amguid El Biod-Hassi Messaoud ridge) and between 50 and 55 mW/m^2 everywhere else. Tectonically less stable, the western part of the basin could have experienced higher than normal heat flows.

- A difference of up to 6 mW/m^2 is observed between the 1D and 2D results. In other words the heat flow values necessary for the calibration of the maturity data are slightly lower when applying the PetroMod 2D program. Such differences probably arise from the fact that PetroMod takes into account the influence of lateral heat transfer on temperature. The estimated amount of overburden eroded during the Hercynian orogeny roughly increases from the south-east to the north-west and seems to be in accordance with the Hercynian subcrop pattern. A minimum of 200 m has been estimated in the Haiad area. A maximum value of about 3000 m has been estimated in the western part of the basin along the Amguid El Biod-Hassi Messaoud ridge. However, this latest value is likely to be an overestimation. Taking into account field observations, a slightly higher heat flow at maximum burial times (66-63 mW/m^2) combined with a Hercynian erosion of only 1860 m would generate a more appropriate model. Furthermore such considered amount of eroded overburden would lead to a more reasonable erosion rate (i.e., 39 in spite of 55 m/Ma).

- The extent of Hercynian erosion, present-day burial and thermal conductivities of rocks are the main factors enhancing or prohibiting the maturation of the

sedimentary organic matter and hydrocarbon generation. Although vitrinite reflectance and other maturity parameters reflect mainly the Meso-Cenozoic burial, the earlier temperature evolution (i.e.,prior to the Hercynian uplift and erosion) is of great importance for hydrocarbon generation in the study area because it determines how much petroleum generation potential was preserved.

- Another important factor which had a great control in prohibiting the maturation of organic matter is the presence of thick evaporite (salt and anhydrite) bearing strata in the post-Hercynian section. Due to their high thermal conductivities, evaporites tend to dissipate the produced energy to the surface (Neunzert et al., 1996, Neunzert, 1998). It was consequently observed that, for the same heat flow density at the base of the sedimentary sequence, the hydrocarbon generation depth is much shallower where sediments of high thermal conductivity are absent.

- Hydrocarbon generation for the Frasnian source rock occurred mainly during the Mesozoic. The earliest time of peak oil generation was 200 Ma; the latest is the present. Peak oil generation along the studied transect occurred at around 120 Ma (Aptian). For the Silurian source rock, the timing of the diagenesis of organic matter in the central part of the basin is Palaeozoic. For the western part of the basin, the hypothesis of a Palaeozoic diagenesis is disputed. A 2D sensitivity analysis revealed that a Late Carboniferous oil generation and expulsion as always postulated shows controversies with the observed field data. Such an hypothesis would lead to rather small oil entrapment efficiencies because the relationship between hydrocarbon generation and structuring was less favourable .

- The calibration of the 2D model against overpressure development reveals that the reverse faults bounding the anticlines in the western part of the basin are most certainly impermeable to fluid movements. The model also shows that the Late Triassic-Early Jurassic extensional faults are open to fluid movements and can be considered, therefore, as important migration pathways within the basin.

- According to the 2D simulation results, the hydrocarbons which were generated during the Palaeozoic cycle, migrated outside the center of the basin at the Late

Carboniferous time towards the Amguid El Biod-Hassi Messaoud axis (western part of the basin) and were trapped there. However, the hydrocarbon accumulations were largely destroyed by progressive exposition of the reservoirs to erosional events and weathering during the Hercynian movements. Therefore, only the hydrocarbons trapped during the Mesozoic time make up the present oil and gas accumulations.

- The contribution of the Frasnian source rock is largely confined to the central part of the basin. Due to more favourable maturity, this source rock is likely to be responsible for the presence of oil fields such as Wed Teh, Berkine East, undrilled in-between structures, as well as Rhourd El Khrouf, Rhourd El Rhouni, Rhourd Messaoud and others. Minor contributions (mostly gas) are attributed to the Silurian shales. Good drainage capabilities are associated with major faults.

- The hydrocarbons trapped along the Amguid El Biod-Hassi Messaoud axis were most certainly sourced by the Silurian source rock. The presence of seals (i.e. faults bounding the anticlines) indicates that these accumulations cannot be fed by the Frasnian source rock, a fact which confirm the hypothesis advanced in Chapter 5.3. The 2D basin modelling results show also that a Mesozoic generation is the most accurate hypothesis which would match the observed accumulations in this hydrocarbon-bearing trend. According to the simulation results, the emplacement of these hydrocarbons in Triassic fields such as Brides, Gassi El Adem, Nezla East, Nezla North, Gassi Touil, Hassi Chergui and even Rhourd El Baguel occurred after the Cretaceous structures were formed. Migration from the source rock to the reservoirs show a succession of expulsion to older more permeable drains (i.e. the sandy horizons of the Ordovician between 161 and 124 Ma (Jurassic-Cretaceous), accumulation in local traps and dismigration as either an oil phase (Gassi El Adem, Nezla North, Gassi Touil, Hassi Chergui and Rhourd El Baguel) or as a gas phase (Brides, Nezla East and others) after the Cretaceous compressive movements. Gas is probably responsible for displacing some oil accumulations in the basin resulting in gas caps within some fields (e.g. Hassi Chergui).

8. References

Albrecht, P., M. Vandenbroucke, and M. Mandengué, 1976, Geochemical studies on the organic matter from the Douala Basin (Cameroon)- I. Evolution of the extractable organic matter and the formation of petroleum: Geochim. Cosmochim. Acta, v.40, p. 791-799.

Alexander, R., R. I. Kagi, and G.W. Woodhouse, 1981, Geochemical correlation of Windalia oils and extracts of Winning group (Cretaceous) potential source rocks, Barrow subbasin, western Australia: AAPG Bulletin, v. 65, p. 235-250.

Allen, P. A., and J.R. Allen, 1990, Basin Analysis: Principles and Applications: Blackwell, Oxford, 451 p.

Attar, A., J. Fournier, A.M. Candilier, and R. Coquel, 1980, Etude palynologique du Devonian terminal et du Carbonifere inferieur du bassin d'Illizi (Fort-Polignac) Algerie: Rev. Inst. Fr.Pétrole, v. 35, p. 585-607.

Awad, G. M., 1984, Habitat of oil in Abu Gharadig and Faiyoum Basins, Western Desert, Egypt: AAPG Bulletin, v. 68, p. 564-573.

Baker. D.R., 1962, Organic geochemistry of Cherokee Group in south-eastern Kansas and noth-eastern Oklahoma: AAPG Bulletin, v. 46, p. 1621-1642.

Balducchi, A., and G. Pommier, 1970, Cambrian oil field of Hassi Messaoud, Algeria, in T.M. Halbouty, ed., Geology of Giant Petroleum Fields, AAPG Memoir. n°.14, p. 477-488 .

BEICIP/SONATRACH, 1979, Etude géologique du champ de Hassi R'Mel: SONATRACH internal report.

BEICIP/SONATRACH, 1991, Basin de Ghadames: Evaluation Pétrolière: SONATRACH internal report.

Benacef, A., S. Beuf, B. Biju-Duval, O. De Charpal, and P. Rognon, 1971, Examples of a cratonic sedimentation: Lower Palaeozoic of Algerian Sahara: AAPG Bulletin, v. 55, p. 2225-2245.

Berner, R. A., and R. Raiswell, 1983, Burial of organic carbon and pyrite sulfur in sediments over Phanerozoic time: A new theory: Geochim. Cosmochim. Acta, v. 47, p. 855-862.

Beuf, S., B. Biju-Duval, O. De Charpal, P. Rognon, O. Gariel, and A. Benacef, 1971, Les grés du Paleozoic inférieur au Sahara, sédimentation et discontinuités, évolution structurale d'un craton: Edition Inst. Fr. Petr., 465 p.

Bishop, W. F., 1975, Geology of Tunisia and adjacent parts of Algeria and Libya: AAPG Bulletin, v. 59, p. 413-450.

Bishop, W. F., 1988, Petroleum geology of East-Central Tunisia: AAPG Bulletin, v. 72, p. 1033-1058.

Bissada, K.K., 1982, Geochemical constraints on petroleum generation and migration- a review: 2nd ASCOPE Conf. Proc. Manilla, Oct, 1981, p. 69-87.

Blackwell, D. D., and J.L. Steel, 1989, Thermal conductivity of sedimentary rocks: Measurements and significance, in N. D. Neaser and T.H. Maculloh, ed., Thermal History of Sedimentary basins- Methods and Case Histories. Springer, Berlin Heidelberg, New York, p. 14-36.

Bossiere, G., and M. Megartzi, 1982, Pétrologie des nodules de pyroxenolites associés á la rushayite d´In Teria (NE d´Illizi), Algerie: Bull. Mineral., v. 105, p. 89-98.

Boudjema, A., 1987, Evolution structurale du basin pétrolier Triasique du Sahara Nord-Oriental (Algerie): unpublished PhD. Thesis, Université Paris- Sud.

Bray, E. E., and E.D. Evans, 1961, Distribution of n-paraffins as a clue to recognition of source beds: Geochim. Cosmochim. Acta, v. 22, p. 2-15.

Bray, E. E., and E.D. Evans, 1965, Hydrocarbons in non-reservoir-rock source beds: AAPG Bulletin, v. 49, p. 248-257.

Brooks, J. D., K. Gould, and J.W. Smith, 1969, Isoprenoid hydrocarbons in coal and petroleum: Nature, v. 222, p. 257-259.

Broughton, P., and A. Trepanier, 1993, Hydrocarbon Generation in the Essaouira Basin of Western Morocco: AAPG Bulletin, v. 77, p. 999-1015.

Brown, R. N., 1978, History of exploration and discovery of Morgan, Ramadan and July oil fields, Gulf of Suez, Egypt, in A.D. Maill, ed.,: Fact and Principles of World Petroleum Occurence, Canadian Soc. Petr. Geo. Mem. n° 6, p.733-764.

Buiskool Toxopeus, J. M. A., 1983, Selection criteria for the use of vitrinite reflectance as a maturity tool, in J.Brooks, ed., Petroleum Geochemistry and Exploration in Europe, Oxford, Blackwell, p. 295-307.

Burke, K. C., and A. Whiteman, 1973, Uplift, rifting and the break-up of Africa, in D. Tarling and S.K. Runcorn, eds., Implications of Continental Drift to the Earth Sciences, London, Academic Press, p. 735-755.

Burke, K. C., and J.F. Dewey, 1974, Two plates in Africa during the Cretaceous?: Nature, v. 249, p. 313-316.

Buhrig, C., 1989, Geopressured Jurassic reservoirs in the Viking Graben: modeling and geological significance: Marine and Petroleum Geology, v.6, p.31-48.

Burnham, A. K., and J.J. Sweeney, 1989, A chemical kinetic model of vitrinite maturation and reflectance: Geochim. Cosmochim. Acta, v. 53, p. 2649-2657.

Burollet, P. F., 1967, General Geology of Tunisia, in Guidebook to the geology and history of Tunisia: Petr. Expl. Soc. Libya, 9th Ann. Field. Conf., p. 51-58.

Burrolet, P. F., 1989, North African epeiric basins (Abs): 28th IGC, p. 217.

Burrus, J., A. Kuhfuss, S. Doligez, and P. Ungerer, 1991, Are numerical models useful in reconstructing the migration of hydrocarbons? A discussion based on the Northern Viking Graben, in W. A. England, and A.J. Fleet, eds., Petroleum Migration, Geological Society Special Publication, n°. 59, p. 89-109.

Busson, G., 1967, Le Mésozoic Saharian, part 1: l'extreme Sud Tunisien: France, Cen. Rech. Zones Arides, Serv. Geo., n°. 8, 194p.

Chaouche, A., 1991, Genese et mise en place des hydrocarbures dans les basins de l'Erg Oriental (Sahara algerien): unpublished PhD. Thesis, Bordeau, France.

Chapman, R. E., 1981, Geology and Water, Development in Applied Earth Sciences 1 Nijhoff-Junk, The Hague, 228p.

Chapman, R. E., 1994, Abnormal pore pressures: Essential theory, possible causes and sliding, in W. H. Fertl, R.E. Chapman, and R.F. Hotz, eds., Studies in Abnormal Pressure, Elsevier Science B.V., p. 51-91.

Chiarelli, A., 1978, Hydrodynamic framework of Eastern Algerian Sahara- Influence on Hydrocarbon Occurence: AAPG Bulletin, v. 62, p. 667-685.

Chiarelli, A., and F. Duffaud, 1980, Pressure origin and distribution in Jurassic of Viking Graben (United Kingdom, Norway): AAPG Bulletin, v. 64, p. 1225-1250.

Choubert, G., and A. Faure-Muret, 1971, The Hercynian period, in Tectonics of Africa: Paris, p. 353-378.

Choubert, G., A. Faure-Muret, J. Fabre, A. Perrodon, and D.C. Turnier, 1971, The Platform Cover, in Tectonics of Africa: Paris, p. 379-408.

Claret, J., and C. Tempere, 1967, Une nouvelle region productive au Sahara Algerien: l'Anticlinorium d'Hassi Touareg, in 7th World Petroleum Congress, Mexico, V. 2, p. 81-100.

Clemenz, 1979, Effects of oil and bitumen saturation on source rock pyrolysis: AAPG Bulletin, v. 63, p. 2227-2232.

Clifford, A. C., 1987, African oil- past, present and future, in M. T. Halbouty, ed., Future Petroleum Provinces of the World, AAPG Mem., n°. 40, p.340-372.

Connan, J., 1974, Diagenese naturelle et diagenese artificielle de la matière organique á éléments végétaux dominants, in B. Tissot, and F. Bienner, eds., Advances in Organic Geochemistry 1973, p. 73-95.

Connan, J., K. Le Tran, and B. Van Der Weide, 1975, Alteration of Petroleum in reservoirs, in Proc. 9th World Petroleum Congress, p. 171-178.

Conrad, J., 1969, L´évolution continentale post-Hercynienne du Sahara Algerien (Saoura, Erg Chech-Tanezrouft, Ahnet-Mouydir): France, Mem. Cent. Rech. Zones Arides, Serv. Geo., Paris 10.

Cox, B. M., and R.W. Gallois, 1981, The stratigraphy of the Kimmeridge Clay of the Dorset type area and its correlation with some other Kimmeridgian sequences: Inst. Geol. Sci. Report, v. 80, 44p.

Creany, S., and Q.R. Passey, 1993, Recurring patterns of total organic carbon and source rock quality within a sequence stratigraphic Framework: AAPG Bulletin, v. 77, p. 386-401.

Dallmeyer, R. D., and J.P. Lecorché, 1989, $^{40}Ar/^{39}Ar$ polyorogenic mineral age record within the central Mauritanide orogen, West Africa: Geol. Soc. Am. Bulletin, v. 101, p. 55-70.

Dautria. J.M., and A. Lesquer, 1989, An example of the relationship between rift and dome: recent geodynamic evolution of the Hoggar swell and its nearby regions (Central Sahara, Southern Algeria and Eastern Niger): Tectonophysics, v. 163, p. 45-61.

Demaison, G., and F.T. Bourgeois, 1984, Environment of deposition of middle Miocene (Alcanar) carbonate source beds, Casablanca field, Tarragona basin, offshore Spain, in Petroleum Geochemistry and Source Rock Potential of Carbonate Rocks, Studies in Geology: AAPG Mem. n°18, p. 151-161.

Deynoux, M., 1983, Late Precambrian and Upper Ordovician glaciations in the Taoudeni Basin, West Africa, in M. Deynoux, ed., West African Paleoglaciation: Characterisation and evolution of glacial phenomena through space and time (Abs): Symposium Till Mauritania, p. 43-86.

Deynoux, M., G. Sougy, and R. Trompette, 1985, Lower Palaeozoic rocks of West Africa and the Western part of Central Africa, in C. H. Holland, ed., Lower Palaeozoic of North-Western and West-Central Africa, p. 337-412.

Doligez, B., P. Ungerer, P.Y. Chenet, J. Burrus, F. Bessis, and G. Bessereau, 1987, Numerical modelling of the sedimentation heat transfer, hydrocarbon formation and fluid migration in the Viking Graben, North Sea, in E. J. Brooks and K. Glennie, eds., Petroleum Geology of North West Europe, p. 1039-1048.

Doliguez, B., F. Bessis, J. Burrus, P. Ungerer, and P.Y. Chenet, 1986, Integrated numerical simulation of the sedimentation heat transfer, hydrocarbon formation and fluid migration in a sedimentary basin: The Themis model, in J. Burrus, ed., Thermal Modelling in Sedimentary Basins: Paris, Editions Technip, p. 173-195.

Dow, W. G., 1977, Kerogen studies and geological interpretation: Journal of Geochemical Exploration, v. 7, p. 77-99.

Dowdle, W.L., and W.M. Cobb, 1975, Static formation temperature from well logs, an empirical method: Journal of Petroleum Techniques, p.1326-1330.

Durand, B., B. Alpern, J.L. Pition, and B. Pradier, 1986, Reflectance of vitrinite as a control of thermal history of sediments, in J. Burrus, ed., Thermal Modelling in Sedimentary Basins: Paris, Editions Technip, p. 441-474.

Durand, B., 1988, Understanding of hydrocarbon migration in sedimentary basins (present state of knowledge): Org. Geochemistry, v. 13, p. 445-459.

England, W. A., M.S. Mackenzie, D.M. Mann, and T.M. Quigley, 1987, The movement and entrapment of petroleum fluids in the subsurface: J. Geol. Society, v. 144, p. 327-347.

Espitalié, J., P. Ungerer, I. Irwin, and F. Marquis, 1988, Primary cracking of kerogens. Experimenting and modelling C1, C2-C5, C6-C15 and C15+ classes of hydrocarbons formed: Org. Geochemistry, v. 13, p. 893-899.

Espitalié, J., J.L. Laporte, M. Madec, F. Marquis, P. Leplat, J. Paulet, and A. Boutefeu, 1977, Methode rapide de characterisation des roches mères, de leur potentiel pétrolier et de leur degré d´évolution: Rev. Inst. Fr.Pétrole, v. 32, p. 23-42.

Espitalié, J., J.M. Madec, and B. Tisssot, 1980, Role of mineral matrix in kerogen pyrolysis: Influence on petroleum generation and migration: AAPG Bulletin, v. 64, p. 59-66.

Espitalié, J., J.M. Madec, and F. Marquis, 1985, La pyrolyse Rock-Eval et ses application, deuxieme partie: Rev. Inst. Fr.Pétrole, v. 40, p. 754-784.

Espitalié, J., J.M. Madec, and F. Marquis, 1986, La pyrolyse Rock-Eval et ses application, troisieme partie: Rev. Inst. Fr.Pétrole, v. 41, p. 73-89.

Fabre, J., 1976, Introduction á la geologie du Sahara Algerien: Alger, Edition SNED, 421p.

Fowler, M. G., and A.G. Douglas, 1987, Saturated hydrocarbon biomarkers in oils of Late Precambrian age from eastern Siberia: Organic Geochemistry, v. 11, p. 201-213.

Furon, R., 1963, Geology of Africa, Edinbourgh, 377 p.

Genik, G. J., 1992, Regional framework, structural and petroleum aspects of rift basins in Niger, Chad and the Central African Republic (CAR): Tectonophysics, v. 213, p. 141-151.

Genik, G. J., 1993, Petroleum geology of Cretaceous-Tertiary rift basins in Niger, Chad, and Central African Republic: AAPG Bulletin, v. 77, p. 1405-1433.

Gontcharov, I., 1992, Tentative de classification des huiles Algériennes: SONATRACH internal report.

Goodarzi, F., M.G. Fowler, M. Bustin, and D.M.Mckiry, 1992, Thermal maturity of Early Paleozoic sediments as determined by the optical properties of marine-derived organic matter- A Review, in M. Schidowski et al., eds., Early Organic Evolution: Implication for Mineral and Energy Ressources, Springer-Verlag, Berlin, Heidelberg, p. 279-295.

Goudarzi, G. H., 1980, Structure of Libya, in M. J. Salem and M.T. Busreweil, eds., The Geology of Libya, Academic Press, London, p. 879-892.

Guiraud, R., Y. Bellion, J. Benkhelil, and C. Moreau, 1987, Post-Hercynian tectonics in Northern and Western Africa: Geol. Journal, v. 22, p. 433-466.

Guiraud, R., and J.C. Maurin, 1992, Early Cretaceous rifts of Western and Central Africa: an overview: Tectonophysics, v. 213, p. 153-168.

Guiraud, R., R.M. Binks, J.D. Fairhead, and M. Wilson, 1992, Chronology and geodynamic setting of Cretaceous-Cenozoic rifting in West and Central Africa: Tectonophysics, v. 213, p. 227-234.

Guiraud, M., 1993, Late Jurassic rifting-Early Cretaceous rifting and Late Cretaceous transpressional inversion in the Upper Benue Basin (NE Nigeria): Elf Aquitaine Bulletin, v. 17, p. 371-383.

Hanebeck, D., 1994, Experimentelle simulation und untersuchung der genese und expulsion von erdölen aus muttergesteinen: Dissertation, RWTH Aachen.

Hartly, R. W., and P.A. Allen, 1994, Interior cratonic basins of Africa: relation to continental break-up and role of mantle convection: Basin Research, v. 6, p. 95-113.

Hermanrud, C., I. Lerche, and K. Meisingset, 1991b, Determination of virgin rock temperature from drill stem tests: J. Pet. Technology, v. 43, p. 1126-1131.

Huang, W. Y., and W.G Meinschein, 1979, Sterols as ecological indicators: Geochim. Cosmochim. Acta, v. 43, p. 739-745.

Hunt, J. M., 1996, Petroleum Geochemistry and Geology, 743p.

Hunt, J. M., 1961, Distribution of hydrocarbons in sedimentary rocks: Geochim. Cosmochim. Acta, v. 22, p. 37-49.

Hutton, A.C., and A.C. Cook, 1980, Influence of alginite on the refelectance of vitrinite from Joadja, NSW, and some ther coals and oil shales containing alginites: Fuel, v.59, p. 711-714.

Ibach, L. E. J., 1982, Relation between sedimentation rate and total organic carbon content in ancient marine sediments: AAPG Bulletin, v. 66, p. 170-188.

I.E.S, 1995, PetroMod reference manual (release 3): I.E.S, Jülich, Germany.

Illich, H. A., 1983, Pristane, phytane, and lower molecular weight isoprenoid distribution: AAPG Bulletin, v. 67, p. 385-397.

Illich, H., J. Zumberge, C. Schiefelbein, and S. Brown, 1997, Petroleum systems of the Ghadames Basin and Illizi Platform (abs): AAPG Annual Meetig Convension, April 6-9, Dallas, Texas.

Jardine, S., and L. Yapaudjian, 1968, Lithostratigraphie et palynologie du Devonien-Gothlandien greseux du bassin de Polignac (Sahara): Rev. Inst. Fr.Pétrole, v. 13, p. 439-462.

Katz, B. J., 1983, Limitations of Rock-Eval pyrolysis for typing organic matter: Org. Geochemistry, v. 4, p. 195-199.

Katz, B. J., R.N. Pheifer, and D.J. Schunk, 1988, Interpretation of dicontinious vitrinite reflectance profiles: AAPG Bulletin, v. 72, p. 926-931.

Kehle, R. O., 1973, Geothermal survey of North America: Annual progress report. Project supported by the Am. Assoc. Petr. Geol.

Killian, C., 1922, Etude de l´Ordovicien et du Silurien du Sahara Algerian: C.R. Soc. Geo. France, p. 25-26.

Klitzch, E., 1970, Structural development of parts of North Africa since Cambrian time, in C. Gray, ed., Symposium on Geology of Libya, Lib. Pet. Expl. Society, p. 253-265.

Klitzch, E. H., 1984, Northwestern Sudan and bordering area: geological development since Cambrian time: Berlin Geowissenschaften Abhandlung, v. 50, p. 23-45.

Klitzch, E., 1990, Palaezoic, in R. Said, ed., The geology of Egypt, p. 393-406.

Larter, S., 1989, Chemical models of vitrinite reflectance evolution: Geo. Rundschau, v. 78, p. 349-359.

Le Pichon, X., F. Bergerat, and M.J. Roulet, 1988, Plate kinematics and tectonics leading to the Alpine belt formation; a new analysis: Geo. Soc. America, v. 218, p. 111-131.

Legrand, P., 1975, Lower Palaeozoic rocks of Algeria, in C. H. Holland, ed., Lower Palaeozoic Rocks of the World, p. 5-89.

Legrand, P., 1981, Essai sur la paléogeographie du Silurien au Sahara Algerien: Compagne Francaise des Pétroles, Memoire n° 16, Paris, p. 10-22.

Legrand, P. H., 1985, Lower Paleozoic rocks of Algeria, in C. H. Holland, ed., Lower Palaeozoic of Northwerstern and West-Central Africa, p. 5-89.

Leischner, K., D.H. Welte, and R. Littke, 1993, Fluid inclusions and organic maturity parameters as calibration tools in basin modelling, in A.G. Dore et al., eds., Basin Modelling: Advances and Applications, p. 161-172.

Lesquer, A., J.F. Beltrao, and F.A.M. De Abreu, 1984, Proterozoic links between north-eastern Brazil and West Africa: a plate tectonic model based on gravity data: Tectonophysics, v. 110, p. 9-26.

Lesquer, A., A. Burmatte, and J.M. Dautria, 1988, Deep structure of the Hoggar domal uplift (Central Sahara, South Algeria) from gravity, thermal and petrological data: Tectonophysics, v. 152, p. 71-87.

Lesquer, A., D. Takhrist, J.M. Dautria, and O. Hadiouche, 1990, Geophysical and petrological evidence for the presence of an "anomalous" upper mantle beneath the Sahara basins (Algeria): Earth and Planet. Sci. Letters, v. 96, p. 407-418.

Leventhal, J. S., 1983, An interpretation of carbon and sulfur relationships in Black Sea sediments as indicators of environments of deposition: Geochim. Cosmochim. Acta, v. 47, p. 133-137.

Littke, R., D.R. Baker, and D. Leythaeuser, 1988, Microscopic and sedimentologic evidence for the generation and migration of hydrocarbons in Toarcian source rocks of different maturities: Org. Geochemistry, v. 13, p. 549-559.

Littke, R., D.R. Baker, and J. Rullkötter, 1991, Keys to the depositional history of the Posidonia Shale (Toarcian) in the Hils syncline, Northern Germany, in R. V. Pearson and T.H. Tyson., eds., Modern and ancient shelf anoxia, p. 311-334.

Littke, R., C. Büker, A. Lückge, R.F. Sachsenhofer, and D.H. Welte, 1994, A new evaluation of palaeoheat flows and eroded thicknesses for the Carboniferous Ruhr basin, western Germany: Intern. Journ. Coal. Geology, v. 26, p. 155-183.

Littke, R., D.R. Baker, and J. Rullkötter, 1997, Deposition of petroleum source rocks, in D. H. Welte, B. Horsfield, and D.R. Baker, eds., Petroleum and Basin Evolution, Springer-Verlag, Berlin, Heidelberg, p. 273-333.

Lopatin, N. V., 1971, Temperature and geologic time as factors in coalification: Akad.Nauk. SSSR izv.ser.Geol., p. 95-106.

Louis, M. C., and B. Tissot, 1967, Influence de la température et de la pression sur la formation des hydrocarbures dans les argiles á kérogene. in Proceedings of the 7th World Petroleum Congress, v.2, p. 47-60.

Macgregor, D. S., 1996, The hydrocarbon systems of North Africa: Marine and Petroleum Geology, v. 13, p. 329-340.

Mackenzie, A. S., and T.M. Quigly, 1988, Principles of geochemical prospect appraisal: AAPG Bulletin, v. 72, p. 399-415.

MacKirdy, D. M., A.K. Aldridge, and P.J.M. Ypma, 1983, A geochemical comparison of some crude oils from pre-Ordovician carbonate rocks, in M. Bjoroy et al., eds., Advances in Organic Geochemistry, 1981, p. 90-107.

Magara, K., 1978, Compaction and fluid migration: Amsterdam, Elsevier, 319 p.

Magliore, P. R., 1970, Triassic gas field of Hassi R´Mel, Algeria, in M.T. Halbouty, ed., Geology of the Giant Petroleum Fields, AAPG Mem. n°. 14, p 489-501.

Makhous, M., 1996, Conditions géologiques et géochimiques de formation des gisements d´hydrocarbures dans les basins Sahariens, unpublished PhD. Thesis, Université de Strasbourg, France, 288 p.

Makhous, M., Y. Galushkin, and N. Lopatin, 1997, Burial history and kinetic modelling for hydrocarbon generation, part I: The Galo Model: AAPG Bulletin, v. 81, p. 1660-1678.

Makhous, M., Y. Galushkin, and N. Lopatin, 1997, Burial history and kinetic modeling for hydrocarbon generation, part II: Applying the GALO Model to Saharan Basins: AAPG Bulletin, v. 81, p. 1979-1699.

Malla, M. S., B. Khatir, N. Yahi, and D. Kessab, 1995, Synthese et analyse des donnees et résultats géochimiques par basin: Illizi-Ghdames: SONATRACH internal report

Malla, M. S., B. Khatir, and N. Yahi, 1997, Revue of the structural evolution and hydrocarbon generation in the Ghadames and Illizi Basins, Algeria (abs): 15th World Petroleum Congress, Beigin.

Massa, D., and A. Moreau-Benoit, 1976, Essai de synthese stratigraphique et palynologique du systeme Devonien en Libye occidentale: Rev. Inst. Fr. Pétr., v. 31, p. 287-316.

Massa, D., and D. Vachard, 1979, Le Carbonifere de Libye occidentale: Biostratigraphie et Micropaléontologie. Position dans le domaine Tethysien de l´Afrique du Nord: Rev. Inst. Fr.Pétrole, v. 34, p. 3-47.

Matsumoto, G., T. Tori, and T. Hanya, 1982, High abundance of algal 24-ethylcholesterol in antarctic lake sediments: Nature, v. 299, p. 52-54.

Maxwell, J. R., R.E. Cox, R.G. Ackman, and S.N. Hooper, 1972, The diagenesis and maturation of phytol: The stereochemistry of 2, 6, 10, 14-tetramethylpentadecane from an ancient sediment, in H. R. Von Geartner and H. Wehner, eds., Advances in Organic Geochemistry 1971, p. 227-291.

Mckenzie, D., 1978, Some remarks on the development of sedimentary basins: Earth and Planet. Sci. Letters, v. 40, p. 25-32.

Mackenzie, A. S., and T.M. Quigley, 1988, Principles of geochemical prospect appraisal: AAPG Bulletin, v. 72, p. 399-415.

Megartzi, M., 1972, Etude des structures circulaires du Nord-Est d´Illizi (ex Fort-Polignac), Sahara Nord-Oriental, Alger.

Mengoli, S., and G. Spenci, 1985, Tectonic evolution of North Africa (from North Sinai to Algeria), in Proceedings of the Seminar on Source Rock and Habitat of Petroleum in the Arabic Countries, Kuwait, Oct. 1984, OAPEC, p.119-174.

Moldowan, J. M., P. Sundaraman, and M. Schoell, 1985, Sensivity of biomarker properties of depositional environment and/or source input in the Lower Toarcian of SW Germany: Org. Geochemistry, v. 10, p. 915-926.

Moldowan, J. M., W.K. Seifert, and E.J. Gallegos, 1985, Relationship between petroleum composition and depositional environment of petroleum source rocks: AAPG Bulletin, v. 69, p. 1255-1268.

Mongelli, F., M. Loddo, and A.Tramacere, 1982, Thermal conductivity and specific heat variation of some Travale field (Tuscany) rocks versus temperature: Tectonophysics, v. 83, p. 33-43.

Neunzert, G.H., R. Gaupp, and R. Littke, 1996, Absenkungs- und Temperatur-geschichte paläozoicher und mesozoischer Formationen im Nordwestdeutschen Becken: Z.Dt. Geol. Ges, v. 147,2, p. 183-208.

Neunzert, G.H., 1998, Simulation der Beckensubsidenz, der Temperaturgeschichte, der Reifung organichen Materials, und der Genese, Migration und Akkumulation von Methan und Stickstoff in Nordwestdeutschland auf der Basis seismischer Interpretationen: Berichte, Forschungzentrum Jülich, 3521, 173p.

Nichols, P. D., A.C. Palmisano, M.S. Rayner, G.A. Smith, and D.C. Wite, 1990, Occurence of novel C30 sterols in Antarctic sea-ice diatom communities during a spring bloom: Org. Geochemistry, v.15,p.503

Oil and Gas Journal, 1998, Sonatrach aims to become major international oil firm, v. 96, n°

Osborne, M.J., and R.E. Swarbrick, 1997, Mechanisms of generating overpressures in sedimentary basins - A reevaluation: AAPG Bulletin, v.81, no.6, p. 1023-1041.

Ourisson, G., P. Albrecht, and M. Rohmer, 1979, The hopanoids. Paleochemistry and biochemistry of a group of natural products: Pure Appl. Chemistry, v. 51, p. 709-729.

Pearson, T. H., and R. Rosenberg, 1978, Macrobenthic succession in relation to organic enrichment and pollution of the marine environment: Ocean and Mar. Biology: an Annual Revue, v. 16, p. 229-311.

Peters, K. E., and J.M. Moldowan, 1991, Effect of source, thermal maturity and biodegradation on the distribution and isomerisation of homohopanes in petroleum: Org. Geochemistry, v. 17, p. 47-61.

Peters, K. E., and J.M. Moldowan, 1993, The biomarker guide, interpreting molecular fossils in petroleum and ancient sediments: New Gersey, Englewood Cliffs, 363p.

Petters, S., 1979, Stratigraphic history of the South-central Saharan region: Geo. Soc. Am. Bulletin, v. 90, p. 753-760.

Petters, K. E., 1986, Guideline for evaluating petroleum source rocks using programed pyrolysis: AAPG Bulletin, v. 70, p. 318-329.

Petters, S. W., 1991, Regional Geology of Africa, Springer-Verlag, Berlin, Heidelberg, 722p.

Philippi, G. T., 1956, Identification of oil source beds by chemical means: Geologia del Petroleo: Congreso Geologico Internacional XX Sesion, Ciudad de Mexico, p. 25-38.

Philippi, G. T., 1965, On the depth, time and mechanism of petroleum generation: Geochim. Cosmochim. Acta, v. 29, p. 1021-1049.

Philippi, G. T., 1975, The deep subsurface temperature controlled origin of the gaseous and gasoline-range hydrocarbons of petroleum: Geochim. Cosmochim. Acta, v. 39, p. 1353-1373.

Poelchau, H. S., D.R. Baker, T. Hantschel, B. Horsfield, and B. Wygrala, 1997, Basin simulation and the design of the conceptual basin model, in D. H. Welte, B. Horsfield, and D.R., Baker, eds., Petroleum and Basin Evolution, Springer-Verlag, Berlin, Heidelberg, p. 5-70.

Powell, T.G., and D.M. McKirdy, 1975, Crude oil composition in Australia and Papua-New Guinea: AAPG Bulletin, v. 59, p. 1176-1197.

Powell, T.G., S. Creany, and L.R. Snowdon, 1982, Limitations of use of organic petrographic techniques for identification of petroleum source rocks: AAPG Bulletin, v. 66, p. 430-435.

Powell., T.G., and D.M. McKirdy, 1973, The effect of source material, rock type and diagenesis on the *n*-alkane content of sediments: Geochim. Cosmochim. Acta, v. 37, p. 623-633.

Price, C.L., 1979, Aqueous solubility of methane at elevated pressures and temperatures: AAPG Bulletin, v. 63, p. 1527-1533.

Quigley, T. M., A.S. Mackenzie, and J.R. Gray, 1987, Kinetic theory of petroleum generation, in B. Doligez, ed., Migration of Hydrocarbon in Sedimentary Basins: Paris, Editions Technip, p. 649-665.

Radke, M., H.G. Sittardt, and D.H. Welte, 1978, Removal of soluble organic matter from rock samples with a flow-through extraction cell: Anal. Chemistry, v. 50, p. 663-665.

Radke, M., H. Willsch, and D.H. Welte, 1980, Preparative hydrocarbon group type determination by automated medium pressure liquid chromatigraphy: Anal. Chemistry, v. 52.

Radke, M., 1981, Class separation of aromatic compounds in rock extracts and crude oils by semipreparative HPLC: KFA, ICH-5, report 500581, 34p.

Radke, M., D.H. Welte, and H. Wilsch, 1982, Geochemical study on a well in the western Canada Basin: relation of the aromatic distribution pattern to maturity of organic matter: Geochim. Cosmochim. Acta, v. 46, p. 1-10.

Radke, M., and D.H. Welte, 1983, The Methylphenanthrene Index (MPI): A maturity parameter based on aromatic hydrocarbons: influence of the organic matter type, in M. Bjoroy et al., eds., Advances in Organic Geochemistry 1981, Wiley, Chister, p.504-512.

Radke, M., D.H. Welte, and H. Willsch, 1986, Maturity parameters based on aromatic hydrocarbons: influence of the organic matter type: Org. Geochemistry, v. 10, p. 51-63.

Radke, M., 1987, Organic geochemistry of aromatic hydrocarbons, in J. Brooks, and D.H. Welte, eds., Advances in Petroleum Geochemistry, London, Academic Press, v. 2, p. 141-207.

Radke, M., 1988, Application of aromatic compounds as maturity indicators in source rocks and crude oils: Mar. Petr. Geology, v. 5, p. 224-236.

Radke, M., B. Horsfield, R. Littke, and J. Rullkötter, 1997, Maturation and petroleum generation, in D. H. Welte, B. Horsfield, and D.R. Baker, eds., Petroleum and Basin Evolution, Springer-Verlag, Berlin, Heidelberg, p. 172-229.

Richardson, J. B., and N. Ioannides, 1973, Silurian palynomorphs from Tanezouft and Accacus formations , Tripolitania, North Africa: Micropaleontology, v. 19, p. 257-307.

Richardson, M., and Arthur, A.A., 1988, The Gulf of Suez-northern Red Sea Neogen rift: a quantitative basin analysis: Mar. Petr. Geology, v. 5, p. 247-270.

Rieke, H. H., and G.V. Chilingarian, 1974, Compaction of argilaceous sediments, Developments in Sedimentology 16, Elsevier, 424p.

Robbins, E. I., 1979, Geothermal gradients, in P. A. Scholle, ed., Geological studies of the Cost GE-1 well, United States South Atlantic Outer Continental shelf Area, US Geol. Survey. Circ., p. 72-73.

Robinson, K. M., 1987, An overview of source rocks and oils in Indonesia: in Proceedings of the Indonesian Petroleum Association, 16th Ann. Convention, Ind. Petr. Ass., v. 1, p. 97-122.

Rullkötter, J., D. Leythaeuser, B. Horsfield, R. Littke, U. Mann, P.J. Müller, M. Radke, R.G. Shaefer, H.J. Schenk, K. Schwochau, E.G. Witte, and D.H. Welte, 1988, Organic matter maturation under the influence of a deep intrusive haet source: A natural experiment for quantification of hydrocarbon generation and expulsion from a petroleum source rock (Toarcian shale, northern Germany): Org. Geochemistry, v. 13, p. 847-856.

Sachsenhofer, R. F., and R. Littke, 1993, Vergleich und Bewertung verschiedener Methoden zur Berechnung der Vitrinitreflexion am Beispiel von Bohrungen im Steirischen Tertiärbecken: Zentralbl. Geol. Paläonto, 1992, v. 1, p. 597-610.

Sahagian, D., 1988, Epeirogenic motion of Africa as inferred from Cretaceous shoreline deposits: Tectonics, v. 7, p. 125-138.

Savostin, L. A., J.C. Sibuet, L.P. Zonenshain, X. Le Pichon, and M.J. Roulet, 1986, Kinematic evolution of the Tethys belt from the Atlantic ocean to the Pamirs since the Triassic: Tectonophysiscs, v. 123, p. 1-35.

Scheidt, G., and R. Littke, 1989, Comparative organic petrology of interlayered sandstones, siltstones, mudstones and coals in the Upper Carboniferous Rhur Basin, Northwest Germany, and their thermal history and methane generation: Geol. Rdsch, v. 78,1, p. 375-390.

Schenk, H.J., B. Horsfield, B. Krooss, R.G. Schaefer, and K. Schwochau, 1997, Kinetics of Petroleum formation and cracking, in D. H. Welte, B. Horsfield, and D.R.

Baker, eds., Petroleum and Basin Evolution, Springer-Verlag, Berlin, Heidelberg, p. 233-269.

Schowalter, T. T., 1979, Mechanisms of secondary migration and entrapment: AAPG Bulletin, v. 63, p. 723-760.

Seifert, W. K., and J.M. Moldowan, 1978, Applications of steranes, terpanes and monoaromatics to the maturation, migration, and source of crude oils: Geochem. Cosmochim. Acta, v. 42, p. 77-95.

Seifert, W. K., and J.M. Moldowan, 1980, The effect of thermal stress on source rock quality as measured by hopane stereochemistry, in A. G. Douglas and J. R. Maxwell, eds., Advances in Organic Geochemistry 1979, Pergamon, Oxford, p. 229-237.

Sieskind, O., G. Joly, and P. Albrecht, 1979, Simulation of the geochimical transformation of sterols: superacid effect of clay minerlals: Geochim. Cosmochim. Acta, v. 43, p. 1675-1679.

Sweeney, J. J., and A.K. Burnham, 1990, Evaluation of a simple model of vitrinite reflectance based on chemical kinetics: AAPG Bulletin, v. 74, p. 1559-1570.

Takhrist, D., and A. Lesquer, 1989, Mise en évidence d´importantes variations régionales du flux de chaleur en Algérie: Can. Jour. Earth Sciences, v. 26, p. 615-626.

Taylor, G.H., M. Teichmüller, A. Davis, C.F.K. Diessel, R. Littke, and P. Robert, 1998, Organic Petrology: Gebrüder Borntraeger, Berlin, Stuttgart, 704p.

Ten Haven, H. L., J.W. De Leeuw, J.S. Sinninghe Damste, P.A. Schenk, S.E. Palmer, and J.E. Zumberge, 1988, Application of biological markers in the recognition of paleohypersaline environments, in A. G. Fleet and M.R. Talbot, eds., Lacustrine Petroleum Source Rocks, Geological Society Special Publication, n°. 40, p. 123-130.

Thiessen, R., K. Burke, and W.S.F. Didd, 1979, African hotspots and their relation to the underlying mantle: Geology, v. 7, p. 263-266.

Tissot, B., Y. Califet-Debyser, G. Deroo, and J.L. Oudin, 1971, Origin and evolution of hydrocarbons in Early Toarcian shales, Paris Basin, France: AAPG Bulletin, v. 55, p. 212179-2193.

Tissot, B., J. Espitaliie, and G. Deroo, 1973, Origin and migration of Hydrocarbons in the Eastern Sahara (Algeria), in G. Demaison, ed., Petroleum Geochemistry and Basin Evaluation, AAPG Mem., n°35, p. 315-334.

Tissot, B., and J. Espitalié, 1975, L´évolution thermique de la matière organique des sédiments: application d´une simulation mathématique: Rev. Inst. Fr.Pétrole, v. 30, p. 743-777.

Tissot, B., R. Pelet, J. Roucaché, and A. Combaz, 1977, Utilisation des alcanes comme fossiles géochimiques indicateurs des environements géologiques, in R. Campos and J. Goni, eds., Advances in Organic Geochemistry 1975, Madrid, p. 117-154.

Tissot, B., and D.H. Welte, 1984, Petroleum Formation and Occurrence: New York, Springer-Verlag, Berlin, 699p.

Tissot, B., R. Pelet, and P. Ungerer, 1987, Thermal history of sedimentary basins, maturation indices, and kinetics of oil and gas generation: AAPG Bulletin, v. 71, p. 1445-1466.

Tyson, R. V., and T.H. Pearson, 1991, Modern and Ancient Continental Shelf Anoxia, v. 58, Geological Society Special Publication, n°. 58, 470p.

Ungerer, P., F. Bessis, P. Y. Chenet, E. Nogaret, A. Chiarelli, J.L Oudin, and J.F. Perrin, 1984, Geological and geochemical models in oil exploration; principles and practical examples: AAPG Mem., v. 35, p. 53-77.

Ungerer, P., and R. Pelet, 1987, Extrapolation of the kinetics of oil and gas formation from laboratory experiments to sedimentary basins: Nature, v. 327, p. 52-54.

Ungerer, P., J. Burrus, B. Doligez, P.Y. Chenet, and F. Bessis, 1990, Basin evaluation by integrated two-dimensional modeling of heat transfer, fluid flow, hydrocarbon generation, and migration: AAPG Bulletin, v. 74, p. 309-335.

Ungerer, P., 1990b, State of the art of research in kinetic modelling of oil formation and expulsion: Org. Geochem, v. 16, p. 1-25.

Vandenbrouke, M., and F. Behar, 1988, Geochemical characterisation of the organic matter from some recent sediments by a new pyrolysis technique. in K. Kelts, A. Fleet, and M. Talbot, eds., Lacustrine Petroleum Source Rocks, Oxford, Blackwell.

Volkman, J. K., 1986, A review of sterol markers for marine and terrigeneous organic matter: Org. Geochemistry, v. 9, p. 83-99.

Volkman, J. K., 1988, Biological marker compounds as indicators of the depositional environments of petroleum source rocks, in A.J. Fleet and M.R. Talbot, eds., Lacustrine Petroleum Source Socks, Oxford, Blackwell, p. 103-122.

Waples, D. W., 1980, Time and temperature in petroleum formation: Application of Lopatin's method to petroleum exploration: AAPG Bulletin, v. 64, p. 916-926.

Waples, D. W., 1985, Geochemistry in petroleum exploration: Boston, International Human Ressources Development, 232 p.

Welte, D. H., and M.A. Yukler, 1981, Petroleum origin and accumulation in basin evolution- a quantitative model: AAPG Bulletin, v. 65, p. 1387-1396.

Welte, D. H., 1987, Migration of hydrocarbons, facts and theory, in B. Doliguez, ed., Migration of Hydrocarbon in Sedimentary Basins: Paris, Editions Technip, p. 393-413.

Welte, D. H., and M.N. Yalcin, 1987, Formation and occurence of petroleum in sedimentary basins as deduced from computer-aided basin modelling, in S. P. Kumar, et al., eds., Petroleum Geochemistry and Exploration in the Afro-Asian Region, Balkema, Rotterdam, p. 17-23.

Welte, D. H., and M.N. Yalcin, 1988, Basin modelling - A new comprehensive method in petroleum geology: Org. Geochemistry, v. 13, p. 141-152.

Wenger, L. M., and D.R. Baker, 1987, Variations in vitrinite reflectance with organic facies- Examples from Pensylvanian cyclotherms of the Midcontinent, USA: Org. Geochemistry, v. 11, p. 411-416.

Whiteman, A. J., 1971, Cambro-Ordovician Rocks of Al Jazair (Algeria)- a Review: AAPG Bulletin, v. 55, p. 1295-1335.

Wignall, P. B., 1994, Black Shales, Oxford, 127p.

Wygrala, B. P., 1988, Integrated computer- aided basin modeling applied to analysis of hydrocarbon generation history in northern Italian oil field, in L. Matavelli and L. Novelli, eds., Advances in Organic Geochemistry 1987, p. 187-197.

Wygrala, B. P., 1989, Integrated study of an oil field in southern Po basin, northern Italy: Dissertation, Universitate Köln, 217 p.

Yalcin, M. N., D.H. Welte, K.N. Misra, S.K. Mandal, K.C. Balan, K.L. Mehrotra, and B.L. Lohar, 1988, Three-dimensional computer-aided basin modeling of Cambay Basin, India- A case history of hydrocarbon generation, in L. K. Kumar et al., eds., Petroleum Geochemistry and Exploration in the Afro-Asian region, Balkema, Rotterdam, p. 417-450.

Yalcin, M. N., and D.H. Welte, 1988, Thermal history evolution of sedimentary basins and significance for hydrocarbon generation: Turk. Asoc. Petr. Geologists, v. 1, p. 12-26.

Yalcin, M. N., R. Littke, and R.F. Sachsenhofer, 1997, Thermal history of sedimentary basins, in D. H. Welte, B. Horsfield, and D.R. Baker, eds., Petroleum and Basin Evolution, Springer-Verlag, Berlin, Heidelberg, p. 73-167.

APPENDIX

Equations Used for the Calculation of Molecular parameters

$$\text{CPI-1} = \frac{2(C23 + C25)}{(C22 + 2C24 + C26}$$

$$\text{CPI-5} = \frac{2(C25 + C27 + C29 + C31)}{(C24 + 2C26 + C28 + C30)}$$

$$\text{LHCPI} = \frac{2(C17 + C18 + C19)}{(C27 + 2C28 + C29)}$$

$$\text{MNR} = \frac{(2\text{-MP})}{(1\text{-MP})}$$

$$\text{MPI 1} = \frac{1.5\,((2\text{-MP}) + (3\text{-MP}))}{(P) + (1\text{-MP}) + (9\text{-MP})}$$

$$\text{ENR} = \frac{(2\text{-EN})}{(1\text{-EN})}$$

MN, methylnaphthalene
EN, ethylnaphthalene
MP, methylphenanthrene

$$\frac{(22S)}{(22S+22R)} \text{ of } C_{32} \text{ hop} \quad \frac{17\alpha\,(H)\text{-Homohopane (22S)}}{17\alpha\,(H)\text{-Homohopane (22S)} + 17\alpha\,(H)\text{-homohopane (22R)}}$$

$$\frac{Ts}{Ts + Tm} = \frac{C27\ 18\alpha\,(H)\text{-trinorhopane}}{C_{27}\ 18\alpha\,(H)\text{-trinorhopane} + C27\ 17\alpha\,(H)\text{-trinorhopane}}$$

$$\frac{Hop}{Hop + Mor} = \frac{17\alpha\,(H)\text{-hopane}}{17\alpha\,(H)\text{-hopane} + 17\beta\,(H)\text{-hopane}}$$

Tab. 1: Total organic carbon (C_{org}), sulfur and Rock-Eval data of the sample set analysed in this study.

Sample N°	Depth (m)	C_{org} (%)	TC (%)	$CaCO_3$ (%)	S (%)	S_1 (mg hc/g)	S_2 (mg hc/g)	S_3 mg CO2/g	T_{max} (°C)	HI mg hc/g C_{org}	OI mg CO2/g C_{org}
E44093	4510.00	1.55	2.17	5.17	1.78	0.09	0.56	0.49		36	32
E44094	4515.00	2.32	3.74	11.83	1.45	0.15	0.29	0.65		13	28
E44095	4519.00	4.25	4.69	3.63	3.42	0.11	0.28	1.10		7	26
E44096	4520.00	8.99	12.3	27.58	4.74	0.13	0.59	1.36		7	15
E44097	4522.00	10.7	12.2	12.5	4.66	0.27	0.72	0.90	498	7	8
E44098	4525.00	3.71	4.85	9.50	2.94	0.06	0.31	0.87	542	8	23
E44099	3665.00	7.50	8.88	11.5	3.97	33.89	23.56	1.48		314	20
E44100	3582.00	3.55	4.43	7.33	3.6	24.93	7.31	1.24	436	206	35
E44101	3606.00	4.26	5.12	7.17	2.72	37.05	11.36	1.08	437	267	25
E44102	3620.00	3.92	5.10	9.83	3.03	41.27	11.45	1.16	437	292	30
E44103	3632.00	4.40	9.19	39.92	2.36	39.72	12.57	1.76	437	286	40
E44230	3736.75	1.06	1.05	0.00	1.72	0.32	0.67	0.06	430	63	6
E44231	3740.15	0.94	0.92	0.00	1.31	0.33	0.99	0.07	429	105	7
E44232	3744.85	1.16	1.19	0.25	1.09	0.28	0.93	0.08	436	80	7
E44233	3856.05	3.60	3.78	1.50	0.18	0.45	3.43	0.23	446	95	6
E44234	3947.00	2.75	2.88	1.08	2.95	0.94	1.73	1.10	429	63	40
E44235	3968.00	2.75	2.82	0.58	4.02	0.64	1.20	0.83	432	44	30
E44236	3992.00	2.62	2.67	0.42	3.99	0.89	1.79	1.51	427	68	58
E44237	4035.00	1.65	3.20	12.92	0.79	0.46	1.23	1.93	444	75	117
E44238	4146.00	1.79	2.27	12.33	1.01	0.48	0.83	1.98	446	46	111
E44239	4176.00	3.10	3.05	0,00	3.46	1.32	1.41	1.61	416	45	52
E44240	4212.00	7.70	7.99	2.42	6.3	2.82	4.57	1.03	438	59	13
E44241	4216.00	5.95	7.55	13.33	5.18	2.38	5.68	0.97	446	95	16
E44242	4219.00	3.68	4.38	5.83	4.48	1.89	2.82	2.4	442	77	65
E44243	4227.00	6.84	7.51	5.58	4.87	3.22	6.19	1.15	447	91	17
E44244	4306.00	4.83	5.58	6.25	3.24	1.71	3.96	0.95	450	82	20
E44245	4324.00	5.60	6.18	4.83	3.29	2.01	2.86	0.94	440	51	17
E44246	4359.00	6.28	8.78	20.83	3.67	2.14	4.16	1.21	458	66	19
E44247	4371.00	7.14	8.72	13.17	3.91	1.87	3.84	1.23	463	54	17
E44248	4406.00	4.21	5.67	12.17	2.21	1.14	2.53	1.52	460	60	28
E44249	4412.00	4.12	6.64	21.00	2.24	1.35	2.76	1.60	461	67	37
E44250	4461.00	2.24	3.29	8.75	2.95	0.68	0.92	1.18	437	41	71
E44251	4467.00	1.58	2.34	6.33	2.51	0.92	1.21	2.46	548	77	75
E44252	4510.00	1.06	1.13	0.58	1.44	0.60	1.91	2.87	545	180	232
E44253	4540.00	1.79	1.89	0.83	4.20	0.80	1.8	2.07	547	101	160
E44254	4570.00	1.71	2.99	10.67	2.23	0.90	0.57	1.5	360	33	121
E44256	4587.00	1.68	2.29	5.08	3.31	0.84	1.48	2.14	548	88	89
E44257	4610.00	1.17	1.80	5.25	1.94	0.62	1.54	2.07	548	132	183
E44258	4622.00	0.82	0.97	1.25	1.01	0.74	2.47	2.19	544	301	252
E44259	4632.00	1.19	1.82	5.25	2.00	0.89	1.47	1.55	548	124	184
E44260	4642.00	1.20	1.70	4.17	2.86	0.89	0.61	2.22		51	129
E44261	4657.00	0.80	1.53	6.08	0.89	1.14	1.53	1.52	547	191	278
E44262	4690.00	2.49	2.72	1.92	2.69	0.51	1.38	1.52	423	55	61
E44263	4692.00	1.28	1.74	3.83	3.02	0.01	0.22	0.20		17	16
E44264	4699.00	2.20	3.39	9.92	3.10	0.01	0.17	0.20	500	8	9
E44265	4708.00	4.53	5.83	10.83	4.60	0.02	0.30	0.33	521	7	7
E44266	4712.00	8.37	9,93	13,00	3.75	0.02	0.29	0.31	527	3	4
E44267	4719.00	9.00	11.10	17.5	11.9	0.02	0.28	0.38	521	3	4
E44268	4723.00	0.43	0.63	1.67	0.47	0,00	0.08	0.06		19	14
E44269	4762.00	19.3	19.4	0.83	3.25	2.12	18.39	15.55	426	95	81
E44270	4772.00	2.03	2.86	6.92	2.93	0.14	0.30	0.47	420	15	23
E44271	3749.00	1.68	3.30	13.5	0.43	0.46	1.48	1.03	448	88	61
E44272	3754.12	2.33	2.89	4.67	0.10	0.58	2.94	0.49	446	126	21
E44273	3758.00	1.96	2.09	1.08	0.23	0.48	2.05	0.20	447	105	10
E44274	3763.00	1.95	1.89	0.25	0.23	0.40	1.98	0.04	449	102	2

E44275	3787.40	1.87	2.02	1.25	0.91	0.51	1.53	0.14	449	82	7
E44276	3792.30	1.89	1.91	0.17	0.25	0.37	1.47	0.03	447	78	2
E44277	3804.00	3.72	4.56	7,00	0.77	28.36	7.20	1.26	435	194	34
E44278	3830.00	3.36	3.95	4.92	3.62	18.77	3.90	1.03	419	116	31
E44279	3862.00	3.53	4.72	9.92	3.19	24.86	6.02	1.08	436	171	31
E44280	3886.00	5.64	6.53	7.42	3.69	36.3	6.62	1.19	432	117	21
E44281	3924.00	4.38	6.45	17.25	2.55	29.2	7.50	1.27	438	171	29
E44283	4112.50	0.8	0.92	1.00	2.89	0.26	0.48	0.12	367	60	15
E44284	4117.45	1.73	2.45	6.00	4.58	0.64	0.74	0.20	447	43	12
E44285	4178.00	3.95	5.09	9.5	2.38	39.95	5.32	1.24	437	135	31
E44286	4196.00	2.39	3.11	6,00	0.72	30.02	4.62	1.17	439	193	49
E44287	4208.00	2.73	3.55	6.83	0.79	35.38	5.64	1.27	438	207	47
E44288	4220.00	2.89	4.07	9.83	1.07	44.35	6.68	1.47	441	231	51
E44289	4224.00	2.76	3.08	2.67	1.52	40.22	5.78	1.47	438	209	53
E44290	4352.00	2.40	3.19	6.58	0.5	31.4	6.02	0.91	431	251	38
E44291	2592.00	0.94	1.40	3.83	2.52	0.64	1.10	2.25	388	117	239
E44293	2620.00	1.31	2.27	8.00	3.59	0.35	0.70	1.12	429	53	86
E44294	2630.00	1.94	3.26	11,00	4.57	0.84	1.77	1.47	430	91	76
E44295	2642.00	1.29	2.40	9.25	3.68	0.43	1.13	0.59	438	88	46
E44296	2652.00	2.02	3.05	8.58	3.90	0.74	1.50	2.02	435	74	100
E44297	2660.00	3.08	4.97	15.75	5.06	0.97	1.85	2.22	438	60	72
E44298	2677.00	1.79	3.23	12.00	3.85	0.61	1.08	1.30	435	60	73
E44299	2682.00	2.68	3.49	6.75	4.59	1.69	1.89	1.51	436	71	56
E44300	2687.oo	4.19	8.08	32.42	4.65	1.33	4.28	1.79	443	102	43

Tab.2: Input data for modelling of burial and temperature history of well BK-2

Event N°	Name	Time at the base (mybp)	Thickness (m)	Lithology	Porosity (%)	Water depth (m)	SWI temp (°C)	Heat flow (mW/m²)
49	Quaternary	2.0	0.0	SANDSTONE	42.0	0.0	21.0	55
48	Pliocene	4.0	-50.0	SAND, silty	39.0	0.0	21.0	55
47	Ol/Miopl	35.0	260.0	SAND, silty	39.0	1.0	21.0	55
46	Alpine	42.0	-50.0	LIME, dolo	39.0	0.0	24.0	55
45	Maest-Eoc	74.0	216.0	LIME, dolo	39.0	45.0	27.0	55
44	Camp-Sant	86.0	232.0	DOLO,evap	34.0	5.0	28.0	55
43	Coniacian	89.0	180.0	SALT	6.0	5.0	29.0	55
42	Turonian	90.0	58.0	LIME, marly	31.0	15.0	29.0	55
41	Upp_Cenom	93.0	128.0	SHALE&ANHYD	6.0	15.0	29.0	55
40	Low_Cenom	97.0	95.0	SHALE, calc	20.0	45.0	29.0	57
39	Albian	112.0	219.0	SAND,shaly	23.0	30.0	30.0	57
38	Aptian	117.0	30.0	LIME, dolo	27.0	45.0	30.0	57
37	Austrian	124.0	-150	SAND, silty	20.0	0.0	30.0	57
36	Barremian	132.0	653.0	SAND, silty	20.0	30.0	30.0	57
35	Neocomian	146.0	313.0	SHALE, sandy	15.0	30.0	29.0	57
34	Malm	161.0	218.0	SHALE&LIME	16.0	45.0	28.0	57
33	Bart-Bajo	173.0	134.0	SHALE, calc	14.0	15.0	27.0	60
32	Toarc_Aal	187.0	109.0	SHALE, calc	13.0	30.0	25.0	60
31	Pliensbac	194.0	299.0	EVAP,shaly	5.0	45.0	24.0	60
30	Sinemurian	203.0	23.0	LIME, shaly	14.0	10.0	24.0	60
29	Hetangian	208.0	476.0	SALT	5.0	5.0	24.0	65
28	Rhaetian	210.0	77.0	SHALE&SALT	5.0	5.0	28.0	65
27	Keup_TAGS	215.0	46.0	SHALE,sandy	10.0	30.0	28.0	70
26	Keup_Calc	224.0	143.0	SILT,calc	9.0	15.0	28.0	70
25	Keup_TAGI	231.0	42.0	SAND,shaly	12.0	30.0	29.0	70
24	Hercynian	260.0	-150.0	SAND,shaly	12.0	0.0	28.0	58
23	Hercynian	268.0	-9999.0	SAND&SHALE	11.0	0.0	24.0	58
22	Hercynian	275.0	-9999.0	SILTSTONE	10.0	0.0	23.0	58
21	Hercynian	278.0	-9999.0	SHALE, calc	9.0	0.0	21.0	58
20	Hercynian	283.0	-9999.0	LIME, shaly	10.0	0.0	21.0	58
19	Hercynian	286.0	-9999.0	SHALE, evap	8.0	0.0	21.0	58
18	Stephan	303.0	120.0	SHALE, evap	8.0	5.0	22.0	60
17	Westphal	315.0	300.0	LIME, shaly	10.0	15.0	24.0	60
16	Namurian	333.0	250.0	SHALE, calc	9.0	10.0	26.0	60
15	Visean_C	342.0	350.0	SILTSTONE	10.0	15.0	24.0	60
14	Visean_B	350.0	250.0	SAND&SHALE	11.0	15.0	23.0	60
13	Tournais	355.0	200	SAND,shaly	12.0	10.0	23.0	60
12	Strunian	363.0	106.0	SILT,sandy	11.0	30.0	23.0	60
11	Famennian	367.0	350	SHALE,silty	8.0	45.0	22.0	60
10	Fras upp	370.0	114	SHALE,calc	8.0	100.0	22.0	60
9	Fras Rad	373.0	116.0	SHALE,calc	8.0	100.0	22.0	60
8	Frasnian	377.0	-50.0	SHALE&LIME	7.0	0.0	23.0	60
7	Givetian	381.0	117.0	SHALE&LIME	7.0	45.0	23.0	62
6	Eifel_Ems	390.0	63	SHALE, silty	7.00	15.0	23.0	62
5	Sieg_Gedi	399.0	359.0	SAND&SHALE	9.0	30.0	23.0	62
4	Gedinian	409.0	320	SANDSTONE	11.0	10.0	23.0	63
3	Taconic	411.0	-25.0	SAND&SHALE	7.0	0.0	23.0	63
2	Ludlow	424.0	650	SAND&SHALE	7.0	30.0	23.0	65
1	Wenlock	435.0	550	SHALE,silty	5.0	100.0	22.0	65

Tab.3: Input data for modelling of burial and temperature history of well WT-1

Event N°	Name	Time (Ma)	Thickness (m)	Lithology	Porosity (%)	Water depth (m)	SWI temp (°C)	Heat flow (mW/m²)
49	Quaternar	2.0	0.0	SANDSTONE	42.0	0.0	21.0	55
48	Pliocene	4.0	-50.0	SAND, silty	39.0	0.0	21.0	55
47	Ol/MioPl	35.0	303.0	SAND, silty	39.0	1.0	21.0	55
46	Alpine	42.0	-50.0	LIME, dolo	39.0	0.0	24.0	55
45	Maest-Eoc	74.0	274.0	LIME, dolo	39.0	45.0	27.0	56
44	Camp-Sant	86.0	252.0	DOLO,evap	34.0	5.0	28.0	56
43	Coniacian	89.0	122.0	SALT	6.0	5.0	29.0	56
42	Turonian	90.0	111.0	LIME, marly	31.0	15.0	29.0	56
41	Cenoman	97.0	241.0	SHALE,evap	23.0	30.0	29.0	58
40	Albian	112.0	237.0	SAND,shaly	23.0	30.0	30.0	58
39	Aptian	117.0	30.00	LIME, dolo	27.0	45.0	30.0	58
38	Austrian	124.0	-100.0	SAND, silty	20.0	0.0	30.0	58
37	Barremian	132.0	620.0	SAND, silty	20.0	30.0	30.0	58
36	Neocomian	146.0	309.0	SHALE, sandy	15.0	30.0	29.0	58
35	Malm	161.0	209.0	SHALE&LIME	16.0	45.0	28.0	58
34	Dogger	187.0	259.0	SHALE;calc	13.0	30.0	25.0	60
33	Pliensbac	194.0	257.0	EVAP,shaly	5.0	45.0	24.0	60
32	Sinemurian	203.0	25.0	LIME, shaly	14.0	10.0	24.0	60
31	Hetangian	208.0	409.0	SALT	5.0	5.0	24.0	65
30	Rhaetian	210.0	61.0	SHALE&SALT	5.0	5.0	28.0	65
29	Keup_TAGS	215.0	65.0	SHALE,sandy	10.0	30.0	28.0	70
28	Keup_Calc	224.0	138.0	SILT,calc	9.0	15.0	28.0	70
27	Keup_TAGI	231.0	63.0	SAND,shaly	12.0	30.0	29.0	70
26	Hercynian	245.0	-200.0	SHALE,calc	8.0	0.0	29.0	58
25	Hercynian	258.0	-9999.0	SHALE,silty	11.0	0.0	29.0	58
24	Hercynian	265.0	-9999.0	SILT,sandy	12.0	0.0	28.0	58
23	Hercynian	270.0	-9999.0	SAND,shaly	11.0	0.0	28.0	58
22	Hercynian	275.0	-9999.0	SAND&SHALE	10.0	0.0	25.0	58
21	Hercynian	278.0	-9999.0	SILTSTONE	9.0	0.0	24.0	58
20	Hercynian	282.0	-9999.0	SHALE, calc	10.0	0.0	21.0	58
19	Hercynian	286.0	-9999.0	LIME, shaly	8.0	0.0	21.0	58
18	Stephan	303.0	120.0	SHALE, evap	8.0	5.0	22.0	60
17	Westphal	315.0	300.0	LIME, shaly	10.0	15.0	24.0	60
16	Namurian	333.0	250.0	SHALE, calc	9.0	10.0	26.0	60
15	Visean_C	342.0	350.0	SILTSTONE	10.0	15.0	24.0	60
14	Visean_B	350.0	250.0	SAND&SHALE	11.0	15.0	23.0	60
13	Tournais	355.0	200.0	SAND,shaly	12.0	10.0	23.0	60
12	Strunian	363.0	106.0	SILT,sandy	11.0	30.0	23.0	60
11	Famennian	367.0	349.0	SHALE,silty	8.0	45.0	22.0	60
10	Fras Upp	370.0	80.0	SHALE,calc	8.0	100.0	22.0	60
9	Fras Rad	373.0	116.0	SHALE,calc	8.0	100.0	21.0	60
8	Frasnian	377.0	-50.0	SHALE&LIME	7.0	0.0	23.0	60
7	Givetian	381.0	96.0	SHALE&LIME	7.0	45.0	23.0	62
6	Eifel_Ems	390.0	90.0	SHALE, silty	7.00	15.0	23.0	62
5	Sieg_Gedi	399.0	371.0	SAND&SHALE	9.0	30.0	23.0	62
4	Gedinian	409.0	310.0	SANDSTONE	11.0	10.0	23.0	63
3	Taconic	411.0	-25.0	SAND&SHALE	7.0	0.0	23.0	63
2	Ludlow F6	424.0	675.0	SAND&SHALE	7.0	30.0	23.0	65
1	Wenlock	435.0	550	SHALE,silty	5.0	100.0	22.0	65

Tab.4: Input data for modelling of burial and temperature history of well HAD-1 (Model A, B and C)

Event N°	Name	Time (Ma)	Thickness (m)	Lithology	Porosity (%)	Water depth (m)	SWI temp (°C)	Heat flow (mW/m²) Mod.A	Mod.B	Mod.C
42	Quaternar	2.0	12.0	SANDSTONE	42.0	0.0	21.0	55	55	55
41	Pliocene	4.0	-50.0	SAND,calc	42.0	0	21.0	55	55	55
40	Ol/Miopl	35.0	96.0	SAND,calc	41.0	10.0	21.0	**55**	**73**	**80**
39	Alpine	42.0	-50.0	LIME,shaly	47.0	0.0	24.0	55	55	55
38	Maest-Eoc	74.0	202.0	LIME,shaly	45.0	45.0	27.0	55	55	55
37	Camp_Sant	86.0	242.0	LIME,shaly	41.0	5.0	28.0	55	55	55
36	Coniacian	89.0	148.0	SALT	6.0	5.0	29.0	55	55	55
35	Turonian	90.0	83.0	LIME,marly	34.0	15.0	29.0	55	55	55
34	Upp_Cenom	93.0	103.0	EVAP,shaly	15.0	15.0	29.0	55	55	55
33	Low_Cenom	97.0	133.0	LIME,marly	31.0	45.0	29.0	58	58	58
32	Albian	112.0	125.0	SAND,shaly	25.0	30.0	30.0	58	58	58
31	Aptian	117.0	24.0	LIME,dolo	30.0	45.0	30.0	58	58	58
30	Austrian	124.0	-100.0	SAND,shaly	24.0	0.0	29.0	58	58	58
29	Barremian	132.0	520.0	SAND,shaly	22.0	30.0	29.0	58	58	58
28	Neocomian	146.0	241.0	SHALE&SAND	19.0	30.0	28.0	58	58	58
27	Malm	161.0	239.0	SHALE&SAND	17.0	30.0	27.0	58	58	58
26	Dogger	187.0	110.0	LIME,marly	21.0	45.0	25.0	60	60	60
25	Liassic	210.0	130.0	SHALE,evap	13.0	30.0	25.0	65	65	65
24	Keup_TAGS	215.0	84.0	EVAP,shaly	10.0	15.0	28.0	70	70	70
23	Keup-Calc	224.0	113.0	SAND,calc	17.0	15.0	28.0	70	70	70
22	Keup-TAGI	231.0	45.0	SAND,silty	16.0	10.0	28.0	70	70	70
21	Hercynian	265.0	-230.0	SHALE&LIME	15.0	0.0	21.0	58	58	58
20	Hercynian	286.0	-9999.0	SHALE,silty	12.0	0.0	21.0	58	58	58
19	Stephan	303.0	120.0	SHALE,silty	12.0	10.0	22.0	60	60	60
18	Westphal	315.0	306.0	SHALE&LIME	15.0	15.0	24.0	60	60	60
17	Namurian	333.0	246.0	SAND&LIME	17.0	10.0	26.0	60	60	60
16	Visean_C	342.0	260.0	SHALE&SAND	13.0	15.0	24.0	60	60	60
15	Visean_B	346.0	345.0	SHALE&SAND	12.0	15.0	24.0	60	60	60
14	Visean_A	350.0	296.0	SHALE,silty	9.0	15.0	24.0	60	60	60
13	Tournais	355.0	69.0	SHALE&SAND	11.0	15.0	23.0	60	60	60
12	Strunian	363.0	100.0	SAND,shaly	12.0	10.0	23.0	60	60	60
11	Famennian	367.0	165.0	SHALE,silty	8.0	45.0	23.0	60	60	60
10	Fras upp	370.0	114.0	SAND&LIME	8.0	100.0	22.0	60	60	60
9	Fras Rad	373.0	82.0	SHALE,calc	8.0	100.0	22.0	60	60	60
8	Frasnian	377.0	-50.0	SHALE,calc	8.0	0.0	23.0	60	60	60
7	Givetian	381.0	86.0	SHALE,calc	7.0	45.0	22.0	62	62	62
6	Ems_Eifel	390.0	129.0	SHALE&SAND	10.0	15.0	23.0	62	62	62
5	Sieg_Gedi	396.0	308.0	SHALE&SAND	9.0	30.0	23.0	62	62	62
4	Gedinian	409.0	270.0	SANDSTONE	11.0	10.0	23.0	63	63	63
3	Taconic	411.0	-25.0	SAND,shaly	9.0	0.0	23.0	63	63	63
2	Ludlow	424.0	650.0	SAND,shaly	9.0	30.0	23.0	65	65	65
1	Wenlock	435.0	475.0	SHALE,silty	5.0	100.0	21.0	65	65	65

Tab.5: Input data for modelling of burial and temperature history of well SF-1 (Model A and B)

Event N°	Name	Time (Ma)	Thickness (m)	Lithology	Porosity (%)	Water depth (m)	SWI temp (°C)	Heat flow (mW/m²) Mod. A	Mod.B
49	Quaternary	2.0	30.0	SANDSTONE	42.0	0.0	17.0	58	58
48	Pliocene	4.0	-50.0	SAND, silty	39.0	0.0	17.0	56	35
47	Ol/MioPl	35.0	192.0	SAND, silty	39.0	1.0	21.0	56	35
46	Alpine	42.0	-50.0	LIME, dolo	39.0	0.0	24.0	56	35
45	Maest-Eoc	74.0	171.0	LIME, dolo	39.0	45.0	27.0	56	35
44	Camp-Sant	86.0	329.0	DOLO,evap	34.0	5.0	28.0	56	35
43	Coniacian	89.0	161.0	SALT	5.0	5.0	29.0	56	35
42	Turonian	90.0	67.0	LIME, marly	31.0	15.0	29.0	56	35
41	Upp_Cenom	93.0	98.0	SHALE&ANHYD	6.0	15.0	29.0	56	35
40	Low_Cenom	97.0	140.0	SHALE, calc	20.0	45.0	29.0	58	35
39	Albian	112.0	99.0	SAND,shaly	23.0	30.0	30.0	58	35
38	Aptian	117.0	25.0	LIME, dolo	27.0	45.0	30.0	58	36
37	Austrian	124.0	-150	SAND, silty	20.0	0.0	30.0	58	40
36	Barremian	132.0	381.0	SAND, silty	20.0	30.0	30.0	58	40
35	Neocomian	146.0	247.0	SHALE, sandy	15.0	30.0	29.0	58	45
34	Malm	161.0	242.0	SHALE&LIME	16.0	45.0	28.0	58	45
33	Bart_Bajo	173.0	132.0	SHALE, calc	14.0	15.0	27.0	58	48
32	Toarc_Aal	187.0	114.0	SHALE, calc	13.0	30.0	25.0	60	55
31	Pliensbac	194.0	230.0	EVAP,shaly	5.0	45.0	24.0	60	55
30	Sinemurian	203.0	25.0	LIME, shaly	14.0	10.0	24.0	60	55
29	Hetangian	208.0	374.0	SALT	5.0	5.0	24.0	65	60
28	Rhaetian	210.0	67.0	SHALE&SALT	5.0	5.0	28.0	65	60
27	Keup_TAGS	215.0	15.0	SHALE,sandy	15.0	10.0	28.0	70	65
26	Keup_Calc	224.0	64.0	SILT,calc	14.0	15.0	28.0	70	65
25	Keup_TAGI	231.0	96.0	SAND,shaly	12.0	30.0	29.0	70	65
24	Hercynian	252.0	-100.0	SAND,shaly	13.0	0.0	28.0	58	50
23	Hercynian	265.0	-9999.0	SAND&SHALE	13.0	0.0	25.0	58	50
22	Hercynian	270.0	-9999.0	SILTSTONE	12.0	0.0	24.0	58	50
21	Hercynian	275.0	-9999.0	SHALE, calc	11.0	0.0	23.0	58	50
20	Hercynian	280.0	-9999.0	LIME, shaly	14.0	0.0	23.0	58	50
19	Hercynian	286.0	-9999.0	SHALE, evap	8.0	0.0	21.0	58	50
18	Stephan	303.0	120.0	SHALE, evap	8.0	5.0	22.0	60	50
17	Westphal	315.0	300.0	LIME, shaly	10.0	15.0	24.0	60	50
16	Namurian	333.0	250.0	SHALE, calc	9.0	10.0	26.0	60	50
15	Visean_C	342.0	350.0	SILTSTONE	10.0	15.0	24.0	60	50
14	Visean_B	350.0	250.0	SAND&SHALE	11.0	10.0	23.0	60	50
13	Tournais	355.0	191.0	SAND,shaly	12.0	10.0	23.0	60	50
12	Strunien	363.0	134.0	SILT,sandy	11.0	30.0	23.0	60	55
11	Famennian	367.0	313.0	SHALE,silty	8.0	45.0	22.0	60	55
10	Fras upp	370.0	128.0	SHALE,calc	8.0	100.0	22.0	60	55
9	Fras Rad	373.0	142.0	SHALE,calc	8.0	100.0	22.0	60	55
8	Frasnian	377.0	-25.0	SHALE&LIME	7.0	0.0	23.0	60	55
7	Givetian	381.0	87.0	SHALE&LIME	7.0	45.0	23.0	62	58
6	Eifel_Ems	390.0	94.0	SHALE, silty	7.0	15.0	23.0	62	58
5	Sieg-Gedi	399.0	256.0	SAND&SHALE	9.0	30.0	23.0	62	58
4	Gedinian	409.0	300.0	SANDSTONE	11.0	10.0	23.0	63	60
3	Taconic	411.0	-5.0	SAND&SHALE	7.0	0.0	23.0	63	60
2	Ludlow	424.0	605.0	SAND&SHALE	7.0	30.0	23.0	65	60
1	Wenlock	435.0	500	SHALE,silty	5.0	100.0	22.0	65	60

Tab.6: Input data for modelling of burial and temperature history of well BBK-1

Event N°	Name	Time (Ma)	Thickness (m)	Lithology	Porosity (%)	Water depth (m)	SWI temp (°C)	Heat flow (mW/m²)
48	Quaternary	2.0	33.0	SANDSTONE	41.0	0.0	21.0	55
47	Pliocene	4.0	-50.0	SANDSTONE	44.0	0.0	21.0	35
46	Ol/Miopl	35.0	220.0	SANDSTONE	36.0	1.0	21.0	35
45	Alpine	42.0	-50.0	DOLOMITE	44.0	0.0	24.0	35
44	Maest-Eoc	74.0	162.0	DOLOMITE	39.0	45.0	27.0	35
43	Camp-Sant	86.0	279.0	DOLO,evap	31.0	5.0	28.0	35
42	Coniacian	89.0	152.0	SALT	6.0	5.0	28.0	35
41	Turonian	90.0	74.0	LIME,dolo	30.0	15.0	29.0	35
40	Cenoman.	97.0	246.0	SHALE&DOLO	19.0	45.0	29.0	37
39	Albian	112.0	95.0	SAND,silty	26.0	30.0	30.0	40
38	Aptian	117.0	26.0	LIME,dolo	30.0	45.0	30.0	40
37	Austrian	124.0	-300.0	SHALE&SAND	23.0	0.0	29.0	45
36	Barremian	132.0	638.0	SHALE&SAND	23.0	30.0	29.0	45
35	Neocomian	146.0	277.0	SHALE,sandy	15.0	30.0	28.0	48
34	Malm	161.0	268.0	SHALE&LIME	15.0	45.0	27.0	55
33	Bart_Bajo	173.0	151.0	SHALE,calc	12.0	10.0	25.0	55
32	Toar_Aalen	187.0	290.0	EVAP,shaly	5.0	15.0	25.0	55
31	Pliensbac	194.0	265.0	EVAPORITE	5.0	5.0	25.0	60
30	Sinum HB	203.0	26.0	LIMESTONE	11.0	10.0	25.0	60
29	Hetangian	208.0	437.0	SALT	5.0	5.0	25.0	65
28	Rhaetian	210.0	10.0	SALT	5.0	5.0	25.0	65
27	Triassic	231.0	219.0	SAND&SHALE	12.0	10.0	28.0	65
26	Hercynian	235.0	-50.0	SHALE,calc	8.0	0.0	26.0	50
25	Hercynian	238.0	-9999.0	SHALE,silty	8.0	0.0	26.0	50
24	Hercynian	250.0	-9999.0	SILT,sandy	8.0	0.0	24.0	50
23	Hercynian	254.0	-9999.0	SAND,shaly	11.0	0.0	24.0	50
22	Hercynian	258.0	-9999.0	SAND&SHALE	12.0	0.0	24.0	50
21	Hercynian	272.0	-9999.0	SILTSTONE	11.0	0.0	21.0	50
20	Hercynian	278.0	-9999.0	SHALE, calc	9.0	0.0	21.0	50
19	Hercynian	283.0	-9999.0	LIME, shaly	10.0	0.0	21.0	50
18	Hercynian	286.0	-9999.0	SHALE, evap	8.0	0.0	21.0	50
17	Stephan	303.0	100.0	SHALE, evap	8.0	5.0	22.0	50
16	Westphal	315.0	250.0	LIME, shaly	10.0	15.0	24.0	50
15	Namurian	333.0	250.0	SHALE, calc	9.0	10.0	26.0	50
14	Visean	350.0	400.0	SHALE,sandy	11.0	15.0	24.0	50
13	Tournaisn	355.0	150.0	SAND,shaly	12.0	10.0	23.0	50
12	Strunien	363.0	80.0	SILT,sandy	11.0	30.0	23.0	50
11	Famennian	367.0	250.0	SHALE,silty	8.0	45.0	22.0	50
10	Fras upp	370.0	90.0	SHALE,calc	8.0	100.0	22.0	50
9	Fras Rad	373.0	125.0	SHALE,calc	8.0	100.0	22.0	55
8	Frasnian	377.0	-50.0	SHALE&LIME	7.0	0.0	23.0	55
7	Givetian	381.0	82.0	SHALE&LIME	7.0	45.0	23.0	55
6	Eifel-Ems	390.0	86.0	SHALE, silty	7.0	15.0	23.0	55
5	Sieg-Gedin	399.0	263.0	SAND&SHALE	9.0	30.0	23.0	55
4	Gedinian	409.0	276.0	SANDSTONE	11.0	10.0	23.0	58
3	Taconic	411.0	-25.0	SAND&SHALE	7.0	0.0	23.0	60
2	Ludlow	424.0	700.0	SAND&SHALE	7.0	30.0	23.0	60
1	Wenlock	435.0	550.0	SHALE,silty	5.0	100.0	22.0	60

Tab.7: Input data for modelling of burial and temperature history of well BRD-4 (Model A and B)

Event N°	Name	Time (Ma)	Thickness (m) Mod. A	Thickness (m) Mod. B	Lithology	Porosity (%)	Water depth (m)	SWI temp (°C)	Heat flow (mW/m²) Mod. A	Heat flow (mW/m²) Mod. B
49	Quaternar	2.0	0.0	0.0	SANDSTONE	46.0	0.0	21.0	63	63
48	Pliocene	4.0	-100.0	-100.0	SAND,silty	42.0	0.0	21.0	63	66
47	Mio-Plio	35.0	292.0	292.0	SAND,silty	38.0	1.0	21.0	63	63
46	Alpine	42.0	-150.0	-150.0	LIME,dolo	38.0	0.0	24.0	63	63
45	Maest_Eoc	74.0	345.0	345.0	LIME,dolo	38.0	45.0	27.0	63	63
44	Camp_Sant	86.0	208.0	208.0	DOLO,evap	35.0	5.0	28.0	63	63
43	Coniacian	89.0	99.0	99.0	SALT	6.0	5.0	29.0	63	63
42	Turonian	90.0	100.0	100.0	LIME,marly	21.0	15.0	29.0	63	63
41	Upp_Cenom	93.0	74.0	74.0	SHALE&ANHYD	16.0	15.0	29.0	63	64
40	Low_Cenom	97.0	131.0	131.0	SHALE,calc	20.0	45.0	30.0	64	64
39	Albian	112.0	125.0	125.0	SAND,shaly	26.0	30.0	30.0	64	64
38	Aptian	117.0	25.0	25.0	LIME, dolo	29.0	45.0	30.0	64	64
37	Austrian	124.0	-350.0	-350.0	SAND, silty	18.0	0.0	29.0	64	64
36	Barremian	132.0	705.0	705.0	SAND, silty	23.0	15.0	30.0	64	64
35	Neocomian	146.0	306.0	306.0	SHALE, sandy	14.0	30.0	29.0	64	64
34	Malm	161.0	248.0	248.0	SHALE&LIME	11.0	45.0	28.0	64	65
33	Bart-Bajo	173.0	227.0	227.0	SHALE, calc	11.0	10.0	27.0	65	65
32	Toarc-Aal	187.0	57.0	57.0	SHALE, calc	12.0	15.0	25.0	65	65
31	Pliensbac	194.0	310.0	310.0	EVAP,shaly	5.0	45.0	24.0	65	65
30	Sinemurian	203.0	25.0	25.0	LIME, shaly	8.0	5.0	24.0	65	65
29	Hetangian	208.0	596.0	596.0	SALT	5.0	5.0	24.0	70	70
28	Rhaetian	210.0	77.0	77.0	SHALE&SALT	11.0	5.0	28.0	70	70
27	Keup_TAGS	215.0	74.0	74.0	SHALE,sandy	22.0	10.0	28.0	75	75
26	Keup_Int	224.0	237.0	237.0	SILT,calc	12.0	15.0	28.0	75	75
25	Keup_TAGI	231.0	33.0	33.0	SAND,shaly	12.0	5.0	29.0	75	75
24	Hercynian	240.0	-75	-35	SAND&SHALE	9.0	0.0	29.0	58	58
23	Hercynian	250.0	-9999.0	-9999.0	SANDSTONE	14.0	0.0	29.0	58	58
22	Hercynian	258.0	-9999.0	-9999.0	SAND&SHALE	11.0	0.0	29.0	58	58
21	Hercynian	264.0	-9999.0	-9999.0	SHALE,silty	9.0	0.0	29.0	58	58
20	Hercynian	268.0	-9999.0	-9999.0	SHALE,sandy	8.0	0.0	29.0	58	58
19	Hercynian	272.0	-9999.0	-9999.0	SAND,shaly	12.0	0.0	29.0	58	58
18	Hercynian	276.0	-9999.0	-9999.0	SAND&SHALE	11.0	0.0	28.0	58	58
17	Hercynian	279.0	-9999.0	-9999.0	SILTSTONE	10.0	0.0	28.0	58	58
16	Hercynian	282.0	-9999.0	-9999.0	SHALE, calc	9.0	0.0	28.0	58	58
15	Hercynian	284.0	-9999.0	-9999.0	LIME, shaly	10.0	0.0	25.0	58	58
14	Hercynian	286.0	-9999.0	-9999.0	SHALE, evap	8.0	0.0	21.0	58	58
13	Stephan	303.0	120.0	70.0	SHALE, evap	8.0	10.0	22.0	60	60
12	Westphal	315.0	300.0	180.0	LIME, shaly	10.0	15.0	26.0	60	60
11	Namurian	333.0	250.0	150.0	SHALE, calc	9.0	15.0	26.0	60	60
10	Visean_C	342.0	350.0	220.0	SILTSTONE	10.0	15.0	26.0	60	60
9	Visean_B	350.0	250.0	150.0	SAND&SHALE	11.0	15.0	26.0	60	60
8	Tournais	355.0	200.0	100.0	SAND,shaly	12.0	15.0	26.0	60	60
7	Fras_Stru	377.0	655.0	420.0	SHALE,sandy	10.0	100.0	22.0	60	60
6	Eifel_Ems	390.0	136.0	50.0	SHALE,silty	9.0	45.0	23.0	62	62
5	Sieg_Gedin	399.0	370.0	250.0	SAND&SHALE	11.0	30.0	23.0	62	62
4	Gedinian	409.0	320.0	210.0	SANDSTONE	13.0	10.0	23.0	63	63
3	Taconic	411.0	-25.0	-25	SHALE&SAND	9.0	0.0	23.0	63	63
2	Ludlow	424.0	625.00	550.0	SHALE&SAND	5.0	30.0	23.0	65	65
1	Wenlock	435.0	510.0	510.0	SHALE, silty	5.0	110.0	21.0	65	65

Tab.8: Input data for modelling of burial and temperature history of well TZM-1

Event N°	Name	Time (Ma)	Thickness (m)	Lithology	Porosity (%)	Water depth (m)	SWI temp (°C)	Heat flow (mW/m²)
42	Quaternar	2.0	8.0	SANDSTONE	42.0	0.0	21.0	56
41	Pliocene	4.0	-9999.0	SAND,silty	42.0	0.0	21.0	56
40	Ol/Miopl	35.0	150.0	SAND,silty	40.0	1.0	21.0	56
39	Alpine	42.0	-200.0	LIME,marly	43.0	0.0	24.0	56
38	Maest_Eoc	74.0	501.0	LIME,marly	35.0	25.0	27.0	56
37	Coniacian	89.0	0.0	SALT	6.0	0.0	28.0	56
36	Turonian	90.0	30.0	LIMESTONE	29.0	25.0	29.0	56
35	Cenoman.	97.0	233.0	SHALE,evap	19.0	5.0	29.0	56
34	Albian	112.0	42.0	SAND,shaly	23.0	30.0	30.0	56
33	Aptian	117.0	24.0	LIME,marly	32.0	15.0	30.0	56
32	Austrian	124.0	-200.0	SAND,shaly	26.0	0.0	30.0	56
31	Barremian	132.0	350.0	SAND,shaly	26.0	10.0	29.0	56
30	Neocomian	146.0	152.0	SHALE,silty	15.0	25.0	29.0	56
29	Malm	161.0	120.0	SHALE,calc	16.0	45.0	28.0	56
28	Dogger	187.0	338.0	SHALE&SANI	17.0	45.0	26.0	60
27	Liassic	210.0	117.0	SHALE,evap	12.0	5.0	24.0	65
26	Trias-Keup	231.0	104.0	SAND,shaly	16.0	5.0	28.0	70
25	Hercynian	251.0	-220.0	LIME,shaly	16.0	0.0	28.0	56
24	Hercynian	286.0	-9999.0	SHLAE,evap	15.0	0.0	21.0	56
23	Stephan	303.0	150.0	SHLAE,evap	15.0	5.0	22.0	60
22	Westphal	315.0	310.0	LIME,shaly	11.0	15.0	24.0	60
21	Namurian	333.0	239.0	SHALE,calc	14.0	25.0	26.0	60
20	Visean	350.0	518.0	SHALE&SANI	11.0	45.0	24.0	60
19	Tournais	355.0	263.0	SHALE,silty	9.0	15.0	23.0	60
18	Strunian	363.0	61.0	SAND,shaly	11.0	15.0	23.0	60
17	Famennian	367.0	76.0	SHALE,silty	8.0	45.0	23.0	60
16	Fras upp	370.0	57.0	SHALE,calc	8.0	65.0	22.0	60
15	Fras Rad	373.0	32.0	SHALE,calc	9.0	100.0	22.0	60
14	Frasnian	376.0	-59.0	SANDSTONE	16.0	0.0	23.0	60
13	Frasnian	381.0	-9999.0	SHALE&SANI	13.0	0.0	23.0	60
12	Eifel-Giv	386.0	0.0	SHALE,calc	13.0	45.0	23.0	62
11	Emsian	390.0	0.0	SHALE,silty	13.0	15.0	23.0	62
10	Sieg_Gedi	399.0	100.0	SHALE&SANI	9.0	15.0	23.0	62
9	Gedinian	409.0	80.0	SANDSTONE	11.0	10.0	23.0	62
8	Taconic	411.0	-50.0	SHALE&SANI	13.0	0.0	23.0	63
7	Ludlow	424.0	438.0	SHALE&SANI	10.0	15.0	23.0	65
6	Wenlock	435.0	312.0	SHALE,silty	6.0	100.0	22.0	65

Tab.9: Input data for modelling of burial and temperature history of well KA-1bis

Event N°	Name	Time (Ma)	Thickness (m)	Lithology	Porosity (%)	Water depth (m)	SWI temp (°C)	Heat flow (mW/m²)
43	Pliocene	4.0	-100.0	SANDSTONE	42.0	0.0	21.0	55
42	Ol/MioPl	35.0	100.0	SANDSTONE	41.0	0.0	21.0	55
41	Alpine	42.0	-50.0	LIME,dolo	42.0	0.0	24.0	55
40	Maest_Eoc	74.0	213.0	LIME,dolo	39.0	45.0	27.0	55
39	Camp_Coni	89.0	114.0	LIME&EVAP	16.0	5.0	28.0	55
38	Turonian	90.0	79.0	LIME,marly	33.0	15.0	29.0	56
37	Cenoman.	97.0	167.0	LIME,shaly	38.0	30.0	29.0	56
36	Albian	112.0	87.0	SAND,shaly	26.0	30.0	30.0	58
35	Aptian	117.0	30.0	LIME,dolo	29.0	45.0	30.0	58
34	Austrian	124.0	-100.0	SAND,silty	27.0	0.0	29.0	58
33	Barremian	132.0	314.0	SAND,silty	22.0	30.0	29.0	58
32	Neocomian	146.0	224.0	SHALE&SAND	20.0	30.0	29.0	58
31	Malm	161.0	250.0	SHALE&LIME	18.0	45.0	27.0	58
30	Bart-Bajo	173.0	200.0	SHALE,sandy	15.0	15.0	26.0	59
29	Toarc_Aal	187.0	241.0	LIME&EVAP	7.0	30.0	24.0	59
28	Pliensbac	194.0	52.0	EVAP,shaly	10.0	45.0	24.0	59
27	Sinemurian	203.0	21.0	LIME,dolo	16.0	10.0	24.0	59
26	Hetangian	208.0	296.0	SALT	5.0	5.0	24.0	65
25	Rhaetian	210.0	142.0	EVAP,shaly	10.0	5.0	25.0	65
24	Keup_TAGS	215.0	78.0	SHALE,sandy	16.0	30.0	28.0	70
23	Keup_Calc	224.0	217.0	SHALE&SAND	22.0	15.0	28.0	70
22	Keup_TAGI	231.0	77.0	SAND,shaly	21.0	30.0	29.0	70
21	Hercynian	246.0	-150.0	SHALE&SAND	13.0	0.0	29.0	58
20	Hercynian	258.0	-9999.0	SANDSTONE	14.0	0.0	26.0	58
19	Hercynian	264.0	-9999.0	SHALE&SAND	17.0	0.0	25.0	58
18	Hercynian	267.0	-9999.0	SHALE,sandy	14.0	0.0	24.0	58
17	Hercynian	268.0	-9999.0	SHALE,calc	13.0	0.0	24.0	58
16	Hercynian	271.0	-9999.0	SHALE,calc	12.0	0.0	24.0	58
15	Hercynian	274.0	-9999.0	SHALE,sandy	13.0	0.0	23.0	58
14	Hercynian	277.0	-9999.0	SHALE&SAND	14.0	0.0	21.0	58
13	Hercynian	280.0	-9999.0	LIME,shaly	16.0	0.0	21.0	58
12	Hercynian	286.0	-9999.0	SHALE,evap	11.0	0.0	21.0	58
11	Stephan	303.0	150.0	SHALE,evap	11.0	5.0	22.0	60
10	West_Nam	333.0	500.0	LIME,shaly	16.0	15.0	25.0	60
9	Tour_Visean	355.0	650.0	SHALE&SAND	14.0	15.0	24.0	60
8	Famen_Strun	367.0	120.0	SHALE,sandy	13.0	45.0	23.0	60
7	Frasnian	377.0	80.0	SHALE,calc	12.0	100.0	22.0	60
6	Givetian	381.0	30.0	SHALE,calc	12.0	45.0	22.0	60
5	Eifel_Ems	390.0	30.0	SHALE,sandy	13.0	15.0	23.0	62
4	Sieg_Gedi	399.0	100.0	SHALE&SAND	14.0	30.0	23.0	62
3	Gedinian	409.0	100.0	SANDSTONE	17.0	10.0	23.0	63
2	Ludlow	424.0	350.0	SHALE&SAND	14.0	30.0	23.0	65
1	Wenlock	435.0	322.0	SHALE,silty	6.0	100.0	22.0	65

Tab. 10: Sediment thicknesses (m) used along the simulated cross section (original model). GP29,GP33,GP42, GP45 and GP94 are BRD-4, BKW-1,WT-1, BK-2 and SF-1 wells, respectively. -9999 means total erosion

Evt. N°	Evt. Name	GP1	GP2	GP3	GP4	GP5	GP6	GP7	GP8	GP9	GP10	GP11	GP12	GP13	GP14	GP15	GP16	GP17	GP18	GP19	GP20	GP21	GP22	GP23
60	Tertiary	184	184	184	184	184	184	184	184	184	184	184	184	184	180	170	168	166	167	176	211	191	191	187
59	Alpine	-169	-169	-168	-168	-168	-168	-168	-168	-167	-166	-165	-164	-164	-164	-164	-164	-164	-164	-163	-97	-58	-145	-145
58	Maest-Eoc.	203	369	266	241	234	228	210	191	190	376	416	385	380	371	367	379	392	407	421	441	442	440	432
57	Santonian	144	144	144	144	144	144	144	144	144	144	185	185	185	185	185	185	185	185	185	185	185	212	211
56	Coniacian	186	166	129	137	131	131	120	116	116	116	116	116	116	116	116	123	122	119	119	97	97	97	97
55	Turonian	73	73	73	73	73	73	73	73	73	97	97	97	97	97	97	97	97	97	97	97	97	120	120
54	Cenoman.	191	195	149	144	147	151	148	137	166	185	177	191	174	174	174	174	174	174	174	174	174	222	227
53	Albian	136	136	168	153	147	145	139	125	125	140	140	140	140	140	140	140	140	140	140	122	104	122	128
52	Aptian	30	30	30	30	30	30	30	30	30	30	30	30	30	30	30	30	30	30	30	30	30	30	30
51	Austrian	0	0	0	0	0	0	-115	-9999	0	0	0	0	0	0	0	0	0	0	0	0	0	0	0
50	Austrian	0	0	0	0	0	-9999	-9999	-9999	0	0	0	0	0	0	0	0	0	0	0	0	0	0	0
49	Austrian	-467	-425	-435	-551	-699	-9999	-9999	-9999	-9999	-441	-365	-436	-448	-488	-565	-565	-480	-435	-385	-150	-170	-185	-190
48	Barremian	706	721	717	706	706	707	725	770	905	690	706	670	670	670	670	670	670	710	725	725	725	770	780
47	Neocomm.	444	403	372	374	419	380	345	318	296	296	296	296	296	260	296	296	247	286	290	308	302	277	284
46	Malm	225	247	237	252	5	280	220	184	277	237	245	266	264	229	229	229	229	276	270	310	320	309	300
45	Dogger	290	264	278	252	156	249	182	123	292	242	270	309	309	309	309	309	309	309	309	309	309	309	309
44	Pliensbach.	284	277	210	208	160	160	160	160	234	200	200	200	180	121	121	121	121	165	170	175	220	240	250
43	Sinemurian	25	25	25	25	25	25	25	25	25	25	25	25	25	25	25	25	25	25	25	25	25	25	25
42	Rhaetian	894	894	894	444	934	963	1000	1000	880	773	746	735	737	664	664	664	664	620	598	603	641	665	663
41	Tr. Keuper	399	399	399	399	399	399	399	399	475	457	374	329	306	317	317	317	317	474	448	391	384	384	392
40	Hercynian	-148	-136	-75	-108	-112	-108	-6	-78	-17	0	0	0	0	0	0	0	0	0	0	0	0	0	0
39	Hercynian	-9999	-9999	-9999	-9999	-9999	-9999	-9999	-9999	-9999	-9999	0	0	0	0	0	0	0	0	0	0	0	0	0
38	Hercynian	-9999	-9999	-9999	-9999	-9999	-9999	-9999	-9999	-9999	-9999	-324	-300	-284	-325	-325	-325	-325	-103	0	0	0	0	0
37	Hercynian	-9999	-9999	-9999	-9999	-9999	-9999	-9999	-9999	-9999	-9999	-9999	-9999	-9999	-9999	-9999	-9999	-9999	-9999	-395	-322	-259	-257	-257
36	Hercynian	-9999	-9999	-9999	-9999	-9999	-9999	-9999	-9999	-9999	-9999	-9999	-9999	-9999	-9999	-9999	-9999	-9999	-9999	-9999	-9999	-9999	-9999	-9999
35	Hercynian	-9999	-9999	-9999	-9999	-9999	-9999	-9999	-9999	-9999	-9999	-9999	-9999	-9999	-9999	-9999	-9999	-9999	-9999	-9999	-9999	-9999	-9999	-9999
34	Hercynian	-9999	-9999	-9999	-9999	-9999	-9999	-9999	-9999	-9999	-9999	-9999	-9999	-9999	-9999	-9999	-9999	-9999	-9999	-9999	-9999	-9999	-9999	-9999
33	Hercynian	-9999	-9999	-9999	-9999	-9999	-9999	-9999	-9999	-9999	-9999	-9999	-9999	-9999	-9999	-9999	-9999	-9999	-9999	-9999	-9999	-9999	-9999	-9999
32	Hercynian	-9999	-9999	-9999	-9999	-9999	-9999	-9999	-9999	-9999	-9999	-9999	-9999	-9999	-9999	-9999	-9999	-9999	-9999	-9999	-9999	-9999	-9999	-9999

31	Hercynian	-9999	-9999	-9999	-9999	-9999	-9999	-9999	-9999	-9999	-9999	-9999	-9999	-9999	-9999	-9999	-9999	-9999	-9999	-9999	-9999	-9999	-9999	-9999
30	Hercynian	-9999	-9999	-9999	-9999	-9999	-9999	-9999	-9999	-9999	-9999	-9999	-9999	-9999	-9999	-9999	-9999	-9999	-9999	-9999	-9999	-9999	-9999	-9999
29	Hercynian	-9999	-9999	-9999	-9999	-9999	-9999	-9999	-9999	-9999	-9999	-9999	-9999	-9999	-9999	-9999	-9999	-9999	-9999	-9999	-9999	-9999	-9999	-9999
28	Hercynian	-9999	-9999	-9999	-9999	-9999	-9999	-9999	-9999	-9999	-9999	-9999	-9999	-9999	-9999	-9999	-9999	-9999	-9999	-9999	-9999	-9999	-9999	-9999
27	Hercynian	-9999	-9999	-9999	-9999	-9999	-9999	-9999	-9999	-9999	-9999	-9999	-9999	-9999	-9999	-9999	-9999	-9999	-9999	-9999	-9999	-9999	-9999	-9999
26	Hercynian	-9999	-9999	-9999	-9999	-9999	-9999	-9999	-9999	-9999	-9999	-9999	-9999	-9999	-9999	-9999	-9999	-9999	-9999	-9999	-9999	-9999	-9999	-9999
25	Hercynian	-9999	-9999	-9999	-9999	-9999	-9999	-9999	-9999	-9999	-9999	-9999	-9999	-9999	-9999	-9999	-9999	-9999	-9999	-9999	-9999	-9999	-9999	-9999
24	Hercynian	-9999	-9999	-9999	-9999	-9999	-9999	-9999	-9999	-9999	-9999	-9999	-9999	-9999	-9999	-9999	-9999	-9999	-9999	-9999	-9999	-9999	-9999	-9999
23	Hercynian	-9999	-9999	-9999	-9999	-9999	-9999	-9999	-9999	-9999	-9999	-9999	-9999	-9999	-9999	-9999	-9999	-9999	-9999	-9999	-9999	-9999	-9999	-9999
22	Stephan.	120	120	120	120	120	120	120	120	120	120	120	120	120	120	120	120	120	120	120	120	120	120	120
21	Westphal.	300	300	300	300	300	300	300	300	300	300	300	300	300	300	300	300	300	300	300	300	300	300	300
20	Namurian	250	250	250	250	250	250	250	250	250	250	250	250	250	250	250	250	250	250	250	250	250	250	250
19	Visean C	350	350	350	350	350	350	350	350	350	350	350	350	350	350	350	350	350	350	350	350	350	350	350
18	Visean B	250	250	250	250	250	250	250	250	250	250	250	250	250	250	250	250	250	250	250	250	250	250	250
17	Tournais.	200	200	200	200	200	200	200	200	200	200	200	200	200	200	200	200	200	200	200	200	200	200	200
16	Strunian	106	106	106	106	106	106	106	106	106	106	106	106	106	106	106	106	106	106	106	106	106	106	106
15	Famennian	349	349	349	349	349	349	349	349	349	349	349	349	349	349	349	349	349	349	349	349	349	349	349
14	Frasnian	200	200	200	200	200	200	200	200	200	200	200	200	200	200	200	200	200	200	200	200	200	200	200
13	Emsian	136	136	136	136	136	136	136	136	136	136	136	136	136	136	136	136	136	136	136	136	136	136	136
12	Ged-Sieg.	320	320	320	320	320	320	320	320	320	320	320	320	320	320	320	320	320	320	320	320	320	320	320
11	ntra.G.Sieg	50	50	50	50	50	50	50	50	50	50	50	50	50	50	50	50	50	50	50	50	50	50	50
10	Gedinnian	265	265	265	265	265	265	265	265	265	265	265	265	265	265	265	265	270	270	270	270	270	270	270
9	Prodolian	50	50	50	50	50	50	50	50	50	50	50	50	50	50	50	50	50	50	50	50	50	50	50
8	Ludlow	600	600	600	600	600	600	600	600	600	600	600	600	600	600	600	600	600	600	600	600	600	600	600
7	Wenlock	460	460	460	460	460	460	460	460	460	460	460	460	460	460	460	460	460	473	450	420	420		
6	Sil.R.Z	50	50	50	50	50	50	50	50	50	50	50	50	50	50	50	50	50	50	50	50	50		
5	Llanvirn	225	225	220	206	206	206	206	206	206	206	206	206	206	206	206	206	265	236	293	293	293	293	
4	Arenigian	300	300	300	293	293	293	293	293	252	250	250	250	270	252	252	252	252	250	250	250	250	250	
3	Tremadoc	260	260	260	250	250	250	250	285	303	280	300	320	320	313	313	313	313	300	300	300	300	300	270
2	Cambrian	500	500	500	500	500	500	500	500	503	500	500	500	326	500	500	500	500	500	500	500	500	500	230
1	Basement	3364	3223	3377	4135	4164	4195	4327	4335	3497	3235	3044	3098	3297	3369	3479	3461	3343	3160	2617	2131	1786	1722	1971

GP24	GP25	GP26	GP27	GP28	GP29	GP30	GP31	GP32	GP33	GP34	GP35	GP36	GP37	GP38	GP39	GP40	GP41	GP42	GP43	GP44	GP45	GP46	GP47	GP48
183	186	185	184	192	192	197	192	250	258	288	267	247	234	224	228	230	232	253	232	218	210	210	210	210
-144	-144	-144	-144	-150	-150	-143	-143	-141	-140	-139	-137	-136	-50	-50	-50	-50	-50	-50	-50	-50	-50	-50	-50	-50
416	396	387	373	345	345	343	352	327	270	271	316	327	293	293	293	285	279	274	218	217	216	217	180	261
212	213	214	216	208	208	208	208	293	348	348	348	348	262	239	240	239	252	252	236	236	236	236	236	245
97	97	97	97	97	97	96	97	155	155	155	155	155	173	156	140	135	127	122	169	180	180	180	180	170
120	100	100	100	100	100	102	100	84	78	78	78	78	78	102	113	115	114	111	70	58	58	58	58	58
226	223	221	215	205	205	205	205	227	242	242	242	242	242	242	231	236	241	241	269	223	223	223	211	193
137	141	143	125	125	125	102	125	219	268	268	268	268	268	238	230	233	237	237	225	219	219	219	219	213
30	30	30	25	25	25	46	25	30	30	30	30	30	30	30	30	30	30	30	30	30	30	30	30	30
0	0	0	0	0	0	0	0	0	0	0	0	0	0	0	0	0	0	0	0	0	0	0	0	0
0	0	0	0	0	0	0	0	0	0	0	0	0	0	0	0	0	0	0	0	0	0	0	0	0
-192	-350	-350	-350	-350	-350	-372	-350	-124	-124	-135	-150	-150	-150	-150	-150	-150	-150	-100	-150	-150	-150	-150	-150	-150
790	705	705	705	705	705	724	705	705	705	705	697	697	645	652	661	664	667	620	653	658	653	635	533	490
299	538	306	306	306	306	302	306	310	316	323	302	306	307	317	310	309	309	309	309	309	313	313	316	335
279	292	498	272	248	248	249	248	274	249	249	229	232	229	223	217	214	209	209	209	218	218	218	216	222
309	309	309	309	309	309	282	309	260	238	240	250	246	256	260	297	298	295	259	259	243	243	243	227	225
260	270	280	310	310	310	311	310	320	320	320	350	350	320	289	280	280	257	257	278	299	299	299	265	225
25	25	25	25	25	25	21	25	25	25	25	25	25	25	25	25	25	25	25	25	25	25	25	25	25
656	661	663	621	673	673	677	673	659	637	634	564	564	549	496	472	476	409	470	514	553	553	553	575	622
408	399	90	362	344	344	346	344	309	232	227	273	261	272	282	279	275	296	266	216	231	231	231	236	261
0	0	0	0	0	0	0	0	0	0	0	0	0	0	0	0	0	0	0	0	0	0	0	0	0
0	0	0	0	0	0	0	0	0	0	0	0	0	0	0	0	0	0	0	0	0	0	0	0	0
0	0	0	0	0	0	0	0	0	0	0	0	0	0	0	0	0	0	0	0	0	0	0	0	0
-229	-218	-180	-181	-150	-75	0	0	0	0	0	0	0	0	0	0	0	0	0	0	0	0	0	0	0
-9999	-9999	-9999	-9999	-9999	-9999	-9999	0	0	0	0	0	0	0	0	0	0	0	0	0	0	0	0	0	0
-9999	-9999	-9999	-9999	-9999	-9999	-9999	-9999	-169	0	0	0	0	0	0	0	0	0	0	0	0	0	0	0	0
-9999	-9999	-9999	-9999	-9999	-9999	-9999	-9999	-9999	-9999	0	0	0	0	0	0	0	0	0	0	0	0	0	0	0
-9999	-9999	-9999	-9999	-9999	-9999	-9999	-9999	-9999	-9999	-9999	0	0	0	0	0	0	0	0	0	0	0	0	0	0
-9999	-9999	-9999	-9999	-9999	-9999	-9999	-9999	-9999	-9999	-9999	-9999	0	0	0	0	0	0	0	0	0	0	0	0	0

-9999	-9999	-9999	-9999	-9999	-9999	-9999	-9999	-9999	-9999	-9999	-9999	-9999	0	0	0	0	0	0	0	0	0	0	0
-9999	-9999	-9999	-9999	-9999	-9999	-9999	-9999	-9999	-9999	-9999	-9999	-9999	-9999	-318	-207	-190	-224	-200	-200	0	0	0	0
-9999	-9999	-9999	-9999	-9999	-9999	-9999	-9999	-9999	-9999	-9999	-9999	-9999	-9999	-9999	-9999	-9999	-9999	-9999	-9999	0	0	0	-70	0
-9999	-9999	-9999	-9999	-9999	-9999	-9999	-9999	-9999	-9999	-9999	-9999	-9999	-9999	-9999	-9999	-9999	-9999	-9999	-9999	-9999	-150	-150	-9999	-9999
-9999	-9999	-9999	-9999	-9999	-9999	-9999	-9999	-9999	-9999	-9999	-9999	-9999	-9999	-9999	-9999	-9999	-9999	-9999	-9999	-9999	-9999	-9999	-9999	-9999
-9999	-9999	-9999	-9999	-9999	-9999	-9999	-9999	-9999	-9999	-9999	-9999	-9999	-9999	-9999	-9999	-9999	-9999	-9999	-9999	-9999	-9999	-9999	-9999	-9999
-9999	-9999	-9999	-9999	-9999	-9999	-9999	-9999	-9999	-9999	-9999	-9999	-9999	-9999	-9999	-9999	-9999	-9999	-9999	-9999	-9999	-9999	-9999	-9999	-9999
-9999	-9999	-9999	-9999	-9999	-9999	-9999	-9999	-9999	-9999	-9999	-9999	-9999	-9999	-9999	-9999	-9999	-9999	-9999	-9999	-9999	-9999	-9999	-9999	-9999
-9999	-9999	-9999	-9999	-9999	-9999	-9999	-9999	-9999	-9999	-9999	-9999	-9999	-9999	-9999	-9999	-9999	-9999	-9999	-9999	-9999	-9999	-9999	-9999	-9999
120	120	120	120	120	120	120	120	120	120	120	120	120	120	120	120	120	120	120	120	120	120	120	120	120
300	300	300	300	300	300	300	300	300	300	300	300	300	300	300	300	300	300	300	300	300	300	300	300	300
250	250	250	250	250	250	250	250	250	250	250	250	250	250	250	250	250	250	250	250	250	250	250	250	250
350	350	350	350	350	350	350	350	350	350	350	350	350	350	350	350	350	350	350	350	350	350	350	350	350
250	250	250	250	250	250	250	250	250	250	250	250	250	250	250	250	250	250	250	250	250	250	250	250	250
200	200	200	200	200	200	200	200	200	200	200	200	200	200	200	200	200	200	200	200	200	200	200	200	200
106	106	106	106	106	106	106	106	106	106	106	106	106	106	106	106	106	106	106	106	106	106	106	106	106
349	349	349	349	349	349	349	349	349	349	349	349	349	349	360	360	349	349	349	330	330	330	350	350	379
200	200	200	200	200	200	200	200	200	200	200	200	200	200	200	200	200	196	196	200	206	206	230	230	250
136	136	136	136	136	136	136	136	136	136	136	136	136	136	136	136	136	136	136	136	162	162	180	180	225
320	320	320	320	320	320	320	320	320	320	320	321	321	321	321	321	321	321	321	309	309	309	309	285	270
50	50	50	50	50	50	50	50	50	50	50	50	50	50	50	50	50	50	50	50	50	50	50	50	50
270	270	270	270	270	270	270	270	282	282	282	270	270	270	270	260	260	260	260	270	270	270	270	260	260
50	50	50	50	50	50	50	50	50	50	50	50	50	50	50	50	50	50	50	50	50	50	50	50	50
600	600	580	580	600	600	600	600	600	600	700	650	700	650	650	650	570	650	650	650	650	650	650	650	650
420	170	393	393	510	510	510	510	550	550	550	550	550	550	550	550	550	550	550	550	550	550	550	550	550
50	50	50	50	50	50	50	50	50	50	50	50	50	50	50	50	40	50	50	50	50	50	50	50	50
293	200	293	293	293	293	293	293	293	293	293	293	293	293	293	293	260	260	260	260	260	260	260	270	270
13	280	280	280	280	280	280	280	250	250	250	250	250	250	250	250	250	250	280	250	250	250	250	260	260
200	260	273	273	273	273	273	273	273	273	273	273	273	273	273	273	250	250	250	250	250	250	250	250	250
460	460	500	500	500	500	500	500	500	500	500	500	500	500	500	500	500	500	500	500	500	500	500	500	500
1988	2004	2012	2020	2015	2000	1888	1775	1240	1122	1113	836	701	648	716	653	753	750	761	465	407	397	407	650	287

GP49	GP50	GP51	GP52	GP53	GP54	GP55	GP56	GP57	GP58	GP59	GP60	GP61	GP62	GP63	GP64	GP65	GP66	GP67	GP68	GP69	GP70	GP71	GP72	GP73
210	206	205	206	207	202	195	196	196	192	192	196	196	194	182	173	174	172	171	168	169	173	174	164	164
-50	-50	-50	-50	-50	-50	-50	-50	-50	-50	-50	-50	-50	-50	-50	-50	-50	-50	-50	-50	-50	-50	-50	-50	-50
310	293	292	289	285	273	272	270	250	275	275	272	272	270	200	332	330	330	330	330	308	275	260	260	260
242	234	223	214	225	243	244	253	256	250	240	234	230	232	266	232	233	234	233	225	236	247	247	247	240
170	166	156	159	159	158	165	164	167	165	172	176	180	187	186	183	181	179	180	181	188	180	180	180	180
58	65	64	51	49	47	46	46	48	52	49	49	51	47	54	45	46	48	48	49	47	51	47	46	46
196	207	215	230	236	237	234	234	230	230	231	234	233	234	228	248	243	237	235	230	233	235	241	245	249
213	215	220	225	225	225	235	235	240	240	235	230	235	235	212	187	187	187	187	187	187	179	175	167	167
30	30	30	30	30	30	30	30	30	30	30	30	30	30	30	30	30	30	30	30	30	30	30	30	30
0	0	0	0	0	0	0	0	0	0	0	0	0	0	0	0	0	0	0	0	0	0	0	0	0
0	0	0	0	0	0	0	0	0	0	0	0	0	0	0	0	0	0	0	0	0	0	0	0	0
-150	-150	-150	-150	-150	-150	-150	-150	-150	-150	-150	-150	-150	-150	-150	-150	-150	-150	-150	-150	-150	-150	-150	-150	-150
492	505	515	490	464	461	490	490	499	514	531	545	550	544	476	478	483	489	491	500	489	488	486	480	483
336	338	342	346	342	332	330	331	325	322	319	317	314	312	312	290	289	287	287	284	290	295	288	284	291
222	218	217	221	225	219	209	207	209	210	211	211	210	210	212	227	231	235	235	235	236	239	235	214	220
228	233	229	224	224	228	206	201	197	199	202	204	207	209	218	243	243	243	245	255	245	228	219	217	215
225	220	225	230	225	238	245	245	245	245	243	240	240	240	250	250	250	245	245	240	245	235	211	211	215
25	25	25	25	25	25	25	25	25	25	25	25	25	25	25	25	25	25	25	25	25	25	25	25	25
624	626	624	633	556	543	536	560	560	561	558	552	543	532	501	445	445	444	443	461	470	425	343	379	375
268	275	272	267	244	263	270	270	268	263	257	253	251	249	231	236	237	238	239	224	123	206	164	164	135
0	0	0	0	0	0	0	0	0	0	0	0	0	0	0	0	0	0	0	0	0	0	0	0	0
0	0	0	0	0	0	0	0	0	0	0	0	0	0	0	0	0	0	0	0	0	0	0	0	0
0	0	0	0	0	0	0	0	0	0	0	0	0	0	0	0	0	0	0	0	0	0	0	0	0
0	0	0	0	0	0	0	0	0	0	0	0	0	0	0	0	0	0	0	0	0	0	0	0	0
0	0	0	0	0	0	0	0	0	0	0	0	0	0	0	0	0	0	0	0	0	0	0	0	0
0	0	0	0	0	0	0	0	0	0	0	0	0	0	0	0	0	0	0	0	0	0	0	0	0
0	0	0	0	0	0	0	0	0	0	0	0	0	0	0	0	0	0	0	0	0	0	0	0	0
0	0	0	0	0	0	0	0	0	0	0	0	0	0	0	0	0	0	0	0	0	0	0	0	0
0	0	0	0	0	0	0	0	0	0	0	0	0	0	0	0	0	0	0	0	0	0	0	0	0
0	0	0	0	0	0	0	0	0	0	0	0	0	0	0	0	0	0	0	0	0	0	0	0	0

0	0	0	0	0	0	0	0	0	0	0	0	0	0	0	0	0	0	0	0	0	0	0	0
0	0	0	0	0	0	0	0	0	0	0	0	0	0	0	0	0	0	0	0	0	0	0	0
0	0	0	0	-54	-78	-59	-57	-26	-13	0	0	0	0	0	0	0	0	0	0	0	0	0	0
-9999	-149	-125	-145	-9999	-9999	-9999	-9999	-9999	-9999	-104	-77	-35	0	0	0	0	0	0	0	0	0	0	0
-9999	-9999	-9999	-9999	-9999	-9999	-9999	-9999	-9999	-9999	-9999	-9999	-9999	-9999	-65	0	0	0	0	0	0	0	0	0
-9999	-9999	-9999	-9999	-9999	-9999	-9999	-9999	-9999	-9999	-9999	-9999	-9999	-9999	-9999	-364	-337	-278	-263	-171	-84	-232	-200	-200
-9999	-9999	-9999	-9999	-9999	-9999	-9999	-9999	-9999	-9999	-9999	-9999	-9999	-9999	-9999	-9999	-9999	-9999	-9999	-9999	-9999	-9999	-9999	-9999
-9999	-9999	-9999	-9999	-9999	-9999	-9999	-9999	-9999	-9999	-9999	-9999	-9999	-9999	-9999	-9999	-9999	-9999	-9999	-9999	-9999	-9999	-9999	-9999
120	120	120	120	120	120	120	120	120	120	120	122	120	120	120	120	120	120	120	120	120	120	120	120
300	300	300	300	300	300	300	300	300	300	300	298	300	300	300	300	300	300	300	300	300	300	300	300
250	250	250	250	250	250	250	250	250	250	250	256	250	250	250	250	250	250	250	250	250	250	250	250
350	350	350	350	350	350	350	350	350	350	350	371	350	350	350	350	350	350	350	350	350	350	350	350
250	250	250	250	250	250	250	250	250	250	250	195	195	195	195	195	195	195	195	192	192	192	192	192
200	200	200	200	200	200	200	200	200	200	115	115	115	115	115	114	114	109	109	109	109	109	109	109
120	120	120	117	117	117	117	117	116	116	116	116	116	116	116	116	116	116	116	116	116	116	116	116
379	379	379	379	379	379	379	379	379	379	379	379	379	379	379	379	379	379	379	379	379	379	379	379
250	250	250	248	248	248	248	248	248	248	248	248	248	248	248	250	250	248	248	248	248	248	248	248
225	200	177	58	177	177	177	177	177	177	177	177	177	177	177	179	178	177	177	177	177	177	177	177
270	270	280	145	233	233	233	233	233	233	233	233	233	233	233	233	233	233	233	233	233	233	233	233
50	50	50	50	50	50	50	50	50	50	50	50	50	50	50	52	52	50	50	50	50	50	50	50
260	270	220	250	250	250	250	250	250	250	250	250	250	250	250	250	250	250	250	250	250	250	250	250
50	50	0	50	50	50	50	50	50	50	50	50	50	50	50	52	52	50	50	50	50	50	50	50
650	650	465	650	650	650	650	635	635	635	650	650	650	650	650	650	650	650	650	650	522	520	650	650	650
550	528	550	550	550	550	550	535	535	535	577	577	577	577	577	577	577	577	577	290	410	550	550	550	550
50	50	5	50	50	50	50	50	50	50	50	50	50	50	50	50	50	50	50	50	50	50	50	50	50
270	87	250	250	250	250	250	250	250	250	275	275	275	275	275	275	275	275	200	250	250	250	250	250	250
260	240	250	250	250	250	250	250	250	250	180	280	280	280	280	280	280	280	100	250	250	250	250	250	250
243	250	250	250	250	250	250	250	250	250	250	290	290	290	290	290	290	206	268	250	250	250	250	250	250
276	470	500	500	500	500	500	500	500	500	470	320	500	500	500	507	441	379	500	500	500	500	500	500	500
464	496	528	557	590	626	617	612	601	597	592	587	370	341	242	210	247	364	373	429	461	497	515	546	542

GP74	GP75	GP76	GP77	GP78	GP79	GP80	GP81	GP82	GP83	GP84	GP85	GP86	GP87	GP88	GP89	GP90	GP91	GP92	GP93	GP94	GP95
172	172	173	171	169	160	168	167	169	176	173	170	169	169	170	171	167	165	164	172	172	172
-50	-50	-50	-50	-50	-50	-50	-50	-50	-50	-50	-50	-50	-50	-50	-50	-50	-50	-50	-50	-50	-50
285	310	315	315	310	280	262	194	178	190	216	230	230	237	238	240	245	245	245	205	171	171
239	230	224	222	224	231	230	268	276	273	276	270	270	270	284	290	294	296	298	329	329	329
177	174	170	170	176	189	185	176	181	179	173	173	173	174	166	161	158	160	161	161	161	161
48	44	47	46	47	51	55	61	60	63	61	60	61	61	64	65	65	62	62	67	67	67
243	236	228	220	213	209	216	221	209	221	214	219	220	222	221	221	224	228	227	238	238	238
167	160	165	165	165	170	170	180	180	165	165	154	150	145	140	138	132	124	120	99	99	99
30	30	25	25	25	25	25	25	25	25	25	25	25	25	25	25	25	25	25	25	25	25
0	0	0	0	0	0	0	0	0	0	0	0	0	0	0	0	0	0	0	0	0	0
0	0	0	0	0	0	0	0	0	0	0	0	0	0	0	0	0	0	0	0	0	0
-150	-150	-150	-150	-150	-150	-150	-150	-150	-150	-150	-150	-150	-150	-150	-150	-150	-150	-150	-150	-150	-150
486	478	483	483	477	440	434	397	370	374	387	383	375	361	357	359	371	386	394	381	381	381
293	292	295	296	298	309	322	311	304	286	281	279	277	271	262	259	254	248	248	250	247	247
222	239	236	235	238	250	250	258	242	231	225	234	240	242	239	240	243	243	237	249	242	242
218	221	230	224	222	219	222	245	256	237	247	253	253	247	251	257	267	261	259	249	246	246
245	235	225	225	225	230	230	240	260	265	255	255	240	250	254	260	260	260	265	229	230	230
25	25	25	25	25	25	25	25	25	25	25	25	25	25	25	25	25	25	25	25	25	25
490	481	478	476	472	467	468	483	499	513	507	494	456	447	453	530	525	514	493	426	441	441
164	163	170	181	190	206	211	211	204	204	198	183	173	175	192	188	186	183	199	163	175	175
0	0	0	0	0	0	0	0	0	0	0	0	0	0	0	0	0	0	0	0	0	0
0	0	0	0	0	0	0	0	0	0	0	0	0	0	0	0	0	0	0	0	0	0
0	0	0	0	0	0	0	0	0	0	0	0	0	0	0	0	0	0	0	0	0	0
0	0	0	0	0	0	0	0	0	0	0	0	0	0	0	0	0	0	0	0	0	0
0	0	0	0	0	0	0	0	0	0	0	0	0	0	0	0	0	0	0	0	0	0
0	0	0	0	0	0	0	0	0	0	0	0	0	0	0	0	0	0	0	0	0	0
0	0	0	0	0	0	0	0	0	0	0	0	0	0	0	0	0	0	0	0	0	0
0	0	0	0	0	0	0	0	0	0	0	0	0	0	0	0	0	0	0	0	0	0
0	0	0	0	0	0	0	0	0	0	0	0	0	0	0	0	0	0	0	0	0	0
0	0	0	0	0	0	0	0	0	0	0	0	0	0	0	0	0	0	0	0	0	0

0	0	0	0	0	0	0	0	0	0	0	0	0	0	0	0	0	0	0	0	0	0
0	0	0	0	0	0	0	0	0	0	0	0	0	0	0	0	0	0	0	0	0	0
0	0	0	0	0	0	0	0	0	0	0	0	0	0	0	0	0	0	0	0	0	0
0	0	0	0	0	0	0	0	0	0	0	0	0	0	0	0	0	0	0	0	0	0
0	0	0	0	0	0	0	-229	-182	-194	-227	-236	-239	-243	-238	-136	-109	-40	-9999	-9999	-9999	-9999
-227	-212	-202	-179	-156	-75	-9999	-9999	-9999	-9999	-9999	-9999	-9999	-9999	-9999	-9999	-9999	-9999	-9999	-9999	-9999	-9999
-9999	-9999	-9999	-9999	-9999	-9999	-9999	-9999	-9999	-9999	-9999	-9999	-9999	-9999	-9999	-9999	-9999	-9999	-9999	-9999	-9999	-9999
-9999	-9999	-9999	-9999	-9999	-9999	-9999	-9999	-9999	-9999	-9999	-9999	-9999	-9999	-9999	-9999	-9999	-9999	-9999	-9999	-9999	-9999
-9999	-9999	-9999	-9999	-9999	-9999	-9999	-9999	-9999	-9999	-9999	-9999	-9999	-9999	-9999	-9999	-9999	-9999	-9999	-9999	-9999	-9999
120	120	120	120	120	120	120	120	120	120	120	120	120	120	120	120	120	120	120	120	120	120
300	300	300	300	300	300	300	300	300	300	300	300	300	300	300	300	300	300	300	300	300	300
250	250	250	250	250	250	250	250	250	250	250	250	250	250	250	250	250	250	250	250	250	250
350	350	350	350	350	350	350	350	350	350	350	350	350	350	350	350	350	350	350	350	350	350
230	230	230	230	250	250	250	250	250	250	250	250	250	250	250	250	250	250	250	250	250	250
130	130	130	130	150	150	150	130	130	130	130	130	130	130	130	150	165	165	191	191	191	191
120	120	120	120	134	134	134	134	134	134	134	134	134	134	120	140	140	140	140	134	134	134
170	379	379	379	379	379	379	360	360	325	325	325	313	313	313	313	313	313	313	313	313	313
248	300	300	300	325	325	325	300	300	300	300	270	270	270	270	54	285	285	285	270	270	270
177	177	177	177	195	195	195	180	180	180	180	156	156	156	156	156	170	170	170	156	156	156
215	250	250	250	300	300	300	270	270	250	245	175	206	206	206	206	206	183	206	206	206	206
50	50	4	50	50	50	50	50	50	50	50	50	50	50	50	50	56	50	50	50	50	50
250	101	330	330	350	350	350	250	250	250	155	250	250	250	250	235	270	270	270	250	250	250
50	50	50	50	50	50	50	50	50	50	10	50	50	50	50	50	50	50	50	50	50	50
640	615	368	650	650	650	650	600	600	600	580	580	600	600	600	600	320	700	700	600	600	600
550	550	550	550	550	550	550	500	500	391	500	500	500	500	500	500	470	550	550	500	500	500
50	50	50	27	50	50	50	50	50	50	50	50	50	50	50	50	50	47	50	50	50	50
250	250	250	50	280	280	280	250	250	250	250	250	250	250	250	250	250	1,01,199	270	250	250	250
250	250	250	250	260	260	260	250	250	250	250	240	250	250	250	250	250	147	260	250	250	250
250	250	250	251	270	270	270	250	250	250	250	249	250	250	250	250	250	250	250	250	250	250
500	500	500	500	500	500	500	500	500	500	500	500	500	500	500	500	500	500	500	500	500	500
535	497	465	418	134	14	97	401	607	830	898	951	981	1037	1054	1050	1008	939	570	980	1082	1166

Tab. 11: Heat flow (mW/m²) used along the simulated cross section (original model). GP29, GP33, GP42, GP45 and GP94 are BRD-4, BKW-1, WT-1, BK-2 and SF-1 wells, respectively.

Evt. Nr.	Evt. Name	GP1	GP2	GP3	GP4	GP5	GP6	GP7	GP8	GP9	GP10	GP11	GP12	GP13	GP14	GP15	GP16	GP17	GP18	GP19	GP20	GP21	GP22	GP23
60	Tertiary	60	60	60	60	60	60	60	60	60	60	60	60	60	60	60	60	60	60	60	60	60	60	60
59	Alpine	60	60	60	60	60	60	60	60	60	60	60	60	60	60	60	60	60	60	60	60	60	60	60
58	Maest-Eoc.	60	60	60	60	60	60	60	60	60	60	60	60	60	60	60	60	60	60	60	60	60	60	60
57	Santonian	60	60	60	60	60	60	60	60	60	60	60	60	60	60	60	60	60	60	60	60	60	60	60
56	Coniacian	60	60	60	60	60	60	60	60	60	60	60	60	60	60	60	60	60	60	60	60	60	60	60
55	Turonian	60	60	60	60	60	60	60	60	60	60	60	60	60	60	60	60	60	60	60	60	60	60	60
54	Cenoman.	60	60	60	60	60	60	60	60	60	60	60	60	60	60	60	60	60	60	60	60	60	60	60
53	Albian	60	60	60	60	60	60	60	60	60	60	60	60	60	60	60	60	60	60	60	60	60	60	60
52	Aptian	60	60	60	60	60	60	60	60	60	60	60	60	60	60	60	60	60	60	60	60	60	60	60
51	Austrian	60	60	60	60	60	60	60	60	60	60	60	60	60	60	60	60	60	60	60	60	60	60	60
50	Austrian	61	61	61	61	61	61	61	61	61	61	61	61	61	61	61	61	61	61	61	61	61	61	61
49	Austrian	61	61	61	61	61	61	61	61	61	61	61	61	61	61	61	61	61	61	61	61	61	61	61
48	Barremian	61	61	61	61	61	61	61	61	61	61	61	61	61	61	61	61	61	61	61	61	61	61	61
47	Neocomm.	62	62	62	62	62	62	62	62	62	62	62	62	62	62	62	62	62	62	62	62	62	62	62
46	Malm	62	62	62	62	62	62	62	62	62	62	62	62	62	62	62	62	62	62	62	62	62	62	62
45	Dogger	63	63	63	63	63	63	63	63	63	63	63	63	63	63	63	63	63	63	63	63	63	63	63
44	Pliensbach.	63	63	63	63	63	63	63	63	63	63	63	63	63	63	63	63	63	63	63	63	63	63	63
43	Sinemurian	63	63	63	63	63	63	63	63	63	63	63	63	63	63	63	63	63	63	63	63	63	63	63
42	Rhaetian	65	65	65	65	65	65	65	65	65	65	65	65	65	65	65	65	65	65	65	65	65	65	65
41	Tr. Keuper	70	70	70	70	70	70	70	70	70	70	70	70	70	70	70	70	70	70	70	70	70	70	70
40	Hercynian	58	58	58	58	58	58	58	58	58	58	58	58	58	58	58	58	58	58	58	58	58	58	58
39	Hercynian	58	58	58	58	58	58	58	58	58	58	58	58	58	58	58	58	58	58	58	58	58	58	58
38	Hercynian	58	58	58	58	58	58	58	58	58	58	58	58	58	58	58	58	58	58	58	58	58	58	58
37	Hercynian	58	58	58	58	58	58	58	58	58	58	58	58	58	58	58	58	58	58	58	58	58	58	58
36	Hercynian	58	58	58	58	58	58	58	58	58	58	58	58	58	58	58	58	58	58	58	58	58	58	58
35	Hercynian	58	58	58	58	58	58	58	58	58	58	58	58	58	58	58	58	58	58	58	58	58	58	58
34	Hercynian	58	58	58	58	58	58	58	58	58	58	58	58	58	58	58	58	58	58	58	58	58	58	58
33	Hercynian	58	58	58	58	58	58	58	58	58	58	58	58	58	58	58	58	58	58	58	58	58	58	58
32	Hercynian	58	58	58	58	58	58	58	58	58	58	58	58	58	58	58	58	58	58	58	58	58	58	58

31	Hercynian	58	58	58	58	58	58	58	58	58	58	58	58	58	58	58	58	58	58	58	58	58	58	58
30	Hercynian	58	58	58	58	58	58	58	58	58	58	58	58	58	58	58	58	58	58	58	58	58	58	58
29	Hercynian	58	58	58	58	58	58	58	58	58	58	58	58	58	58	58	58	58	58	58	58	58	58	58
28	Hercynian	58	58	58	58	58	58	58	58	58	58	58	58	58	58	58	58	58	58	58	58	58	58	58
27	Hercynian	58	58	58	58	58	58	58	58	58	58	58	58	58	58	58	58	58	58	58	58	58	58	58
26	Hercynian	58	58	58	58	58	58	58	58	58	58	58	58	58	58	58	58	58	58	58	58	58	58	58
25	Hercynian	58	58	58	58	58	58	58	58	58	58	58	58	58	58	58	58	58	58	58	58	58	58	58
24	Hercynian	58	58	58	58	58	58	58	58	58	58	58	58	58	58	58	58	58	58	58	58	58	58	58
23	Hercynian	58	58	58	58	58	58	58	58	58	58	58	58	58	58	58	58	58	58	58	58	58	58	58
22	Stephan.	60	60	60	60	60	60	60	60	60	60	60	60	60	60	60	60	60	60	60	60	60	60	60
21	Westphal.	60	60	60	60	60	60	60	60	60	60	60	60	60	60	60	60	60	60	60	60	60	60	60
20	Namurian	60	60	60	60	60	60	60	60	60	60	60	60	60	60	60	60	60	60	60	60	60	60	60
19	Visean C	60	60	60	60	60	60	60	60	60	60	60	60	60	60	60	60	60	60	60	60	60	60	60
18	Visean B	60	60	60	60	60	60	60	60	60	60	60	60	60	60	60	60	60	60	60	60	60	60	60
17	Tournais.	60	60	60	60	60	60	60	60	60	60	60	60	60	60	60	60	60	60	60	60	60	60	60
16	Strunian	60	60	60	60	60	60	60	60	60	60	60	60	60	60	60	60	60	60	60	60	60	60	60
15	Famennian	60	60	60	60	60	60	60	60	60	60	60	60	60	60	60	60	60	60	60	60	60	60	60
14	Frasnian	60	60	60	60	60	60	60	60	60	60	60	60	60	60	60	60	60	60	60	60	60	60	60
13	Emsian	60	60	60	60	60	60	60	60	60	60	60	60	60	60	60	60	60	60	60	60	60	60	60
12	Ged-Sieg.	62	62	62	62	62	62	62	62	62	62	60	60	60	60	60	60	60	60	60	60	60	60	60
11	intra.G.Sieg	62	62	62	62	62	62	62	62	62	62	62	62	62	62	62	62	62	62	62	62	62	62	62
10	Gedinnian	62	62	62	62	62	62	62	62	62	62	62	62	62	62	62	62	62	62	62	62	62	62	62
9	Prodolian	63	63	63	63	63	63	63	63	63	63	63	63	63	63	63	63	63	63	63	63	63	63	63
8	Ludlow	63	63	63	63	63	63	63	63	63	63	63	63	63	63	63	63	63	63	63	63	63	63	63
7	Wenlock	65	65	65	65	65	65	65	65	65	65	65	65	65	65	65	65	65	65	65	65	65	65	65
6	Sil.R.Z	65	65	65	65	65	65	65	65	65	65	65	65	65	65	65	65	65	65	65	65	65	65	65
5	Llanvirn	70	70	70	70	70	70	70	70	70	70	70	70	70	70	70	70	70	70	70	70	70	70	70
4	Arenigian	70	70	70	70	70	70	70	70	70	70	70	70	70	70	70	70	70	70	70	70	70	70	70
3	Tremadoc	75	75	75	75	75	75	75	75	75	75	75	75	75	75	75	75	75	75	75	75	75	75	75
2	Cambrian	75	75	75	75	75	75	75	75	75	75	75	75	75	75	75	75	75	75	75	75	75	75	75
1	Basement	40	40	40	40	40	40	40	40	40	40	40	40	40	40	40	40	40	40	40	40	40	40	40

GP24	GP25	GP26	GP27	GP28	GP29	GP30	GP31	GP32	GP33	GP34	GP35	GP36	GP37	GP38	GP39	GP40	GP41	GP42	GP43	GP44	GP45	GP46	GP47	GP48
60	60	60	60	60	60	60	60	60	60	60	60	60	60	60	50	50	50	50	50	50	50	50	50	50
60	60	60	60	60	60	60	60	60	60	60	60	60	60	60	50	50	50	50	50	50	50	50	50	50
60	60	60	60	60	60	60	60	60	60	60	60	60	60	60	50	50	50	50	50	50	50	50	50	50
60	60	60	60	60	60	60	60	60	60	60	60	60	60	60	50	50	50	50	50	50	50	50	50	50
60	60	60	60	60	60	60	60	60	60	60	60	60	60	60	50	50	50	50	50	50	50	50	50	50
60	60	60	60	60	60	60	60	60	60	60	60	60	60	60	50	50	50	50	50	50	50	50	50	50
60	60	60	60	60	60	60	60	60	60	60	60	60	60	60	50	50	50	50	50	50	50	50	50	50
60	60	60	60	60	60	60	60	60	60	60	60	60	60	60	50	50	50	50	50	50	50	50	50	50
60	60	60	60	60	60	60	60	60	60	60	60	60	60	60	50	50	50	50	50	50	50	50	50	50
60	60	60	60	60	60	60	60	60	60	60	60	60	60	60	50	50	50	50	50	50	50	50	50	50
61	61	61	61	61	61	61	61	61	61	61	61	61	61	61	53	53	53	53	53	53	53	53	53	53
61	61	61	61	61	61	61	61	61	61	61	61	61	61	61	53	53	53	53	53	53	53	53	53	53
61	61	61	61	61	61	61	61	61	61	61	61	61	61	61	53	53	53	53	53	53	53	53	53	53
62	62	62	62	62	62	62	62	62	62	62	62	62	62	62	55	55	55	55	55	55	55	55	55	55
62	62	62	62	62	62	62	62	62	62	62	62	62	62	62	55	55	55	55	55	55	55	55	55	55
63	63	63	63	63	63	63	63	63	63	63	63	63	63	63	58	58	58	58	58	58	58	58	58	58
63	63	63	63	63	63	63	63	63	63	63	63	63	63	63	58	58	58	58	58	58	58	58	58	58
63	63	63	63	63	63	63	63	63	63	63	63	63	63	63	58	58	58	58	58	58	58	58	58	58
65	65	65	65	65	65	65	65	65	65	65	65	65	65	65	60	60	60	60	60	60	60	60	60	60
70	70	70	70	70	70	70	70	70	70	70	70	70	70	70	65	65	65	65	65	65	65	65	65	65
58	58	58	58	58	58	58	58	58	58	58	58	58	58	58	58	58	58	58	58	58	58	58	58	58
58	58	58	58	58	58	58	58	58	58	58	58	58	58	58	58	58	58	58	58	58	58	58	58	58
58	58	58	58	58	58	58	58	58	58	58	58	58	58	58	58	58	58	58	58	58	58	58	58	58
58	58	58	58	58	58	58	58	58	58	58	58	58	58	58	58	58	58	58	58	58	58	58	58	58
58	58	58	58	58	58	58	58	58	58	58	58	58	58	58	58	58	58	58	58	58	58	58	58	58
58	58	58	58	58	58	58	58	58	58	58	58	58	58	58	58	58	58	58	58	58	58	58	58	58
58	58	58	58	58	58	58	58	58	58	58	58	58	58	58	58	58	58	58	58	58	58	58	58	58
58	58	58	58	58	58	58	58	58	58	58	58	58	58	58	58	58	58	58	58	58	58	58	58	58
58	58	58	58	58	58	58	58	58	58	58	58	58	58	58	58	58	58	58	58	58	58	58	58	58
58	58	58	58	58	58	58	58	58	58	58	58	58	58	58	58	58	58	58	58	58	58	58	58	58

58	58	58	58	58	58	58	58	58	58	58	58	58	58	58	58	58	58	58	58	58	58	58	58	58
58	58	58	58	58	58	58	58	58	58	58	58	58	58	58	58	58	58	58	58	58	58	58	58	58
58	58	58	58	58	58	58	58	58	58	58	58	58	58	58	58	58	58	58	58	58	58	58	58	58
58	58	58	58	58	58	58	58	58	58	58	58	58	58	58	58	58	58	58	58	58	58	58	58	58
58	58	58	58	58	58	58	58	58	58	58	58	58	58	58	58	58	58	58	58	58	58	58	58	58
58	58	58	58	58	58	58	58	58	58	58	58	58	58	58	58	58	58	58	58	58	58	58	58	58
58	58	58	58	58	58	58	58	58	58	58	58	58	58	58	58	58	58	58	58	58	58	58	58	58
58	58	58	58	58	58	58	58	58	58	58	58	58	58	58	58	58	58	58	58	58	58	58	58	58
58	58	58	58	58	58	58	58	58	58	58	58	58	58	58	58	58	58	58	58	58	58	58	58	58
58	58	58	58	58	58	58	58	58	58	58	58	58	58	58	58	58	58	58	58	58	58	58	58	58
60	60	60	60	60	60	60	60	60	60	60	60	60	60	60	60	60	60	60	60	60	60	60	60	60
60	60	60	60	60	60	60	60	60	60	60	60	60	60	60	60	60	60	60	60	60	60	60	60	60
60	60	60	60	60	60	60	60	60	60	60	60	60	60	60	60	60	60	60	60	60	60	60	60	60
60	60	60	60	60	60	60	60	60	60	60	60	60	60	60	60	60	60	60	60	60	60	60	60	60
60	60	60	60	60	60	60	60	60	60	60	60	60	60	60	60	60	60	60	60	60	60	60	60	60
60	60	60	60	60	60	60	60	60	60	60	60	60	60	60	60	60	60	60	60	60	60	60	60	60
60	60	60	60	60	60	60	60	60	60	60	60	60	60	60	60	60	60	60	60	60	60	60	60	60
60	60	60	60	60	60	60	60	60	60	60	60	60	60	60	60	60	60	60	60	60	60	60	60	60
60	60	60	60	60	60	60	60	60	60	60	60	60	60	60	60	60	60	60	60	60	60	60	60	60
60	60	60	60	60	60	60	60	60	60	60	60	60	60	60	60	60	60	60	60	60	60	60	60	60
60	60	60	60	60	60	60	60	60	60	60	60	60	60	60	60	60	60	60	60	60	60	60	60	60
60	60	60	60	60	60	60	60	60	60	60	60	60	60	60	60	60	60	60	60	60	60	60	60	60
62	62	62	62	62	62	62	62	62	62	62	62	62	62	62	62	62	62	62	62	62	62	62	62	62
62	62	62	62	62	62	62	62	62	62	62	62	62	62	62	62	62	62	62	62	62	62	62	62	62
62	62	62	62	62	62	62	62	62	62	62	62	62	62	62	62	62	62	62	62	62	62	62	62	62
63	63	63	63	63	63	63	63	63	63	63	63	63	63	63	63	63	63	63	63	63	63	63	63	63
63	63	63	63	63	63	63	63	63	63	63	63	63	63	63	63	63	63	63	63	63	63	63	63	63
65	65	65	65	65	65	65	65	65	65	65	65	65	65	65	65	65	65	65	65	65	65	65	65	65
65	65	65	65	65	65	65	65	65	65	65	65	65	65	65	65	65	65	65	65	65	65	65	65	65
70	70	70	70	70	70	70	70	70	70	70	70	70	70	70	70	70	70	70	70	70	70	70	70	70
70	70	70	70	70	70	70	70	70	70	70	70	70	70	70	70	70	70	70	70	70	70	70	70	70
75	75	75	75	75	75	75	75	75	75	75	75	75	75	75	75	75	75	75	75	75	75	75	75	75
75	75	75	75	75	75	75	75	75	75	75	75	75	75	75	75	75	75	75	75	75	75	75	75	75
40	40	40	40	40	40	40	40	40	40	40	40	40	40	40	40	40	40	40	40	40	40	40	40	40

GP49	GP50	GP51	GP52	GP53	GP54	GP55	GP56	GP57	GP58	GP59	GP60	GP61	GP62	GP63	GP64	GP65	GP66	GP67	GP68	GP69	GP70	GP71	GP72	GP73
50	50	50	50	50	50	50	50	50	50	50	50	50	50	50	50	50	50	50	50	50	50	50	50	50
50	50	50	50	50	50	50	50	50	50	50	50	50	50	50	50	50	50	50	50	50	50	50	50	50
50	50	50	50	50	50	50	50	50	50	50	50	50	50	50	50	50	50	50	50	50	50	50	50	50
50	50	50	50	50	50	50	50	50	50	50	50	50	50	50	50	50	50	50	50	50	50	50	50	50
50	50	50	50	50	50	50	50	50	50	50	50	50	50	50	50	50	50	50	50	50	50	50	50	50
50	50	50	50	50	50	50	50	50	50	50	50	50	50	50	50	50	50	50	50	50	50	50	50	50
50	50	50	50	50	50	50	50	50	50	50	50	50	50	50	50	50	50	50	50	50	50	50	50	50
50	50	50	50	50	50	50	50	50	50	50	50	50	50	50	50	50	50	50	50	50	50	50	50	50
50	50	50	50	50	50	50	50	50	50	50	50	50	50	50	50	50	50	50	50	50	50	50	50	50
50	50	50	50	50	50	50	50	50	50	50	50	50	50	50	50	50	50	50	50	50	50	50	50	50
53	53	53	53	53	53	53	53	53	53	53	53	53	53	53	53	53	53	53	53	53	53	53	53	53
53	53	53	53	53	53	53	53	53	53	53	53	53	53	53	53	53	53	53	53	53	53	53	53	53
53	53	53	53	53	53	53	53	53	53	53	53	53	53	53	53	53	53	53	53	53	53	53	53	53
55	55	55	55	55	55	55	55	55	55	55	55	55	55	55	55	55	55	55	55	55	55	55	55	55
55	55	55	55	55	55	55	55	55	55	55	55	55	55	55	55	55	55	55	55	55	55	55	55	55
58	58	58	58	58	58	58	58	58	58	58	58	58	58	58	58	58	58	58	58	58	58	58	58	58
58	58	58	58	58	58	58	58	58	58	58	58	58	58	58	58	58	58	58	58	58	58	58	58	58
58	58	58	58	58	58	58	58	58	58	58	58	58	58	58	58	58	58	58	58	58	58	58	58	58
60	60	60	60	60	60	60	60	60	60	60	60	60	60	60	60	60	60	60	60	60	60	60	60	60
65	65	65	65	65	65	65	65	65	65	65	65	65	65	65	65	65	65	65	65	65	65	65	65	65
58	58	58	58	58	58	58	58	58	58	58	58	58	58	58	58	58	58	58	58	58	58	58	58	58
58	58	58	58	58	58	58	58	58	58	58	58	58	58	58	58	58	58	58	58	58	58	58	58	58
58	58	58	58	58	58	58	58	58	58	58	58	58	58	58	58	58	58	58	58	58	58	58	58	58
58	58	58	58	58	58	58	58	58	58	58	58	58	58	58	58	58	58	58	58	58	58	58	58	58
58	58	58	58	58	58	58	58	58	58	58	58	58	58	58	58	58	58	58	58	58	58	58	58	58
58	58	58	58	58	58	58	58	58	58	58	58	58	58	58	58	58	58	58	58	58	58	58	58	58
58	58	58	58	58	58	58	58	58	58	58	58	58	58	58	58	58	58	58	58	58	58	58	58	58
58	58	58	58	58	58	58	58	58	58	58	58	58	58	58	58	58	58	58	58	58	58	58	58	58
58	58	58	58	58	58	58	58	58	58	58	58	58	58	58	58	58	58	58	58	58	58	58	58	58
58	58	58	58	58	58	58	58	58	58	58	58	58	58	58	58	58	58	58	58	58	58	58	58	58
58	58	58	58	58	58	58	58	58	58	58	58	58	58	58	58	58	58	58	58	58	58	58	58	58

58	58	58	58	58	58	58	58	58	58	58	58	58	58	58	58	58	58	58	58	58	58	58	58	58	58
58	58	58	58	58	58	58	58	58	58	58	58	58	58	58	58	58	58	58	58	58	58	58	58	58	58
58	58	58	58	58	58	58	58	58	58	58	58	58	58	58	58	58	58	58	58	58	58	58	58	58	58
58	58	58	58	58	58	58	58	58	58	58	58	58	58	58	58	58	58	58	58	58	58	58	58	58	58
58	58	58	58	58	58	58	58	58	58	58	58	58	58	58	58	58	58	58	58	58	58	58	58	58	58
58	58	58	58	58	58	58	58	58	58	58	58	58	58	58	58	58	58	58	58	58	58	58	58	58	58
58	58	58	58	58	58	58	58	58	58	58	58	58	58	58	58	58	58	58	58	58	58	58	58	58	58
58	58	58	58	58	58	58	58	58	58	58	58	58	58	58	58	58	58	58	58	58	58	58	58	58	58
58	58	58	58	58	58	58	58	58	58	58	58	58	58	58	58	58	58	58	58	58	58	58	58	58	58
60	60	60	60	60	60	60	60	60	60	60	60	60	60	60	60	60	60	60	60	60	60	60	60	60	60
60	60	60	60	60	60	60	60	60	60	60	60	60	60	60	60	60	60	60	60	60	60	60	60	60	60
60	60	60	60	60	60	60	60	60	60	60	60	60	60	60	60	60	60	60	60	60	60	60	60	60	60
60	60	60	60	60	60	60	60	60	60	60	60	60	60	60	60	60	60	60	60	60	60	60	60	60	60
60	60	60	60	60	60	60	60	60	60	60	60	60	60	60	60	60	60	60	60	60	60	60	60	60	60
60	60	60	60	60	60	60	60	60	60	60	60	60	60	60	60	60	60	60	60	60	60	60	60	60	60
60	60	60	60	60	60	60	60	60	60	60	60	60	60	60	60	60	60	60	60	60	60	60	60	60	60
60	60	60	60	60	60	60	60	60	60	60	60	60	60	60	60	60	60	60	60	60	60	60	60	60	60
60	60	60	60	60	60	60	60	60	60	60	60	60	60	60	60	60	60	60	60	60	60	60	60	60	60
60	60	60	60	60	60	60	60	60	60	60	60	60	60	60	60	60	60	60	60	60	60	60	60	60	60
62	62	62	62	62	62	62	62	62	62	62	62	62	62	62	62	62	62	62	62	62	62	62	62	62	62
62	62	62	62	62	62	62	62	62	62	62	62	62	62	62	62	62	62	62	62	62	62	62	62	62	62
62	62	62	62	62	62	62	62	62	62	62	62	62	62	62	62	62	62	62	62	62	62	62	62	62	62
63	63	63	63	63	63	63	63	63	63	63	63	63	63	63	63	63	63	63	63	63	63	63	63	63	63
63	63	63	63	63	63	63	63	63	63	63	63	63	63	63	63	63	63	63	63	63	63	63	63	63	63
65	65	65	65	65	65	65	65	65	65	65	65	65	65	65	65	65	65	65	65	65	65	65	65	65	65
65	65	65	65	65	65	65	65	65	65	65	65	65	65	65	65	65	65	65	65	65	65	65	65	65	65
70	70	70	70	70	70	70	70	70	70	70	70	70	70	70	70	70	70	70	70	70	70	70	70	70	70
70	70	70	70	70	70	70	70	70	70	70	70	70	70	70	70	70	70	70	70	70	70	70	70	70	70
75	75	75	75	75	75	75	75	75	75	75	75	75	75	75	75	75	75	75	75	75	75	75	75	75	75
75	75	75	75	75	75	75	75	75	75	75	75	75	75	75	75	75	75	75	75	75	75	75	75	75	75
40	40	40	40	40	40	40	40	40	40	40	40	40	40	40	40	40	40	40	40	40	40	40	40	40	40

GP74	GP75	GP76	GP77	GP78	GP79	GP80	GP81	GP82	GP83	GP84	GP85	GP86	GP87	GP88	GP89	GP90	GP91	GP92	GP93	GP94	GP95
50	50	50	50	50	50	50	50	50	50	50	50	50	50	50	50	50	50	50	50	50	50
50	50	50	50	50	50	50	50	50	50	50	50	50	50	50	50	50	50	50	50	50	50
50	50	50	50	50	50	50	50	50	50	50	50	50	50	50	50	50	50	50	50	50	50
50	50	50	50	50	50	50	50	50	50	50	50	50	50	50	50	50	50	50	50	50	50
50	50	50	50	50	50	50	50	50	50	50	50	50	50	50	50	50	50	50	50	50	50
50	50	50	50	50	50	50	50	50	50	50	50	50	50	50	50	50	50	50	50	50	50
50	50	50	50	50	50	50	50	50	50	50	50	50	50	50	50	50	50	50	50	50	50
50	50	50	50	50	50	50	50	50	50	50	50	50	50	50	50	50	50	50	50	50	50
50	50	50	50	50	50	50	50	50	50	50	50	50	50	50	50	50	50	50	50	50	50
50	50	50	50	50	50	50	50	50	50	50	50	50	50	50	50	50	50	50	50	50	50
50	50	50	50	50	50	50	50	50	50	50	50	50	50	50	50	50	50	50	50	50	50
53	53	53	53	53	53	53	53	53	53	53	53	53	53	53	53	53	53	53	53	53	53
53	53	53	53	53	53	53	53	53	53	53	53	53	53	53	53	53	53	53	53	53	53
53	53	53	53	53	53	53	53	53	53	53	53	53	53	53	53	53	53	53	53	53	53
55	55	55	55	55	55	55	55	55	55	55	55	55	55	55	55	55	55	55	55	55	55
55	55	55	55	55	55	55	55	55	55	55	55	55	55	55	55	55	55	55	55	55	55
58	58	58	58	58	58	58	58	58	58	58	58	58	58	58	58	58	58	58	58	58	58
58	58	58	58	58	58	58	58	58	58	58	58	58	58	58	58	58	58	58	58	58	58
58	58	58	58	58	58	58	58	58	58	58	58	58	58	58	58	58	58	58	58	58	58
60	60	60	60	60	60	60	60	60	60	60	60	60	60	60	60	60	60	60	60	60	60
65	65	65	65	65	65	65	65	65	65	65	65	65	65	65	65	65	65	65	65	65	65
58	58	58	58	58	58	58	58	58	58	58	58	58	58	58	58	58	58	58	58	58	58
58	58	58	58	58	58	58	58	58	58	58	58	58	58	58	58	58	58	58	58	58	58
58	58	58	58	58	58	58	58	58	58	58	58	58	58	58	58	58	58	58	58	58	58
58	58	58	58	58	58	58	58	58	58	58	58	58	58	58	58	58	58	58	58	58	58
58	58	58	58	58	58	58	58	58	58	58	58	58	58	58	58	58	58	58	58	58	58
58	58	58	58	58	58	58	58	58	58	58	58	58	58	58	58	58	58	58	58	58	58
58	58	58	58	58	58	58	58	58	58	58	58	58	58	58	58	58	58	58	58	58	58
58	58	58	58	58	58	58	58	58	58	58	58	58	58	58	58	58	58	58	58	58	58
58	58	58	58	58	58	58	58	58	58	58	58	58	58	58	58	58	58	58	58	58	58
58	58	58	58	58	58	58	58	58	58	58	58	58	58	58	58	58	58	58	58	58	58

58	58	58	58	58	58	58	58	58	58	58	58	58	58	58	58	58	58	58	58	58	58
58	58	58	58	58	58	58	58	58	58	58	58	58	58	58	58	58	58	58	58	58	58
58	58	58	58	58	58	58	58	58	58	58	58	58	58	58	58	58	58	58	58	58	58
58	58	58	58	58	58	58	58	58	58	58	58	58	58	58	58	58	58	58	58	58	58
58	58	58	58	58	58	58	58	58	58	58	58	58	58	58	58	58	58	58	58	58	58
58	58	58	58	58	58	58	58	58	58	58	58	58	58	58	58	58	58	58	58	58	58
58	58	58	58	58	58	58	58	58	58	58	58	58	58	58	58	58	58	58	58	58	58
58	58	58	58	58	58	58	58	58	58	58	58	58	58	58	58	58	58	58	58	58	58
58	58	58	58	58	58	58	58	58	58	58	58	58	58	58	58	58	58	58	58	58	58
60	60	60	60	60	60	60	60	60	60	60	60	60	60	60	60	60	60	60	60	60	60
60	60	60	60	60	60	60	60	60	60	60	60	60	60	60	60	60	60	60	60	60	60
60	60	60	60	60	60	60	60	60	60	60	60	60	60	60	60	60	60	60	60	60	60
60	60	60	60	60	60	60	60	60	60	60	60	60	60	60	60	60	60	60	60	60	60
60	60	60	60	60	60	60	60	60	60	60	60	60	60	60	60	60	60	60	60	60	60
60	60	60	60	60	60	60	60	60	60	60	60	60	60	60	60	60	60	60	60	60	60
60	60	60	60	60	60	60	60	60	60	60	60	60	60	60	60	60	60	60	60	60	60
60	60	60	60	60	60	60	60	60	60	60	60	60	60	60	60	60	60	60	60	60	60
60	60	60	60	60	60	60	60	60	60	60	60	60	60	60	60	60	60	60	60	60	60
60	60	60	60	60	60	60	60	60	60	60	60	60	60	60	60	60	60	60	60	60	60
62	62	62	62	62	62	62	62	62	62	62	62	62	62	62	62	62	62	62	62	62	62
62	62	62	62	62	62	62	62	62	62	62	62	62	62	62	62	62	62	62	62	62	62
62	62	62	62	62	62	62	62	62	62	62	62	62	62	62	62	62	62	62	62	62	62
63	63	63	63	63	63	63	63	63	63	63	63	63	63	63	63	63	63	63	63	63	63
63	63	63	63	63	63	63	63	63	63	63	63	63	63	63	63	63	63	63	63	63	63
65	65	65	65	65	65	65	65	65	65	65	65	65	65	65	65	65	65	65	65	65	65
65	65	65	65	65	65	65	65	65	65	65	65	65	65	65	65	65	65	65	65	65	65
70	70	70	70	70	70	70	70	70	70	70	70	70	70	70	70	70	70	70	70	70	70
70	70	70	70	70	70	70	70	70	70	70	70	70	70	70	70	70	70	70	70	70	70
75	75	75	75	75	75	75	75	75	75	75	75	75	75	75	75	75	75	75	75	75	75
75	75	75	75	75	75	75	75	75	75	75	75	75	75	75	75	75	75	75	75	75	75
40	40	40	40	40	40	40	40	40	40	40	40	40	40	40	40	40	40	40	40	40	40

Tab. 12: Sediment thicknesses (m) used along the simulated cross section (alternative model). GP29, GP33,GP42, GP45 and GP94 are BRD-4, BKW-1,WT-1, BK-2 and SF-1wells, respectively. -9999 means total erosion

Evt. N°	Evt. Name	GP1	GP2	GP3	GP4	GP5	GP6	GP7	GP8	GP9	GP10	GP11	GP12	GP13	GP14	GP15	GP16	GP17	GP18	GP19	GP20	GP21	GP22	GP23
60	Tertiary	184	184	184	184	184	184	184	184	184	184	184	184	184	180	170	168	166	167	176	211	191	191	187
59	Alpine	-169	-169	-168	-168	-168	-168	-168	-168	-167	-166	-165	-164	-164	-164	-164	-164	-164	-164	-163	-97	-58	-145	-145
58	Maest-Eoc.	203	369	266	241	234	228	210	191	190	376	416	385	380	371	367	379	392	407	421	441	442	440	432
57	Santonian	144	144	144	144	144	144	144	144	144	144	185	185	185	185	185	185	185	185	185	185	185	212	211
56	Coniacian	186	166	129	137	131	131	120	116	116	116	116	116	116	116	116	123	122	119	119	97	97	97	97
55	Turonian	73	73	73	73	73	73	73	73	73	97	97	97	97	97	97	97	97	97	97	97	120	120	120
54	Cenoman.	191	195	149	144	147	151	148	137	166	185	177	191	174	174	174	174	174	174	174	174	174	222	227
53	Albian	136	136	168	153	147	145	139	125	125	140	140	140	140	140	140	140	140	140	122	104	122	128	
52	Aptian	30	30	30	30	30	30	30	30	30	30	30	30	30	30	30	30	30	30	30	30	30	30	
51	Austrian	0	0	0	0	0	0	-115	-9999	0	0	0	0	0	0	0	0	0	0	0	0	0	0	
50	Austrian	0	0	0	0	0	-9999	-9999	-9999	0	0	0	0	0	0	0	0	0	0	0	0	0	0	
49	Austrian	-467	-425	-435	-551	-699	-9999	-9999	-9999	-9999	-441	-365	-436	-448	-488	-565	-565	-480	-435	-385	-150	-170	-185	-190
48	Barremian	706	721	717	706	706	707	725	770	905	690	706	670	670	670	670	670	670	710	725	725	725	770	780
47	Neocomm.	444	403	372	374	419	380	345	318	296	296	296	296	296	260	296	296	247	286	290	308	302	277	284
46	Malm	225	247	237	252	10349	280	220	184	277	237	245	266	264	229	229	229	229	276	270	310	320	309	300
45	Dogger	290	264	278	252	156	249	182	123	292	242	270	309	309	309	309	309	309	309	309	309	309	309	309
44	Pliensbach.	284	277	210	208	160	160	160	160	234	200	200	200	180	121	121	121	121	165	170	175	220	240	250
43	Sinemurian	25	25	25	25	25	25	25	25	25	25	25	25	25	25	25	25	25	25	25	25	25	25	25
42	Rhaetian	894	894	894	444	934	963	1000	1000	880	773	746	735	737	664	664	664	664	620	598	603	641	665	663
41	Tr. Keuper	399	399	399	399	399	399	399	399	475	457	374	329	306	317	317	317	317	474	448	391	384	384	392
40	Hercynian	-148	-136	-75	-108	-112	-108	-6	-78	17	0	0	0	0	0	0	0	0	0	0	0	0	0	0
39	Hercynian	-9999	-9999	-9999	-9999	-9999	-9999	-9999	-9999	-9999	-9999	0	0	0	0	0	0	0	0	0	0	0	0	0
38	Hercynian	-9999	-9999	-9999	-9999	-9999	-9999	-9999	-9999	-9999	-9999	-324	-300	-284	-325	-325	-325	-325	-103	0	0	0	0	0
37	Hercynian	-9999	-9999	-9999	-9999	-9999	-9999	-9999	-9999	-9999	-9999	-9999	-9999	-9999	-9999	-9999	-9999	-9999	-9999	-9999	-395	-322	-259	-257
36	Hercynian	-9999	-9999	-9999	-9999	-9999	-9999	-9999	-9999	-9999	-9999	-9999	-9999	-9999	-9999	-9999	-9999	-9999	-9999	-9999	-9999	-9999	-9999	-9999
35	Hercynian	-9999	-9999	-9999	-9999	-9999	-9999	-9999	-9999	-9999	-9999	-9999	-9999	-9999	-9999	-9999	-9999	-9999	-9999	-9999	-9999	-9999	-9999	-9999
34	Hercynian	-9999	-9999	-9999	-9999	-9999	-9999	-9999	-9999	-9999	-9999	-9999	-9999	-9999	-9999	-9999	-9999	-9999	-9999	-9999	-9999	-9999	-9999	-9999
33	Hercynian	-9999	-9999	-9999	-9999	-9999	-9999	-9999	-9999	-9999	-9999	-9999	-9999	-9999	-9999	-9999	-9999	-9999	-9999	-9999	-9999	-9999	-9999	-9999
32	Hercynian	-9999	-9999	-9999	-9999	-9999	-9999	-9999	-9999	-9999	-9999	-9999	-9999	-9999	-9999	-9999	-9999	-9999	-9999	-9999	-9999	-9999	-9999	-9999

31	Hercynian	-9999	-9999	-9999	-9999	-9999	-9999	-9999	-9999	-9999	-9999	-9999	-9999	-9999	-9999	-9999	-9999	-9999	-9999	-9999	-9999	-9999	-9999	-9999
30	Hercynian	-9999	-9999	-9999	-9999	-9999	-9999	-9999	-9999	-9999	-9999	-9999	-9999	-9999	-9999	-9999	-9999	-9999	-9999	-9999	-9999	-9999	-9999	-9999
29	Hercynian	-9999	-9999	-9999	-9999	-9999	-9999	-9999	-9999	-9999	-9999	-9999	-9999	-9999	-9999	-9999	-9999	-9999	-9999	-9999	-9999	-9999	-9999	-9999
28	Hercynian	-9999	-9999	-9999	-9999	-9999	-9999	-9999	-9999	-9999	-9999	-9999	-9999	-9999	-9999	-9999	-9999	-9999	-9999	-9999	-9999	-9999	-9999	-9999
27	Hercynian	-9999	-9999	-9999	-9999	-9999	-9999	-9999	-9999	-9999	-9999	-9999	-9999	-9999	-9999	-9999	-9999	-9999	-9999	-9999	-9999	-9999	-9999	-9999
26	Hercynian	-9999	-9999	-9999	-9999	-9999	-9999	-9999	-9999	-9999	-9999	-9999	-9999	-9999	-9999	-9999	-9999	-9999	-9999	-9999	-9999	-9999	-9999	-9999
25	Hercynian	-9999	-9999	-9999	-9999	-9999	-9999	-9999	-9999	-9999	-9999	-9999	-9999	-9999	-9999	-9999	-9999	-9999	-9999	-9999	-9999	-9999	-9999	-9999
24	Hercynian	-9999	-9999	-9999	-9999	-9999	-9999	-9999	-9999	-9999	-9999	-9999	-9999	-9999	-9999	-9999	-9999	-9999	-9999	-9999	-9999	-9999	-9999	-9999
23	Hercynian	-9999	-9999	-9999	-9999	-9999	-9999	-9999	-9999	-9999	-9999	-9999	-9999	-9999	-9999	-9999	-9999	-9999	-9999	-9999	-9999	-9999	-9999	-9999
22	Stephan.	50	51	52	52	53	53	53	53	54	57	59	60	60	60	60	61	61	61	62	54	67	68	68
21	Westphal.	150	152	154	154	154	154	154	155	156	161	164	165	166	166	166	167	167	168	168	172	176	178	179
20	Namurian	100	103	106	106	107	107	107	108	110	118	123	126	126	126	127	128	129	130	130	137	144	147	148
19	Visean C	120	125	130	130	131	131	132	133	136	148	157	161	161	162	163	165	166	167	169	179	191	196	196
18	Visean B	120	122	124	124	124	124	124	125	126	131	134	135	136	136	136	137	137	138	138	142	146	148	149
17	Tournais.	125	123	122	122	122	122	121	121	120	116	113	112	112	112	111	111	110	110	110	106	103	101	101
16	Strunian	50	50	50	50	50	50	50	50	50	50	50	50	50	50	50	50	50	50	50	50	50	50	50
15	Famennian	220	220	220	220	220	220	220	220	220	220	220	220	220	220	220	220	220	220	220	220	220	220	220
14	Frasnian	150	150	150	150	150	150	150	150	150	150	150	150	150	150	150	150	150	150	150	150	150	150	150
13	Emsian	50	50	50	50	50	50	50	50	50	50	50	50	50	50	50	50	50	50	50	50	50	50	50
12	Ged-Sieg.	200	200	200	200	200	200	200	200	200	200	200	200	200	200	200	200	200	200	200	200	200	200	200
11	Intra.G.Sieg	50	50	50	50	50	50	50	50	50	50	50	50	50	50	50	50	50	50	50	50	50	50	50
10	Gedinnian	160	160	160	160	160	160	160	160	160	160	160	160	160	160	160	160	160	160	160	160	160	160	160
9	Prodolian	50	50	50	50	50	50	50	50	50	50	50	50	50	50	50	50	50	50	50	50	50	50	50
8	Ludlow	500	500	500	500	500	500	500	500	500	500	500	500	500	500	500	500	500	500	600	600	600	600	600
7	Wenlock	460	460	460	460	460	460	460	460	460	460	460	460	460	460	460	460	460	460	460	473	450	420	420
6	Sil.R.Z	50	50	50	50	50	50	50	50	50	50	50	50	50	50	50	50	50	50	50	50	50	50	50
5	Llanvirn	225	225	220	206	206	206	206	206	206	206	206	206	206	206	206	206	206	265	236	293	293	293	293
4	Arenigian	300	300	300	293	293	293	293	293	252	250	250	250	270	252	252	252	252	250	250	250	250	250	250
3	Tremadoc	260	260	260	250	250	250	250	285	303	280	300	320	320	313	313	313	313	300	300	300	300	300	270
2	Cambrian	500	500	500	500	500	500	500	500	503	500	500	500	326	500	500	500	500	500	500	500	500	500	230
1	Basement	3364	3223	3377	4135	4164	4195	4327	4335	3497	3235	3044	3098	3297	3369	3479	3461	3343	3160	2617	2131	1786	1722	1971

GP24	GP25	GP26	GP27	GP28	GP29	GP30	GP31	GP32	GP33	GP34	GP35	GP36	GP37	GP38	GP39	GP40	GP41	GP42	GP43	GP44	GP45	GP46	GP47	GP48
183	186	185	184	192	192	197	192	250	288	288	267	247	234	224	228	230	232	253	232	218	210	210	210	210
-144	-144	-144	-144	-150	-150	-143	-143	-141	-140	-139	-137	-136	-50	-50	-50	-50	-50	-50	-50	-50	-50	-50	-50	-50
416	396	387	373	345	343	343	352	327	270	271	316	327	293	293	293	285	279	274	218	217	216	217	180	261
212	213	214	216	208	208	208	208	293	348	348	348	348	262	239	240	239	252	252	236	236	236	236	236	245
97	97	97	97	97	97	96	97	155	155	155	155	155	173	156	140	135	127	122	169	180	180	180	180	170
120	100	100	100	100	100	102	100	84	78	78	78	78	78	102	113	115	114	11	70	58	58	58	58	58
226	223	221	215	205	205	205	205	227	242	242	242	242	242	242	231	236	241	241	269	223	223	223	211	193
137	141	143	125	125	125	102	125	219	268	268	268	268	268	238	230	233	237	237	225	219	219	219	219	213
30	30	30	25	25	25	46	25	30	30	30	30	30	30	30	30	30	30	30	30	30	30	30	30	30
0	0	0	0	0	0	0	0	0	0	0	0	0	0	0	0	0	0	0	0	0	0	0	0	0
0	0	0	0	0	0	0	0	0	0	0	0	0	0	0	0	0	0	0	0	0	0	0	0	0
-192	-350	-350	-350	-350	-350	-372	-350	-124	-124	-135	-150	-150	-150	-150	-150	-150	-150	-100	-150	-150	-150	-150	-150	-150
790	705	705	705	705	705	724	705	705	705	705	697	697	645	652	661	664	667	620	653	658	653	635	533	490
299	538	306	306	306	306	302	306	310	316	323	302	306	307	317	310	309	309	309	309	309	313	313	316	335
279	292	498	272	248	248	249	248	274	249	249	229	232	229	223	217	214	209	209	209	218	218	218	216	222
309	309	309	309	309	309	282	309	260	228	240	250	246	256	260	297	298	295	259	259	243	243	243	227	225
260	270	280	310	310	310	311	310	320	320	320	350	350	320	289	280	280	257	257	278	299	299	299	265	225
25	25	25	25	25	25	35906	25	25	25	25	25	25	25	25	25	25	25	25	25	25	25	25	25	25
656	661	663	621	673	673	677	673	659	637	634	564	564	549	496	472	476	409	470	514	553	553	553	575	622
408	399	90	362	344	344	346	344	309	232	227	273	261	272	282	279	275	296	266	216	231	231	231	236	261
0	0	0	0	0	0	0	0	0	0	0	0	0	0	0	0	0	0	0	0	0	0	0	0	0
0	0	0	0	0	0	0	0	0	0	0	0	0	0	0	0	0	0	0	0	0	0	0	0	0
0	0	0	0	0	0	0	0	0	0	0	0	0	0	0	0	0	0	0	0	0	0	0	0	0
-229	-218	-180	-181	-50	-100	0	0	0	0	0	0	0	0	0	0	0	0	0	0	0	0	0	0	0
-9999	-9999	-9999	-9999	-9999	-9999	-9999	0	0	0	0	0	0	0	0	0	0	0	0	0	0	0	0	0	0
-9999	-9999	-9999	-9999	-9999	-9999	-9999	-9999	-169	0	0	0	0	0	0	0	0	0	0	0	0	0	0	0	0
-9999	-9999	-9999	-9999	-9999	-9999	-9999	-9999	-9999	-9999	0	0	0	0	0	0	0	0	0	0	0	0	0	0	0
-9999	-9999	-9999	-9999	-9999	-9999	-9999	-9999	-9999	-9999	-9999	0	0	0	0	0	0	0	0	0	0	0	0	0	0
-9999	-9999	-9999	-9999	-9999	-9999	-9999	-9999	-9999	-9999	-9999	-9999	0	0	0	0	0	0	0	0	0	0	0	0	0

-9999	-9999	-9999	-9999	-9999	-9999	-9999	-9999	-9999	-9999	-9999	-9999	-9999	0	0	0	0	0	0	0	0	0	0	0
-9999	-9999	-9999	-9999	-9999	-9999	-9999	-9999	-9999	-9999	-9999	-9999	-9999	-9999	-318	-207	-190	-224	-200	0	0	0	0	0	0
-9999	-9999	-9999	-9999	-9999	-9999	-9999	-9999	-9999	-9999	-9999	-9999	-9999	-9999	-9999	-9999	-9999	-9999	-9999	-9999	0	0	0	-70	0
-9999	-9999	-9999	-9999	-9999	-9999	-9999	-9999	-9999	-9999	-9999	-9999	-9999	-9999	-9999	-9999	-9999	-9999	-9999	-9999	-9999	-150	-9999	-9999	-9999
-9999	-9999	-9999	-9999	-9999	-9999	-9999	-9999	-9999	-9999	-9999	-9999	-9999	-9999	-9999	-9999	-9999	-9999	-9999	-9999	-9999	-9999	-9999	-9999	-9999
-9999	-9999	-9999	-9999	-9999	-9999	-9999	-9999	-9999	-9999	-9999	-9999	-9999	-9999	-9999	-9999	-9999	-9999	-9999	-9999	-9999	-9999	-9999	-9999	-9999
-9999	-9999	-9999	-9999	-9999	-9999	-9999	-9999	-9999	-9999	-9999	-9999	-9999	-9999	-9999	-9999	-9999	-9999	-9999	-9999	-9999	-9999	-9999	-9999	-9999
-9999	-9999	-9999	-9999	-9999	-9999	-9999	-9999	-9999	-9999	-9999	-9999	-9999	-9999	-9999	-9999	-9999	-9999	-9999	-9999	-9999	-9999	-9999	-9999	-9999
68	69	69	69	70	70	75	80	85	90	95	95	100	105	110	120	120	120	120	120	120	120	120	120	120
179	179	180	180	180	180	190	205	210	215	220	220	240	260	270	300	300	300	300	300	300	300	300	300	300
148	149	149	150	150	150	170	190	200	105	210	210	220	230	250	250	250	250	250	250	250	250	250	250	250
197	199	199	200	200	220	240	260	280	300	305	305	315	320	350	350	350	350	350	350	350	350	350	350	350
149	149	150	150	150	150	160	165	170	180	205	205	210	220	250	250	250	250	250	250	250	250	250	250	250
100	100	100	100	100	100	110	120	125	140	160	160	170	180	200	200	200	200	200	200	200	200	200	200	200
50	50	50	50	50	50	60	70	70	75	80	80	90	95	106	106	106	106	106	106	106	106	106	106	106
220	220	220	220	220	220	220	240	260	280	290	300	305	330	360	360	349	349	349	330	330	330	350	350	379
150	150	150	150	150	150	150	200	200	200	200	200	200	200	200	200	200	196	196	200	206	206	230	230	250
50	50	50	50	50	50	55	60	70	80	100	105	110	125	136	136	136	136	136	136	162	162	180	180	225
200	200	200	200	200	200	200	320	320	320	320	321	321	321	321	321	321	321	321	309	309	309	309	285	270
50	50	50	50	50	50	50	50	50	50	50	50	50	50	50	50	50	50	50	50	50	50	50	50	50
160	160	160	160	160	160	170	180	180	200	200	220	230	230	240	260	260	260	260	270	270	270	270	260	260
50	50	50	50	50	50	50	50	50	50	50	50	50	50	50	50	50	50	50	50	50	50	50	50	50
600	600	550	580	550	550	550	600	600	600	700	650	700	650	650	650	570	650	650	650	650	650	650	650	650
420	170	393	393	510	510	510	510	550	550	550	550	550	550	550	550	550	550	550	550	550	550	550	550	550
50	50	50	50	50	50	50	50	50	50	50	50	50	50	50	50	40	50	50	50	50	50	50	50	50
293	200	293	293	293	293	293	293	293	293	293	293	293	293	293	293	260	260	260	260	260	260	260	270	270
13	280	280	280	280	280	280	280	250	250	250	250	250	250	250	250	250	250	250	250	250	250	250	260	260
200	260	273	273	273	273	273	273	273	273	273	273	273	273	273	273	250	250	250	250	250	250	250	250	250
460	460	500	500	500	500	500	500	500	500	500	500	500	500	500	500	500	500	500	500	500	500	500	500	500
1988	2004	2012	2020	2015	2000	1888	1775	1240	1132	1113	836	701	648	716	653	753	750	751	465	407	397	407	650	287

GP49	GP50	GP51	GP52	GP53	GP54	GP55	GP56	GP57	GP58	GP59	GP60	GP61	GP62	GP63	GP64	GP65	GP66	GP67	GP68	GP69	GP70	GP71	GP72	GP73
210	206	205	206	207	202	195	196	196	192	192	196	196	194	182	173	174	172	171	168	169	173	174	164	164
-50	-50	-50	-50	-50	-50	-50	-50	-50	-50	-50	-50	-50	-50	-50	-50	-50	-50	-50	-50	-50	-50	-50	-50	-50
310	293	292	289	285	273	272	270	250	275	275	272	272	270	200	332	330	330	330	330	308	275	260	260	260
242	234	223	214	225	243	244	253	256	250	240	234	230	232	266	232	233	234	233	225	236	247	247	247	240
170	166	156	159	159	158	165	164	167	165	172	176	180	187	186	183	181	179	180	181	188	180	180	180	180
58	65	64	51	49	47	46	46	48	52	49	49	51	47	54	45	46	48	48	49	47	51	47	46	46
196	207	215	230	236	237	234	234	230	230	231	234	233	234	228	248	243	237	235	230	233	235	241	245	249
213	215	220	225	225	225	235	235	240	240	235	230	235	235	212	187	187	187	187	187	187	179	175	167	167
30	30	30	30	30	30	30	30	30	30	30	30	30	30	30	30	30	30	30	30	30	30	30	30	30
0	0	0	0	0	0	0	0	0	0	0	0	0	0	0	0	0	0	0	0	0	0	0	0	0
0	0	0	0	0	0	0	0	0	0	0	0	0	0	0	0	0	0	0	0	0	0	0	0	0
-150	-150	-150	-150	-150	-150	-150	-150	-150	-150	-150	-150	-150	-150	-150	-150	-150	-150	-150	-150	-150	-150	-150	-150	-150
492	505	515	490	464	461	490	490	499	514	531	545	550	544	476	478	483	489	491	500	489	488	486	480	483
336	338	342	346	342	332	330	331	325	322	319	317	314	312	312	290	289	287	287	284	290	295	288	284	291
222	218	217	221	225	219	209	207	209	210	211	211	210	210	212	227	231	235	235	235	236	239	235	214	220
228	233	229	224	224	228	206	201	197	199	202	204	207	209	218	243	243	243	245	255	245	228	219	217	215
225	220	225	230	225	238	245	245	245	245	243	240	240	240	250	250	250	245	245	240	245	235	211	211	215
25	25	25	25	25	25	25	25	25	25	25	25	25	25	25	25	25	25	25	25	25	25	25	25	25
624	626	624	633	556	543	536	560	560	561	558	552	543	532	501	445	445	444	443	461	470	425	343	379	375
268	275	272	267	244	263	270	270	268	263	257	253	251	249	231	236	237	238	239	224	123	206	164	164	135
0	0	0	0	0	0	0	0	0	0	0	0	0	0	0	0	0	0	0	0	0	0	0	0	0
0	0	0	0	0	0	0	0	0	0	0	0	0	0	0	0	0	0	0	0	0	0	0	0	0
0	0	0	0	0	0	0	0	0	0	0	0	0	0	0	0	0	0	0	0	0	0	0	0	0
0	0	0	0	0	0	0	0	0	0	0	0	0	0	0	0	0	0	0	0	0	0	0	0	0
0	0	0	0	0	0	0	0	0	0	0	0	0	0	0	0	0	0	0	0	0	0	0	0	0
0	0	0	0	0	0	0	0	0	0	0	0	0	0	0	0	0	0	0	0	0	0	0	0	0
0	0	0	0	0	0	0	0	0	0	0	0	0	0	0	0	0	0	0	0	0	0	0	0	0
0	0	0	0	0	0	0	0	0	0	0	0	0	0	0	0	0	0	0	0	0	0	0	0	0
0	0	0	0	0	0	0	0	0	0	0	0	0	0	0	0	0	0	0	0	0	0	0	0	0

0	0	0	0	0	0	0	0	0	0	0	0	0	0	0	0	0	0	0	0	0	0	0	0	0
0	0	0	0	0	0	0	0	0	0	0	0	0	0	0	0	0	0	0	0	0	0	0	0	0
0	0	0	0	-54	-78	-59	-57	-26	-13	0	0	0	0	0	0	0	0	0	0	0	0	0	0	0
-9999	-149	-125	-145	-9999	-9999	-9999	-9999	-9999	-9999	-104	-77	35	0	0	0	0	0	0	0	0	0	0	0	0
-9999	-9999	-9999	-9999	-9999	-9999	-9999	-9999	-9999	-9999	-9999	-9999	-9999	-9999	-65	0	0	0	0	0	0	0	0	0	0
-9999	-9999	-9999	-9999	-9999	-9999	-9999	-9999	-9999	-9999	-9999	-9999	-9999	-9999	-9999	-364	-337	-278	-263	-171	-84	-232	-200	-200	-200
-9999	-9999	-9999	-9999	-9999	-9999	-9999	-9999	-9999	-9999	-9999	-9999	-9999	-9999	-9999	-9999	-9999	-9999	-9999	-9999	-9999	-9999	-9999	-9999	-9999
-9999	-9999	-9999	-9999	-9999	-9999	-9999	-9999	-9999	-9999	-9999	-9999	-9999	-9999	-9999	-9999	-9999	-9999	-9999	-9999	-9999	-9999	-9999	-9999	-9999
-9999	-9999	-9999	-9999	-9999	-9999	-9999	-9999	-9999	-9999	-9999	-9999	-9999	-9999	-9999	-9999	-9999	-9999	-9999	-9999	-9999	-9999	-9999	-9999	-9999
120	120	120	120	120	120	120	120	120	120	120	122	120	120	120	120	120	120	120	120	120	120	120	120	120
300	300	300	300	300	300	300	300	300	300	300	298	300	300	300	300	300	300	300	300	300	300	300	300	300
250	250	250	250	250	250	250	250	250	250	250	256	250	250	250	250	250	250	250	250	250	250	250	250	250
350	350	350	350	350	350	350	350	350	350	350	371	350	350	350	350	350	350	350	350	350	350	350	350	350
250	250	250	250	250	250	250	250	250	250	250	195	195	195	195	195	195	195	195	192	192	192	192	192	192
200	200	200	200	200	200	200	200	200	200	115	115	115	115	115	114	114	109	109	109	109	109	109	109	109
120	120	120	117	117	117	117	117	116	116	116	116	116	116	116	116	116	116	116	116	116	116	116	116	116
379	379	379	379	379	379	379	379	379	379	379	379	379	379	379	379	379	379	379	379	379	379	379	379	379
250	250	250	248	248	248	248	248	248	248	248	248	248	248	248	250	250	248	248	248	248	248	248	248	248
225	200	177	58	177	177	177	177	177	177	177	177	177	177	177	179	178	177	177	177	177	177	177	177	177
270	270	280	145	233	233	233	233	233	233	233	233	233	233	233	233	233	233	233	233	233	233	233	233	233
50	50	50	50	50	50	50	50	50	50	50	50	50	50	50	52	52	50	50	50	50	50	50	50	50
260	270	220	250	250	250	250	250	250	250	250	250	250	250	250	250	250	250	250	250	250	250	250	250	250
50	50	0	50	50	50	50	50	50	50	50	50	50	50	50	52	52	50	50	50	50	50	50	50	50
650	650	465	650	650	650	650	635	635	635	650	650	650	650	650	650	650	650	650	650	522	520	650	650	650
550	528	550	550	550	550	550	535	535	535	577	577	577	577	577	577	577	577	577	290	410	550	550	550	550
50	28946	50	50	50	50	50	50	50	50	50	50	50	50	50	50	50	50	50	50	50	50	50	50	50
270	87	250	250	250	250	250	250	250	250	275	275	275	275	275	275	275	275	200	250	250	250	250	250	250
260	240	250	250	250	250	250	250	250	250	180	280	280	280	280	280	280	280	100	250	250	250	250	250	250
243	250	250	250	250	250	250	250	250	250	250	290	290	290	290	290	290	206	268	250	250	250	250	250	250
276	470	500	500	500	500	500	500	500	500	470	320	500	500	500	507	441	379	500	500	500	500	500	500	500
464	496	528	557	590	626	617	612	601	597	592	587	370	341	242	210	247	364	373	429	461	497	515	546	542

GP74	GP75	GP76	GP77	GP78	GP79	GP80	GP81	GP82	GP83	GP84	GP85	GP86	GP87	GP88	GP89	GP90	GP91	GP92	GP93	GP94	GP95
172	172	173	171	169	160	168	167	169	176	173	170	169	169	170	171	167	165	164	172	172	172
-50	-50	-50	-50	-50	-50	-50	-50	-50	-50	-50	-50	-50	-50	-50	-50	-50	-50	-50	-50	-50	-50
285	310	315	315	310	280	262	194	178	190	216	230	230	237	238	240	245	245	245	205	171	171
239	230	224	222	224	231	230	268	276	273	276	270	270	270	284	290	294	296	298	329	329	329
177	174	170	170	176	189	185	176	181	179	173	173	173	174	166	161	158	160	161	161	161	161
48	44	47	46	47	51	55	61	60	63	61	60	61	61	64	65	65	62	62	67	67	67
243	236	228	220	213	209	216	221	209	221	214	219	220	222	221	221	224	228	227	238	238	238
167	160	165	165	165	170	170	180	180	165	165	154	150	145	140	138	132	124	120	99	99	99
30	30	25	25	25	25	25	25	25	25	25	25	25	25	25	25	25	25	25	25	25	25
0	0	0	0	0	0	0	0	0	0	0	0	0	0	0	0	0	0	0	0	0	0
0	0	0	0	0	0	0	0	0	0	0	0	0	0	0	0	0	0	0	0	0	0
-150	-150	-150	-150	-150	-150	-150	-150	-150	-150	-150	-150	-150	-150	-150	-150	-150	-150	-150	-150	-150	-150
486	478	483	483	477	440	434	397	370	374	387	383	375	361	357	359	371	386	394	381	381	381
293	292	295	296	298	309	322	311	304	286	281	279	277	271	262	259	254	248	248	250	247	247
222	239	236	235	238	250	250	258	242	231	225	234	240	242	239	240	243	243	237	249	242	242
218	221	230	224	222	219	222	245	256	237	247	253	253	247	251	257	267	261	259	249	246	246
245	235	225	225	225	230	230	240	260	265	255	255	240	250	254	260	260	260	265	229	230	230
25	25	25	25	25	25	25	25	25	25	25	25	25	25	25	25	25	25	25	25	25	25
490	481	478	476	472	467	468	483	499	513	507	494	456	447	453	530	525	514	493	426	441	441
164	163	170	181	190	206	211	211	204	204	198	183	173	175	192	188	186	183	199	163	175	175
0	0	0	0	0	0	0	0	0	0	0	0	0	0	0	0	0	0	0	0	0	0
0	0	0	0	0	0	0	0	0	0	0	0	0	0	0	0	0	0	0	0	0	0
0	0	0	0	0	0	0	0	0	0	0	0	0	0	0	0	0	0	0	0	0	0
0	0	0	0	0	0	0	0	0	0	0	0	0	0	0	0	0	0	0	0	0	0
0	0	0	0	0	0	0	0	0	0	0	0	0	0	0	0	0	0	0	0	0	0
0	0	0	0	0	0	0	0	0	0	0	0	0	0	0	0	0	0	0	0	0	0
0	0	0	0	0	0	0	0	0	0	0	0	0	0	0	0	0	0	0	0	0	0
0	0	0	0	0	0	0	0	0	0	0	0	0	0	0	0	0	0	0	0	0	0
0	0	0	0	0	0	0	0	0	0	0	0	0	0	0	0	0	0	0	0	0	0

0	0	0	0	0	0	0	0	0	0	0	0	0	0	0	0	0	0	0	0	0	0
0	0	0	0	0	0	0	0	0	0	0	0	0	0	0	0	0	0	0	0	0	0
0	0	0	0	0	0	0	0	0	0	0	0	0	0	0	0	0	0	0	0	0	0
0	0	0	0	0	0	0	0	0	0	0	0	0	0	0	0	0	0	0	0	0	0
0	0	0	0	0	0	0	0	0	0	0	0	0	0	0	0	0	0	0	0	0	0
0	0	0	0	0	0	0	-229	-182	-194	-227	-236	-239	-243	-238	-136	-109	-40	-9999	-9999	-9999	-9999
-227	-212	-202	-179	-156	-75	-9999	-9999	-9999	-9999	-9999	-9999	-9999	-9999	-9999	-9999	-9999	-9999	-9999	-9999	-9999	-9999
-9999	-9999	-9999	-9999	-9999	-9999	-9999	-9999	-9999	-9999	-9999	-9999	-9999	-9999	-9999	-9999	-9999	-9999	-9999	-9999	-9999	-9999
-9999	-9999	-9999	-9999	-9999	-9999	-9999	-9999	-9999	-9999	-9999	-9999	-9999	-9999	-9999	-9999	-9999	-9999	-9999	-9999	-9999	-9999
-9999	-9999	-9999	-9999	-9999	-9999	-9999	-9999	-9999	-9999	-9999	-9999	-9999	-9999	-9999	-9999	-9999	-9999	-9999	-9999	-9999	-9999
120	120	120	120	120	120	120	120	120	120	120	120	120	120	120	120	120	120	120	120	120	120
300	300	300	300	300	300	300	300	300	300	300	300	300	300	300	300	300	300	300	300	300	300
250	250	250	250	250	250	250	250	250	250	250	250	250	250	250	250	250	250	250	250	250	250
350	350	350	350	350	350	350	350	350	350	350	350	350	350	350	350	350	350	350	350	350	350
230	230	230	230	250	250	250	250	250	250	250	250	250	250	250	250	250	250	250	250	250	250
130	130	130	130	150	150	150	130	130	130	130	130	130	130	130	150	165	165	191	191	191	191
120	120	120	120	134	134	134	134	134	134	134	134	134	134	120	140	140	140	140	134	134	134
170	379	379	379	379	379	379	360	360	325	325	325	313	313	313	313	313	313	313	313	313	313
248	300	300	300	325	325	325	300	300	300	300	270	270	270	270	54	285	285	285	270	270	270
177	177	177	177	195	195	195	180	180	180	180	156	156	156	156	156	170	170	170	156	156	156
215	250	250	250	300	300	300	270	270	250	245	175	206	206	206	206	206	183	206	206	206	206
50	11780	50	50	50	50	50	50	50	50	50	50	50	50	50	50	56	50	50	50	50	50
250	101	330	330	350	350	350	250	250	250	155	250	250	250	250	235	270	270	270	250	250	250
50	50	50	50	50	50	50	50	50	50	10	50	50	50	50	50	50	50	50	50	50	50
640	615	368	650	650	650	650	600	600	600	580	580	600	600	600	600	320	700	700	600	600	600
550	550	550	550	550	550	550	500	500	391	500	500	500	500	500	500	470	550	550	500	500	500
50	50	50	27	50	50	50	50	50	50	50	50	50	50	50	50	50	47	50	50	50	50
250	250	250	50	280	280	280	250	250	250	250	250	250	250	250	250	250	35796	270	250	250	250
250	250	250	250	260	260	260	250	250	250	250	240	250	250	250	250	250	147	260	250	250	250
250	250	250	251	270	270	270	250	250	250	250	249	250	250	250	250	250	250	250	250	250	250
500	500	500	500	500	500	500	500	500	500	500	500	500	500	500	500	500	500	500	500	500	500
535	497	465	418	134	14	97	401	607	830	898	951	981	1037	1054	1050	1008	939	570	980	1082	1166

Tab. 13: Heat flow (mW/m²) used along the simulated cross section (alternative model). GP29,GP33,GP42, GP45 and GP94 are BRD-4, BKW-1,WT-1, BK-2 and SF-1 wells, respectively.

Evt. N°	Evt. Name	GP1	GP2	GP3	GP4	GP5	GP6	GP7	GP8	GP9	GP10	GP11	GP12	GP13	GP14	GP15	GP16	GP17	GP18	GP19	GP20	GP21	GP22	GP23
60	Tertiary	63	63	63	63	63	63	63	63	63	63	63	63	63	63	63	63	63	63	63	63	63	63	63
59	Alpine	63	63	63	63	63	63	63	63	63	63	63	63	63	63	63	63	63	63	63	63	63	63	63
58	Maest-Boc.	63	63	63	63	63	63	63	63	63	63	63	63	63	63	63	63	63	63	63	63	63	63	63
57	Santonian	63	63	63	63	63	63	63	63	63	63	63	63	63	63	63	63	63	63	63	63	63	63	63
56	Coniacian	63	63	63	63	63	63	63	63	63	63	63	63	63	63	63	63	63	63	63	63	63	63	63
55	Turonian	63	63	63	63	63	63	63	63	63	63	63	63	63	63	63	63	63	63	63	63	63	63	63
54	Cenoman.	63	63	63	63	63	63	63	63	63	63	63	63	63	63	63	63	63	63	63	63	63	63	63
53	Albian	63	63	63	63	63	63	63	63	63	63	63	63	63	63	63	63	63	63	63	63	63	63	63
52	Aptian	63	63	63	63	63	63	63	63	63	63	63	63	63	63	63	63	63	63	63	63	63	63	63
51	Austrian	63	63	63	63	63	63	63	63	63	63	63	63	63	63	63	63	63	63	63	63	63	63	63
50	Austrian	63	63	63	63	63	63	63	63	63	63	63	63	63	63	63	63	63	63	63	63	63	63	63
49	Austrian	63	63	63	63	63	63	63	63	63	63	63	63	63	63	63	63	63	63	63	63	63	63	63
48	Barremian	64	64	64	64	64	64	64	64	64	64	64	64	64	64	64	64	64	64	64	64	64	64	64
47	Neocomm.	64	64	64	64	64	64	64	64	64	64	64	64	64	64	64	64	64	64	64	64	64	64	64
46	Malm	64	64	64	64	64	64	64	64	64	64	64	64	64	64	64	64	64	64	64	64	64	64	64
45	Dogger	65	65	65	65	65	65	65	65	65	65	65	65	65	65	65	65	65	65	65	64	64	64	64
44	Pliensbach.	65	65	65	65	65	65	65	65	65	65	65	65	65	65	65	65	65	65	65	65	65	65	65
43	Sinemurian	65	65	65	65	65	65	65	65	65	65	65	65	65	65	65	65	65	65	65	65	65	65	65
42	Rhaetian	68	68	68	68	68	68	68	68	68	68	68	68	68	68	68	68	68	68	68	68	68	68	68
41	Tr. Keuper	70	70	70	70	70	70	70	70	70	70	70	70	70	70	70	70	70	70	70	70	70	70	70
40	Hercynian	58	58	58	58	58	58	58	58	58	58	58	58	58	58	58	58	58	58	58	58	58	58	58
39	Hercynian	58	58	58	58	58	58	58	58	58	58	58	58	58	58	58	58	58	58	58	58	58	58	58
38	Hercynian	58	58	58	58	58	58	58	58	58	58	58	58	58	58	58	58	58	58	58	58	58	58	58
37	Hercynian	58	58	58	58	58	58	58	58	58	58	58	58	58	58	58	58	58	58	58	58	58	58	58
36	Hercynian	58	58	58	58	58	58	58	58	58	58	58	58	58	58	58	58	58	58	58	58	58	58	58
35	Hercynian	58	58	58	58	58	58	58	58	58	58	58	58	58	58	58	58	58	58	58	58	58	58	58
34	Hercynian	58	58	58	58	58	58	58	58	58	58	58	58	58	58	58	58	58	58	58	58	58	58	58
33	Hercynian	58	58	58	58	58	58	58	58	58	58	58	58	58	58	58	58	58	58	58	58	58	58	58
32	Hercynian	58	58	58	58	58	58	58	58	58	58	58	58	58	58	58	58	58	58	58	58	58	58	58

31	Hercynian	58	58	58	58	58	58	58	58	58	58	58	58	58	58	58	58	58	58	58	58	58	58	58
30	Hercynian	58	58	58	58	58	58	58	58	58	58	58	58	58	58	58	58	58	58	58	58	58	58	58
29	Hercynian	58	58	58	58	58	58	58	58	58	58	58	58	58	58	58	58	58	58	58	58	58	58	58
28	Hercynian	58	58	58	58	58	58	58	58	58	58	58	58	58	58	58	58	58	58	58	58	58	58	58
27	Hercynian	58	58	58	58	58	58	58	58	58	58	58	58	58	58	58	58	58	58	58	58	58	58	58
26	Hercynian	58	58	58	58	58	58	58	58	58	58	58	58	58	58	58	58	58	58	58	58	58	58	58
25	Hercynian	58	58	58	58	58	58	58	58	58	58	58	58	58	58	58	58	58	58	58	58	58	58	58
24	Hercynian	58	58	58	58	58	58	58	58	58	58	58	58	58	58	58	58	58	58	58	58	58	58	58
23	Hercynian	58	58	58	58	58	58	58	58	58	58	58	58	58	58	58	58	58	58	58	58	58	58	58
22	Stephan.	60	60	60	60	60	60	60	60	60	60	60	60	60	60	60	60	60	60	60	60	60	60	60
21	Westphal.	60	60	60	60	60	60	60	60	60	60	60	60	60	60	60	60	60	60	60	60	60	60	60
20	Namurian	60	60	60	60	60	60	60	60	60	60	60	60	60	60	60	60	60	60	60	60	60	60	60
19	Visean C	60	60	60	60	60	60	60	60	60	60	60	60	60	60	60	60	60	60	60	60	60	60	60
18	Visean B	60	60	60	60	60	60	60	60	60	60	60	60	60	60	60	60	60	60	60	60	60	60	60
17	Tournais.	60	60	60	60	60	60	60	60	60	60	60	60	60	60	60	60	60	60	60	60	60	60	60
16	Strunian	60	60	60	60	60	60	60	60	60	60	60	60	60	60	60	60	60	60	60	60	60	60	60
15	Famennian	60	60	60	60	60	60	60	60	60	60	60	60	60	60	60	60	60	60	60	60	60	60	60
14	Frasnian	60	60	60	60	60	60	60	60	60	60	60	60	60	60	60	60	60	60	60	60	60	60	60
13	Emsian	60	60	60	60	60	60	60	60	60	60	60	60	60	60	60	60	60	60	60	60	60	60	60
12	Ged-Sieg.	62	62	62	62	62	62	62	62	62	62	62	62	62	62	62	62	62	62	62	62	62	62	62
11	ntra.G.Sieg	62	62	62	62	62	62	62	62	62	62	62	62	62	62	62	62	62	62	62	62	62	62	62
10	Gedinnian	62	62	62	62	62	62	62	62	62	62	62	62	62	62	62	62	62	62	62	62	62	62	62
9	Prodolian	63	63	63	63	63	63	63	63	63	63	63	63	63	63	63	63	63	63	63	63	63	63	63
8	Ludlow	63	63	63	63	63	63	63	63	63	63	63	63	63	63	63	63	63	63	63	63	63	63	63
7	Wenlock	65	65	65	65	65	65	65	65	65	65	65	65	65	65	65	65	65	65	65	65	65	65	65
6	Sil.R.Z	65	65	65	65	65	65	65	65	65	65	65	65	65	65	65	65	65	65	65	65	65	65	65
5	Llanvirn	70	70	70	70	70	70	70	70	70	70	70	70	70	70	70	70	70	70	70	70	70	70	70
4	Arenigian	70	70	70	70	70	70	70	70	70	70	70	70	70	70	70	70	70	70	70	70	70	70	70
3	Tremadoc	75	75	75	75	75	75	75	75	75	75	75	75	75	75	75	75	75	75	75	75	75	75	75
2	Cambrian	75	75	75	75	75	75	75	75	75	75	75	75	75	75	75	75	75	75	75	75	75	75	75
1	Basement	40	40	40	40	40	40	40	40	40	40	40	40	40	40	40	40	40	40	40	40	40	40	40

GP24	GP25	GP26	GP27	GP28	GP29	GP30	GP31	GP32	GP33	GP34	GP35	GP36	GP37	GP38	GP39	GP40	GP41	GP42	GP43	GP44	GP45	GP46	GP47	GP48
63	63	63	63	63	63	63	63	63	63	63	63	63	63	63	50	50	50	50	50	50	50	50	50	50
63	63	63	63	63	63	63	63	63	63	63	63	63	63	63	50	50	50	50	50	50	50	50	50	50
63	63	63	63	63	63	63	63	63	63	63	63	63	63	63	50	50	50	50	50	50	50	50	50	50
63	63	63	63	63	63	63	63	63	63	63	63	63	63	63	50	50	50	50	50	50	50	50	50	50
63	63	63	63	63	63	63	63	63	63	63	63	63	63	63	50	50	50	50	50	50	50	50	50	50
63	63	63	63	63	63	63	63	63	63	63	63	63	63	63	50	50	50	50	50	50	50	50	50	50
63	63	63	63	63	63	63	63	63	63	63	63	63	63	63	50	50	50	50	50	50	50	50	50	50
63	63	63	63	63	63	63	63	63	63	63	63	63	63	63	50	50	50	50	50	50	50	50	50	50
63	63	63	63	63	63	63	63	63	63	63	63	63	63	63	50	50	50	50	50	50	50	50	50	50
63	63	63	63	63	63	63	63	63	63	63	63	63	63	63	50	50	50	50	50	50	50	50	50	50
63	63	63	63	63	63	63	63	63	63	63	63	63	63	63	50	50	50	50	50	50	50	50	50	50
63	63	63	63	63	63	63	63	63	63	63	63	63	63	63	50	50	50	50	50	50	50	50	50	50
63	63	63	63	63	63	63	63	63	63	63	63	63	63	63	53	53	53	53	53	53	53	53	53	53
64	64	64	64	64	64	64	64	64	64	64	64	64	64	64	53	53	53	53	53	53	53	53	53	53
64	64	64	64	64	64	64	64	64	64	64	64	64	64	64	55	55	55	55	55	55	55	55	55	55
64	64	64	64	64	64	64	64	64	64	64	64	64	64	64	55	55	55	55	55	55	55	55	55	55
65	65	65	65	65	65	65	65	65	65	65	65	65	65	65	58	58	58	58	58	58	58	58	58	58
65	65	65	65	65	65	65	65	65	65	65	65	65	65	65	58	58	58	58	58	58	58	58	58	58
65	65	65	65	65	65	65	65	65	65	65	65	65	65	65	58	58	58	58	58	58	58	58	58	58
68	68	68	68	68	68	68	68	68	68	68	68	68	68	68	60	60	60	60	60	60	60	60	60	60
70	70	70	70	70	70	70	70	70	70	70	70	70	70	70	65	65	65	65	65	65	65	65	65	65
58	58	58	58	58	58	58	58	58	58	58	58	58	58	58	58	58	58	58	58	58	58	58	58	58
58	58	58	58	58	58	58	58	58	58	58	58	58	58	58	58	58	58	58	58	58	58	58	58	58
58	58	58	58	58	58	58	58	58	58	58	58	58	58	58	58	58	58	58	58	58	58	58	58	58
58	58	58	58	58	58	58	58	58	58	58	58	58	58	58	58	58	58	58	58	58	58	58	58	58
58	58	58	58	58	58	58	58	58	58	58	58	58	58	58	58	58	58	58	58	58	58	58	58	58
58	58	58	58	58	58	58	58	58	58	58	58	58	58	58	58	58	58	58	58	58	58	58	58	58
58	58	58	58	58	58	58	58	58	58	58	58	58	58	58	58	58	58	58	58	58	58	58	58	58
58	58	58	58	58	58	58	58	58	58	58	58	58	58	58	58	58	58	58	58	58	58	58	58	58
58	58	58	58	58	58	58	58	58	58	58	58	58	58	58	58	58	58	58	58	58	58	58	58	58
58	58	58	58	58	58	58	58	58	58	58	58	58	58	58	58	58	58	58	58	58	58	58	58	58

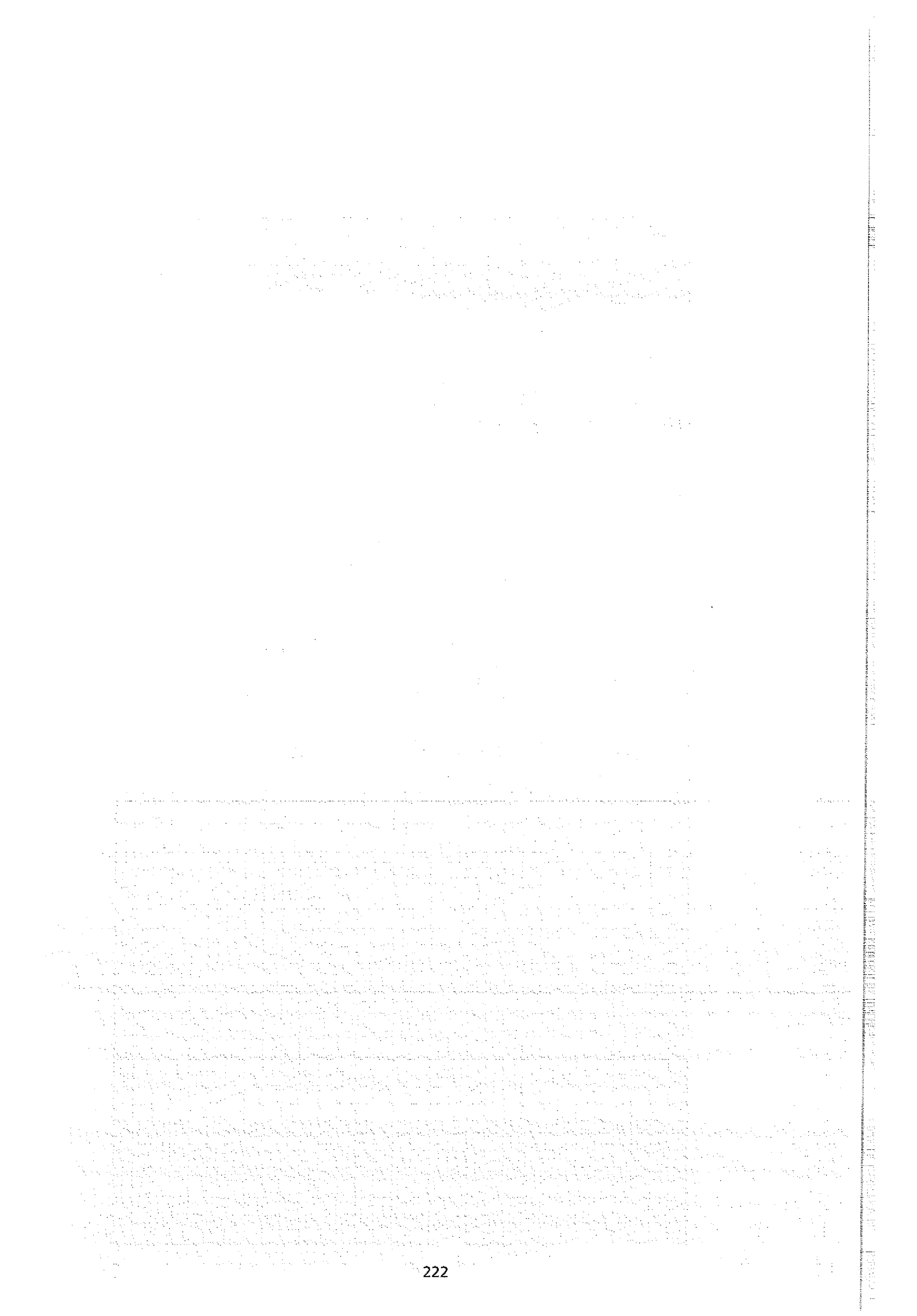
58	58	58	58	58	58	58	58	58	58	58	58	58	58	58	58	58	58	58	58	58	58	58	58	58
58	58	58	58	58	58	58	58	58	58	58	58	58	58	58	58	58	58	58	58	58	58	58	58	58
58	58	58	58	58	58	58	58	58	58	58	58	58	58	58	58	58	58	58	58	58	58	58	58	58
58	58	58	58	58	58	58	58	58	58	58	58	58	58	58	58	58	58	58	58	58	58	58	58	58
58	58	58	58	58	58	58	58	58	58	58	58	58	58	58	58	58	58	58	58	58	58	58	58	58
58	58	58	58	58	58	58	58	58	58	58	58	58	58	58	58	58	58	58	58	58	58	58	58	58
58	58	58	58	58	58	58	58	58	58	58	58	58	58	58	58	58	58	58	58	58	58	58	58	58
58	58	58	58	58	58	58	58	58	58	58	58	58	58	58	58	58	58	58	58	58	58	58	58	58
58	58	58	58	58	58	58	58	58	58	58	58	58	58	58	58	58	58	58	58	58	58	58	58	58
58	58	58	58	58	58	58	58	58	58	58	58	58	58	58	58	58	58	58	58	58	58	58	58	58
60	60	60	60	60	60	60	60	60	60	60	60	60	60	60	60	60	60	60	60	60	60	60	60	60
60	60	60	60	60	60	60	60	60	60	60	60	60	60	60	60	60	60	60	60	60	60	60	60	60
60	60	60	60	60	60	60	60	60	60	60	60	60	60	60	60	60	60	60	60	60	60	60	60	60
60	60	60	60	60	60	60	60	60	60	60	60	60	60	60	60	60	60	60	60	60	60	60	60	60
60	60	60	60	60	60	60	60	60	60	60	60	60	60	60	60	60	60	60	60	60	60	60	60	60
60	60	60	60	60	60	60	60	60	60	60	60	60	60	60	60	60	60	60	60	60	60	60	60	60
60	60	60	60	60	60	60	60	60	60	60	60	60	60	60	60	60	60	60	60	60	60	60	60	60
60	60	60	60	60	60	60	60	60	60	60	60	60	60	60	60	60	60	60	60	60	60	60	60	60
60	60	60	60	60	60	60	60	60	60	60	60	60	60	60	60	60	60	60	60	60	60	60	60	60
60	60	60	60	60	60	60	60	60	60	60	60	60	60	60	60	60	60	60	60	60	60	60	60	60
60	60	60	60	60	60	60	60	60	60	60	60	60	60	60	60	60	60	60	60	60	60	60	60	60
60	60	60	60	60	60	60	60	60	60	60	60	60	60	60	60	60	60	60	60	60	60	60	60	60
60	60	60	60	60	60	60	60	60	60	60	60	60	60	60	60	60	60	60	60	60	60	60	60	60
62	62	62	62	62	62	62	62	62	62	62	62	62	62	62	62	62	62	62	62	62	62	62	62	62
62	62	62	62	62	62	62	62	62	62	62	62	62	62	62	62	62	62	62	62	62	62	62	62	62
62	62	62	62	62	62	62	62	62	62	62	62	62	62	62	62	62	62	62	62	62	62	62	62	62
63	63	63	63	63	63	63	63	63	63	63	63	63	63	63	63	63	63	63	63	63	63	63	63	63
63	63	63	63	63	63	63	63	63	63	63	63	63	63	63	63	63	63	63	63	63	63	63	63	63
65	65	65	65	65	65	65	65	65	65	65	65	65	65	65	65	65	65	65	65	65	65	65	65	65
65	65	65	65	65	65	65	65	65	65	65	65	65	65	65	65	65	65	65	65	65	65	65	65	65
70	70	70	70	70	70	70	70	70	70	70	70	70	70	70	70	70	70	70	70	70	70	70	70	70
70	70	70	70	70	70	70	70	70	70	70	70	70	70	70	70	70	70	70	70	70	70	70	70	70
75	75	75	75	75	75	75	75	75	75	75	75	75	75	75	75	75	75	75	75	75	75	75	75	75
75	75	75	75	75	75	75	75	75	75	75	75	75	75	75	75	75	75	75	75	75	75	75	75	75
40	40	40	40	40	40	40	40	40	40	40	40	40	40	40	40	40	40	40	40	40	40	40	40	40

GP49	GP50	GP51	GP52	GP53	GP54	GP55	GP56	GP57	GP58	GP59	GP60	GP61	GP62	GP63	GP64	GP65	GP66	GP67	GP68	GP69	GP70	GP71	GP72	GP73
50	50	50	50	50	50	50	50	50	50	50	50	50	50	50	50	50	50	50	50	50	50	50	50	50
50	50	50	50	50	50	50	50	50	50	50	50	50	50	50	50	50	50	50	50	50	50	50	50	50
50	50	50	50	50	50	50	50	50	50	50	50	50	50	50	50	50	50	50	50	50	50	50	50	50
50	50	50	50	50	50	50	50	50	50	50	50	50	50	50	50	50	50	50	50	50	50	50	50	50
50	50	50	50	50	50	50	50	50	50	50	50	50	50	50	50	50	50	50	50	50	50	50	50	50
50	50	50	50	50	50	50	50	50	50	50	50	50	50	50	50	50	50	50	50	50	50	50	50	50
50	50	50	50	50	50	50	50	50	50	50	50	50	50	50	50	50	50	50	50	50	50	50	50	50
50	50	50	50	50	50	50	50	50	50	50	50	50	50	50	50	50	50	50	50	50	50	50	50	50
50	50	50	50	50	50	50	50	50	50	50	50	50	50	50	50	50	50	50	50	50	50	50	50	50
50	50	50	50	50	50	50	50	50	50	50	50	50	50	50	50	50	50	50	50	50	50	50	50	50
53	53	53	53	53	53	53	53	53	53	53	53	53	53	53	53	53	53	53	53	53	53	53	53	53
53	53	53	53	53	53	53	53	53	53	53	53	53	53	53	53	53	53	53	53	53	53	53	53	53
53	53	53	53	53	53	53	53	53	53	53	53	53	53	53	53	53	53	53	53	53	53	53	53	53
55	55	55	55	55	55	55	55	55	55	55	55	55	55	55	55	55	55	55	55	55	55	55	55	55
55	55	55	55	55	55	55	55	55	55	55	55	55	55	55	55	55	55	55	55	55	55	55	55	55
58	58	58	58	58	58	58	58	58	58	58	58	58	58	58	58	58	58	58	58	58	58	58	58	58
58	58	58	58	58	58	58	58	58	58	58	58	58	58	58	58	58	58	58	58	58	58	58	58	58
58	58	58	58	58	58	58	58	58	58	58	58	58	58	58	58	58	58	58	58	58	58	58	58	58
60	60	60	60	60	60	60	60	60	60	60	60	60	60	60	60	60	60	60	60	60	60	60	60	60
65	65	65	65	65	65	65	65	65	65	65	65	65	65	65	65	65	65	65	65	65	65	65	65	65
58	58	58	58	58	58	58	58	58	58	58	58	58	58	58	58	58	58	58	58	58	58	58	58	58
58	58	58	58	58	58	58	58	58	58	58	58	58	58	58	58	58	58	58	58	58	58	58	58	58
58	58	58	58	58	58	58	58	58	58	58	58	58	58	58	58	58	58	58	58	58	58	58	58	58
58	58	58	58	58	58	58	58	58	58	58	58	58	58	58	58	58	58	58	58	58	58	58	58	58
58	58	58	58	58	58	58	58	58	58	58	58	58	58	58	58	58	58	58	58	58	58	58	58	58
58	58	58	58	58	58	58	58	58	58	58	58	58	58	58	58	58	58	58	58	58	58	58	58	58
58	58	58	58	58	58	58	58	58	58	58	58	58	58	58	58	58	58	58	58	58	58	58	58	58
58	58	58	58	58	58	58	58	58	58	58	58	58	58	58	58	58	58	58	58	58	58	58	58	58
58	58	58	58	58	58	58	58	58	58	58	58	58	58	58	58	58	58	58	58	58	58	58	58	58
58	58	58	58	58	58	58	58	58	58	58	58	58	58	58	58	58	58	58	58	58	58	58	58	58

58	58	58	58	58	58	58	58	58	58	58	58	58	58	58	58	58	58	58	58	58	58	58	58
58	58	58	58	58	58	58	58	58	58	58	58	58	58	58	58	58	58	58	58	58	58	58	58
58	58	58	58	58	58	58	58	58	58	58	58	58	58	58	58	58	58	58	58	58	58	58	58
58	58	58	58	58	58	58	58	58	58	58	58	58	58	58	58	58	58	58	58	58	58	58	58
58	58	58	58	58	58	58	58	58	58	58	58	58	58	58	58	58	58	58	58	58	58	58	58
58	58	58	58	58	58	58	58	58	58	58	58	58	58	58	58	58	58	58	58	58	58	58	58
58	58	58	58	58	58	58	58	58	58	58	58	58	58	58	58	58	58	58	58	58	58	58	58
58	58	58	58	58	58	58	58	58	58	58	58	58	58	58	58	58	58	58	58	58	58	58	58
58	58	58	58	58	58	58	58	58	58	58	58	58	58	58	58	58	58	58	58	58	58	58	58
58	58	58	58	58	58	58	58	58	58	58	58	58	58	58	58	58	58	58	58	58	58	58	58
60	60	60	60	60	60	60	60	60	60	60	60	60	60	60	60	60	60	60	60	60	60	60	60
60	60	60	60	60	60	60	60	60	60	60	60	60	60	60	60	60	60	60	60	60	60	60	60
60	60	60	60	60	60	60	60	60	60	60	60	60	60	60	60	60	60	60	60	60	60	60	60
60	60	60	60	60	60	60	60	60	60	60	60	60	60	60	60	60	60	60	60	60	60	60	60
60	60	60	60	60	60	60	60	60	60	60	60	60	60	60	60	60	60	60	60	60	60	60	60
60	60	60	60	60	60	60	60	60	60	60	60	60	60	60	60	60	60	60	60	60	60	60	60
60	60	60	60	60	60	60	60	60	60	60	60	60	60	60	60	60	60	60	60	60	60	60	60
60	60	60	60	60	60	60	60	60	60	60	60	60	60	60	60	60	60	60	60	60	60	60	60
60	60	60	60	60	60	60	60	60	60	60	60	60	60	60	60	60	60	60	60	60	60	60	60
60	60	60	60	60	60	60	60	60	60	60	60	60	60	60	60	60	60	60	60	60	60	60	60
60	60	60	60	60	60	60	60	60	60	60	60	60	60	60	60	60	60	60	60	60	60	60	60
60	60	60	60	60	60	60	60	60	60	60	60	60	60	60	60	60	60	60	60	60	60	60	60
62	62	62	62	62	62	62	62	62	62	62	62	62	62	62	62	62	62	62	62	62	62	62	62
62	62	62	62	62	62	62	62	62	62	62	62	62	62	62	62	62	62	62	62	62	62	62	62
62	62	62	62	62	62	62	62	62	62	62	62	62	62	62	62	62	62	62	62	62	62	62	62
63	63	63	63	63	63	63	63	63	63	63	63	63	63	63	63	63	63	63	63	63	63	63	63
63	63	63	63	63	63	63	63	63	63	63	63	63	63	63	63	63	63	63	63	63	63	63	63
65	65	65	65	65	65	65	65	65	65	65	65	65	65	65	65	65	65	65	65	65	65	65	65
65	65	65	65	65	65	65	65	65	65	65	65	65	65	65	65	65	65	65	65	65	65	65	65
70	70	70	70	70	70	70	70	70	70	70	70	70	70	70	70	70	70	70	70	70	70	70	70
70	70	70	70	70	70	70	70	70	70	70	70	70	70	70	70	70	70	70	70	70	70	70	70
75	75	75	75	75	75	75	75	75	75	75	75	75	75	75	75	75	75	75	75	75	75	75	75
75	75	75	75	75	75	75	75	75	75	75	75	75	75	75	75	75	75	75	75	75	75	75	75
40	40	40	40	40	40	40	40	40	40	40	40	40	40	40	40	40	40	40	40	40	40	40	40

GP74	GP75	GP76	GP77	GP78	GP79	GP80	GP81	GP82	GP83	GP84	GP85	GP86	GP87	GP88	GP89	GP90	GP91	GP92	GP93	GP94	GP95
50	50	50	50	50	50	50	50	50	50	50	50	50	50	50	50	50	50	50	50	50	50
50	50	50	50	50	50	50	50	50	50	50	50	50	50	50	50	50	50	50	50	50	50
50	50	50	50	50	50	50	50	50	50	50	50	50	50	50	50	50	50	50	50	50	50
50	50	50	50	50	50	50	50	50	50	50	50	50	50	50	50	50	50	50	50	50	50
50	50	50	50	50	50	50	50	50	50	50	50	50	50	50	50	50	50	50	50	50	50
50	50	50	50	50	50	50	50	50	50	50	50	50	50	50	50	50	50	50	50	50	50
50	50	50	50	50	50	50	50	50	50	50	50	50	50	50	50	50	50	50	50	50	50
50	50	50	50	50	50	50	50	50	50	50	50	50	50	50	50	50	50	50	50	50	50
50	50	50	50	50	50	50	50	50	50	50	50	50	50	50	50	50	50	50	50	50	50
50	50	50	50	50	50	50	50	50	50	50	50	50	50	50	50	50	50	50	50	50	50
50	50	50	50	50	50	50	50	50	50	50	50	50	50	50	50	50	50	50	50	50	50
53	53	53	53	53	53	53	53	53	53	53	53	53	53	53	53	53	53	53	53	53	53
53	53	53	53	53	53	53	53	53	53	53	53	53	53	53	53	53	53	53	53	53	53
53	53	53	53	53	53	53	53	53	53	53	53	53	53	53	53	53	53	53	53	53	53
55	55	55	55	55	55	55	55	55	55	55	55	55	55	55	55	55	55	55	55	55	55
55	55	55	55	55	55	55	55	55	55	55	55	55	55	55	55	55	55	55	55	55	55
58	58	58	58	58	58	58	58	58	58	58	58	58	58	58	58	58	58	58	58	58	58
58	58	58	58	58	58	58	58	58	58	58	58	58	58	58	58	58	58	58	58	58	58
58	58	58	58	58	58	58	58	58	58	58	58	58	58	58	58	58	58	58	58	58	58
60	60	60	60	60	60	60	60	60	60	60	60	60	60	60	60	60	60	60	60	60	60
65	65	65	65	65	65	65	65	65	65	65	65	65	65	65	65	65	65	65	65	65	65
58	58	58	58	58	58	58	58	58	58	58	58	58	58	58	58	58	58	58	58	58	58
58	58	58	58	58	58	58	58	58	58	58	58	58	58	58	58	58	58	58	58	58	58
58	58	58	58	58	58	58	58	58	58	58	58	58	58	58	58	58	58	58	58	58	58
58	58	58	58	58	58	58	58	58	58	58	58	58	58	58	58	58	58	58	58	58	58
58	58	58	58	58	58	58	58	58	58	58	58	58	58	58	58	58	58	58	58	58	58
58	58	58	58	58	58	58	58	58	58	58	58	58	58	58	58	58	58	58	58	58	58
58	58	58	58	58	58	58	58	58	58	58	58	58	58	58	58	58	58	58	58	58	58
58	58	58	58	58	58	58	58	58	58	58	58	58	58	58	58	58	58	58	58	58	58
58	58	58	58	58	58	58	58	58	58	58	58	58	58	58	58	58	58	58	58	58	58
58	58	58	58	58	58	58	58	58	58	58	58	58	58	58	58	58	58	58	58	58	58

58	58	58	58	58	58	58	58	58	58	58	58	58	58	58	58	58	58	58	58	58	58
58	58	58	58	58	58	58	58	58	58	58	58	58	58	58	58	58	58	58	58	58	58
58	58	58	58	58	58	58	58	58	58	58	58	58	58	58	58	58	58	58	58	58	58
58	58	58	58	58	58	58	58	58	58	58	58	58	58	58	58	58	58	58	58	58	58
58	58	58	58	58	58	58	58	58	58	58	58	58	58	58	58	58	58	58	58	58	58
58	58	58	58	58	58	58	58	58	58	58	58	58	58	58	58	58	58	58	58	58	58
58	58	58	58	58	58	58	58	58	58	58	58	58	58	58	58	58	58	58	58	58	58
58	58	58	58	58	58	58	58	58	58	58	58	58	58	58	58	58	58	58	58	58	58
58	58	58	58	58	58	58	58	58	58	58	58	58	58	58	58	58	58	58	58	58	58
58	58	58	58	58	58	58	58	58	58	58	58	58	58	58	58	58	58	58	58	58	58
60	60	60	60	60	60	60	60	60	60	60	60	60	60	60	60	60	60	60	60	60	60
60	60	60	60	60	60	60	60	60	60	60	60	60	60	60	60	60	60	60	60	60	60
60	60	60	60	60	60	60	60	60	60	60	60	60	60	60	60	60	60	60	60	60	60
60	60	60	60	60	60	60	60	60	60	60	60	60	60	60	60	60	60	60	60	60	60
60	60	60	60	60	60	60	60	60	60	60	60	60	60	60	60	60	60	60	60	60	60
60	60	60	60	60	60	60	60	60	60	60	60	60	60	60	60	60	60	60	60	60	60
60	60	60	60	60	60	60	60	60	60	60	60	60	60	60	60	60	60	60	60	60	60
60	60	60	60	60	60	60	60	60	60	60	60	60	60	60	60	60	60	60	60	60	60
60	60	60	60	60	60	60	60	60	60	60	60	60	60	60	60	60	60	60	60	60	60
60	60	60	60	60	60	60	60	60	60	60	60	60	60	60	60	60	60	60	60	60	60
60	60	60	60	60	60	60	60	60	60	60	60	60	60	60	60	60	60	60	60	60	60
62	62	62	62	62	62	62	62	62	62	62	62	62	62	62	62	62	62	62	62	62	62
62	62	62	62	62	62	62	62	62	62	62	62	62	62	62	62	62	62	62	62	62	62
62	62	62	62	62	62	62	62	62	62	62	62	62	62	62	62	62	62	62	62	62	62
63	63	63	63	63	63	63	63	63	63	63	63	63	63	63	63	63	63	63	63	63	63
63	63	63	63	63	63	63	63	63	63	63	63	63	63	63	63	63	63	63	63	63	63
65	65	65	65	65	65	65	65	65	65	65	65	65	65	65	65	65	65	65	65	65	65
65	65	65	65	65	65	65	65	65	65	65	65	65	65	65	65	65	65	65	65	65	65
70	70	70	70	70	70	70	70	70	70	70	70	70	70	70	70	70	70	70	70	70	70
70	70	70	70	70	70	70	70	70	70	70	70	70	70	70	70	70	70	70	70	70	70
75	75	75	75	75	75	75	75	75	75	75	75	75	75	75	75	75	75	75	75	75	75
75	75	75	75	75	75	75	75	75	75	75	75	75	75	75	75	75	75	75	75	75	75
40	40	40	40	40	40	40	40	40	40	40	40	40	40	40	40	40	40	40	40	40	40



Forschungszentrum Jülich

Jül-3677
July 1999
ISSN 0944-2952